Chem Soc Rev

Organoboron-based multiple-resonance emitters: synthesis, structure–property correlations, and prospects†

Masashi Mamada, (ID) ‡ Masahiro Hayakawa, (ID) ‡ Junki Ochi (ID) ‡ and Takuji Hatakeyama (ID) *

Boron-based multiple-resonance (MR) emitters exhibit the advantages of narrowband emission, high absolute photoluminescence quantum yield, thermally activated delayed fluorescence (TADF), and sufficient stability during the operation of organic light-emitting diodes (OLEDs). Thus, such MR emitters have been widely applied as blue emitters in triplet–triplet-annihilation-driven fluorescent devices used in smartphones and televisions. Moreover, they hold great promise as TADF or terminal emitters in TADF-assisted fluorescence or phosphor-sensitised fluorescent OLEDs. Herein we comprehensively review organoboron-based MR emitters based on their synthetic strategies, clarify structure–photophysical property correlations, and provide design guidelines and future development prospects.

1. Introduction

Given their advantageous optical and electrochemical properties, π-conjugated compounds featuring tricoordinated sp²-hybridised boron (B_{sp^2}) atoms with empty p_z orbitals have attracted significant attention in the field of materials chemistry.[1–21] The inherent

Department of Chemistry, Graduate School of Science, Kyoto University, Sakyo-ku, Kyoto 606-8502, Japan. E-mail: hatake@kuchem.kyoto-u.ac.jp

† Electronic supplementary information (ESI) available: List of compounds. See DOI: **https://doi.org/10.1039/d3cs00837a**

‡ These authors equally contributed to this work.

Masashi Mamada

Masashi Mamada obtained his PhD degree in 2010 from Tokyo Institute of Technology under the supervision of Prof. Yoshiro Yamashita. After working as a postdoctoral researcher in Prof. Pavel Anzenbacher's group at Bowling Green State University, USA, until 2011, he joined Innovation Center for Organic Electronics (INOEL) of Yamagata University as an assistant professor. In 2016, he moved to Prof. Chihaya Adachi's group of Center for Organic Photonics and Electronics Research (OPERA) at Kyushu University as an assistant professor to contribute to the Molecular Exciton Engineering Project. He is currently an associate professor in the Department of Chemistry, Graduate School of Science at Kyoto University. His research is focused on synthesis and photophysics of novel organic materials for optoelectronic applications such as OLEDs, OFETs, and organic lasers.

Masahiro Hayakawa

Masahiro Hayakawa received his BSc (2017), MSc (2019), and PhD (2022) degrees in Chemistry from Nagoya University under the supervision of Prof. Shigehiro Yamaguchi and Prof. Aiko Fukazawa. In 2022, he joined the group of Prof. Takuji Hatakeyama and started his academic career as an assistant professor in the Department of Chemistry, Graduate School of Science at Kyoto University. His current research interest is the development of unusual π-conjugated compounds.
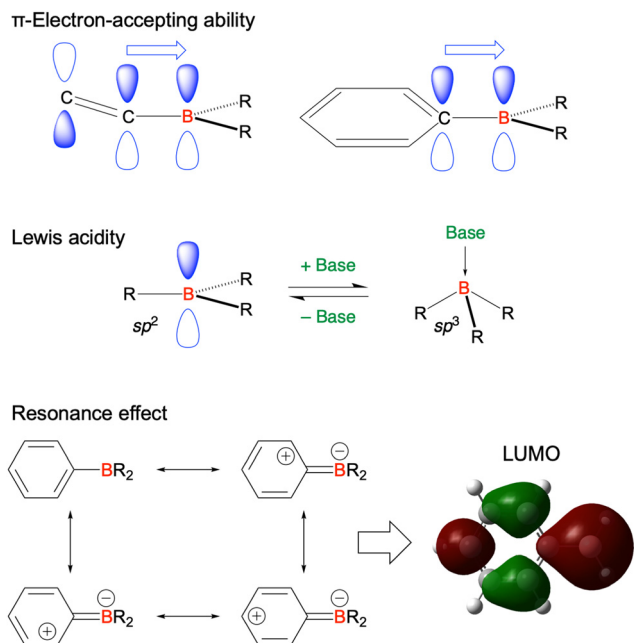
1624 | *Chem. Soc. Rev.*, 2024, **53**, 1624–1692

This journal is © The Royal Society of Chemistry 2024

Fig. 1 Representative features of a tricoordinated sp^2-hybridised boron (B_{sp^2}) atom.

Fig. 2 Molecular design and physical properties of multiple-resonance (MR) emitters.

vulnerability of B_{sp^2}–C bonds to moisture and oxygen necessitates the adoption of protective measures such as steric shielding[22–24] (*e.g.*, Mes_2B group (Mes = mesityl)), intramolecular π-electron donation[25–34] (*e.g.*, aza- and oxaborines), and planarity constraints[35,36] (*e.g.*, boron-doped polycyclic aromatic hydrocarbons (PAHs)) to achieve sufficient stability for use in, *e.g.*, nonlinear optics, optoelectronics, stimuli-responsive systems, bioimaging, sensing, and catalysis. Although the observed functionalities mostly originate from the π-electron-accepting ability or Lewis acidity of B_{sp^2}, the resonance effect of such
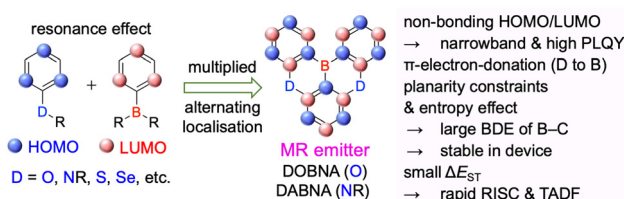
centres has not been intentionally exploited in material design (Fig. 1).

In 2015 and 2016, a new molecular design utilising the opposite resonance effects of B_{sp^2} and electron-donating atoms (*e.g.*, oxygen[37] and nitrogen[38]) at relative *ortho*-positions in a polycyclic aromatic skeleton was proposed by Hatakeyama *et al.* (Fig. 2). In such structures, the highest occupied molecular orbital (HOMO) is mainly localised on electron-donating atoms and carbons *ortho*/*para* relative to them, whereas the lowest unoccupied molecular orbital (LUMO) is mainly localised on the boron atom and carbons *ortho*/*para* relative to it in adjacent benzene rings. This alternating localisation of frontier molecular orbitals (FMOs) results in narrowband emission, high absolute photoluminescence (PL) quantum yield (Φ_{PL}), thermally activated delayed fluorescence (TADF),[39–41] and sufficient stability during the operation of organic light-emitting diodes (OLEDs).[42,43] Consequently, more than 400 organoboron-based multiple-resonance (MR) emitters have been developed[44–53] after the pioneering reports on 5,9-dioxa-13b-boranaphtho[3,2,1-*de*]anthracene (**DOBNA**)[37] and 5,9-diaza-13b-boranaphtho[3,2,1-*de*]anthracene (**DABNA**).[38]

For organic emitters, the full width at half maximum (FWHM) of the emission peak is generally correlated with the degree of structural relaxation in the first singlet excited state (S_1).[54,55]

Junki Ochi received his BSc (2018), MSc (2020), and PhD (2023) degrees in Chemistry from Kyoto University under the supervision of Prof. Yoshiki Chujo and Prof. Kazuo Tanaka. In 2023, he joined the group of Prof. Takuji Hatakeyama in the Department of Chemistry, Graduate School of Science at Kyoto University, as a Program-Specific Assistant Professor. His current research interest is developing heteroatom-containing luminescent materials.

Junki Ochi

Takuji Hatakeyama received his PhD degree in 2005 from the University of Tokyo under the supervision of Prof. Eiichi Nakamura. After working as a postdoctoral researcher in Prof. Rustem F. Ismagilov's group at Chicago University, he joined the group of Prof. Masaharu Nakamura at Kyoto University as an assistant professor in 2006. In 2013, he initiated his independent research career as an associate professor at

Takuji Hatakeyama

Kwansei Gakuin University, and was promoted to a full professor in 2018. Since 2022, he has been a full professor in the Department of Chemistry, Graduate School of Science at Kyoto University. His research interests include the development of carbon–heteroatom bond formation reactions and synthesis of novel boron-based materials for optoelectronic applications.
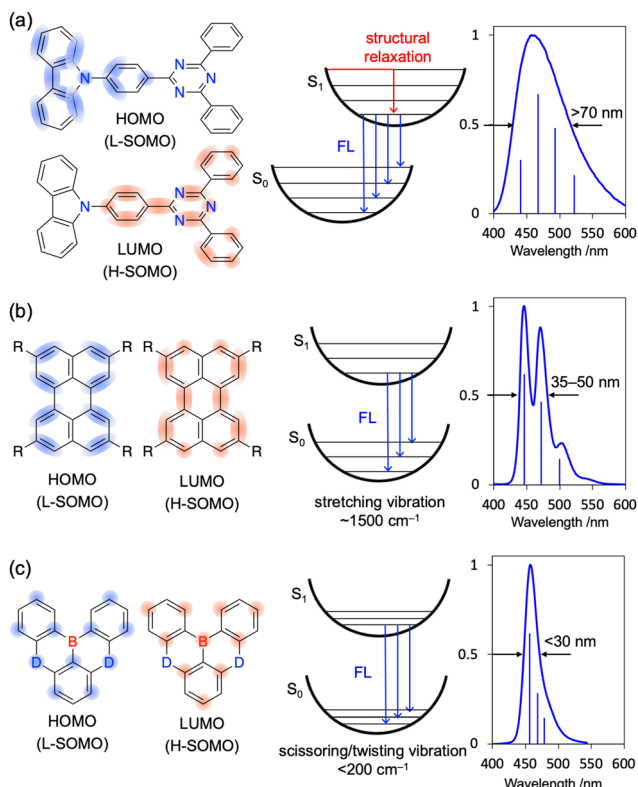
This journal is © The Royal Society of Chemistry 2024

Chem. Soc. Rev., 2024, **53**, 1624–1692 | **1625**

Fig. 3 Typical vibronic spectra of (a) D–A-type, (b) LE, and (c) MR emitters.

The number of vibrational modes (stretching, bending, scissoring, rocking, wagging, twisting, *etc.*) and vibronic transitions (0–1, 0–2, 0–3, *etc.*) in each mode that can couple with electronic excitation and, hence, the extent of emission peak broadening, are positively correlated with the extent of structural differences between the ground (S_0) and S_1 states (Fig. 3a). This correlation is the underlying reason for the broad emission (FWHM > 70 nm) of donor–acceptor (D–A)-type emitters featuring intramolecular charge-transfer (ICT) excited states. For π-conjugated compounds with a rigid framework and no strong donor or acceptor groups (*e.g.*, pyrene and perylene), locally excited (LE) character becomes dominant to result in narrower emission (FWHM < 50 nm). Moreover, LE emitters show small Stokes shifts (10–20 nm) because of their minimal structural relaxation in the S_1 state. However, in terms of colour purity, even LE emitters cannot compete with inorganic ones (*e.g.*, GaN-based light-emitting diodes (LEDs)[56] and CdS/ZnS quantum dots[57,58]) because of the unfavourable vibronic peaks with energy intervals of ∼1500 cm^{-1} observed in the former case (Fig. 3b).[42,57,58] This behaviour indicates strong vibronic coupling between the S_1–S_0 electronic transition and stretching vibrations originating from the bonding/anti-bonding character of FMOs.[54,59] In contrast, MR emitters do not show obvious vibronic peaks because of the non-bonding character of their FMOs and feature S_1–S_0 electronic transition coupling with the scissoring/twisting vibrations at <200 cm^{-1} and not with the stretching vibrations at ∼1500 cm^{-1}.[60] As a result, all vibronic transitions with energy

intervals of <200 cm^{-1} are included in one emission peak with a FWHM of <30 nm (Fig. 3c). Given the minimal vibronic coupling between the electronic transition and stretching vibrations, the non-radiative transition from S_1 to S_0 is efficiently suppressed, and most MR emitters therefore exhibit high Φ_{PL} (>90%).[61–63]

The pioneering work of Adachi *et al.* (2012)[41,64,65] inspired numerous studies on organic TADF emitters for optoelectronic devices. Unlike conventional fluorescent emitters, which can harvest only singlet excitons, TADF emitters can harvest both singlet and triplet excitons *via* efficient reverse intersystem crossing (RISC) from the triplet excited (T_1) state to the S_1 state, which enables the realisation of OLEDs with internal quantum efficiencies (IQEs) of up to 100% (Fig. 4).[41] According to first-order perturbation theory, namely Fermi's golden rule, the rate constant for the RISC between two states (k_{RISC}) is proportional to the spin–orbit coupling (SOC) matrix element ($\langle S_n|\hat{H}_{SOC}|T_n\rangle$) and inversely proportional to the exciton singlet–triplet energy gap (ΔE_{ST}), *i.e.*, $k_{RISC} \propto \langle S_n|\hat{H}_{SOC}|T_n\rangle \exp(-\Delta E_{ST}/k_B T)$, where k_B is the Boltzmann constant and T is the absolute temperature.[66–69] To simultaneously realise a small ΔE_{ST} and sufficient transition oscillator strength (f) of conventional TADF emitters, twisted D–A structures with D and A units of variable electron-donating and -accepting abilities can be used to achieve an appropriate overlap of FMO wavefunctions.[70–73] The balance between ΔE_{ST} and f can be also optimised by introducing π-spacer introduction. However, as mentioned above, D–A-type TADF emitters exhibit broad emission peaks because of their substantial structural relaxation in the S_1 state. In contrast, MR emitters feature both TADF properties and narrowband emission because their alternating HOMO–LUMO separation efficiently suppresses the exchange interaction between FMOs and vibronic coupling with stretching vibrations in excited states. Therefore, MR emitters are usually denoted as MR-TADF emitters to clearly distinguish them from D–A-type TADF emitters. From a theoretical viewpoint, MR-TADF emitters are characterised by short-range charge-transfer (CT) character and long-range electronic delocalisation in the excited state, which collectively result in a small ΔE_{ST} + large f, which is ideal for TADF emitters.[74] These distinctive features enable light
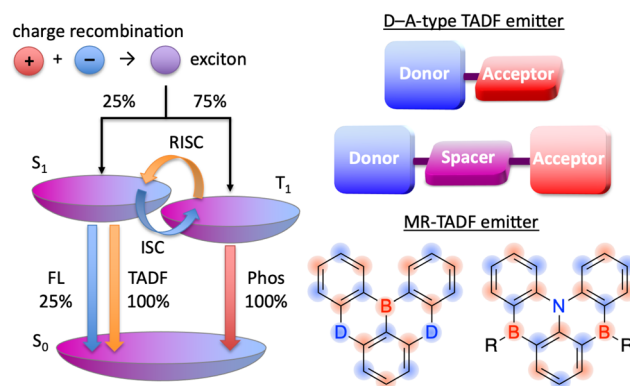

Fig. 4 HOMO–LUMO separation in D–A-type TADF and MR-TADF emitters (D = O, NR, S, Se, *etc.*; A = BR, CO, *etc.*).

amplification for solid-state laser applications despite the difficulty of lasing with most TADF materials.[75–77] Moreover, because of their planar structures, MR-TADF emitters prefer a horizontal orientation in vacuum-deposited OLEDs, which results in high outcoupling efficiency and external quantum efficiency (EQE).[78–81] One drawback of MR-TADF emitters is their insufficiently fast RISC ($k_{RISC} = 10^4$–10^5 s^{-1}) due to the weak SOC between their S_1 and T_n states. Although state-of-the-art D–A-type TADF emitters exhibit strong SOC between their ^{3}LE (T_n) and ^{1}CT (S_1) states because of the twisted D–A structures,[67–74] the generation of sufficient SOC in the planar and rigid π-conjugated frameworks of MR emitters is challenging.[82–85]

Over the last three decades, much effort has been dedicated to developing emitters based on B_{sp^2},[1–21] although their industrial applicability is questionable because of their rapid degradation via the cleavage of B_{sp^2}–C bonds during device operation (Fig. 5). This behaviour is due to the critically small bond dissociation energy (BDE)[86] of the radical-cation species that decomposes to produce a borinium ion and C_{sp^2}-centred radical species; the BDE ($\Delta H^{\ddagger}$) of triphenylborane (Ph$_3$B) in radical-cation and neutral states is 51.1 and 116.9 kcal mol^{-1}, respectively. Although the incorporation of electron-donating atoms in phenoxaborin and phenazaborin increases the BDE ($\Delta H^{\ddagger}$) of the radical-cation state by 35.7 and 39.0 kcal mol^{-1}, respectively, through the stabilisation of this state and destabilisation of borinium ions, the $\Delta G^{\ddagger}$ of bond dissociation is much smaller

than the $\Delta H^{\ddagger}$ because of the entropy gain due to the generation of two species from one. For MR emitters, the BDE ($\Delta H^{\ddagger}$) of the radical-cation state is even higher, equalling 105.5 kcal mol^{-1} for **DOBNA** and 116.6 kcal mol^{-1} for **DABNA**. Notably, the differences between the $\Delta H^{\ddagger}$ and $\Delta G^{\ddagger}$ BDE values of these MR emitters are negligibly small, suggesting a substantial contribution of the intramolecular (ring-fusion) effect to the suppression of bond dissociation. However, this effect alone is insufficient, as exemplified by the much smaller BDE ($\Delta G^{\ddagger}$) of 72.5 kcal mol^{-1} observed for 5,9-dihydro-13b-boranaphtho[3,2,1-*de*]anthracene (**BNA**).

These intrinsic features of MR emitters make them ideal for practical applications, as evidenced by the fact that patents have been filed for more than 3000 related molecules in the last few years. As a result, **DABNA** derivatives are now widely commercialised as blue emitters in triplet–triplet annihilation (TTA)-driven fluorescent devices for smartphones and televisions.[87–91] However, MR emitters have not been implemented as TADF emitters because of their rapid degradation through the long-lived T_1 state in TADF-OLEDs.[87] One of the most effective ways of realising reliable TADF devices is boosting the RISC of MR emitters. However, promising approaches such as the introduction of heavy atoms[92–95] lead to structural weakness (e.g., small BDE of heavy atoms and strain energy), which adversely affects the device lifetime despite the increased k_{RISC}. Another promising approach is the extension of the MR skeleton to enhance charge delocalisation and decrease ΔE_{ST}.[60,74] However, most large molecules suffer from poor synthetic efficiency or require solution-phase processing and are therefore difficult to commercialise. The use of MR emitters as terminal emitters (TEs) in TADF-assisted fluorescence (TAF, i.e., hyperfluorescence)[96–100] or phosphor-sensitised fluorescence (PSF) OLEDs[101,102] is a more promising approach, as in this case, all the intrinsic features of MR emitters (e.g., narrowband emission, high Φ_{PL}, small Stokes shift, high molar extinction coefficient, and horizontal dipole orientation) positively affect device properties. The precise adjustment of TE's ionisation potential and electron affinity of a TE is necessary to prevent carrier trapping in the emissive layer (comprising a sensitiser and host material), and thus maximise the characteristics of TAF- and PSF-based OLEDs, especially the device lifetime. However, adjustment based on the introduction of donor or acceptor groups leads to structural weakness. Establishing a molecular design that fulfils all of the requirements for practical applications requires an understanding of the available chemical space of MR emitters. Therefore, we herein comprehensively review organoboron-based MR emitters, highlight their synthetic strategies classified as one-pot borylation, one-shot borylation, and late-stage functionalisation, and establish material structure–photophysical property correlations to accelerate the practical application of these compounds in OLED displays and open up new applications that remain largely unexplored.[103,104]

Given that some MR emitters have been named differently in different papers, we list all compound names in chronological order in the tables and schemes, and the earliest reported compound name is adopted as a representative one afterwards.

	Ph$_3$B	phenoxaborin	phenazaborin
$\Delta H^{\ddagger}$ (kcal mol^{-1})	51.1	86.8	90.1
$\Delta G^{\ddagger}$ (kcal mol^{-1})	37.8	73.0	76.3

	DOBNA	DABNA	BNA
$\Delta H^{\ddagger}$ (kcal mol^{-1})	105.5	116.6	74.3
$\Delta G^{\ddagger}$ (kcal mol^{-1})	104.5	115.2	72.5

	Ph$_3$B	phenoxaborin	phenazaborin
$\Delta H^{\ddagger}$ (kcal mol^{-1})	116.9	119.3	118.4
$\Delta G^{\ddagger}$ (kcal mol^{-1})	99.5	104.6	103.6

	DOBNA	DABNA	BNA
$\Delta H^{\ddagger}$ (kcal mol^{-1})	133.0	132.0	122.2
$\Delta G^{\ddagger}$ (kcal mol^{-1})	131.3	127.9	117.2

Fig. 5 Bond dissociation energies of B_{sp^2}–C bonds (highlighted in blue) in representative compounds calculated at the B3LYP/6-31G(d) level of theory.

This journal is © The Royal Society of Chemistry 2024

Chem. Soc. Rev., 2024, 53, 1624–1692 | 1627

Table 1 List of abbreviations (general terms) used in the text

Abbreviations	Full meaning	Abbreviations	Full meaning
acac	Acetylacetonate	LE	Locally excited
ACQ	Aggregation caused quenching	^{3}LLCT	Ligand-to-ligand CT
AIE	Aggregation-induced emission	LUMO	Lowest unoccupied molecular orbital
ArLi	Aryl lithium species	MR	Multiple resonance
BDE	Bond dissociation energy	^{3}MLCT	Metal-to-ligand CT
Bpin	Boronic acid pinacol ester	NMR	Nuclear magnetic resonance
CT	Charge transfer	OLED	Organic light-emitting diode
CIE	Commission internationale de l'éclairage	PAH	Polycyclic aromatic hydrocarbons
CPL	Circularly polarised luminescence	Φ_{PL}	Photoluminescence quantum yield, PLQY
D–A	Donor–acceptor	PL	Photoluminescence
ΔE_{ST}	S_1–T_1 energy gap	PSF	Phosphor-sensitised fluorescence
DFT	Density functional theory	RISC	Reverse intersystem crossing
EPR	Electron paramagnetic resonance	rt	Room temperature
EQE	External quantum efficiency	S_NAr	Nucleophilic aromatic substitution reaction
equiv	Equivalent	SMe	Methylthio (group)
f	Oscillator strength	SOC	Spin–orbit coupling
FMOs	Frontier molecular orbitals	S_0	Singlet ground (state)
FWHM	Full width at half maximum	S_1	The first singlet excited (state)
$\lvert g_{PL} \rvert$	Dissymmetry values	TADF	Thermally activated delayed fluorescence
HOMO	Highest occupied molecular orbital	τ_d	Delayed fluorescence lifetime
Hyperfluorescence	TADF-assisted fluorescence (TAF)	TE	Terminal emitter
ICT	Intramolecular charge-transfer	TTA	Triplet–triplet annihilation
^{3}ILCT	Intraligand CT	T_1	The first triplet excited (state)
IQE	Internal quantum efficiency	UV-Vis	Ultraviolet-visible
k_{RISC}	RISC rate constant		

If the earliest paper uses compound numbers and does not provide specific compound names, we use the earliest reported compound name instead of the number. MR emitters with no names established to date are newly named, and the name is enclosed in parentheses. In addition, we list the abbreviations for general terms (Table 1) and reagents and OLED materials (Table 2).

2. One-pot borylation

As the versatile methodology for the construction of cyclic π-conjugated compounds with B_{sp^2} atoms connected to aromatic residues, a "one-pot borylation"[105] protocol has been developed in the past decade. This protocol consists of three tandem steps, namely the lithiation of carbon–hydrogen or carbon–halogen bonds by an alkyllithium reagent, transmetalation by boron tribromide (BBr_3), and tandem intramolecular bora-Friedel–Crafts reaction[106] (i.e., electrophilic C–H borylation) (Scheme 1). The final cyclisation step generally proceeds in the absence of Lewis acid additives, which are generally used as efficient promoters of electrophilic C–H borylation,[25,107–110] as the nucleophilicity of arene rings is increased by two electron-rich atoms (X_1 and X_2 in Scheme 1). Moreover, these electron-donating atoms induce the MR effect and impart photophysical properties desirable for OLED fabrication, such as narrowband emission, high Φ_{PL}, TADF, and sufficient stability in the device. Given that the above development has inspired the design and synthesis of numerous MR-TADF optoelectronic materials, the present section overviews those prepared by one-pot borylation and classifies them according to their synthesis method. In particular, the synthesis route of one-pot borylation precursors

has to be thoughtfully designed because an appropriate directing group for lithiation should be included.

2.1 DOBNA and its derivatives

2.1.1 Directed ortho-lithiation. The one-pot borylation method was first proposed by Hatakeyama et al. (2015) and relied on directed ortho-lithiation, i.e., the ability of aromatic C–H bonds adjacent to coordinative functional groups to be lithiated in a regioselective manner.[37] Table 3 lists the conditions used to synthesise O,B,O-embedded **DOBNA** based on the selective lithiation of 1,3-diphenoxybenzene at the position between the two directing aryloxy groups. After the successive addition of n-butyllithium (^{n}BuLi) and BBr_3, the reaction mixture was supplemented with an amine and heated at 120 °C for 5 h. Screening of the reaction conditions identified the optimal amine loading as 2.0 equivalent (equiv.) (entries 1–4) and the optimal amines as N,N-diisopropylethylamine (NEt^{i}Pr$_2$), 1,2,2,6,6-pentamethylpiperidine (PMP), and N,N-dimethyl-p-toluidine (entries 5–9). Under optimal conditions (entry 3), which are still regarded as the standard for one-pot borylation, **DOBNA** was obtained in an isolated yield of 62%.

A similar procedure was used to prepare DOBNA derivatives via directed ortho-lithiation (Fig. 6 and Table 4).[37,111–113] In the first step, lithiation by alkyllithiums (^{n}BuLi, sec-butyllithium (^{s}BuLi), and tert-butyllithium (^{t}BuLi)) proceeded at a relatively high temperature (room temperature (rt) – 90 °C) for several hours. Subsequent borylation with BBr_3 (1.2–2.0 equiv.) proceeded at rt – 50 °C, and the final intramolecular cyclisation was conducted in the presence of NEt^{i}Pr$_2$ upon heating at 100–120 °C to afford DOBNA derivatives, including those with phenoxazine (**DOBNA-Phenox**) and carbazole (**TMCz-BO**, **TMCz-3P**, and **TDBA-Cz**) functional groups, in moderate yields.

1628 | Chem. Soc. Rev., 2024, **53**, 1624–1692

This journal is © The Royal Society of Chemistry 2024

Table 2 List of abbreviations (reagents and OLED materials) used in the text

Abbreviations	Full meaning	Abbreviations	Full meaning
AIBN	2-Azoisobutyronitrile	MeI	Iodomethane
$AlCl_3$	Aluminium chloride	MeOH	Methyl alcohol
BBr_3	Boron tribromide	2-MeTHF	2-Methyltetrahydrofuran
BCl_3	Boron trichloride	$MesB(OMe)_2$	Dimethyl mesitylboronate
BI_3	Boron triiodide	MesMgBr	Mesityl magnesium bromide
BCPO	Bis-4(N-carbazolyl)phenylphosphine oxide	mCPBA	3-Chloroperbenzoic acid
Bepp2	Bis[2-(2-hydroxyphenyl)-pyridine] beryllium	mCPBC	9-(3-(9H-Carbazol-9-yl)phenyl)-9H-3,9′-bicarbazole
$BF_3 \cdot Et_2O$	Boron trifluoride diethyl ether complex	mCPCN	9-(3-(9H-Carbazol-9-yl)phenyl)-9H-carbazole-3-carbonitrile
$(Bpin)_2$	Bis(pinacolato)diboron	mMTDATA	4,4′,4″-Tris(N-3-methylphenyl-N-phenylamino)triphenylamine
Bu_2O	Dibutyl ether	NaH	Sodium hydride
CBP	4,4′-Di(9H-carbazol-9-yl)-1,1′-biphenyl	$NaHCO_3$	Sodium hydrogencarbonate
$Co_2(CO)_8$	Octacarbonyldicobalt	NaOH	Sodium hydroxide
Cs_2CO_3	Cesium carbonate	NaOAc	Sodium acetate
$[Cu(CH_3CN)_4]PF_6$	Tetrakis(acetonitrile)copper(I) hexafluorophosphate	NaO^tBu	Sodium tert-butoxide
CuCl	Copper(I) chloride	Na_2CO_3	Sodium carbonate
$Cu(ClO_4)_2 \cdot 6H_2O$	Copper(II) perchlorate hexahydrate	NECO-296	Bis(di-tert-butyl(3-methyl-2-butenyl)phosphine)dichloro palladium
CuCN	Copper(I) cyanide	NEt^iPr_2	N,N-Diisopropylethylamine
CuI	Copper(I) iodide	^nBuLi	n-Butyllithium
3CTF	2,4,6-Tris(2-(3,6-di-tert-butyl-9H-carbazol-9-yl)-5-(trifluoromethyl)phenyl)-1,3,5-triazine	NBS	N-Bromosuccinimide
DBFDPO	4,6-Bis(diphenylphosphoryl)dibenzofuran	NMP	N-Methyl-2-pyrrolidone
DBFPO (PPF)	Dibenzo[b,d]furan-2,8-diylbis(diphenylphosphine oxide)	NPB	$N^4,N^{4'}$-Di(naphthalen-1-yl)-$N^4,N^{4'}$-diphenyl-[1,1′-biphenyl]-4,4′-diamine
DBU	1,8-Diazabicyclo[5.4.0]undec-7-ene	$PdCl_2(amphos)_2$	Bis[di-tert-butyl(4-dimethylaminophenyl)phosphine]dichloropalladium(II)
26DCzPPy	2,6-Bis(3-(9H-carbazol-9-yl)phenyl)pyridine	$PdCl_2(dppf)$	[1,1′-Bis(diphenylphosphino)ferrocene]palladium(II) dichloride
DDQ	2,3-Dichloro-5,6-dicyano-1,4-benzoquinone	$PdCl_2(PPh_3)_2$	Bis(triphenylphosphine)palladium(II) dichloride
DIC-TRz	11-(4,6-diphenyl-1,3,5-triazin-2-yl)-12-phenyl-11,12-dihydroindolo[2,3-a]carbazole	$Pd(OAc)_2$	palladium(II) acetate
DMAc	N,N-Dimethylacetamide	$Pd[P(o\text{-tol})_3]_2Cl_2$	Bis(tri-o-tolylphosphine)palladium(II) dichloride
DMAP	4-Dimethylaminopyridine	$Pd(PPh_3)_4$	Tetrakis(triphenylphosphine)palladium(0)
DMF	N,N-Dimethylformamide	$Pd_2(dba)_3$	Tris(dibenzylideneacetone)dipalladium(0)
DMFBD-TRZ	2-(3′-(9,9-Dimethyl-9H-fluoren-2-yl)-[1,1′-biphenyl]-3-yl)-4,6-diphenyl-1,3,5-triazine	$PhBCl_2$	Dichlorophenylborane
DMMN	Dimethylmalononitrile	$PhB(OH)_2$	Phenylboronic acid
DMIC-TRZ	1,3-Dihydro-1,1-dimethyl-3-(3-(4,6-diphenyl-1,3,5-triazin-2-yl)phenyl)indeno-[2,1-b]carbazole	PhCzBCz	9-(2-(9-Phenyl-9H-carbazol-3-yl)phenyl)-9H-3,9′-bicarbazole
DPEPO	Bis[2-(diphenylphosphino)phenyl]ether oxide	Ph_2PH	Diphenylphosphane
dtbpy	4,4′-Di-tert-butyl-2,2′-bipyridyl	Ph_3B	Triphenylborane
DTBPY	2,6-Di-tert-butylpyridine	PMMA	Polymethylmethacrylate
EtOH	Ethyl alcohol	PMP	1,2,2,6,6-Pentamethylpiperidine
NEt_3	Triethylamine	$P(OEt)_3$	Triethyl phosphite
$FeCl_3$	Iron(III) chloride	PO-T2T	2,4,6-Tris[3-(diphenylphosphinyl)phenyl]-1,3,5-triazine
FF	Fluorenofluorene	PPF (DBFPO)	Dibenzo[b,d]furan-2,8-diylbis(diphenylphosphine oxide)
HBC	Hexabenzocoronene	PPh_3	Triphenylphosphine
HBr	Hydrogen bromide/hydrobromic acid	PS	Polystyrene
HCl	Hydrogen chloride/hydrochloric acid	^sBuLi	sec-Butyllithium
HI	Hydrogen iodide/hydriodic acid	SF3TRZ	2-(9,9′-Spirobi[fluoren]-3-yl)-4,6-diphenyl-1,3,5-triazine
HOAc	Acetic acid	SiCzCz	9-(3-(Triphenylsilyl)phenyl)-9H-3,9′-bicarbazole
IF	Indenofluorene	$SiTrzCz_2$	9,9′-(6-(3-(Triphenylsilyl)phenyl)-1,3,5-triazine-2,4-diyl)bis(9H-carbazole)
$^iPrOBpin$	2-Isopropoxy-4,4,5,5-tetramethyl-1,3,2-dioxaborolane	$SnCl_2$	Tin(II) chloride
$IrCl_3$	Iridium trichloride	$SOCl_2$	Thionyl chloride
$[Ir(cod)(OCH_3)]_2$	(1,5-Cyclooctadiene)(methoxy)iridium(I) dimer	SPhos	2-Dicyclohexylphosphino-2′,6′-dimethoxybiphenyl
KOAc	Potassium acetate	TBAF	Tetrabutylammonium fluoride
KO^tBu	Potassium tert-butoxide	^{t}Bu-Benzene	tert-Butylbenzene
KPF_6	Potassium hyxafluorophosphate	^tBuLi	tert-Butyllithium
K_2CO_3	Potassium carbonate	$[^tBu_3PH]BF_4$	Tri-tert-butylphosphonium tetrafluoroborate
K_2PtCl_4	Potassium tetrachloroplatinate(II)	TBTA	Tris[(1-benzyl-1H-1,2,3-triazol-4-yl)methyl]amine
K_3PO_4	Tripotassium phosphate	TCTA	Tris(4-(9H-carbazol-9-yl)phenyl)amine
$K_4[Fe(CN)_6]$	Potassium ferrocyanide	TfOH	Trifluoromethanesulfonic acid
MADN	2-Methyl-9,10-bis(naphthalen-2-yl)anthracene	THF	Tetrahydrofuran
mCBP	3,3′-Di(9H-carbazol-9-yl)-1,1′-biphenyl	TMS	Trimethylsilyl
mCBP-CN	3′,5-Di(9H-carbazol-9-yl)-[1,1′-biphenyl]-3-carbonitrile	TPSS	2,2′,7,7′-Tetraphenyl-9,9′-spirobi[thioxanthene]
mCP	1,3-Di(9H-carbazol-9-yl)benzene	XPhos	2-Dicyclohexylphosphino-2′,4′,6′-triisopropylbiphenyl
MeCN	Acetonitrile		

This journal is © The Royal Society of Chemistry 2024

Chem. Soc. Rev., 2024, 53, 1624–1692 | 1629
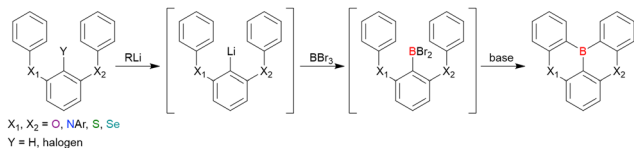
Scheme 1 General synthesis procedure of one-pot borylation.

Table 3 Synthesis of **DOBNA** via directed ortho-lithiation in ref. 37

Entry[a]	Amine	X	Yield[b] [%]
1	None	0	16
2	NEt^{i}Pr$_2$	1.0	62
3	NEt^{i}Pr$_2$	2.0	71^c
4	NEt^{i}Pr$_2$	3.0	44
5	NEt$_3$	2.0	13
6	2,2,6,6-Tetramethylpiperidine	2.0	2
7	PMP	2.0	68
8	2,6-Lutidine	2.0	41
9	N,N-Dimethyl-p-toluidine	2.0	71^c

^{a} Reactions were carried out on a 1.0 mmol scale. ^{b} Yield determined by ^{1}H nuclear magnetic resonance (NMR) measurements using dibromomethane as an internal standard. ^{c} Average of two experiments.

DOBNA, DOBNA-Ph-2, DOBNA-Ph-3, and **DOBNA-Phenox** were later named in ref. 105.

In the case of **DOBNA-Helix** (Scheme 2, denoted as **4** in the original paper), which was the major product (33%) despite its sterically hindered [6]helicene substructure, borylation–cyclisation proceeded in a regioselective manner, with the less distorted isomer ("byproduct" in Scheme 2) formed in only 2%

yield. This result suggests that electronic effects (i.e. HOMO distribution) are more important than steric ones under the optimised conditions of one-pot borylation.

2.1.2 Lithium–halogen exchange. Although directed ortho-lithiation provides access to MR-TADF frameworks, its low reactivity and regioselectivity sometimes prevent effective borylation–cyclisation. Therefore, the development of an alternative methodology was required and borylation via lithium–halogen exchange is now widely adopted as a more practical route. This route requires the regioselective modification of 1,2,3-trisubstituted benzenes to maintain a halogen atom between the two aryloxy groups. To achieve this selectivity, nucleophilic aromatic substitution (S$_N$Ar), which proceeds preferentially on the fluorine substituent, plays an important role.

Commercially available 2-bromo-1,3-difluorobenzene is one of the most promising starting materials for one-pot borylation via lithium–halogen exchange. The first example of such synthesis was reported at the same time as the first directed ortho-lithiation method (Scheme 3).[37] The double S$_N$Ar reaction of 2-bromo-1,3-difluorobenzene with [1,1-biphenyl]-3-ol furnished the bromine-containing precursor in 87% yield, with subsequent one-pot borylation under standard conditions affording **2c** (later named **DOBNA-Ph-1**,[105] or simply **DOBNA-Ph**[114]) in 74% yield.

Fig. 7 and Table 5 summarise DOBNA derivatives synthesised using lithium–halogen exchange.[115–121] **DOBNA-Ph, B1, B2-OH, BOS, BSS,** and **tBuAcBO** were synthesised from 1-bromo-2,6-difluorobenzene, while the other compounds in Fig. 7 were derived from 1,3-difluoro-2-iodobenzene.

Unlike directed ortho-lithiation, lithium–halogen exchange proceeded under mild conditions (-78 °C to rt). In addition to the oxygen-bridged precursor characteristic of DOBNA derivatives, sulphur-bridged ones could also be used (**BOS** and **BSS**). Although triazole functional groups were tolerated under
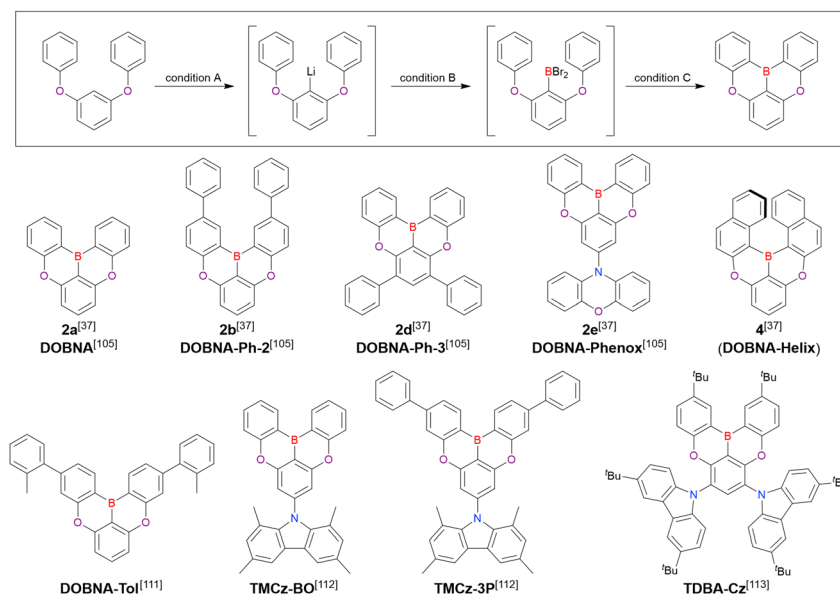

**Fig. 6** DOBNA derivatives synthesised by directed ortho-lithiation.

1630 | Chem. Soc. Rev., 2024, **53**, 1624–1692

This journal is © The Royal Society of Chemistry 2024

Table 4 Conditions used to synthesise the compounds shown in Fig. 6

Compound	Condition A[a]	Condition B[a]	Condition C[a]	Solvent	Yield [%]	Ref.
DOBNA	[n]BuLi (1.1)/70 °C, 4 h	BBr$_3$ (1.2)/40 °C, 1 h	NEt^{i}Pr$_2$ (2.0)/120 °C, 5 h	[t]Bu-Benzene	62	37 and 105
DOBNA-Ph-2	[n]BuLi (1.1)/70 °C, 1 h	BBr$_3$ (1.2)/rt, 1 h	NEt^{i}Pr$_2$ (2.0)/120 °C, 4 h	o-Xylene	54	37 and 105
DOBNA-Ph-3	[t]BuLi (1.2)/rt, 12 h	BBr$_3$ (1.5)/50 °C, 4 h	NEt^{i}Pr$_2$ (2.0)/120 °C, 24 h	[t]Bu-Benzene	42	37 and 105
DOBNA-Phenox	[n]BuLi (1.2)/50 °C, 12 h	BBr$_3$ (1.5)/rt, 12 h	NEt^{i}Pr$_2$ (2.0)/120 °C, 24 h	[t]Bu-Benzene	56	37 and 105
DOBNA-Helix	[n]BuLi (1.5)/90 °C, 4 h	BBr$_3$ (2.0)/rt, 13 h	NEt^{i}Pr$_2$ (2.0)/100 °C, 24 h	[t]Bu-Benzene	33	37
DOBNA-Tol	[s]BuLi (1.2)/70 °C, 3 h	BBr$_3$ (1.2)/rt, 1 h	NEt^{i}Pr$_2$ (2.0)/120 °C, 3 h	Xylene	16	111
TMCz-BO	[n]BuLi (1.2)/50 °C, 4 h	BBr$_3$ (1.5)/40 °C, 1 h	NEt^{i}Pr$_2$ (2.0)/120 °C, 5 h	[t]Bu-Benzene	15	112
TMCz-3P	[n]BuLi (1.2)/50 °C, 4 h	BBr$_3$ (1.5)/40 °C, 1 h	NEt^{i}Pr$_2$ (2.0)/120 °C, 5 h	[t]Bu-Benzene	15	112
TDBA-Cz	[t]BuLi (2.0)/60 °C, 2 h	BBr$_3$ (2.0)/rt, 1 h	NEt^{i}Pr$_2$ (2.0)/140 °C, 20 h	[t]Bu-Benzene	35	113

[a] Numbers in parentheses refer to reagent loadings (equivalents).
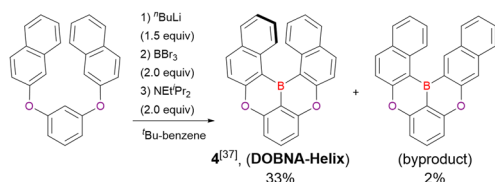
Scheme 2 Regioselectivity of borylation–cyclisation reaction.
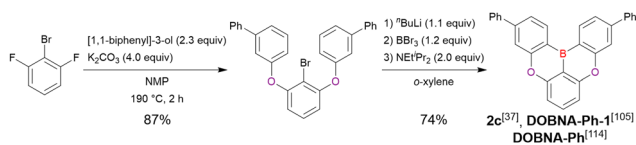
Scheme 3 Synthesis of **DOBNA-Ph** via lithium–halogen exchange.

standard conditions, the related yields were rather low (5% for **B1**, 22% for **B2-OH**, and 6% for **B3**). This result suggests that the coordination of N$_{sp^2}$ to boron atoms can inhibit intramolecular electrophilic C–H borylation. As discussed in the next subsection, bromine-containing products can be synthesised using the same methodology.

One indicative result is the synthesis of **B2-OH** (Scheme 4), in which the introduction of boron was accompanied by the removal of a methoxy group under the action of BBr$_3$, and the resulting phenoxy group was used for subsequent chemical modification (Scheme 55 in Section 4). Given that the reagents used in one-pot borylation (aryllithium species (ArLi) and BBr$_3$) are highly reactive, one should consider functional group tolerance when designing the synthesis route.

2.1.3 Borylation of tetrasubstituted precursors. As shown in the previous subsection, trisubstituted benzenes are the key starting materials for constructing DOBNA-based scaffolds.
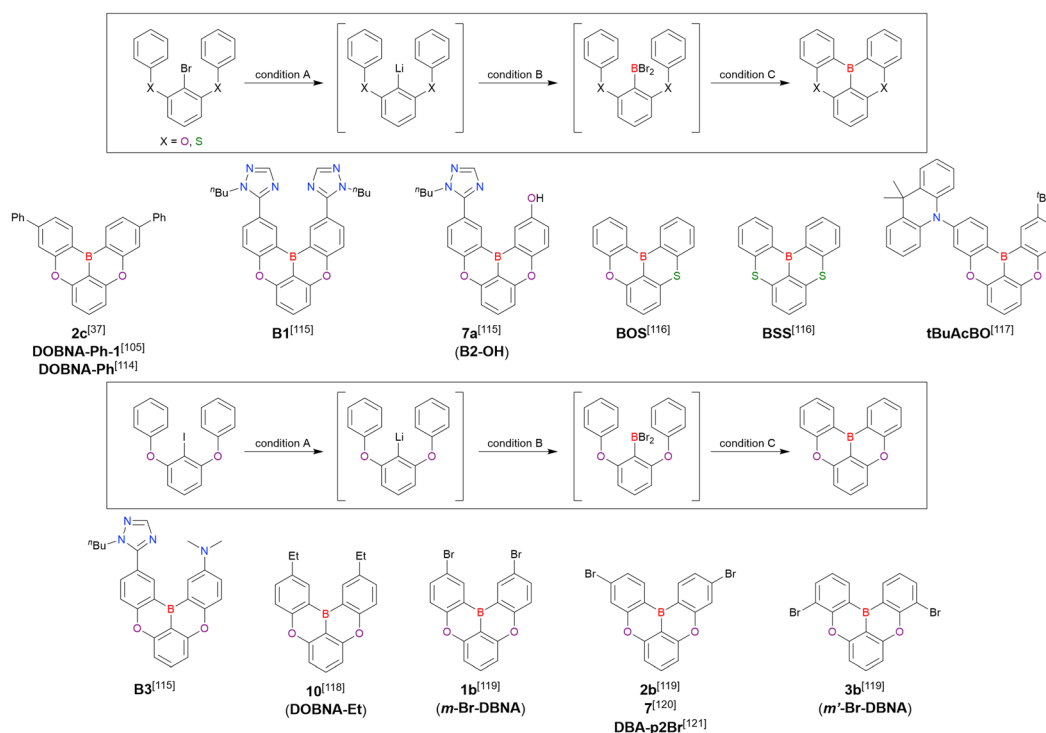

Fig. 7 DOBNA derivatives synthesised via lithium–halogen exchange.

This journal is © The Royal Society of Chemistry 2024

Chem. Soc. Rev., 2024, **53**, 1624–1692 | **1631**

Table 5 Conditions used to synthesise the compounds shown in Fig. 7

| Compound	Condition A[a]	Condition B[a]	Condition C[a]	Solvent	Yield [%]	Ref.
DOBNA-Ph	^{n}BuLi (1.1)/-40 °C to rt	BBr$_3$ (1.2)/rt, 1 h	NEt^{i}Pr$_2$ (2.0)/130 °C, 3 h	o-Xylene	74	37 and 105
B1	^{t}BuLi (2.0)/-30 °C, 2 h	BBr$_3$ (1.2)/rt, 1 h	NEt^{i}Pr$_2$ (2.0)/150 °C, 24 h	^{t}Bu-Benzene	5	115
B2-OH	^{n}BuLi (1.2)/-30 °C, 2 h	BBr$_3$ (2.0)/rt, 1 h	NEt^{i}Pr$_2$ (2.0)/140 °C, 24 h	^{t}Bu-Benzene	22	115
BOS	^{n}BuLi (1.1)/50 °C, 1 h	BBr$_3$ (1.2)/rt, 1 h	NEt^{i}Pr$_2$ (2.0)/125 °C, 12 h	m-Xylene	25	116
BSS	^{n}BuLi (1.1)/50 °C, 1 h	BBr$_3$ (1.2)/rt, 1 h	NEt^{i}Pr$_2$ (2.0)/125 °C, 12 h	m-Xylene	40	116
tBuAcBO	^{n}BuLi (2.0)/rt, 2 h	BBr$_3$ (—)/rt, 2 h	NEt^{i}Pr$_2$ (—)/180 °C, 24 h	^{t}Bu-Benzene	16	117
B3	^{t}BuLi (2.0)/-30 °C, 2 h	BBr$_3$ (1.2)/rt, 1 h	NEt^{i}Pr$_2$ (2.0)/150 °C, 24 h	^{t}Bu-Benzene	6	115
DOBNA-Et	^{n}BuLi (1.1)/-78 °C, 10 min	BBr$_3$ (1.2)/0 °C, 1 h	NEt^{i}Pr$_2$ (2.0)/120 °C, 21 h	Toluene	30	118
m-Br-DBNA	^{n}BuLi (1.0)/-30 °C, 2 h	BBr$_3$ (1.2)/rt, 1 h	NEt^{i}Pr$_2$ (2.0)/140 °C, 24 h	m-Xylene	52	119
DBA-p2Br	^{n}BuLi (1.0)/-30 °C, 2 h	BBr$_3$ (1.2)/rt, 1 h	NEt^{i}Pr$_2$ (2.0)/140 °C, 24 h	m-Xylene	25	119
	^{n}BuLi (1.1)/-30 °C, 1 h	BBr$_3$ (1.2)/rt, 1 h	NEt^{i}Pr$_2$ (2.0)/140 °C, 3 h	^{t}Bu-Benzene	37	120
	^{n}BuLi (1.0)/-30 °C, 1 h	BBr$_3$ (1.1)/-30 °C to rt	NEt^{i}Pr$_2$ (5.0)/120 °C, 14 h	^{t}Bu-Benzene	72	121
m'-Br-DBNA	^{n}BuLi (1.0)/-30 °C, 2 h	BBr$_3$ (1.2)/rt, 1 h	NEt^{i}Pr$_2$ (2.0)/140 °C, 24 h	m-Xylene	40	119

[a] Numbers in parentheses refer to reagent loadings (equivalents).
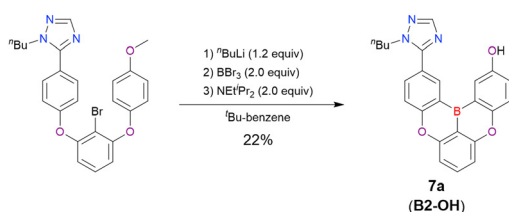
Scheme 4 Accompanying deprotection reaction (methoxy group removal) induced by BBr$_3$.

Hence, tetrasubstituted benzenes were expected to be promising starting materials for accessing more diverse MR-TADF frameworks. In an early example reported by Kwon *et al.* (Scheme 5),[122] **Br-TDBA** was synthesised from 1,4-dibromo-2,6-difluorobenzene in two steps. The first step, a double S$_N$Ar reaction, proceeded in high yield (80%) to afford the borylation precursor, and the second step involved one-pot borylation under standard conditions. Although the precursor contained two bromine atoms capable of reacting with ^{n}BuLi, lithium–bromine exchange mainly proceeded at the *ortho*-position relative to the aryloxy groups because of their directing effect. As a result, **Br-TDBA** was obtained in 15% yield.

From the viewpoint of material chemistry, bromine groups are highly important because they allow for further functionalisation, as exemplified by the tuning of photophysical properties and the addition of various functionalities through the chemical modification of bromine-containing MR-TADF frameworks (see Section 4). Therefore, various bromine-containing DOBNA derivatives have been synthesised using selective lithium–halogen exchange (Fig. 8 and Table 6).[116,120,122–138]
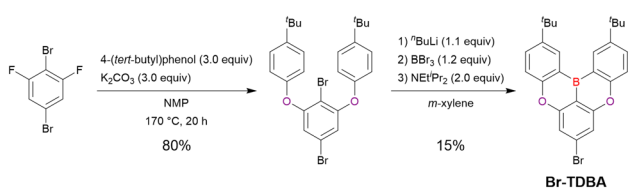
Scheme 5 Synthesis of **Br-TDBA** from a tetrasubstituted benzene.

The reaction temperature of the first lithium–halogen exchange was kept relatively low (-78 °C to rt), probably to suppress the undesired exchange at the remaining bromine atom. Although the yield of **Br-TDBA** was relatively low (15%) in Kwon's work,[122] the same product was synthesised later with up to 49% yield,[129] which suggests that lithium–halogen exchange proceeds with high selectivity. The variations in product yield probably originated from the actual concentration of alkyllithium reagents or the purity of BBr$_3$. The effect of the halogen type (Br *versus* I) on the reaction yield was small, as the yields of **Br-TDBA** prepared from Br (15–49%)[122,123,125–129] and I (41%)[124] derivatives were similar. Interestingly, a pyridine-containing derivative, **DOBNA-Pyr**, could be synthesised in much higher yield (92%), although the detailed purification and characterisation data were not reported.[139]

2.1.4 Photophysical properties. Unlike the MR effect of the recently reported MR-TADF frameworks, the MR effect of DOBNA derivatives has not been a research focus because of the low electron-donating ability of oxygen atoms. However, some reports investigated the photophysical properties of these derivatives in detail. Table 7 summarises λ_{PL}^{max}, FWHM, Φ_{PL}, ΔE_{ST}, and k_{RISC} values as representative photophysical parameters of the MR-TADF emitters presented in Fig. 6–8. Compounds whose photophysical data have not been reported are excluded from Table 7. Given that ΔE_{ST} and k_{RISC} can be estimated in several ways, the values presented herein need to be compared with caution. When grafted with diarylamine and carbazolyl groups, the DOBNA scaffold acts as an electron acceptor and induces long-range D–A-type CT emission (**DOBNA-Phenox**,[37] **TMCz-BO**,[112] **TMCz-3P**,[112] **TDBA-Cz**,[113] **B3**,[115] and **tBuAcBO**[117]). As such emission does not fully reflect the photophysical properties derived from the MR effect, they are not discussed in this section (long-range D–A-type CT emission is reviewed in Section 4). In general, non-D–A-type DOBNA derivatives (**DOBNA**,[37,116] **DOBNA-Ph**,[37] **DOBNA-Ph-2**,[37] **DOBNA-Ph-3**,[37] **B1**,[115] **BOS**,[116] and **BSS**[116]) feature a high transition energy ($\lambda_{PL}^{max} \approx 400$ nm, $T_1 = 2.9$–3.0 eV), moderate Φ_{PL} (0.60–0.80), and moderate k_{RISC} (10^3–10^4 s^{-1}), and are therefore widely used as host materials for the emitting layers of OLEDs, benefiting from the high T_1 energy.

For example, OLEDs containing **DOBNA-Ph** and **DOBNA-Ph-3** as host materials exhibited performances superior to that of
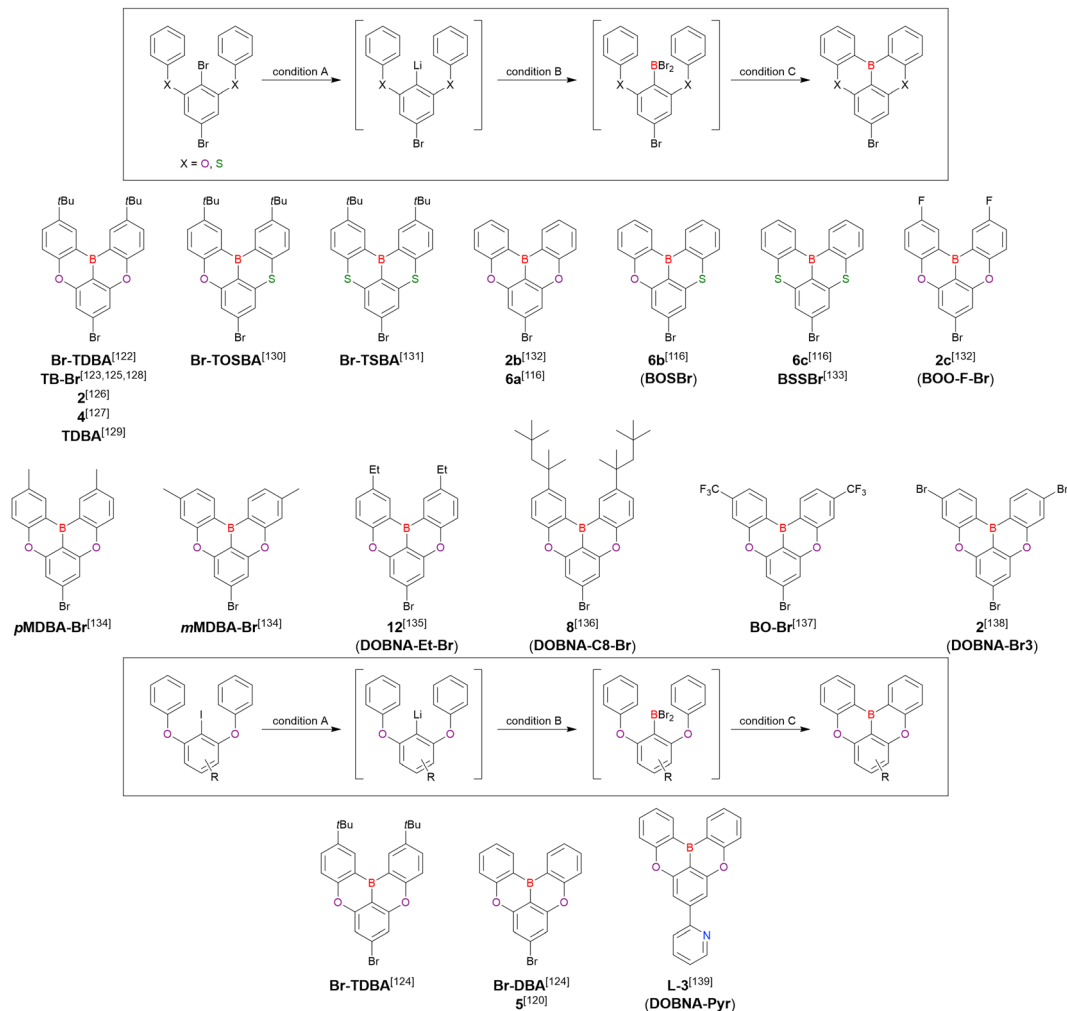
1632 | *Chem. Soc. Rev.*, 2024, **53**, 1624–1692

This journal is © The Royal Society of Chemistry 2024

Fig. 8   DOBNA derivatives synthesised from tetrasubstituted benzenes.

4,4′-di(9H-carbazol-9-yl)-1,1′-biphenyl (CBP) in terms of driving voltage, current efficiency, power efficiency, and external quantum efficiency at 1000 cd m^{-2}.[37] Currently, **DOBNA-Ph** and **DOBNA-Tol** are widely used as host materials for OLEDs. Importantly, the replacement of oxygen by sulphur (**BOS** and **BSS**) causes red-shifted emission (λ_{PL}^{max} = 434 nm for **BOO** and 457 nm for **BOS**) and accelerated RISC (k_{RISC} = 6.1 × 10^4 s^{-1} for **BOO** and 1.18 × 10^5 s^{-1} for **BOS**) because of the heavy-atom effect.[116]

2.2 DABNA and its derivatives

2.2.1 One-pot borylation of triarylamine precursors. The one-pot borylation-based synthesis of **DOBNA** proposed in 2015 highlights the potential of fully cyclised π-conjugated materials containing boron and electron-rich atoms. In addition to O,B,O-embedded DOBNA-type scaffolds, O,B,S- and S,B,S-embedded frameworks can be constructed using similar procedures, as shown above. The powerful route involving an S$_N$Ar reaction is, however, not highly effective for the synthesis of triarylamine-based N,B,N-embedded scaffolds. In 2016, Hatakeyama et al. established an alternative strategy for accessing **DABNA** and its derivatives (Scheme 6).[38]

The corresponding one-pot borylation precursors were synthesised from the commercially available 1-bromo-2,3-dichlorobenzene by Buchwald–Hartwig coupling. The reaction of this starting material with diphenylamine (2.2 equiv.) afforded the key borylation precursor in 66% yield (Scheme 6, left). The chlorine atom for the subsequent lithium–halogen exchange was retained because of its sterically hindered environment. A non-symmetric intermediate could be synthesised by the sequential coupling of N^1,N^1,N^3-triphenylbenzene-1,3-diamine and di([1,1′-biphenyl]-3-yl)amine based on the difference in reactivity between bromine and chlorine atoms (Scheme 6, right). The final one-pot borylation afforded N,B,N-embedded π-conjugated compounds, **DABNA-1** and **DABNA-2**, in yields of 32% and 31%, respectively. In the case of **DABNA-2**, tandem electrophilic C–H borylation occurred at the para-position relative to the diphenylamine group, probably because of its electron-donating nature and bulkiness. These processes were robust and scalable, as confirmed by the synthesis of the target compounds in amounts of 6.0 g.

The chemical structures of derivatives possessing the DABNA skeleton and the related synthesis results are summarised in

Table 6 Conditions used to synthesise the compounds shown in Fig. 8

Compound	Condition A[a]	Condition B[a]	Condition C[a]	Solvent	Yield [%]	Ref.
Br-TDBA	^{n}BuLi (1.1)/rt, 1 h	BBr$_3$ (1.2)/45 °C, 50 min	NEt^{i}Pr$_2$ (2.0)/120 °C, 20 h	m-Xylene	15	122
	^{n}BuLi (1.1)/rt, 1 h	BBr$_3$ (1.2)/50 °C, 1 h	NEt^{i}Pr$_2$ (2.0)/180 °C, 10 h	m-Xylene	41	123
	^{n}BuLi (1.1)/−20 °C, 2 h	BBr$_3$ (1.2)/rt, 1 h	NEt^{i}Pr$_2$ (2.4)/120 °C, 12 h	m-Xylene	41	124
	^{n}BuLi (1.1)/rt, 1 h	BBr$_3$ (1.2)/50 °C, 1 h	NEt^{i}Pr$_2$ (2.0)/180 °C, 10 h	m-Xylene	38	125
	^{n}BuLi (1.1)/0 °C, 2 h	BBr$_3$ (1.2)/rt, 20 min	NEt^{i}Pr$_2$ (0.9)/180 °C, 12 h	o-Dichlorobenzene	27	126
	^{n}BuLi (1.0)/−30 °C, 2 h	BBr$_3$ (1.2)/rt, 1 h	NEt^{i}Pr$_2$ (2.4)/120 °C, 12 h	m-Xylene	43	127
	^{n}BuLi (1.1)/rt, 2 h	BBr$_3$ (1.2)/50 °C, 50 min	NEt^{i}Pr$_2$ (6.0)/120 °C, 20 h	Xylene	19	128
	^{n}BuLi (1.1)/rt, 2 h	BBr$_3$ (1.2)/45 °C, 1 h	NEt^{i}Pr$_2$ (2.0)/135 °C, 20 h	Xylene	49	129
Br-TOSBA	^{n}BuLi (0.7)/rt, 1 h	BBr$_3$ (0.8)/45 °C, 50 min	NEt^{i}Pr$_2$ (1.3)/120 °C, 20 h	m-Xylene	19	130
Br-TSBA	^{n}BuLi (0.7)/rt, 1 h	BBr$_3$ (0.8)/45 °C, 50 min	NEt^{i}Pr$_2$ (1.3)/120 °C, 20 h	m-Xylene	19	131
Br-DBA	^{n}BuLi (1.1)/−30 °C, 2 h	BBr$_3$ (1.2)/rt, 1 h	NEt^{i}Pr$_2$ (3.8)/130 °C, 20 h	m-Xylene	20	132
	^{n}BuLi (1.1)/−30 °C, 2 h	BBr$_3$ (1.2)/rt, 1 h	NEt^{i}Pr$_2$ (3.8)/130 °C, 20 h	m-Xylene	49	116
	^{n}BuLi (1.1)/−20 °C, 2 h	BBr$_3$ (1.2)/rt, 1 h	NEt^{i}Pr$_2$ (2.4)/120 °C, 12 h	^{t}Bu-Benzene	45	124
	^{n}BuLi (1.1)/−30 °C, 1 h	BBr$_3$ (1.2)/rt, 1 h	NEt^{i}Pr$_2$ (2.0)/140 °C, 3 h	m-Xylene	42	120
BOSBr	^{n}BuLi (1.0)/−30 °C, 2 h	BBr$_3$ (1.2)/rt, 1 h	NEt^{i}Pr$_2$ (2.0)/130 °C, 20 h	m-Xylene	44	116
BSSBr	^{n}BuLi (1.0)/−30 °C, 2 h	BBr$_3$ (1.2)/rt, 1 h	NEt^{i}Pr$_2$ (2.0)/125 °C, 20 h	m-Xylene	40	116
	^{n}BuLi (1.0)/−30 °C, 2 h	BBr$_3$ (1.3)/rt, 1 h	NEt^{i}Pr$_2$ (2.0)/125 °C, 20 h	m-Xylene	68	133
BOO-F-Br	^{n}BuLi (1.1)/−30 °C, 2 h	BBr$_3$ (1.2)/rt, 1 h	NEt^{i}Pr$_2$ (2.0)/130 °C, 20 h	m-Xylene	30	132
p**MDBA-Br**	^{n}BuLi (1.1)/rt, 2 h	BBr$_3$ (1.2)/50 °C, 50 min	NEt^{i}Pr$_2$ (2.0)/120 °C, 20 h	m-Xylene	64	134
m**MDBA-Br**	^{n}BuLi (1.1)/rt, 2 h	BBr$_3$ (1.2)/50 °C, 50 min	NEt^{i}Pr$_2$ (2.0)/120 °C, 20 h	m-Xylene	46	134
DOBNA-Et-Br	^{n}BuLi (1.0)/−78 °C, 10 min	BBr$_3$ (1.2)/0 °C, 0.5 h	NEt^{i}Pr$_2$ (2.0)/110 °C, 14 h	Toluene	43	135
DOBNA-C8-Br	^{n}BuLi (1.1)/−78 °C, 10 min	BBr$_3$ (1.2)/0 °C, 10 min	NEt^{i}Pr$_2$ (2.0)/110 °C, 14 h	Toluene	34	136
BO-Br	—[b]	—[b]	—[b]		30	137
DOBNA-Br3	^{n}BuLi (1.1)/25 °C, 1 h	BBr$_3$ (1.2)/0 °C, 1 h	NEt^{i}Pr$_2$ (1.9)/130 °C, 12 h	Xylene	61	138
DOBNA-Pyr	^{n}BuLi (1.3)/rt, 1 h	BBr$_3$ (1.3)/rt, 1 h	NEt^{i}Pr$_2$ (2.1)/120 °C, 12 h	m-Xylene	92	139

[a] Numbers in parentheses refer to reagent loadings (equivalents). [b] Not described.

Table 7 Photophysical properties of the compounds shown in Fig. 6–8

| Compound	Condition	λ_{PL}^{max} [nm]	FWHM [nm]	Φ_{PL} [—]	ΔE_{ST} [eV]	k_{RISC} [s^{-1}]	Ref.
DOBNA	CH$_2$Cl$_2$/1 wt%-PMMA[b]	398/398	—/33	0.72/0.80	0.15/0.18	—/1.7× 10^3	37
	Toluene/1 wt%-PS[b]	396/—	30/—	—/0.70	0.18/—	—/1.1 × 10^4	116
DOBNA-Ph	CH$_2$Cl$_2$	410	—	0.60	0.31	—	37
DOBNA-Ph-2	CH$_2$Cl$_2$	410	—	0.65	0.21	—	37
DOBNA-Ph-3	CH$_2$Cl$_2$	436	—	0.57	0.14	—	37
B1	CH$_2$Cl$_2$/5 wt%-PMMA[b]	409/407	—/—	—/0.75	0.21/—	—/—	115
BOS	Toluene/1 wt%-PS[b]	434/—	29/—	—/0.63	0.17/—	—/6.1 × 10^4	116
BSS	Toluene/1 wt%-PS[b]	457/—	27/—	—/0.58	0.15/—	—/1.18 × 10^5	116
DOBNA-Phenox[a]	1 wt%-PMMA[b]	492	—	0.92	0.06	—	37
TMCz-BO[a]	Toluene/30 wt%-PPF[b]	446/467	—/—	0.81/0.98	—/0.020	—/1.9 × 10^6	112
TMCz-3P[a]	Toluene/30 wt%-PPF[b]	455/477	—/—	0.56/0.76	—/0.134	—/3.3 × 10^4	112
TDBA-Cz[a]	Toluene/10 wt%-DPEPO[b]/neat-film	461/456/462	43/46/41	—/1.00/0.88	0.14/—/—	—/—/1.40 × 10^6	113
B3[a]	CH$_2$Cl$_2$/5 wt%-PMMA[b]	535/497	—/—	—/0.51	0.11/—	—/—	115
tBuAcBO[a]	Toluene/5 wt%-mCP[b]	464/468	—/61	—/0.66	—/0.10	—/1.24 × 10^6	117

[a] Compounds showing long-range D–A-type CT emission. [b] See Table 2 for the full compound name.

Fig. 9 and Table 8.[38,88,102,104,140–149] In addition to 1-bromo-2,3-dichlorobenzene, some studies used 1,3-dibromo-2-chlorobenzene as a starting material. **t-DABNA**, **TBE01**, **TBE02**, and **Tp-DABNA** can be viewed as a straightforward expansion of **DABNA-1** *via* functional group addition. The diarylamine group of the precursor was changed to the 9,10-dihydroacridine group to obtain carbon-bridged MR-TADF frameworks (**BN-DMAC**, **BN-DPAC**, **BN2**). Similarly, structures bridged by oxygen (**2PXZBN**), nitrogen (**TCZ-F-DABNA** and **BNIP-tBuDPAC**), sulphur (**2PTZBN**, **BN4**, **BN5**, and **helicene-BN**), and selenium atoms (**BNSSe** and **BNSeSe**) were obtained. Moreover, a triangulene analogue, **BN3**, was synthesised using the basic one-pot borylation protocol. Tetrasubstituted starting materials (**M-tDABNA**, **TPXZBN**, and

DPXZCZBN) were also used, as shown for DOBNA-type compounds. The first step (lithium–chlorine exchange) proceeded in the presence of ^{t}BuLi at high temperatures (50–80 °C), probably because of the low reactivity of chlorine groups. In most cases, the reaction yield was moderate (20–40%).

Although the replacement of chlorine with bromine is the most straightforward solution to the problem of sluggish lithium–chlorine exchange, this alternative route has been underexplored because of the commercial rarity of the corresponding starting materials. The few compounds successfully prepared from tribromobenzene are listed in Fig. 10 and Table 9.[150–152] The synthesis of these compounds, especially that of **DTBA-BN2**, is characterised by lithium–bromine exchange
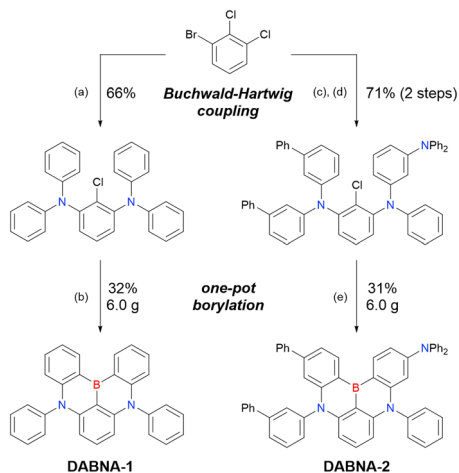
Scheme 6 Synthesis of **DABNA-1** and **DABNA-2**. (a) HNPh$_2$ (2.2 equiv.), ^{t}BuOK (2.5 equiv.), (AmPhos)$_2$PdCl$_2$ (1.0 mol%), o-xylene, 80 °C, 2 h then 120 °C, 3 h. (b) ^{t}BuLi (1.2 equiv.), ^{t}Bu-benzene, 60 °C, 2 h; BBr$_3$ (1.2 equiv.), rt, 0.5 h; NEt^{i}Pr$_2$ (2.0 equiv.), 120 °C, 3 h. (c) HNPh(m-Ph$_2$N-C$_6$H$_4$) (1.0 equiv.), ^{t}BuOK (1.5 equiv.), (AmPhos)$_2$PdCl$_2$ (0.5 mol%), o-xylene, 90 °C, 2.5 h. (d) HN(m-Ph-C$_6$H$_4$)$_2$ (1.0 equiv.), ^{t}BuOK (1.5 equiv.), (AmPhos)$_2$PdCl$_2$ (1.0 mol%), o-xylene, 120 °C, 1 h. (e) ^{t}BuLi (2.0 equiv.), ^{t}Bu-benzene, 60 °C, 3 h; BBr$_3$ (2.0 equiv.), rt, 0.5 h; NEt^{i}Pr$_2$ (2.0 equiv.), 120 °C, 1.5 h.

conditions (^{n}BuLi, −60 °C, 1 h) that are milder than those of lithium–chlorine exchange. Thus, the choice of the halogen atom in one-pot borylation precursors should be carefully considered on the balance of reactivity and accessibility.

The one-pot borylation of a 1,3-diamino-5-carbazolyl-substituted precursor via directed ortho-lithiation was attempted as another route to synthesising DABNA derivatives (Scheme 7).[153] The resulting compound (**TBN-TPA**) was identified by Huang et al. as being borylated between the two diarylamine groups. This structure was later corrected (**CzDABNA-NP-TB**) by Hatakeyama et al., by showing that the boron atom is inserted at the carbon between the diarylamino and carbazolyl groups.[111] This behaviour can be ascribed to the less pronounced electron-donating character of carbazole groups than diarylamino groups, which can facilitate the nucleophilic reaction with ^{n}BuLi at the adjacent position. Therefore, directed ortho-lithiation can suffer from unpredictable or poor regioselectivity. In particular, the directing effects of diarylamine and carbazole groups are inferior to that of aryloxy groups because of the delocalisation of the nitrogen lone pair.

2.2.2 Photophysical properties. Although **DOBNA** and its derivatives were the initial examples of MR-TADF emitters, the development of the one-pot borylation protocol for DABNA derivatives in 2016 enabled the development of numerous
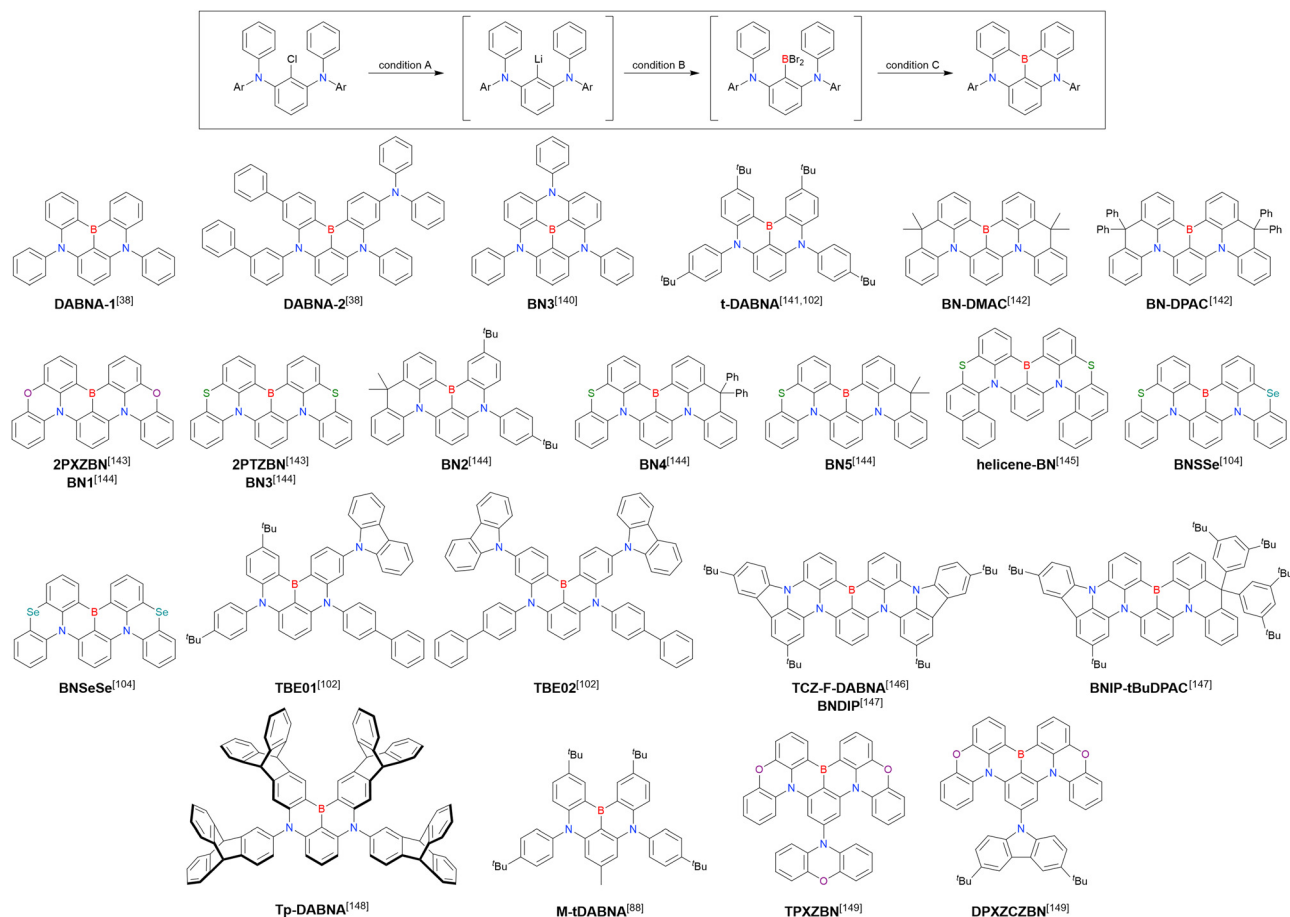

Fig. 9 DABNA-based MR-TADF emitters.

This journal is © The Royal Society of Chemistry 2024

Chem. Soc. Rev., 2024, 53, 1624–1692 | 1635

Table 8 Conditions used to synthesise the compounds shown in Fig. 9

Compound	Condition A[a]	Condition B[a]	Condition C[a]	Solvent	Yield [%]	Ref.
DABNA-1	^{t}BuLi (1.2)/60 °C, 2 h	BBr$_3$ (1.2)/rt, 0.5 h	NEt^{i}Pr$_2$ (2.0)/120 °C, 3 h	^{t}Bu-Benzene	32	38
DABNA-2	^{t}BuLi (2.0)/60 °C, 3 h	BBr$_3$ (2.0)/rt, 0.5 h	NEt^{i}Pr$_2$ (2.0)/120 °C, 1.5 h	^{t}Bu-Benzene	31	38
BN3	^{t}BuLi (1.0)/50 °C, 0.5 h	BBr$_3$ (2.1)/−45 °C	NEt^{i}Pr$_2$ (2.2)/reflux, 14 h	^{t}Bu-Benzene	45	140
t-DABNA	^{t}BuLi (2.0)/60 °C, 2 h	BBr$_3$ (2.0)/rt, 0.5 h	NEt^{i}Pr$_2$ (2.0)/100 °C, 2 h	^{t}Bu-Benzene	31	141
	^{t}BuLi (1.2)/70 °C, 3 h	BBr$_3$ (1.5)/rt, 2 h	NEt^{i}Pr$_2$ (2.0)/70 °C, 12 h	^{t}Bu-Benzene	21	102
BN-DMAC	^{t}BuLi (2.0)/60 °C, 2 h	BBr$_3$ (2.0)/rt, 1 h	NEt^{i}Pr$_2$ (2.0)/reflux, overnight	Mesitylene	25	142
BN-DPAC	^{t}BuLi (2.0)/60 °C, 2 h	BBr$_3$ (2.0)/rt, 1 h	NEt^{i}Pr$_2$ (2.0)/reflux, overnight	Mesitylene	13	142
2PXZBN	^{t}BuLi (2.2)/60 °C, 2 h	BBr$_3$ (1.5)/rt, 1 h	NEt^{i}Pr$_2$ (2.0)/160 °C, 24 h	Mesitylene	23	143
	^{t}BuLi (2.7)/60 °C, 2 h	BBr$_3$ (2.8)/rt, 0.5 h	NEt^{i}Pr$_2$ (2.8)/120 °C, 3 h	^{t}Bu-Benzene	32	144
2PTZBN	^{t}BuLi (2.2)/60 °C, 2 h	BBr$_3$ (1.5)/rt, 1 h	NEt^{i}Pr$_2$ (2.0)/160 °C, 24 h	Mesitylene	25	143
	^{t}BuLi (2.5)/60 °C, 2 h	BBr$_3$ (2.5)/rt, 0.5 h	NEt^{i}Pr$_2$ (2.5)/120 °C, 3 h	^{t}Bu-Benzene	39	144
BN2	^{t}BuLi (2.5)/60 °C, 2 h	BBr$_3$ (2.5)/rt, 0.5 h	NEt^{i}Pr$_2$ (2.5)/120 °C, 3 h	^{t}Bu-Benzene	39	144
BN4	^{t}BuLi (2.0)/60 °C, 2 h	BBr$_3$ (2.0)/rt, 0.5 h	NEt^{i}Pr$_2$ (2.0)/120 °C, 3 h	^{t}Bu-Benzene	41	144
BN5	^{t}BuLi (3.0)/60 °C, 2 h	BBr$_3$ (3.0)/rt, 0.5 h	NEt^{i}Pr$_2$ (3.0)/120 °C, 3 h	^{t}Bu-Benzene	39	144
helicene-BN	^{t}BuLi (2.2)/60 °C, 1 h	BBr$_3$ (2.5)/rt, 1 h	NEt^{i}Pr$_2$ (1.2)/130 °C, 24 h	^{t}Bu-Benzene	15	145
BNSSe	^{t}BuLi (2.5)/60 °C, 5 h	BBr$_3$ (2.5)/rt, 0.5 h	NEt^{i}Pr$_2$ (2.5)/160 °C, 14 h	Mesitylene	21	104
BNSeSe	^{t}BuLi (2.5)/60 °C, 5 h	BBr$_3$ (2.5)/rt, 0.5 h	NEt^{i}Pr$_2$ (5.0)/160 °C, 14 h	Mesitylene	30	104
TBE01	^{t}BuLi (2.0)/70 °C, 3 h	BBr$_3$ (2.0)/rt, 2 h	NEt^{i}Pr$_2$ (2.4)/70 °C, 12 h	^{t}Bu-Benzene	24	102
TBE02	^{t}BuLi (2.0)/70 °C, 3 h	BBr$_3$ (2.0)/rt, 2 h	NEt^{i}Pr$_2$ (2.7)/70 °C, 12 h	^{t}Bu-Benzene	21	102
TCZ-F-DABNA	^{t}BuLi (2.5)/60 °C, 3 h	BBr$_3$ (1.5)/rt, 6 h	NEt^{i}Pr$_2$ (2.5)/130 °C, 12 h	^{t}Bu-Benzene	82	146
	^{t}BuLi (2.2)/60 °C, 1 h	BBr$_3$ (1.5)/rt, 1 h	NEt^{i}Pr$_2$ (1.2)/130 °C, 24 h	^{t}Bu-Benzene	48	147
BNIP-tBuDPAC	^{t}BuLi (2.2)/60 °C, 1 h	BBr$_3$ (1.5)/rt, 1 h	NEt^{i}Pr$_2$ (1.2)/130 °C, 24 h	^{t}Bu-Benzene	38	147
Tp-DABNA	^{t}BuLi (3.0)/80 °C, 4 h	BBr$_3$ (3.0)/60 °C, 1 h	NEt^{i}Pr$_2$ (3.0)/120 °C, 12 h	^{t}Bu-Benzene	18	148
M-tDABNA	^{t}BuLi (1.2)/60 °C, 3 h	BBr$_3$ (1.2)/rt, 1 h	NEt^{i}Pr$_2$ (2.0)/120 °C, 12 h	^{t}Bu-Benzene	27	88
TPXZBN	^{t}BuLi (4.5)/60 °C, 2 h	BBr$_3$ (2.4)/rt, 0.5 h	NEt^{i}Pr$_2$ (3.8)/120 °C, 12 h	^{t}Bu-Benzene	19	149
DPXCZBN	^{t}BuLi (4.5)/60 °C, 2 h	BBr$_3$ (2.4)/rt, 0.5 h	NEt^{i}Pr$_2$ (3.8)/120 °C, 12 h	^{t}Bu-Benzene	15	149

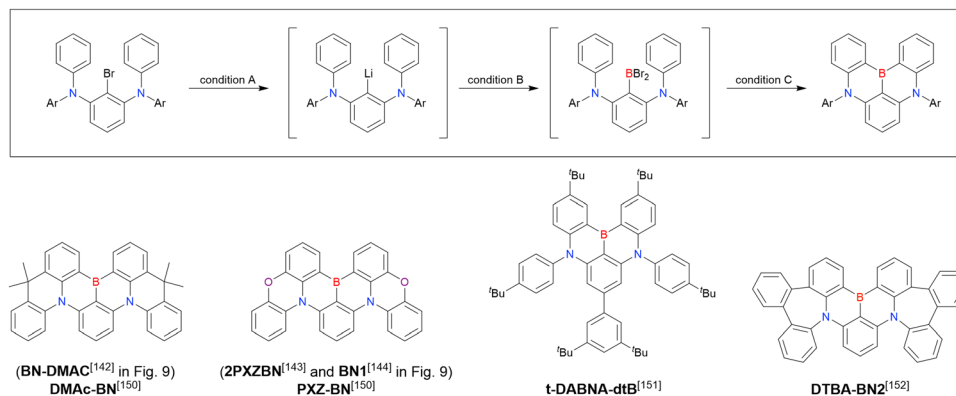[a] Numbers in parentheses refer to reagent loadings (equivalents).

Fig. 10 DABNA derivatives synthesised by lithium−bromine exchange.

(BN-DMAC[142] in Fig. 9) DMAc-BN[150]

(2PXZBN[143] and BN1[144] in Fig. 9) PXZ-BN[150]

t-DABNA-dtB[151]

DTBA-BN2[152]

Table 9 Conditions used to synthesise the compounds shown in Fig. 10

Compound	Condition A[a]	Condition B[a]	Condition C[a]	Solvent	Yield [%]	Ref.
DMAc-BN[b]	^{n}BuLi (1.1)/60 °C, 0.5 h	BBr$_3$ (1.2)/rt, 0.5 h	NEt^{i}Pr$_2$ (2.0)/110 °C, overnight	Toluene	38	150
PXZ-BN[b]	^{n}BuLi (1.1)/60 °C, 0.5 h	BBr$_3$ (1.2)/rt, 0.5 h	NEt^{i}Pr$_2$ (2.0)/110 °C, overnight	Toluene	41	150
t-DABNA-dtB	^{n}BuLi (2.0)/rt, 0.5 h	BBr$_3$ (2.0)/rt, 6 h	NEt^{i}Pr$_2$ (2.0)/120 °C, overnight	o-Xylene	38	151
DTBA-BN2	^{n}BuLi (2.2)/−60 °C, 1 h	BBr$_3$ (1.5)/rt, 1 h	NEt^{i}Pr$_2$ (4.0)/120 °C, 12 h	Toluene	40	152

[a] Numbers in parentheses refer to reagent loadings (equivalents). [b] Same compound appeared in Fig. 9 and Table 8.

MR-TADF emitters suitable for use in the emitting layers of OLEDs. In the original paper,[38] **DABNA-1** and **DABNA-2** were used as MR-TADF emitters in OLEDs for the first time and achieved pure blue emission at 459–467 nm with a narrow FWHM of 28 nm and an IQE of ~100%, thus achieving a record-setting performance for blue OLEDs.

Table 10 lists the photophysical properties of DABNA-based MR-TADF emitters. The most notable feature is the sharp PL

1636 | Chem. Soc. Rev., 2024, 53, 1624–1692

This journal is © The Royal Society of Chemistry 2024
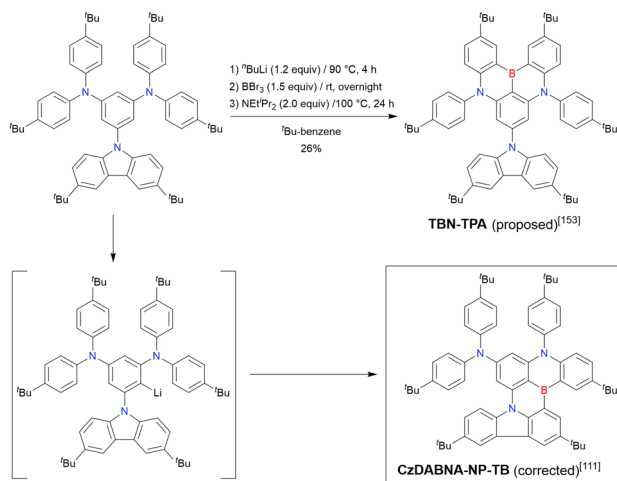
Scheme 7 Two possible chemical structures derived from the directed *ortho*-lithiation of a 1,3-diamino-5-carbazozyl substituted precursor.

band (FWHM = 20–40 nm) and small ΔE_{ST} (0.1–0.2 eV) due to the MR effect of boron and nitrogen atoms. Moreover, the corresponding Φ_{PL} is above 0.90 in most cases, and the average λ_{PL}^{max} values (460–510 nm) are ~50 nm higher than those of DOBNA-based emitters. This spectral shift is attributed to the higher atomic orbital energies of nitrogen compared to those of oxygen, which enhances the conjugation between the lone pair of nitrogen and the π-orbitals of the benzene ring. Note that

BN3, a triangulene analogue, showed relatively low Φ_{PL}, probably due to the small oscillator strength (0.1138).[140]

Table 10 reveals some trends useful for designing DABNA-based emitters. **BN-DMAC**, **DMAc-BN**, **BN-DPAC**, and **BN2** were constructed by inserting sp³-carbon into the DABNA skeleton.[142,144,150] Compared to **DABNA-1**, the λ_{PL}^{max} bands of these materials were red-shifted (462 nm to 475–490 nm) because of the extended π-conjugation. The helical structures induced by intramolecular locking were beneficial for increasing k_{RISC} (9.9 × 10³ s⁻¹ to 2.4 × 10⁴–1.26 × 10⁵ s⁻¹).

The analysis of **TCZ-F-DABNA**, **BNDIP**, and **BNIP-tBuDPAC** shows that additional nitrogen atoms at *ortho*-positions relative to the original nitrogen atoms (*i.e.*, at *meta*-positions relative to boron atoms) can extend π-conjugation and increase the bathochromic shift in PL spectra to 550 nm.[146,147] Although the k_{RISC} values are generally the same as those of DOBNA derivatives (10³–10⁴ s⁻¹), the heavy-atom effect can increase them to >1.0 × 10⁵ s⁻¹ when sulphur and/or selenium atoms are introduced, as exemplified by **2PTZBN**, **BN4**, **BNSSe**, and **BNSeSe**.[104,143,144] The more distorted structures due to the long C–S or C–Se bonds can also increase the SOC to accelerate RISC.
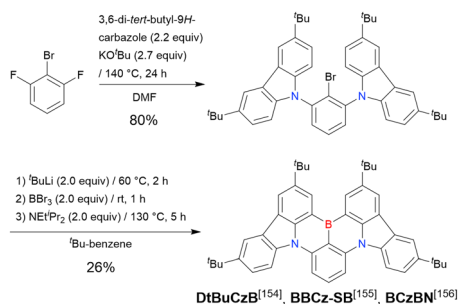
2.3 Carbazole-based MR-TADF emitters

2.3.1 One-pot borylation of carbazole-based precursors. As summarised in this section, the synthesis of DOBNA and DABNA derivatives have inspired the preparation of numerous MR-TADF emitters. From a synthesis viewpoint, these two

Table 10 Photophysical properties of the compounds shown in Fig. 9 and 10

Compound	Condition	λ_{PL}^{max} [nm]	FWHM [nm]	Φ_{PL} [—]	ΔE_{ST} [eV]	k_{RISC} [s⁻¹]	Ref.
DABNA-1	CH₂Cl₂/EtOH/1 wt%-mCBP[a]	462/458/460	33/36/30	0.89/0.84/0.88	—/0.15/0.18	—/—/9.9 × 10³	38
DABNA-2	CH₂Cl₂/EtOH/1 wt%-mCBP[a]	470/463/469	34/34/28	0.85/0.90/0.90	—/0.15/0.14	—/—/1.48 × 10⁴	38
BN3	CH₂Cl₂/1 wt%-PMMA[a]	403/399	—/26	0.362/0.54	—/0.21	—/—	140
t-DABNA	Solution[b]/DPEPO[a]	443[c]/—	—/—	—/0.85	0.17/—	—/2.44 × 10³	141
t-DABNA	Toluene/SiCzCz:SiTrzCz₂[a]	456/—	21/—	0.993/—	0.21/—	—/2.7 × 10³	102
BN-DMAC[d]	Toluene/1 wt%-mCBP[a]	485/489	29/39	—/0.63	0.14/—	—/9.6 × 10⁴	142
DMAc-BN[d]	2-MeTHF/3 wt%-mCBP[a]	484/—	33/—	—/0.88	0.16/—	—/2.4 × 10⁴	150
BN-DPAC	Toluene/1 wt%-mCBP[a]	490/493	30/38	—/0.86	0.11/—	—/1.26 × 10⁵	142
2PXZBN[e]	Toluene/1 wt%-mCBP/PO-T2T[a]	504/515	34/40	0.78/0.84	0.19/0.18	1.03 × 10⁵/0.56 × 10⁵	143
BN1[e]	Toluene	502	41	0.61	0.20	—	144
PXZ-BN[e]	2-MeTHF/3 wt%-mCBP[a]	502/—	38/—	—/0.90	0.17/—	—/0.9 × 10⁴	150
2PTZBN[f]	Toluene/1 wt%-mCBP/PO-T2T[a]	510/519	39/44	0.58/0.80	0.15/0.14	2.76 × 10⁵/1.17 × 10⁵	143
BN3[f]	Toluene	511	46	0.72	0.16	1.0 × 10⁵	144
BN2	Toluene	475	34	0.88	0.20	—	144
BN4	Toluene/3 wt%-mCPCN[a]	500/522	43/50	0.88/0.96	0.14/—	1.6 × 10⁵/3.7 × 10⁴	144
BN5	Toluene/3 wt%-mCPCN[a]	497/512	44/49	0.87/0.92	0.14/—	7.4 × 10⁴/3.3 × 10⁴	144
helicene-BN	Toluene/1 wt%-DMIC-TRZ[a]	520/525	46/48	—/0.98	0.18/0.15	—/4.6 × 10⁴	145
BNSSe	Toluene/1 wt%-DMIC-TRZ[a]	505/520	39/—	—/0.99	0.17/0.12	—/6.0 × 10⁵	104
BNSeSe	Toluene/1 wt%-DMIC-TRZ[a]	502/514	38/—	—/1.00	0.17/0.14	—/2.0 × 10⁶	104
TBE01	Toluene/0.4 wt%-SiCzCz:SiTrzCz₂[a]	459/—	21/—	0.911/—	0.16/—	—/5.1 × 10³	102
TBE02	Toluene/0.4 wt%-SiCzCz:SiTrzCz₂[a]	459/—	21/—	0.891/—	0.14/—	—/1.03 × 10⁴	102
TCZ-F-DABNA[g]	Toluene/8 wt%-PhCzBCz[a]	558/—	38/—	—/0.99	0.12/—	—/7.80 × 10⁴	146
BNDIP[g]	Toluene/1 wt%-DMIC-TRZ[a]	558/584	38/61	—/0.96	0.13/0.09	—/2.3 × 10⁴	147
BNIP-tBuDPAC	Toluene/1 wt%-DMIC-TRZ[a]	544/557	43/53	—/0.98	0.14/0.11	—/1.2 × 10⁴	147
Tp-DABNA	Toluene/2 wt%-mCBP:DPEPO[a]	458/463	19/24	0.96/0.99	0.17/0.15	—/5.7 × 10³	148
M-tDABNA	Toluene/3 wt%-MADN[a]	—/461	—/27	—/0.77	0.11/—	—/—	88
TPXZBN	Toluene/5 wt%-mCBP[a]	502/—	33/—	0.91/0.99	0.16/—	—/4.8 × 10⁴	149
DPXCZBN	Toluene/5 wt%-mCBP[a]	500/—	32/—	0.90/0.94	0.13/—	—/1.11 × 10⁵	149
t-DABNA-dtB	Toluene/3 wt%-mCBP[a]	465/473	22/30	—/0.97	0.19/—	—/2.08 × 10⁴	151
DTBA-BN2	Toluene/3 wt%-26DCzPPy[a]	490/496	41/—	0.96/0.97	0.13/—	2.3 × 10⁵/4.8 × 10⁵	152

[a] See Table 2 for the full compound name. [b] Solvent was not identified. [c] Calculated from the reported S₁ energy in eV. [d] Same compound named differently. [e] Same compound named differently. [f] Same compound named differently. [g] Same compound named differently.

This journal is © The Royal Society of Chemistry 2024

Chem. Soc. Rev., 2024, **53**, 1624–1692 | **1637**

Scheme 8 Synthesis of a carbazole-based MR-TADF emitter.

frameworks are complementary, with the oxygen atoms in DOBNA scaffolds inserted *via* an S_NAr reaction and the nitrogen atoms in DABNA scaffolds inserted *via* Buchwald–Hartwig coupling. Consequently, different methods of introducing nitrogen atoms are worth investigating to expand the chemical space of MR-TADF emitters. More importantly, almost all DABNA derivatives were obtained *via* lithium–chlorine exchange under harsh conditions because of the limited availability of starting materials. Thus, a general procedure providing access to N,B,N-embedded frameworks *via* lithium–bromine exchange is desired to improve functional group tolerance.

In 2020, Wang *et al.* reported the first MR-TADF emitter synthesised *via* an S_NAr reaction involving carbazolyl groups (Scheme 8).[154] The bis(di(*tert*-butyl)carbazolyl)phenylene parent skeleton was synthesised in 80% yield starting from 2-bromo-1,3-difluorobenzene, with the subsequent basic one-pot borylation affording **DtBuCzB** (also known as **BCzBN**) in 26% yield. Similar to the case of the S_NAr substitution-based DOBNA skeleton construction, the carbazolyl group successfully and selectively substituted a fluorine atom, while the bromine atom was preserved for the subsequent one-pot borylation. Therefore, a bromine group could be easily introduced into the one-pot borylation precursor because of the commercial availability of 1-bromo-2,6-difluorobenzene.

Currently, the carbazole-based N,B,N-embedded framework (called **CzBN** in this review) is the one most widely used for the construction of MR-TADF emitters. The abundant methods for carbazolyl group pre-functionalisation allow numerous substructures to be attached to B,N,B-embedded frameworks (Fig. 11 and Table 11).[155–165] In most cases, the *para*-positions of the carbazole nitrogen atoms were pre-functionalised and used in the S_NAr-based one-pot borylation protocol. The highly functionalised carbazolyl subunits (*e.g.*, those in **BN-ICz-1**, **BN-ICz-2**, and **BN-DICz**) were also completely constructed before
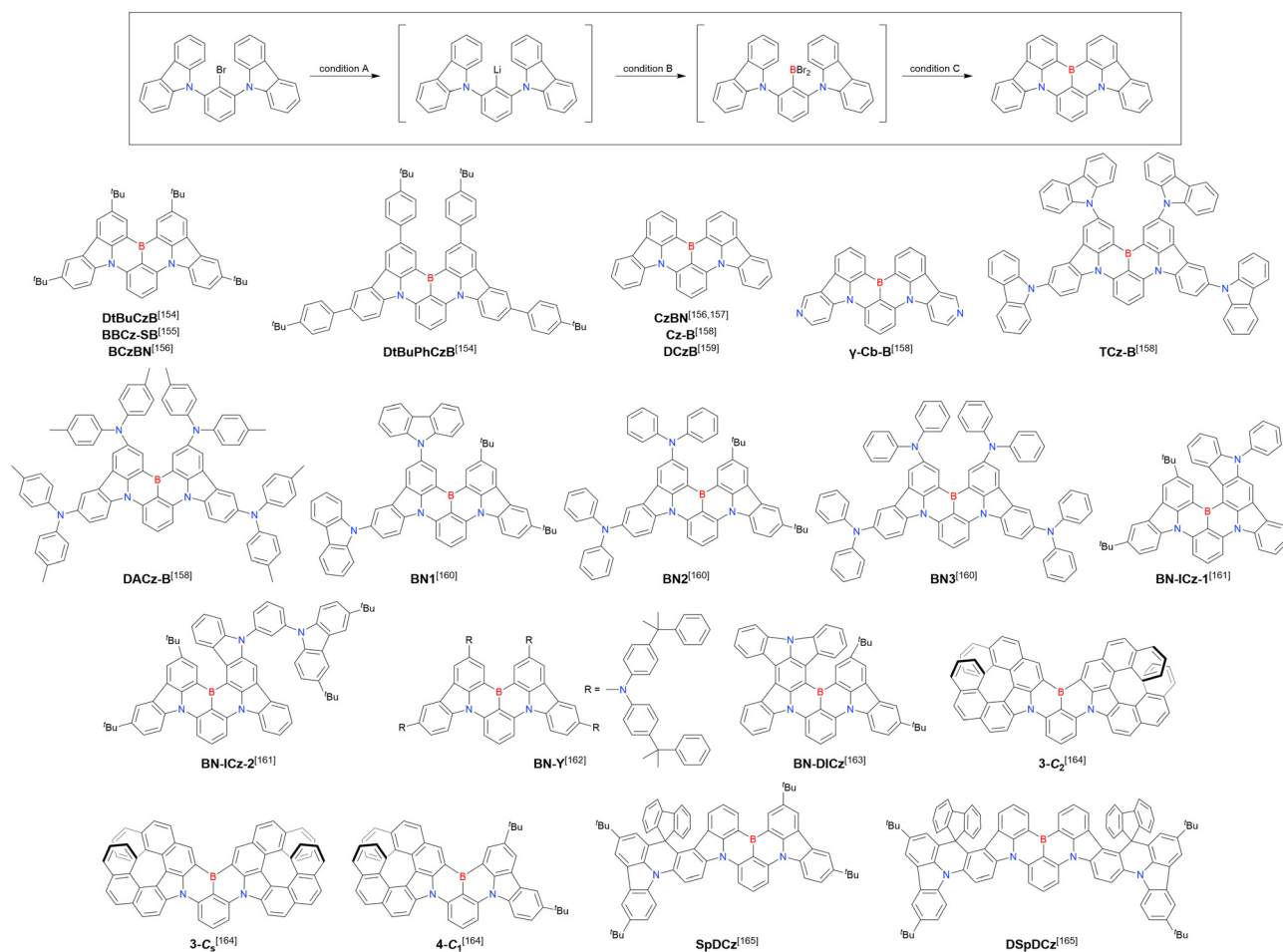

Fig. 11 Carbazole moiety-containing MR-TADF emitters.

1638 | *Chem. Soc. Rev.*, 2024, **53**, 1624–1692

This journal is © The Royal Society of Chemistry 2024

Table 11 Conditions used to synthesise the compounds shown in Fig. 11

Compound	Condition A[a]	Condition B[a]	Condition C[a]	Solvent	Yield [%]	Ref.
DtBuCzB	^{t}BuLi (2.0)/60 °C, 2 h	BBr$_3$ (2.0)/rt, 1 h	NEt^{i}Pr$_2$ (2.0)/130 °C, 5 h	^{t}Bu-Benzene	26	154
	^{n}BuLi (1.7)/rt, 4 h	BBr$_3$ (1.7)/rt, 12 h	NEt^{i}Pr$_2$ (2.7)/170 °C, 24 h	^{t}Bu-Benzene	24	155
	^{n}BuLi (1.2)/rt, 2 h	BBr$_3$ (1.2)/rt, 0.5 h	NEt^{i}Pr$_2$ (2.0)/120 °C, 3 h	^{t}Bu-Benzene	47	156
DtBuPhCzB	^{t}BuLi (2.0)/60 °C, 2 h	BBr$_3$ (2.0)/rt, 1 h	NEt^{i}Pr$_2$ (2.0)/130 °C, 5 h	^{t}Bu-Benzene	17	154
CzBN	^{n}BuLi (1.2)/rt, 2 h	BBr$_3$ (1.2)/rt, 0.5 h	NEt^{i}Pr$_2$ (2.0)/120 °C, 3 h	^{t}Bu-Benzene	41	156
	^{n}BuLi (1.2)/60 °C, 2 h	BBr$_3$ (1.2)/rt, 1 h	NEt^{i}Pr$_2$ (2.0)/110 °C, 8 h	Toluene	29	157
	^{n}BuLi (1.5)/rt, 2 h	BBr$_3$ (1.5)/rt, 2 h	NEt^{i}Pr$_2$ (2.0)/110 °C, 24 h	Toluene	37	158
	^{t}BuLi (2.0)/60 °C, 2 h	BBr$_3$ (2.0)/rt, 1 h	NEt^{i}Pr$_2$ (2.0)/130 °C, 6 h	^{t}Bu-Benzene	20	159
γ-Cb-B	^{n}BuLi (2.0)/rt, 2 h	BBr$_3$ (2.0)/rt, 2 h	PMP (3.0)/170 °C, 24 h	^{t}Bu-Benzene	12	158
TCz-B	^{n}BuLi (1.1)/0 °C, 1 h	BBr$_3$ (1.2)/rt, 2 h	NEt^{i}Pr$_2$ (2.0)/140 °C, 18 h	o-Xylene	56	158
DACz-B	^{n}BuLi (1.1)/0 °C, 1 h	BBr$_3$ (1.2)/rt, 2 h	NEt^{i}Pr$_2$ (2.0)/170 °C, 32 h	^{t}Bu-Benzene	12	158
BN1	^{t}BuLi (2.0)/60 °C, 2 h	BBr$_3$ (2.0)/rt, 1 h	NEt^{i}Pr$_2$ (2.0)/130 °C, 5 h	^{t}Bu-Benzene	21	160
BN2	^{t}BuLi (2.0)/60 °C, 2 h	BBr$_3$ (2.0)/rt, 1 h	NEt^{i}Pr$_2$ (2.0)/130 °C, 5 h	^{t}Bu-Benzene	41	160
BN3	^{t}BuLi (2.0)/60 °C, 2 h	BBr$_3$ (2.0)/rt, 1 h	NEt^{i}Pr$_2$ (2.0)/130 °C, 5 h	^{t}Bu-Benzene	35	160
BN-ICz-1	^{n}BuLi (3.0)/60 °C, 24 h	BBr$_3$ (3.0)/rt, 0.5 h	NEt^{i}Pr$_2$ (4.5)/120 °C, 5 h	^{t}Bu-Benzene	23	161
BN-ICz-2	^{n}BuLi (3.0)/60 °C, 24 h	BBr$_3$ (3.0)/rt, 0.5 h	NEt^{i}Pr$_2$ (4.5)/120 °C, 5 h	^{t}Bu-Benzene	22	161
BN-Y	^{t}BuLi (2.0)/40 °C, 2 h	BBr$_3$ (1.0)/rt, 1 h	NEt^{i}Pr$_2$ (2.0)/120 °C, 8 h	^{t}Bu-Benzene	82	162
BN-DICz	^{n}BuLi (3.0)/60 °C, 24 h	BBr$_3$ (3.0)/rt, 0.5 h	NEt^{i}Pr$_2$ (4.5)/120 °C, 5 h	^{t}Bu-Benzene	22	163
3-C_2/3-C_s	^{n}BuLi (2.5)/rt, 4 h	BBr$_3$ (3.0)/rt, 15 h	NEt^{i}Pr$_2$ (3.5)/175 °C, 24 h	o-Dichlorobenzene	18	164
4-C_1	^{n}BuLi (2.3)/rt, 4 h	BBr$_3$ (3.0)/rt, 15 h	NEt^{i}Pr$_2$ (3.5)/175 °C, 24 h	o-Dichlorobenzene	19	164
SpDCz	^{n}BuLi (1.1)/40 °C, 1 h	BBr$_3$ (3.1)/50 °C, 3 h	NEt^{i}Pr$_2$ (3.1)/125 °C, 20 h	m-Xylene	65	165
DSpDCz	^{n}BuLi (1.1)/40 °C, 1 h	BBr$_3$ (3.1)/50 °C, 3 h	NEt^{i}Pr$_2$ (3.1)/125 °C, 20 h	m-Xylene	58	165

[a] Numbers in parentheses refer to reagent loadings (equivalents).

being merged into the central phenyl ring. Even an aza[7]helicene subunit could be introduced into the MR-TADF framework (3-C_2, 3-C_s, 4-C_1).

In addition to di-carbazolyl frameworks, a combination of carbazolyl and chalcogen groups was easily achieved using sequential nucleophilic substitutions followed by basic one-pot borylation (Fig. 12, Table 12).[94,166–171] Oxygen-bridged (**CzBO**, **BON-D0**, **BON-D1**, **BON-D2**, **CzBNO**, and **SOBN**) and sulphur-bridged (**CzBS** and **Cz-BSN**) compounds were successfully prepared from 2-bromo-1,3-difluorobenzene. Additionally, selenium-bridged

compounds were demonstrated, which was not addressed in previous subsections. The corresponding precursors were synthesised from 2-bromo-3-fluoroaniline using a Sandmeyer-type reaction (**CzBSe**)[94] or from 2-bromo-1,3-difluorobenzene using an S$_N$Ar reaction (**Cz-BSeN**).[169]

Carbazole-based MR-TADF emitters derived from tetrasubstituted benzene can be accessed in a similar manner as DOBNA- and DABNA-based ones (Fig. 13, 14 and Tables 13, 14).[172–187] Although a methoxy group was deprotected by BBr$_3$ in the one-pot borylation procedure (Scheme 4), the methylthio (SMe)
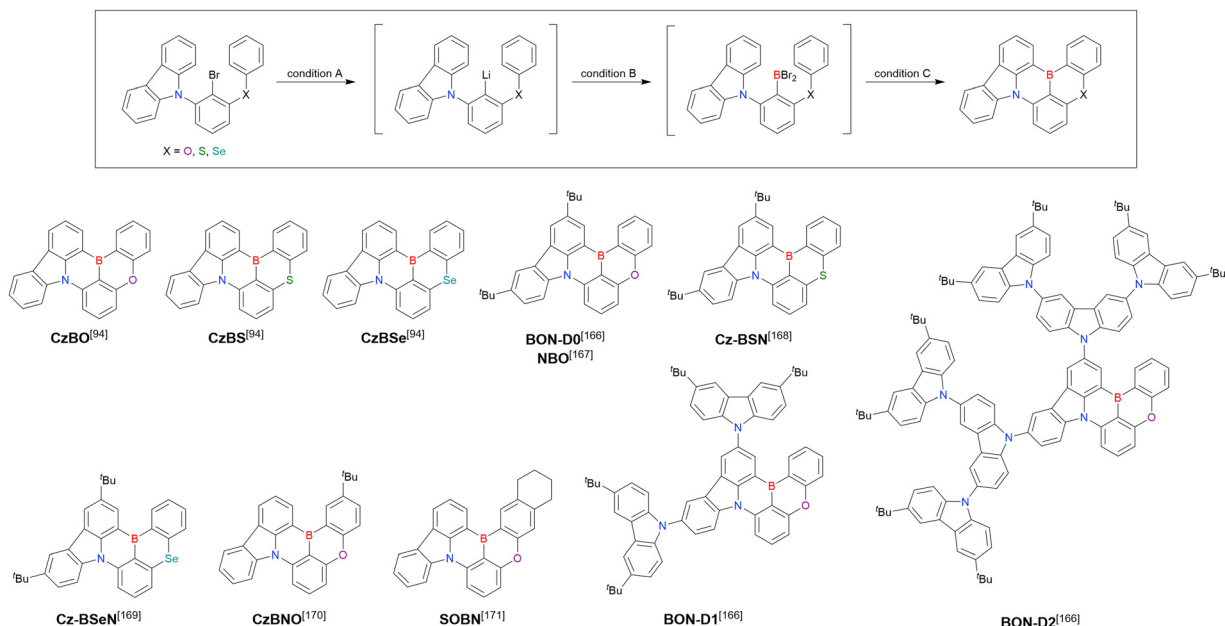

Fig. 12 MR-TADF emitters synthesised by sequential S$_N$Ar reactions.

This journal is © The Royal Society of Chemistry 2024

Chem. Soc. Rev., 2024, **53**, 1624–1692 | **1639**

Table 12 Conditions used to synthesise the compounds shown in Fig. 12

Compound	Condition A[a]	Condition B[a]	Condition C[a]	Solvent	Yield [%]	Ref.
CzBO	^{n}BuLi (1.1)/−30 °C, 1 h	BBr$_3$ (1.2)/rt, 2 h	NEt^{i}Pr$_2$ (2.0)/140 °C, 12 h	^{t}Bu-Benzene	28	94
CzBS	^{n}BuLi (1.1)/−30 °C, 1 h	BBr$_3$ (1.2)/rt, 2 h	NEt^{i}Pr$_2$ (2.0)/140 °C, 12 h	^{t}Bu-Benzene	36	94
CzBSe	^{n}BuLi (1.1)/−30 °C, 1 h	BBr$_3$ (1.2)/rt, 2 h	NEt^{i}Pr$_2$ (2.0)/140 °C, 12 h	^{t}Bu-Benzene	32	94
BON-D0	^{n}BuLi (1.1)/60 °C, 2 h	BBr$_3$ (1.2)/rt, 0.5 h	NEt^{i}Pr$_2$ (2.0)/120 °C, 5 h	m-Xylene	31	166
	^{n}BuLi (1.1)/60 °C, 2 h	BBr$_3$ (1.2)/rt, 0.5 h	NEt^{i}Pr$_2$ (2.0)/110 °C, overnight	Toluene	17	167
Cz-BSN	^{n}BuLi (1.1)/60 °C, 2 h	BBr$_3$ (1.2)/rt, 1 h	NEt^{i}Pr$_2$ (2.0)/130 °C, 24 h	o-Xylene	20	168
Cz-BSeN	^{n}BuLi (1.1)/50 °C, 2 h	BBr$_3$ (1.2)/−30 °C, 0.5 h	NEt^{i}Pr$_2$ (2.0)/130 °C, 48 h	o-Xylene	15	169
CzBNO	^{t}BuLi (2.0)/60 °C, 2 h	BBr$_3$ (2.0)/rt, 1 h	NEt^{i}Pr$_2$ (2.0)/140 °C, 24 h	^{t}Bu-Benzene	32	170
SOBN	^{n}BuLi (4.0)/90 °C, 2 h	BBr$_3$ (4.0)/rt, 1 h	NEt^{i}Pr$_2$ (11)/120 °C, 12 h	^{t}Bu-Benzene	20	171
BON-D1	^{n}BuLi (1.0)/60 °C, 2 h	BBr$_3$ (1.2)/rt, 0.5 h	NEt^{i}Pr$_2$ (2.0)/120 °C, 5 h	m-Xylene	23	166
BON-D2	^{n}BuLi (1.0)/60 °C, 2 h	BBr$_3$ (1.2)/rt, 0.5 h	NEt^{i}Pr$_2$ (2.0)/120 °C, 5 h	m-Xylene	22	166

[a] Numbers in parentheses refer to reagent loadings (equivalents).

group was preserved under the same conditions (**BN(p)SCH$_3$**, Fig. 13). Bromine-containing compounds suitable for subsequent chemical modification were also obtained (**BNCz-Br** and **BNCz-Br-Cz2**, Fig. 14).

At this point, one should mention some indicative results. In 2023, the synthesis of indole-fused MR-TADF frameworks was reported (Scheme 9).[188] The first attempt to obtain the non-substituted indole derivative **InBN** failed in the borylation part, probably because the reactive β-position of the indole unit inhibited the desired reaction during the electrophilic borylation step. Hence, methyl-protected precursors were prepared

and smoothly converted into indole-based MR-TADF emitters (**TMInBN**, **Mes-InBN**, **Cz-InBN**, and **TCz-InBN**) with yields of 8–12%.

As described in Section 2.1.3, the synthesis of bromine-substituted MR-TADF skeletons is an intriguing topic. In particular, sulphur- and selenium-containing compounds are favourable for improving the TADF character. **Br-Cz-BSN** and **Cz-BSeN-Br** were successfully synthesised as heavy-atom-containing MR-type building blocks (Scheme 10).[168,169] Similar to the synthesis of bromo-containing DOBNA derivatives (Section 2.1.3), the commercial availability of the starting material,
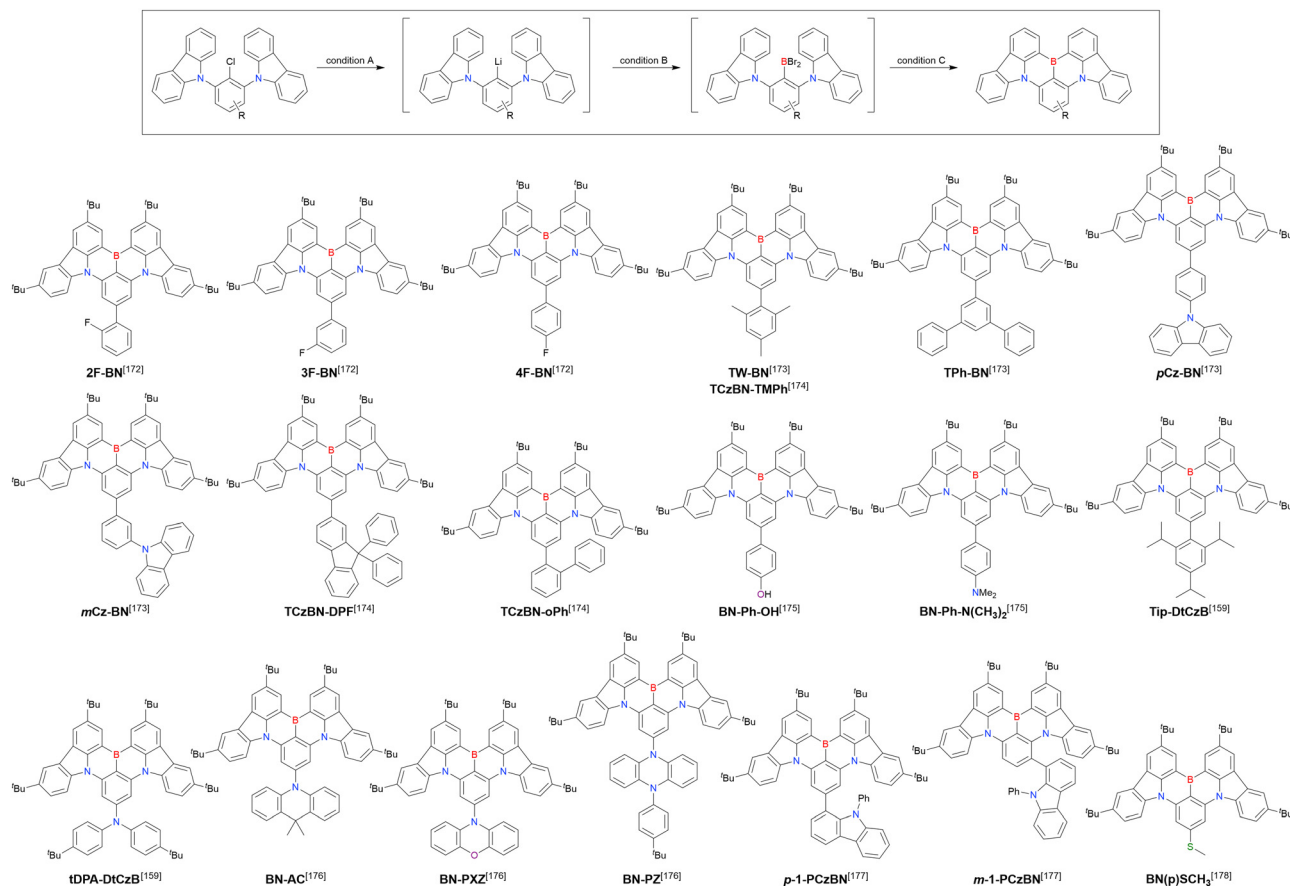

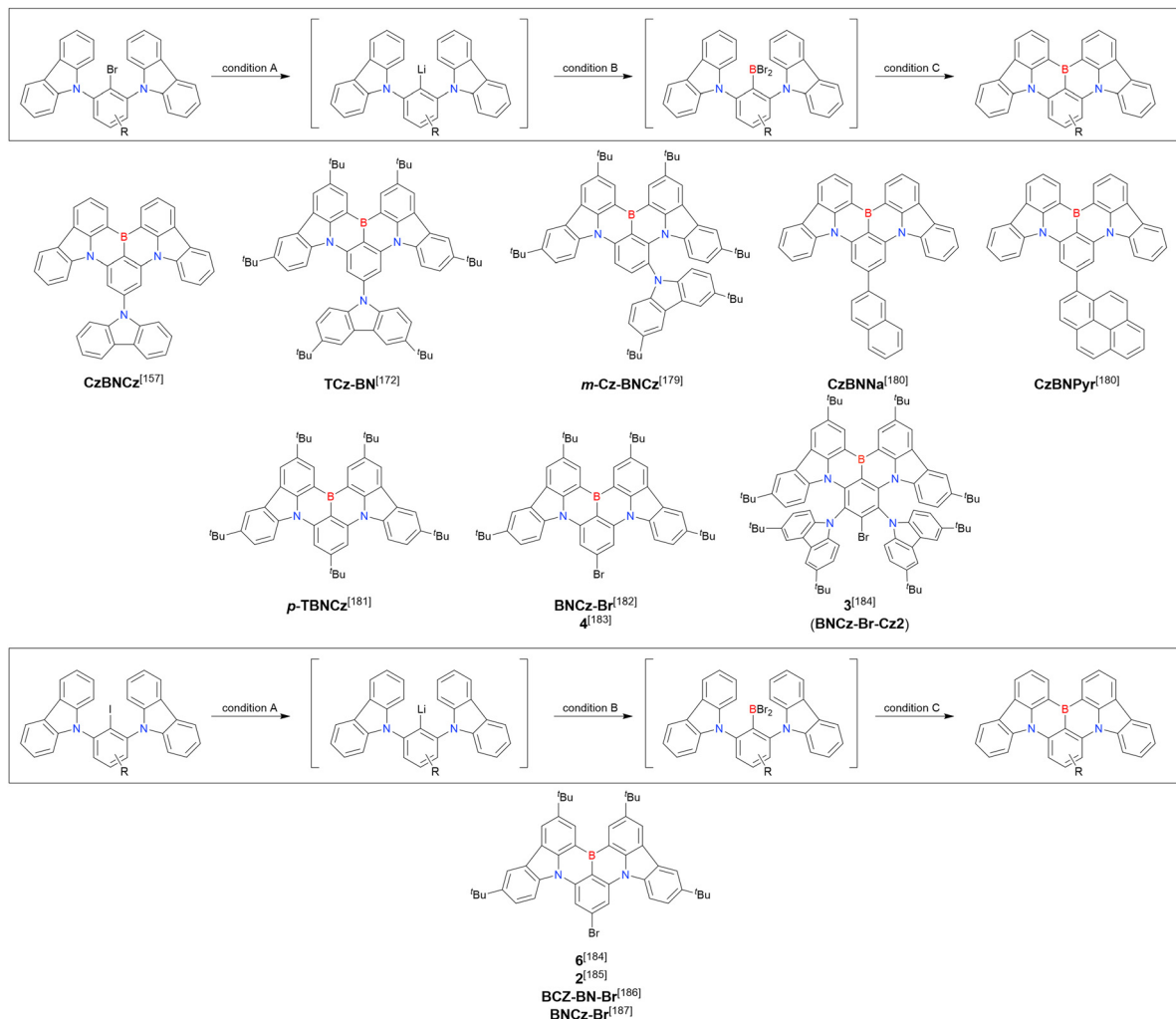**Fig. 13** Carbazole-based MR-TADF emitters synthesised from tetrasubstituted benzene (1).

1640 | *Chem. Soc. Rev.*, 2024, **53**, 1624–1692

This journal is © The Royal Society of Chemistry 2024

Fig. 14 Carbazole-based MR-TADF emitters synthesised from tetrasubstituted benzene (2).

Table 13 Conditions used to synthesise the compounds shown in Fig. 13

Compound	Condition A[a]	Condition B[a]	Condition C[a]	Solvent	Yield [%]	Ref.
2F-BN	^{t}BuLi (3.0)/60 °C, 2 h	BBr$_3$ (3.0)/rt, 0.5 h	NEt^{i}Pr$_2$ (4.8)/120 °C, 5 h	^{t}Bu-Benzene	25	172
3F-BN	^{t}BuLi (3.0)/60 °C, 2 h	BBr$_3$ (3.0)/rt, 0.5 h	NEt^{i}Pr$_2$ (4.8)/120 °C, 5 h	^{t}Bu-Benzene	31	172
4F-BN	^{t}BuLi (3.0)/60 °C, 2 h	BBr$_3$ (3.0)/rt, 0.5 h	NEt^{i}Pr$_2$ (4.8)/120 °C, 5 h	^{t}Bu-Benzene	26	172
TW-BN	^{t}BuLi (2.0)/60 °C, 2 h	BBr$_3$ (2.0)/rt, 1 h	NEt^{i}Pr$_2$ (2.0)/130 °C, 6 h	^{t}Bu-Benzene	32	173
	^{t}BuLi (2.0)/60 °C, 2 h	BBr$_3$ (2.0)/rt, 1 h	NEt^{i}Pr$_2$ (2.0)/130 °C, 5 h	^{t}Bu-Benzene	35	174
TPh-BN	^{t}BuLi (2.0)/60 °C, 2 h	BBr$_3$ (2.0)/rt, 1 h	NEt^{i}Pr$_2$ (2.0)/130 °C, 6 h	^{t}Bu-Benzene	25	173
pCz-BN	^{t}BuLi (2.0)/60 °C, 2 h	BBr$_3$ (2.0)/rt, 1 h	NEt^{i}Pr$_2$ (2.0)/130 °C, 6 h	^{t}Bu-Benzene	22	173
mCz-BN	^{t}BuLi (2.0)/60 °C, 2 h	BBr$_3$ (2.0)/rt, 1 h	NEt^{i}Pr$_2$ (2.0)/130 °C, 6 h	^{t}Bu-Benzene	20	173
TCzBN-DPF	^{t}BuLi (2.0)/60 °C, 2 h	BBr$_3$ (2.0)/rt, 1 h	NEt^{i}Pr$_2$ (2.0)/130 °C, 5 h	^{t}Bu-Benzene	34	174
TCzBN-oPh	^{t}BuLi (2.0)/60 °C, 2 h	BBr$_3$ (2.0)/rt, 1 h	NEt^{i}Pr$_2$ (2.0)/130 °C, 5 h	^{t}Bu-Benzene	38	174
BN-Ph-OH	^{n}BuLi (1.5)/70 °C, 2 h	BBr$_3$ (1.8)/rt, 0.5 h	NEt^{i}Pr$_2$ (2.5)/120 °C, 10 h	^{t}Bu-Benzene	20	175
BN-PhN(CH3)2	^{n}BuLi (1.5)/70 °C, 2 h	BBr$_3$ (1.8)/rt, 0.5 h	NEt^{i}Pr$_2$ (2.5)/120 °C, 10 h	^{t}Bu-Benzene	18	175
Tip-DtCzB	^{t}BuLi (2.0)/60 °C, 2 h	BBr$_3$ (2.0)/rt, 1 h	NEt^{i}Pr$_2$ (2.0)/130 °C, 6 h	^{t}Bu-Benzene	38	159
tDPA-DtCzB	^{t}BuLi (2.0)/60 °C, 2 h	BBr$_3$ (2.0)/rt, 1 h	NEt^{i}Pr$_2$ (2.0)/130 °C, 6 h	^{t}Bu-Benzene	25	159
BN-AC	^{t}BuLi (2.9)/90 °C, 2 h	BBr$_3$ (2.9)/rt, 2 h	NEt^{i}Pr$_2$ (8.0)/130 °C, 24 h	^{t}Bu-Benzene	44	176
BN-PXZ	^{t}BuLi (2.9)/90 °C, 2 h	BBr$_3$ (2.9)/rt, 2 h	NEt^{i}Pr$_2$ (8.0)/130 °C, 24 h	^{t}Bu-Benzene	59	176
BN-PZ	^{t}BuLi (2.9)/90 °C, 2 h	BBr$_3$ (2.9)/rt, 2 h	NEt^{i}Pr$_2$ (8.0)/130 °C, 24 h	^{t}Bu-Benzene	34	176
p-1-PCzBN	^{t}BuLi (4.0)/80 °C, 2 h	BBr$_3$ (4.5)/rt, 40 min	NEt^{i}Pr$_2$ (4.0)/125 °C, 17 h	^{t}Bu-Benzene	92	177
m-1-PCzBN	^{t}BuLi (4.0)/80 °C, 2 h	BBr$_3$ (4.5)/rt, 40 min	NEt^{i}Pr$_2$ (4.0)/125 °C, 17 h	^{t}Bu-Benzene	45	177
BN(p)SCH$_3$	^{t}BuLi (3.0)/60 °C, 2 h	BBr$_3$ (3.0)/rt, 0.5 h	NEt^{i}Pr$_2$ (5.0)/120 °C, 5 h	Mesitylene	21	178

[a] Numbers in parentheses refer to reagent loadings (equivalents).

This journal is © The Royal Society of Chemistry 2024

Chem. Soc. Rev., 2024, **53**, 1624–1692 | **1641**

Table 14 Conditions used to synthesise the compounds shown in Fig. 14

Compound	Condition A[a]	Condition B[a]	Condition C[a]	Solvent	Yield [%]	Ref.
CzBNCz	^{n}BuLi (1.2)/60 °C, 2 h	BBr$_3$ (1.2)/rt, 2 h	NEt^{i}Pr$_2$ (2.4)/110 °C, 10 h	Toluene	34	157
TCz-BN	^{t}BuLi (3.0)/60 °C, 2 h	BBr$_3$ (3.0)/rt, 0.5 h	NEt^{i}Pr$_2$ (4.8)/120 °C, 5 h	^{t}Bu-Benzene	22	172
m-Cz-BNCz	^{t}BuLi (2.0)/60 °C, 2 h	BBr$_3$ (2.0)/rt, 1 h	NEt^{i}Pr$_2$ (2.0)/130 °C, 6 h	^{t}Bu-Benzene	15	179
CzBNNa	^{n}BuLi (1.2)/60 °C, 2 h	BBr$_3$ (1.5)/rt, 2 h	NEt^{i}Pr$_2$ (2.2)/110 °C, 10 h	Toluene	28	180
CzBNpyr	^{n}BuLi (1.2)/60 °C, 2 h	BBr$_3$ (1.5)/rt, 2 h	NEt^{i}Pr$_2$ (2.3)/110 °C, 10 h	Xylene	35	180
p-TBNCz	^{t}BuLi (2.0)/60 °C, 4 h	BBr$_3$ (2.0)/rt, 6 h	NEt^{i}Pr$_2$ (4.0)/120 °C, 24 h	^{t}Bu-Benzene	52	181
BNCz-Br	^{n}BuLi (1.1)/−0 °C to rt	BBr$_3$ (2.0)/rt, 0.5 h	NEt^{i}Pr$_2$ (2.0)/180 °C, 12 h	Mesitylene	74	182
	^{n}BuLi (1.1)/60 °C, 2 h	BBr$_3$ (1.2)/rt, 0.5 h	NEt^{i}Pr$_2$ (2.0)/120 °C, 5 h	m-Xylene	55	183
	^{n}BuLi (1.1)/−60 °C, 1 h	BBr$_3$ (1.5)/rt, 1 h	NEt^{i}Pr$_2$ (4.0)/120 °C, 8 h	Toluene	42	184
	^{n}BuLi (1.1)/rt, 3 h	BBr$_3$ (1.5)/rt, 3 h	NEt^{i}Pr$_2$ (2.3)/160 °C, 24 h	^{t}Bu-Benzene	31	185
	^{n}BuLi (1.1)/−78 °C, 3 h	BBr$_3$ (1.5)/rt, 1 h	NEt^{i}Pr$_2$ (4.0)/130 °C, 8 h	Toluene	20	186
	^{n}BuLi (1.2)/rt, 1 h	BBr$_3$ (1.5)/rt, 1 h	NEt^{i}Pr$_2$ (4.0)/130 °C, 10 h	Xylene	16	187
BNCz-Br-Cz2	^{n}BuLi (1.1)/−60 °C, 1 h	BBr$_3$ (1.5)/rt, 1 h	NEt^{i}Pr$_2$ (4.0)/120 °C, 8 h	Toluene	45	184

[a] Numbers in parentheses refer to reagent loadings (equivalents).
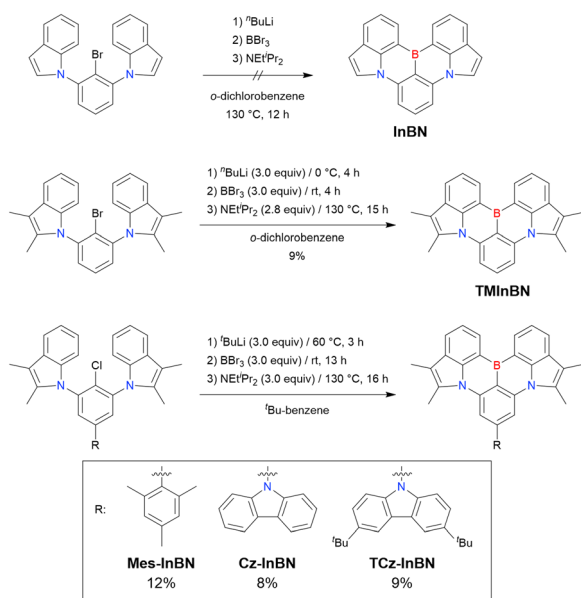
Scheme 9 Synthesis of indole-based MR-TADF emitters reported in ref. 188.

1,4-dibromo-2,6-difluorobenzene, and the regioselectivity of aryloxy group-directed lithium–halogen exchange make these
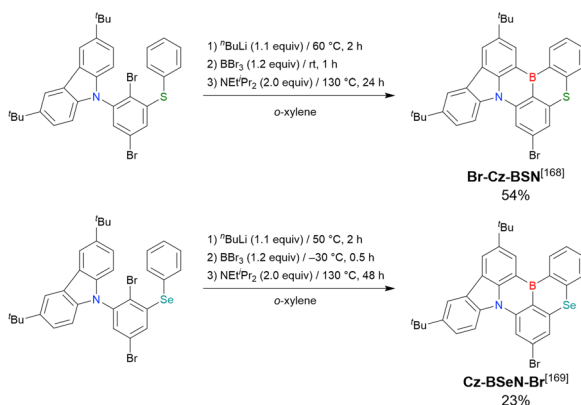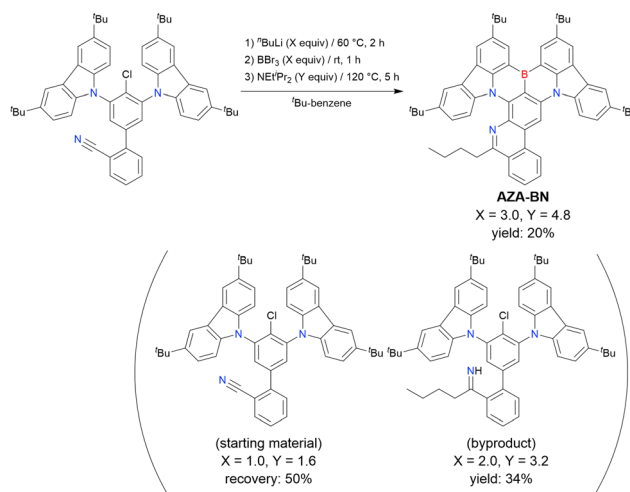

Scheme 10 Synthesis of sulphur- and selenium-containing MR-TADF emitters.

compounds easily accessible. Given that the remaining bromo group facilitates subsequent chemical modification, these compounds can be versatile platforms for the synthesis of various types of functional emitters.
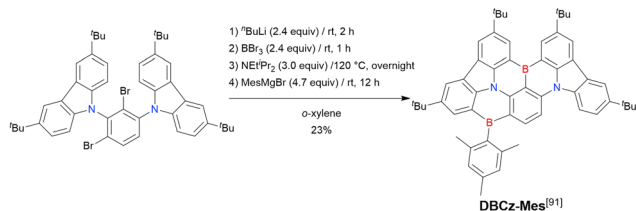
A one-pot multiple cyclisation method for synthesising highly substituted MR-TADF molecules via a combination of imino nitrogen-centred radical-based cyclisation and borylation–cyclisation was proposed in 2020 (Scheme 11).[189] The cyano-substituted starting material was prepared by Suzuki–Miyaura coupling, and **AZA-BN** was obtained in 20% yield under optimal conditions (3.0 equiv. of ^{n}BuLi and 4.8 equiv. of BBr$_3$). Lower reagent ratios resulted in failed boron introduction, which indicated that the addition of ^{n}BuLi to the CN group occurred prior to the substitution of the chlorine atom. In addition, other lithium reagents such as phenyllithium and ^{t}BuLi did not give the desired product.

Recently, a novel boron-bridged compound, **DBCz-Mes**, was synthesised from a dibrominated precursor (Scheme 12).[91] Two boron atoms were simultaneously introduced using 2.4 equiv. of ^{n}BuLi and BBr$_3$, and the reactive B–Br site remaining after intramolecular cyclisation was trapped by a mesityl Grignard reagent (MesMgBr) to afford **DBCz-Mes** in a total yield of 23%,

Scheme 11 Synthesis of aza-fused MR-TADF emitters reported in ref. 189.

1642 | Chem. Soc. Rev., 2024, **53**, 1624–1692

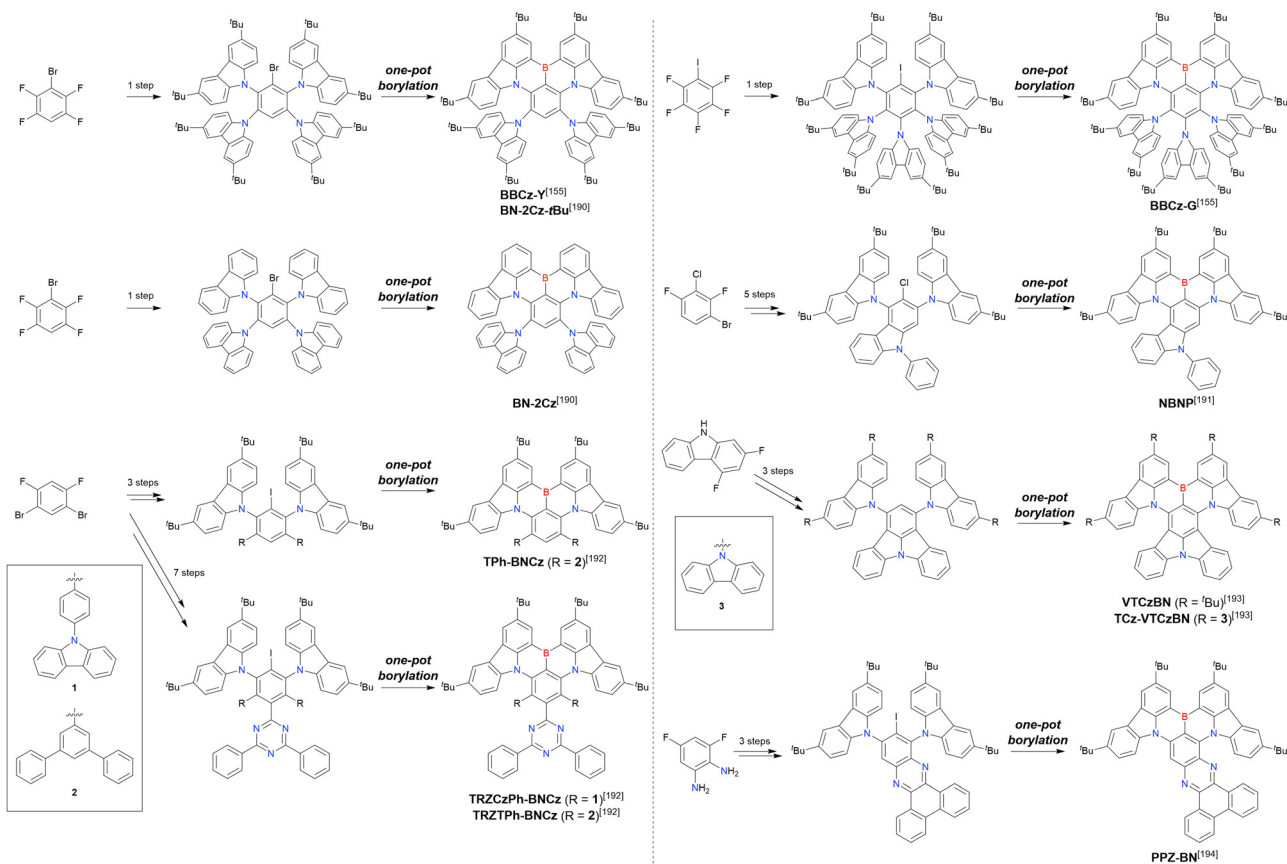This journal is © The Royal Society of Chemistry 2024

Scheme 12 Synthesis of the boron-bridged compound reported in ref. 91.

which is as high as those of other general one-pot borylation protocols.

Although tri- and tetrasubstituted MR-TADF emitters can be easily accessed from commercially available starting materials, the synthesis of penta- and hexa-substituted N,B,N-embedded frameworks require multi-step chemical modification towards borylation precursors (Scheme 13 and Table 15).[155,190–194] **BBCz-Y**, **BBCz-G**, and **BN-2Cz** were conveniently obtained through the simultaneous introduction of multiple carbazolyl groups. Highly cyclised compounds, **NBNP**, **VTCzBN**, **TCz-VTCzBN**, and **PPZ-BN**, were synthesised in a stepwise manner using intra-molecular cyclisation. Finally, the synthesis of **TRZCzPh-BNCz**, **TRZTPh-BNCz**, and **TPh-BNCz** involved iodination after the introduction of carbazolyl groups *via* a substitution reaction. The final one-pot borylation step was achieved *via* directed *ortho*-lithiation or lithium–halogen exchange under standard conditions.

2.3.2 Photophysical properties. As summarised above, the construction of MR-TADF frameworks *via* S_NAr reactions is currently the most common procedure because of their uncomplicated nature and the ready availability of the starting materials (1-bromo-2,6-difluorobenzene and its family). Additionally, coupling partners with carbazole- and chalcogen-containing substituents can also be endowed with diverse structures through pre-functionalisation. Therefore, the resulting MR-TADF emitters show diverse photophysical properties (Tables 16 and 17). As discussions of specific examples are outside the scope of this review, we briefly summarise the overall trends.

First, compared to that of DABNA derivatives, λ_{PL}^{max} shifts to longer wavelengths. For example, the simplest carbazole-based MR-TADF compound, **CzBN**, exhibits a PL maximum at 479 nm in CH_2Cl_2 solution, which is red-shifted by 17 nm relative to that of **DABNA-1**.[156] This change is attributed to the extension of π-conjugation and the increase in the ICT localisation area for a more efficient MR effect. Overall, simple carbazole-based MR-TADF emitters cover the PL colour range of sky-blue, green, and yellow, with blue emission remaining difficult to achieve, except for examples utilising pyridine units (**γ-CB-B**[158]) or oxygen bridges (**CzBO**,[94] **BON-D0**,[166] and **CzBNO**[170]). The carbazole unit is more rigid and planar than carbon-, oxygen-, sulphur-, and selenium-bridged diarylamino units, which are included in some compounds listed in Fig. 9 and 10. This is

Scheme 13 Penta- and hexa-substituted MR-TADF emitters.

Table 15 Conditions used to synthesise the compounds shown in Scheme 13

Compound	Condition A[a]	Condition B[a]	Condition C[a]	Solvent	Yield [%]	Ref.
BBCz-Y	^{n}BuLi (1.5)/rt, 4 h	BBr$_3$ (1.5)/rt, 12 h	NEt^{i}Pr$_2$ (2.4)/170 °C, 24 h	^{t}Bu-Benzene	28	155
	^{n}BuLi (2.1)/rt, 4 h	BBr$_3$ (2.1)/rt, 2 h	NEt^{i}Pr$_2$ (2.1)/160 °C, 6 h	^{t}Bu-Benzene	15	190
BBCz-G	^{n}BuLi (1.5)/rt, 4 h	BBr$_3$ (1.5)/rt, 12 h	NEt^{i}Pr$_2$ (2.4)/170 °C, 24 h	^{t}Bu-Benzene	23	155
BN-2Cz-tBu	^{n}BuLi (2.1)/rt, 4 h	BBr$_3$ (2.1)/rt, 2 h	NEt^{i}Pr$_2$ (2.1)/160 °C, 6 h	^{t}Bu-Benzene	17	190
NBNP	^{n}BuLi (3.0)/70 °C, 1 h	BBr$_3$ (4.0)/rt, 0.5 h	NEt^{i}Pr$_2$ (2.9)/130 °C, 20 h	^{t}Bu-Benzene	14	191
TPh-BNCz	^{n}BuLi (1.5)/rt, 1 h	BBr$_3$ (1.5)/rt, 1 h	NEt^{i}Pr$_2$ (4.0)/180 °C, 12 h	o-Dichlorobenzene	37	192
TRZCzPh-BNCz	^{n}BuLi (1.5)/rt, 1 h	BBr$_3$ (1.5)/rt, 1 h	NEt^{i}Pr$_2$ (4.0)/180 °C, 12 h	o-Dichlorobenzene	35	192
TRZTPh-BNCz	^{n}BuLi (1.5)/rt, 1 h	BBr$_3$ (1.5)/rt, 1 h	NEt^{i}Pr$_2$ (4.0)/180 °C, 12 h	o-Dichlorobenzene	43	192
VTCzBN	^{t}BuLi (4.0)/70 °C, 1 h	BBr$_3$ (4.4)/rt, 0.5 h	NEt^{i}Pr$_2$ (3.7)/130 °C, 24 h	^{t}Bu-Benzene	15	193
TCz-VTCzBN	^{t}BuLi (4.0)/70 °C, 1 h	BBr$_3$ (4.4)/rt, 0.5 h	NEt^{i}Pr$_2$ (3.7)/130 °C, 24 h	^{t}Bu-Benzene	10	193
PPZ-BN	^{n}BuLi (3.0)/rt, 1 h	BBr$_3$ (3.0)/rt, 5 h	NEt^{i}Pr$_2$ (4.5)/120 °C, 12 h	Xylene	21	194

[a] Numbers in parentheses refer to reagent loadings (equivalents).

beneficial for obtaining small FWHMs (generally 20–30 nm) in the solution state. On the other hand, planarity often induces intermolecular interactions with the host material and causes PL spectrum broadening (10–20 nm). To overcome this drawback, peripheral bulky substituents have been introduced. For example, dicarbazole-based symmetric compounds, **TCzBN-DPF**,[174] **TCzBN-oPh**,[174] **p-1-PCzBN**,[177] **m-1-PCzBN**,[177] **DBCz-Mes**,[91] and **TRZCzPh-BNCz**,[192] successfully suppressed spectral broadening within 3 nm, even in host materials. In addition, the highly planar carbazole-based MR skeleton is disadvantageous for accelerating RISC (k_{RISC} typically below 1.0×10^5 s^{-1}). Thus, TAF and PSF OLEDs are often fabricated to achieve high EL performance.[97–100,102]

Second, electron-donating groups at the *para*-position of nitrogen (also the *meta*-position of boron) cause a drastic bathochromic shift in the PL spectra. Tables 16 and 17 list numerous examples of PL wavelength tuning; generally, λ_{PL}^{max} can be increased to >500 nm by introducing one or more electron-donating groups. In some cases, PL wavelengths

exceeding 550 nm (572 nm for **DACz-B**,[158] 562 nm for **BN3**,[160] 567 nm for **BN-Y**,[162] and 613 nm for **PPZ-BN**[194]) were realised through peripheral functionalisation. The other photophysical parameters, namely FWHM, Φ_{PL}, ΔE_{ST}, and k_{RISC}, are comparable to those of DABNA-type MR-TADF emitters.

2.4 Other routes to MR-TADF emitters based on one-pot borylation

2.4.1 Combination of two complementary reactions. Previous subsections overviewed the synthetic routes to DOBNA, DABNA, and CzBN frameworks. The merging of S_NAr and Buchwald–Hartwig coupling reactions is another powerful route used to access other MR-TADF skeletons. In 2021, Yang *et al.* reported the sequential construction of a carbazole-triarylamine-fused compound, **DPACzBN1**, starting from 1-bromo-2-chloro-3-fluorobenzene (Scheme 14).[195] The successive introduction of 9H-carbazole and diphenylamine moieties afforded the key intermediate in 49% yield (two steps). Although the following one-pot borylation required harsh

Table 16 Photophysical properties of the compounds shown in Fig. 11

Compound	Condition	λ_{PL}^{max} [nm]	FWHM [nm]	Φ_{PL} [—]	ΔE_{ST} [eV]	k_{RISC} [s^{-1}]	Ref.
DtBuCzB[a]	Toluene/1 wt%-mCBP[b]	481/493	22/35	0.91/0.88	0.13/—	—/—	154
BBCz-SB[a]	Toluene/2 wt%-mCBP[b]	489/490	23/25	0.98/0.98	0.15/—	1.4×10^4/2.0×10^4	155
BCzBN[a]	CH$_2$Cl$_2$/EtOH/toluene/neat film	497/—/—/517·571	—/—/—/—	—/—/0.863/—	—/0.11/—/—	—/—/1.48 × 10^4/—	156
DtBuPhCzB	Toluene/1 wt%-mCBP[b]	496/508	21/43	0.97/0.90	0.09/—	—/—	154
CzBN[c]	CH$_2$Cl$_2$/EtOH/toluene/neat film	479/—/—/502·570	—/—/—/—	—/—/0.871/—	—/0.12/—/—	—/—/1.69 × 10^4/—	156
CzBN[c]	Toluene/1 wt%-mCBP[b]	473/485	25/32	0.91/0.99	0.15/—	—/1.24 × 10^4	157
Cz-B[c]	Toluene/1 wt%-mCBP[b]	477/484	25/30	0.98/0.97	0.14/—	1.2×10^4/2.7×10^4	158
DCzB[c]	Toluene/1 wt%-PhCzBCz[b]	474/484	24/36	0.81/0.78	0.13/—	—/5.0 × 10^3	159
γ-Cb-B	Toluene/1 wt%-oCBP[b]	460/461	23/30	0.83/0.89	0.12/—	3.1×10^4/5.8×10^4	158
TCz-B	Toluene/1 wt%-mCBP[b]	512/517	27/31	1.00/0.89	0.09/—	2.0×10^4/1.3×10^4	158
DACz-B	Toluene/1 wt%-mCBP[b]	572/576	34/44	0.87/0.87	0.14/—	1.8×10^4/1.0×10^4	158
BN1	Toluene/1 wt%-mCBP[b]	496/499	23/38	0.99/0.93	0.11/—	—/1.9 × 10^5	160
BN2	Toluene/1 wt%-mCBP[b]	534/538	30/41	0.98/0.89	0.13/—	—/1.5 × 10^5	160
BN3	Toluene/1 wt%-mCBP[b]	562/563	30/44	0.98/0.86	0.09/—	—/1.4 × 10^5	160
BN-ICz-1	Toluene/3 wt%-3CTF:mCBP[b]	521/522	21/24	0.992/0.98	0.22/—	2.9×10^4/—	161
BN-ICz-2	Toluene/3 wt%-3CTF:mCBP[b]	521/522	22/24	0.983/0.97	0.18/—	6.4×10^4/—	161
BN-Y	Toluene	567	34	0.95	0.12	—	162
BN-DICz	Toluene/3 wt%-mCBP[b]	533/534	20/32	0.994/—	0.26/—	7.8×10^4/—	163
3-C_2	Toluene/2-MeTHF	543/544	23/—	0.72/—	—/0.35	—/—	164
3-C_s	Toluene/2-MeTHF	546/546	23/—	0.78/—	—/0.35	—/—	164
4-C_1	Toluene/2-MeTHF	520/523	28/—	0.85/—	—/0.32	—/—	164
SpDCz	Toluene/1 wt%-mCP[b]	498/498	26/29	—/0.97	0.14/—	—/3.1 × 10^5	165
DSpDCz	Toluene/1 wt%-mCP[b]	505/505	25/31	—/0.99	0.12/—	—/3.0 × 10^5	165

[a] Same compound named differently. [b] See Table 2 for the full compound name. [c] Same compound named differently.

1644 | *Chem. Soc. Rev.*, 2024, **53**, 1624–1692

This journal is © The Royal Society of Chemistry 2024

Table 17 Photophysical properties of the compounds shown in Fig. 12–14 and Schemes 9, 11–13

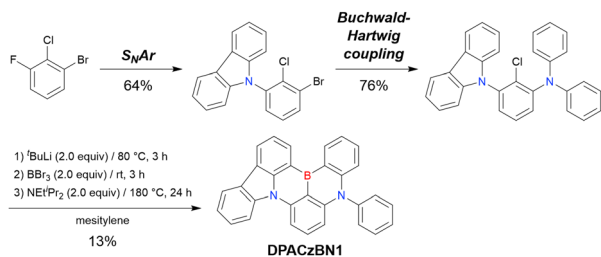| Compound	Condition	λ_{PL}^{max} [nm]	FWHM [nm]	Φ_{PL} [—]	ΔE_{ST} [eV]	k_{RISC} [s^{-1}]	Ref.
CzBO	Toluene/1 wt%-mCBP^a	445/448	26/29	0.98/0.99	0.15/0.16	—/9.0 × 10^3	94
CzBS	Toluene/1 wt%-mCBP^a	471/472	28/30	0.99/0.98	0.11/0.14	4.0 × 10^5/2.2 × 10^5	94
CzBSe	Toluene/1 wt%-mCBP^a	477/479	33/34	0.98/0.98	0.12/0.15	1.5 × 10^8/1.8 × 10^8	94
BON-D0^b	Toluene/5 wt%-mCP^a	450/—	23/—	—/0.85	0.18/—	—/6.73 × 10^4	166
NBO^b	Toluene/3 wt%-mCBP^a	448/458	25/45	—/0.99	—/0.103	—/1.2 × 10^4	167
BON-D1	Toluene/5 wt%-mCP^a	476/—	28/—	—/0.94	0.14/—	—/7.72 × 10^4	166
BON-D2	Toluene/5 wt%-mCP^a	472/—	31/—	—/0.98	0.10/—	—/9.81 × 10^4	166
Cz-BSN	Toluene/1 wt%-PS^a	476/—	24/—	—/0.82	0.13/—	—/9.6 × 10^4	168
Cz-BSeN	Toluene/1 wt%-PS^a	479/—	30/—	—/0.87	0.15/—	—/7.5 × 10^6	169
CzBNO	Toluene/3 wt%-26DCzPPy^a	443/450	23/30	—/0.96	0.21/—	—/3.47 × 10^4	170
SOBN	Toluene/5 wt%-26DCzPPy^a	449/—	22/—	0.78/0.82	0.19/—	—/1.4 × 10^4	171
2F-BN	Toluene/6 wt%-mCPBC^a	494/—	24/—	—/0.887	0.16/—	—/2.2 × 10^4	172
3F-BN	Toluene/6 wt%-mCPBC^a	499/—	24/—	—/0.834	0.08/—	—/3.9 × 10^4	172
4F-BN	Toluene/6 wt%-mCPBC^a	496/—	25/—	—/0.914	0.11/—	—/4.4 × 10^4	172
TW-BN^c	Toluene/3 wt%-mCBP^a	486/485	20/25	0.86/0.92	0.12/—	—/7.56 × 10^3	173
TCzBN-TMPh^c	Toluene/1 wt%-SF3TRZ^a	486/487	23/25	—/0.94	0.12/—	—/1.83 × 10^4	174
TPh-BN	Toluene/3 wt%-mCBP^a	492/495	21/28	0.91/0.94	0.09/—	—/1.43 × 10^4	173
pCz-BN	Toluene/3 wt%-mCBP^a	491/496	21/30	0.90/0.95	0.15/—	—/6.42 × 10^3	173
mCz-BN	Toluene/3 wt%-mCBP^a	495/494	21/29	0.85/0.88	0.14/—	—/1.64 × 10^4	173
TCzBN-DPF	Toluene/1 wt%-SF3TRZ^a	491/495	24/26	—/0.969	0.13/—	—/3.92 × 10^4	174
TCzBN-oPh	Toluene/1 wt%-SF3TRZ^a	489/491	23/24	—/0.961	0.14/—	—/1.62 × 10^4	174
BN-Ph-OH	Toluene/3 wt%-mCBP^a	485/494	26/—	—/0.80	0.14/—	—/2.85 × 10^4	175
BN-PhN(CH3)2	Toluene/3 wt%-mCBP^a	486/500	24/—	—/0.71	0.14/—	—/8.10 × 10^4	175
Tip-DtCzB	Toluene/1 wt%-PhCzBCz^a	477/486	19/29	0.96/0.95	0.13/—	—/9.2 × 10^3	159
tDPA-DtCzB	Toluene/1 wt%-PhCzBCz^a	470/484	21/30	0.86/0.85	0.11/—	—/2.45 × 10^4	159
BN-AC	Toluene/15 wt%-mCBP^a	479/484	26/—	—/0.94	0.14/—	—/1.1 × 10^5	176
BN-PXZ	Toluene/15 wt%-mCBP^a	480/486	28/—	—/0.97	0.12/—	—/7.5 × 10^5	176
BN-PZ	Toluene/15 wt%-mCBP^a	634/610	82/—	—/0.98	0.03/—	—/1.85 × 10^6	176
p-1-PCzBN	Toluene/4 wt%-26DCzPPy^a	489/495^d	25/26^d	—/0.92	0.14/—	—/7.0 × 10^4	177
m-1-PCzBN	Toluene/4 wt%-26DCzPPy^a	502/500^d	27/30^d	—/0.95	0.09/—	—/6.3 × 10^4	177
CzBNCz	Toluene/1 wt%-mCBP^a	465/470	22/26	0.92/0.95	0.18/—	—/7.6 × 10^3	157
TCz-BN	Toluene	477	22	—	—	—	172
m-Cz-BNCz	Toluene/solid/1 wt%-PhCzBCz^a	519/521/520	38/39/47	0.97/—/0.92	0.08/—/—	—/—/8.6 × 10^5	179
CzBNNa	Toluene/1 wt%-mCBP^a	483/487	25/29	0.78/0.98	0.15/—	—/3.07 × 10^4	180
CzBNpyr	Toluene/1 wt%-mCBP^a	480/485	25/29	0.85/0.90	0.15/—	—/—	180
p-TBNCz	Toluene/1 wt%-PhCzBCz^a	484/490	23/29	0.92/0.92	0.12/—	—/1.4 × 10^4	181
TMInBN	Toluene/1 wt%-mCPBC^a	475/480^d	23/31^d	0.66/—	0.39/—	4.6 × 10^4/—	188
Mes-InBN	Toluene/1 wt%-mCPBC^a	475/479^d	23/40^d	0.70/—	0.40/—	4.6 × 10^4/—	188
Cz-InBN	Toluene/1 wt%-mCPBC^a	470/470^d	22/30^d	0.66/—	0.41/—	5.9 × 10^4/—	188
TCz-InBN	Toluene/1 wt%-mCPBC^a	470/473^d	22/45^d	0.69/—	0.42/—	5.4 × 10^4/—	188
AZA-BN	Toluene/4 wt%-mCBP^a	522/526	28/36	0.997/0.94	0.18/—	—/7.53 × 10^3	189
DBCz-Mes	Toluene/1 wt%-mCBP^a	452/452	14/16	0.99/0.98	0.14/—	2.9 × 10^4/—	91
BBCz-Y^e	Toluene/2 wt%-mCBP^a	549/549	42/48	0.85/0.90	0.14/—	1.0 × 10^5/1.1 × 10^5	155
BN-2Cz-tBu^e	Toluene	543	—	0.84	—	1.39 × 10^5	190
BBCz-G	Toluene/2 wt%-mCBP^a	517/519	34/50	0.90/0.99	0.14/—	1.8 × 10^5/1.9 × 10^5	155
BN-2Cz-tBu	Toluene	522	—	0.70	—	1.83 × 10^5	190
NBNP	Toluene/4 wt%-mCBP^a	500/502^d	29/33^d	—/0.93	0.09/—	—/3.0 × 10^5	191
TRZCzPh-BNCz	Toluene/3 wt%-CBP^a	514/516	34/37^d	0.930/0.976	0.13/—	2.13 × 10^6/8.8 × 10^5	192
TRZTPh-BNCz	Toluene/3 wt%-CBP^a	513/516	29/33^d	0.947/0.990	0.11/—	1.55 × 10^6/7.5 × 10^5	192
TPh-BNCz	Toluene	509	33	—	—	—	192
VTCzBN	Toluene/4 wt%-26DCzPPy^a	496/—	34/—	—/0.98	0.06/—	—/1.0 × 10^6	193
TCz-VTCzBN	Toluene/4 wt%-26DCzPPy^a	521/—	29/—	—/0.98	<0.01/—	—/0.9 × 10^6	193
PPZ-BN	Toluene/0.5 wt%-CBP^a	613/619	48/59	0.88/0.82	0.25/—	2.2 × 10^4/—	194

^{a} See Table 2 for the full compound name. ^{b} Same compound named differently. ^{c} Same compound named differently. ^{d} Taken from the EL spectrum. ^{e} Same compound named differently.

conditions because of the sluggishness of lithium–chlorine exchange, the N,B,N-embedded skeleton, **DPACzBN1**, was formed in 13% yield.

MR-TADF emitters synthesised by similar protocols are summarised in Fig. 15 and Table 18.[103,147,170,195–199] As all compounds were derived from 1-bromo-2-chloro-3-fluorobenzene, the final borylation step was conducted under harsh conditions. The phenothiazine group could be introduced using both S$_N$Ar (**PTZBN1**)[196] and Buchwald–Hartwig coupling (**Cz-PTZ-BN**)[197,198] reactions.

2.4.2 Late-stage bromination. The first DOBNA framework was synthesised *via* directed *ortho*-lithiation (see Section 2.1.1). Subsequently, borylation *via* lithium–halogen exchange became the most common one-pot borylation procedure. In this case, the halogen atom required for borylation is already contained in the starting material, and electron-rich substituents are sequentially introduced using the remaining key halogen atoms. As an alternative route, bromination just before borylation was attempted in some reports (Scheme 15 and Table 19).[191,200,201] The *ortho*-position of the two carbazolyl groups was easily

This journal is © The Royal Society of Chemistry 2024

Chem. Soc. Rev., 2024, **53**, 1624–1692 | **1645**

Scheme 14 Example of sequential MR-TADF precursor construction reported in ref. 195.

brominated by Br_2 or *N*-bromosuccinimide (NBS), probably because of the directing effect of these electron-donating groups. In the synthesis of **NBO** and **LTCz-BN**, bromination and subsequent one-pot borylation were conducted without purification. Although the synthesis of **tCzphB-ph** and **tCzphB-Fl** consisted of two independent steps, the first bromination by NBS proceeded in an almost quantitative yield. This late-stage bromination

procedure can facilitate the synthesis of complex structures, as it helps to avoid the use of difficult-to-obtain starting materials such as highly substituted benzenes.

2.4.3 Stepwise borylation and cyclisation. MR-TADF frameworks are generally constructed by one-pot methods with BBr_3 as a boron source. In some reports, an alternative stepwise procedure was applied (Fig. 16 and Table 20).[202–204] In this procedure, the key intermediate possessing a boronic acid pinacol ester (Bpin) group is synthesised in high or moderate yield by the sequential addition of ^{n}BuLi and 2-isopropoxy-4,4,5,5-tetramethyl-1,3,2-dioxaborolane (^{i}PrOBpin) to a bromine-containing precursor, with the subsequent intramolecular bora-Friedel–Crafts reaction affording fully cyclised target compounds.

The intermediate can be either isolated (**B-O-dpa**, **B-O-Cz**, **B-O-dmAc**, **B-dpa-Cz**, **B-dpa-dmAc**, and **B-dpa-SpiroAc**) or used without purification (**Br-DBA** and **B-O-dpAc**). Notably, **Br-DBA** was also synthesised by the basic one-pot borylation method (Fig. 8 and Table 6) with a comparable total yield ($\sim$40%).[120,124]
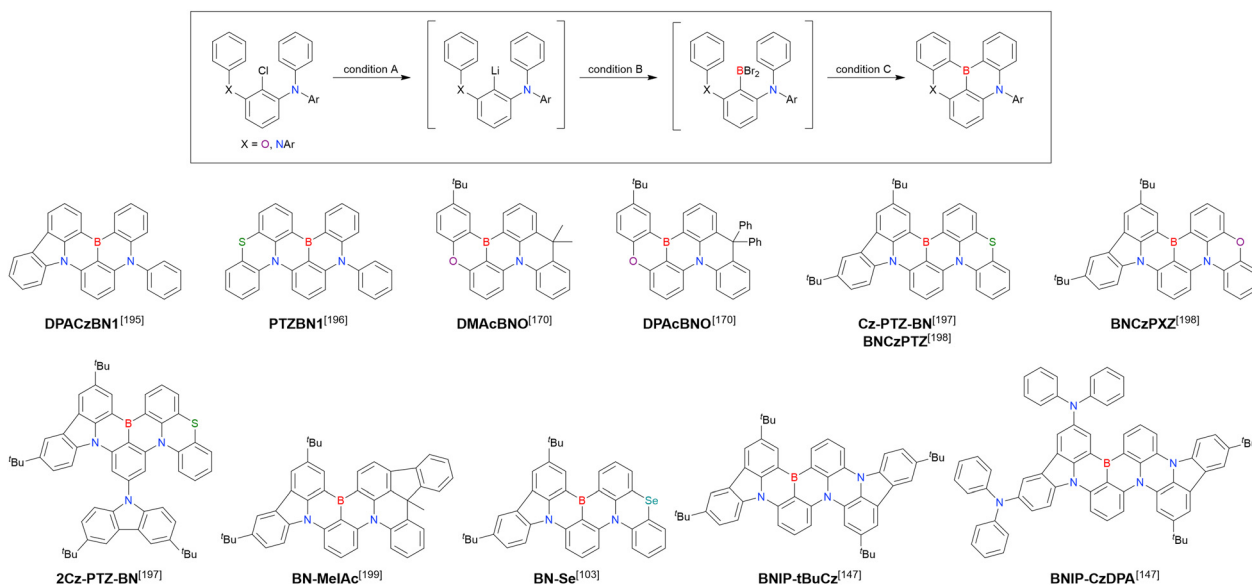

Fig. 15 MR-TADF emitters synthesised by sequential electrophilic aromatic substitution and Buchwald–Hartwig coupling reactions.

Table 18 Conditions used to synthesise the compounds shown in Fig. 15

Compound	Condition A[a]	Condition B[a]	Condition C[a]	Solvent	Yield [%]	Ref.
DPACzBN1	^{t}BuLi (2.0)/80 °C, 3 h	BBr_3 (2.0)/rt, 3 h	NEt^{i}Pr$_2$ (2.0)/180 °C, 24 h	Mesitylene	13	195
PTZBN1	^{t}BuLi (2.4)/60 °C, 2 h	BBr_3 (1.5)/rt, 1 h	NEt^{i}Pr$_2$ (2.0)/160 °C, 24 h	Mesitylene	25	196
DMAcBNO	^{t}BuLi (2.0)/60 °C, 2 h	BBr_3 (2.0)/rt, 1 h	NEt^{i}Pr$_2$ (2.0)/140 °C, 24 h	^{t}Bu-Benzene	25	170
DPAcBNO	^{t}BuLi (2.0)/60 °C, 2 h	BBr_3 (2.0)/rt, 1 h	NEt^{i}Pr$_2$ (2.0)/140 °C, 24 h	^{t}Bu-Benzene	32	170
Cz-PTZ-BN	^{t}BuLi (2.0)/60 °C, 2 h	BBr_3 (2.0)/rt, 1 h	NEt^{i}Pr$_2$ (2.0)/150 °C, 6 h	^{t}Bu-Benzene	22	197
	^{t}BuLi (2.0)/60 °C, 2 h	BBr_3 (2.0)/rt, 1 h	NEt^{i}Pr$_2$ (2.0)/150 °C, 8 h	^{t}Bu-Benzene	20	198
BNCzPXZ	^{t}BuLi (2.0)/60 °C, 2 h	BBr_3 (2.0)/rt, 1 h	NEt^{i}Pr$_2$ (2.0)/150 °C, 8 h	^{t}Bu-Benzene	18	198
2Cz-PTZ-BN	^{t}BuLi (2.0)/60 °C, 2 h	BBr_3 (2.0)/rt, 1 h	NEt^{i}Pr$_2$ (2.0)/150 °C, 6 h	^{t}Bu-Benzene	16	197
BN-MelAc	^{t}BuLi (2.0)/60 °C, 2 h	BBr_3 (2.0)/rt, 1 h	NEt^{i}Pr$_2$ (2.0)/150 °C, 24 h	Mesitylene	35	199
BN-Se	^{t}BuLi (2.0)/60 °C, 3 h	BBr_3 (2.0)/rt, 1 h	NEt^{i}Pr$_2$ (2.0)/150 °C, 12 h	^{t}Bu-Benzene	34	103
BNIP-tBuCz	^{t}BuLi (2.2)/60 °C, 1 h	BBr_3 (1.5)/rt, 1 h	NEt^{i}Pr$_2$ (1.2)/130 °C, 24 h	^{t}Bu-Benzene	54	147
BNIP-CzDPA	^{t}BuLi (2.2)/60 °C, 1 h	BBr_3 (1.5)/rt, 1 h	NEt^{i}Pr$_2$ (1.2)/130 °C, 24 h	^{t}Bu-Benzene	40	147

[a] Numbers in parentheses refer to reagent loadings (equivalents).

1646 | *Chem. Soc. Rev.*, 2024, **53**, 1624–1692

This journal is © The Royal Society of Chemistry 2024

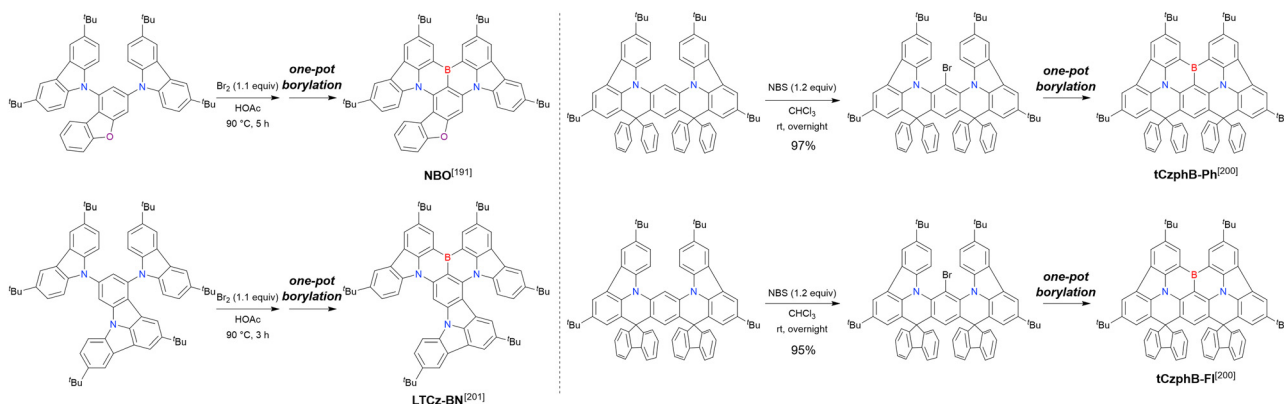**Scheme 15** MR-TADF emitters synthesised *via* late-stage bromination.

Table 19 Conditions used to synthesise the compounds shown in Scheme 15

Compound	Condition A[a]	Condition B[a]	Condition C[a]	Solvent	Yield [%]	Ref.
NBO	^{n}BuLi (3.0)/70 °C, 1 h	BBr$_3$ (4.0)/rt, 0.5 h	NEt^{i}Pr$_2$ (2.9)/130 °C, 18 h	^{t}Bu-Benzene	12 (2 steps)	191
tCzphB-Ph	^{n}BuLi (1.5)/−40 °C, 2 h	BBr$_3$ (2.9)/rt, overnight	NEt^{i}Pr$_2$ (2.9)/130 °C, 4 h	^{t}Bu-Benzene	61	200
tCzphB-Fl	^{n}BuLi (1.5)/−40 °C, 2 h	BBr$_3$ (2.9)/rt, overnight	NEt^{i}Pr$_2$ (2.9)/130 °C, 4 h	^{t}Bu-Benzene	55	200
LTCz-BN	^{t}BuLi (4.0)/70 °C, 1 h	BBr$_3$ (4.2)/rt, 0.5 h	NEt^{i}Pr$_2$ (3.2)/130 °C, 24 h	^{t}Bu-Benzene	10 (2 steps)	201

[a] Numbers in parentheses refer to reagent loadings (equivalents).
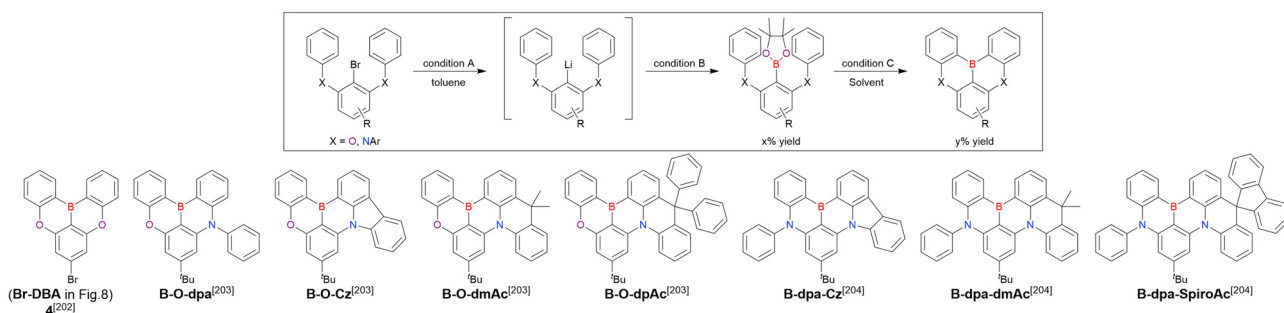
Fig. 16 MR-TADF emitters synthesised by stepwise borylation–cyclisation.

2.4.4 Photophysical properties.
The photophysical properties of the compounds discussed in Section 2.4 are summarised in Table 21. Although a wide variety of structures are included, their properties are in line with previous discussions in Sections 2.1.4, 2.2.2, and 2.3.2.

2.5 Simultaneous introduction of two boron atoms

2.5.1 One nitrogen and two boron atoms. In 2019, Hatakeyama *et al.* developed a boron-enriched MR-TADF material, azadiboranaphthoanthracene (**ADBNA**), which contains two boron atoms and one nitrogen atom and corresponds to

Table 20 Conditions used to synthesise the compounds shown in Fig. 16

Compound	Condition A[a]	Condition B[a]	x [%]	Condition C[a]	Solvent	y [%]	Ref.
Br-DBA	^{n}BuLi (—)/rt, 2 h	^{i}PrOBpin (1.2)/rt, 2 h	—	AlCl$_3$ (4.8)/100 °C, 3 h	Toluene	37 (2 steps)	202
B-O-dpa	^{n}BuLi (1.2)/−20 °C, 1 h	^{i}PrOBpin (3.0)/rt, 1 h	65	AlCl$_3$ (4.0), NEt^{i}Pr$_2$ (5.0)/110 °C, 2 h	Chlorobenzene	43	203
B-O-Cz	^{n}BuLi (1.5)/−20 °C, 1 h	^{i}PrOBpin (3.9)/rt, 1 h	76	AlCl$_3$ (4.0), NEt^{i}Pr$_2$ (5.0)/110 °C, 2 h	Chlorobenzene	47	203
B-O-dmAc	^{n}BuLi (2.5)/−20 °C, 1 h	^{i}PrOBpin (4.5)/rt, 1 h	49	AlCl$_3$ (4.0), NEt^{i}Pr$_2$ (5.0)/110 °C, 2 h	Chlorobenzene	36	203
B-O-dpAc	^{n}BuLi (2.5)/−20 °C, 1 h	^{i}PrOBpin (5.0)/rt, 1 h	—	AlCl$_3$ (6.0), NEt^{i}Pr$_2$ (2.4)/110 °C, 2 h	Chlorobenzene	33 (2 steps)	203
B-dpa-Cz	^{n}BuLi (2.0)/−20 °C, 1 h	^{i}PrOBpin (4.0)/rt, 1 h	65	AlCl$_3$ (5.0), NEt^{i}Pr$_2$ (2.0)/110 °C, 2 h	Chlorobenzene	57	204
B-dpa-dmAc	^{n}BuLi (2.5)/−20 °C, 1 h	^{i}PrOBpin (4.5)/rt, 1 h	84	AlCl$_3$ (3.0), NEt^{i}Pr$_2$ (1.0)/110 °C, 2 h	Toluene	25	204
B-dpa-SpiroAc	^{n}BuLi (2.8)/−20 °C, 1 h	^{i}PrOBpin (5.0)/rt, 1 h	44	AlCl$_3$ (5.0), NEt^{i}Pr$_2$ (2.0)/110 °C, 2 h	Toluene	50	204

[a] Numbers in parentheses refer to reagent loadings (equivalents).

This journal is © The Royal Society of Chemistry 2024

Chem. Soc. Rev., 2024, **53**, 1624–1692 | **1647**

Table 21 Photophysical properties of the compounds shown in Fig. 15, 16 and Scheme 15

Compound	Condition	λ_{PL}^{max} [nm]	FWHM [nm]	Φ_{PL} [—]	ΔE_{ST} [eV]	k_{RISC} [s^{-1}]	Ref.
DPACzBN1	Toluene/3 wt%-26DCzPPy^a	469/479	23/31	—/0.98	—/0.11	—/1.2 × 10^4	195
PTZBN1	Toluene/2 wt%-26DCzPPy^a	490/497	41/44	—/0.98	—/0.16	—/1.11 × 10^5	196
DMAcBNO	Toluene/3 wt%-26DCzPPy^a	462/470	34/41	—/0.99	0.23/—	—/1.40 × 10^4	170
DPAcBNO	Toluene/3 wt%-26DCzPPy^a	462/468	33/39	—/0.98	0.19/—	—/1.75 × 10^4	170
Cz-PTZ-BN^b	Toluene/3 wt%-PhCzBCz^a	510/524	37/50	0.84/0.91	0.11/—	—/8.1 × 10^4	197
BNCzPTZ^b	Toluene/15 wt%-PhCzBCz^a	509/—	42/—	0.84/0.91	0.09/—	—/1.54 × 10^5	198
BNCzPXZ	Toluene/7 wt%-PhCzBCz^a	508/—	36/—	0.88/0.94	0.13/—	—/2.31 × 10^4	198
2Cz-PTZ-BN	Toluene/3 wt%-PhCzBCz^a	505/512	38/48	0.87/0.96	0.09/—	—/1.05 × 10^5	197
BN-MelAc	Toluene/2-MeTHF/1 wt%-DMIC-TRZ^a	497/—/503	30/30/33	—/—/0.96	—/0.11/—	—/—/6.3 × 10^4	199
BN-Se	Toluene/1 wt%-DMIC-TRZ^a	502/505	42/44	0.99/0.98	0.08/—	1.6 × 10^6/1.2 × 10^6	103
BNIP-tBuCz	Toluene/1 wt%-DMIC-TRZ^a	564/570	60/61	—/0.96	0.08/0.13	—/0.9 × 10^4	147
BNIP-CzDPA	Toluene/1 wt%-DMIC-TRZ^a	583/585	49/57	—/0.95	0.06/0.12	—/0.9 × 10^4	147
NBO	Toluene/4 wt%-mCBP^a	487/—	27/—	—/0.92	0.12/—	—/9.3 × 10^5	191
tCzphB-Ph	Toluene/2 wt%-TPSS^a	523/527	21/23	—/0.98	—/0.04	—/—	200
tCzphB-Fl	Toluene/2 wt%-TPSS^a	531/535	21/25	—/0.93	—/0.04	—/—	200
LTCz-BN	Toluene/5 wt%-mCBP^a	497/—	27/—	—/0.93	0.10/—	—/8.3 × 10^5	201
B-O-dpa	Toluene/10 wt%-DPEPO^a	433/—	28/—	—/0.86	0.18/—	—/0.83 × 10^4	203
B-O-Cz	Toluene/10 wt%-DPEPO^a	441/—	27/—	—/0.94	0.15/—	—/4.02 × 10^4	203
B-O-dmAc	Toluene/10 wt%-DPEPO^a	461/—	38/—	—/0.91	0.11/—	—/1.82 × 10^4	203
B-O-dpAc	Toluene/10 wt%-DPEPO^a	463/—	38/—	—/0.94	0.06/—	—/3.12 × 10^4	203
B-dpa-Cz	Toluene/3 wt%-mCPB^a	466/469	27/33	—/0.94	0.15/—	—/2.74 × 10^4	204
B-dpa-dmAc	Toluene/3 wt%-mCPB^a	472/476	31/38	—/0.98	0.16/—	—/4.48 × 10^4	204
B-dpa-SpiroAc	Toluene/3 wt%-mCPB^a	472/476	31/38	—/0.92	0.14/—	—/4.97 × 10^4	204

^{a} See Table 2 for the full compound name. ^{b} Same compound named differently.

DABNA-1 inverted through the interchange of boron and nitrogen positions (Fig. 17a).[205] The one-pot borylation of the tribrominated starting material afforded an intermediate possessing two B–Br bonds, which was then reacted with the desired Grignard reagents to afford ADBNA derivatives. One year later, Wang *et al.* reported a different route to synthesise ADBNA-based frameworks (Fig. 17b).[206] The key intermediate, **Pre-ADBNA**, was prepared in 65% yield by treating the lithiated starting material with dimethyl mesitylboronate (MesB(OMe)$_2$) (2.0 equiv.) and subsequently reacted with BBr$_3$ and ArLi to afford cyclised B,N,B-embedded compounds. Notably, both symmetric and non-symmetric products were obtained by controlling the reagent amounts. When 1.0 equiv. of BBr$_3$ and 1.2 equiv. of ArLi were used, the B–Ar group was introduced only at the acyclic site of **Pre-ADBNA**. However, treatment with 5.0 equiv. of BBr$_3$ for a longer time and the use of 2.4 equiv. of ArLi resulted in the replacement of the remaining B-Mes site of **Pre-ADBNA** with an additional B–Ar group.

2.5.2 One-pot double borylation. Finally, the simultaneous introduction of two fully cyclised boron atoms using the basic one-pot borylation procedure are discussed. In 2020, Yasuda *et al.* reported the synthesis of a doubly borylated compound, **BBCz-R** (Scheme 16), starting from 1-bromo-2,6-difluorobenzene.[155] One equivalent of 3,6-di-*tert*-butylcarbazole was introduced by the standard S$_N$Ar reaction. Subsequently, a similar type of reaction with 2,8-di-*tert*-butyl-5,11-dihydroindolo[3,2-*b*]carbazole was conducted at the remaining fluorine group to form the dibrominated precursor. The final one-pot borylation step did not proceed regioselectively, *i.e.*, a regioisomer (**BBCz-Y-II**, 7% yield) was obtained in addition to the desired **BBCz-R** (5% yield).

The procedure proposed by Yasuda *et al.* is now one of the most common strategies for one-pot double borylation (Fig. 18 and Table 22).[117,155,163,167,207,208] The sequential S$_N$Ar reactions

of 2-bromo-1,6-difluorobenzene (first mono-substitution, then dimerisation) afforded diverse doubly borylated compounds. The data presented in ref. 207 (**SBON** and **SBSN**) suggest that protonation after lithium–bromine exchange is a common side reaction and can affect the yield of the final product. The possible proton sources are residual water in the solvents, HBr contained in BBr$_3$, protons generated during C–H borylation, and so on.

Scheme 17 presents another versatile route to synthesise doubly borylated MR-TADF emitters.[209] This procedure starts from 1,4-dibromo-2,3,5,6-tetrafluorobenzene and affords the dibrominated precursor through multiple S$_N$Ar reactions. A hexasubstituted doubly N,B,N-embedded framework is then constructed by subsequent one-pot borylation. This protocol was adopted in some studies to prepare the desired MR-TADF frameworks (Fig. 19 and Table 23).[210–214] In addition to tetra-carbazolyl substituted compounds (**R-BN**, **R-TBN**, **R-TPhBN**, and **BNS**), the combination of a carbazolyl group and chalcogen bridge (**BNO1**, **BNO2**, **BNO3**, **DBNS**, **DBNS-*t*Bu**, and **BNNO**) was also achieved. As mentioned in the following subsection, these species possess *para*-positioned boron and electron-donating atoms, which is beneficial for obtaining long-wavelength fluorescence.

Other synthesis routes for doubly borylated compounds are summarised in Fig. 20 and Table 24.[92,155,181,215,216] Overall, the reaction yields are lower than those observed for single borylation. Regioselectivity in electrophilic C–H borylation should be considered because poor selectivity causes the formation of undesired isomers after one-pot borylation. For example, the precursors of ***m*-DBCz** and **DBTN-2** have similar chemical structures except for ^{t}Bu groups on the central two benzene rings, which results in different regioselectivity in one-pot borylation. Although double lithiation at the same benzene ring is a good way to avoid the regioselectivity problem, the
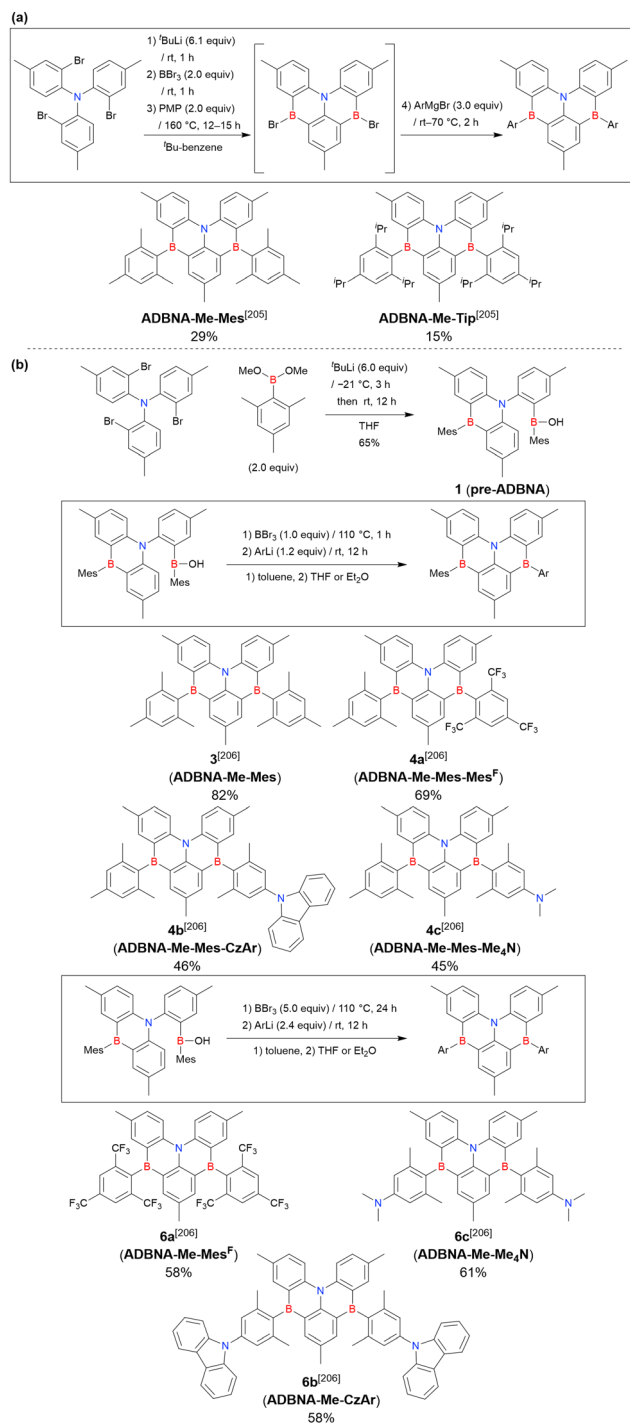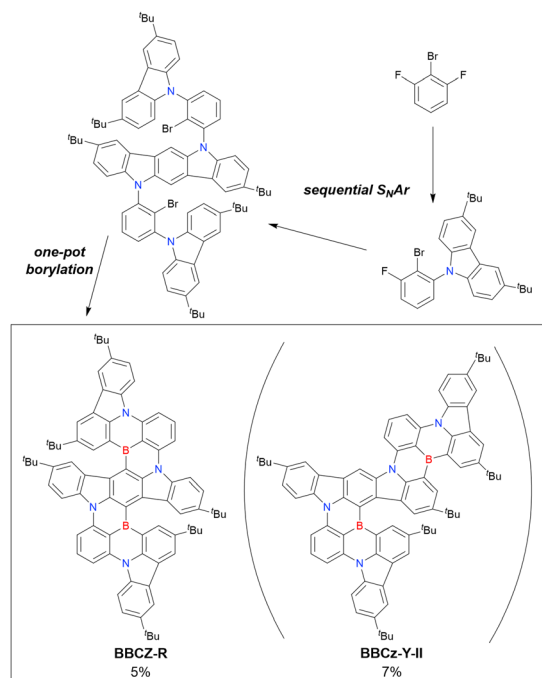
1648 | *Chem. Soc. Rev.*, 2024, **53**, 1624–1692

This journal is © The Royal Society of Chemistry 2024

Fig. 17 Synthesis of boron-bridged compounds reported in ref. 205 and 206.

Scheme 16 Synthesis of doubly borylated compound from 1-bromo-2,6-difluorobenzene reported in ref. 155.

red-shifted emission wavelength. This difference in λ_{PL}^{max} was attributed to the FMO energy levels. Although both HOMO and LUMO energy levels of **ADBNA** are lower than those of **DABNA-1**, the larger decrease in the LUMO energy level of **ADBNA** results in a smaller HOMO–LUMO energy gap.[205] In the case of compounds obtained by one-pot double borylation, λ_{PL}^{max} largely depends on the relative position of boron and electron-donating atoms (or groups). If two electron-donating atoms are placed in the *para*-position, λ_{PL}^{max} substantially increases to >600 nm (*e.g.*, 615 nm for **BBCz-R**).[155] In particular, given that the compounds in Fig. 19 were obtained from 1,4-dibromo-2,3,5,6-tetrafluorobenzene, *para*-type substitution was inevitable and led to orange or red emission with λ_{PL}^{max} > 600 nm (660–662 nm for **R-BN**,[209,210] 684–692 nm for **R-TBN**,[209,210] 696 nm for **R-TPhBN**,[210] 605 nm for **BNO1**,[211] 609 nm for **BNO2**,[211] 616 nm for **BNO3**,[211] 631 nm for **DBNS**,[212] 641 nm for **DBNS-*t*Bu**,[212] 737 nm for **BNS**,[213] and 637 nm for **BNNO**[214]). On the other hand, two electron-donating atoms in a *meta*-relationship had a smaller effect on the PL wavelength, resulting in λ_{PL}^{max} = 440–520 nm.

The relative position of the two boron atoms strongly influences the TADF properties. When two boron atoms are placed in a *meta*-position, a decrease in ΔE_{ST} and an increase in k_{RISC} can be expected because the enlarged π-plane enhances long-range electronic delocalisation.[74] Wang *et al.* evaluated the effect of double borylation by comparing ***p*-TBNCz** and ***m*-DBCz** (Fig. 21)[181] and showed that with an increase in the number of boron atoms, ΔE_{ST} decreased, whereas k_{RISC} increased. On the other hand, two *para*-positioned boron atoms do not improve the TADF properties because the MR effect is partially broken by the undesired π-extension. In this case, the positive effect of enhanced long-range electronic delocalisation is negated, and ΔE_{ST} (0.1–0.2 eV) and

reaction yields remain low (**BBCz-DB**,[155] **BSBS-N1**,[92] **BOBO-Z**,[215] **BOBS-Z**,[215] and **BSBS-Z**[215]). Moreover, the simultaneous introduction of three or more boron atoms has not been achieved to date.

2.5.3 Photophysical properties. Table 25 lists the photophysical properties of doubly borylated MR-TADF emitters, showing that compounds possessing one nitrogen and two boron atoms (ADBNA derivatives) exhibit photophysical parameters comparable to those of DABNA derivatives, except for the

This journal is © The Royal Society of Chemistry 2024

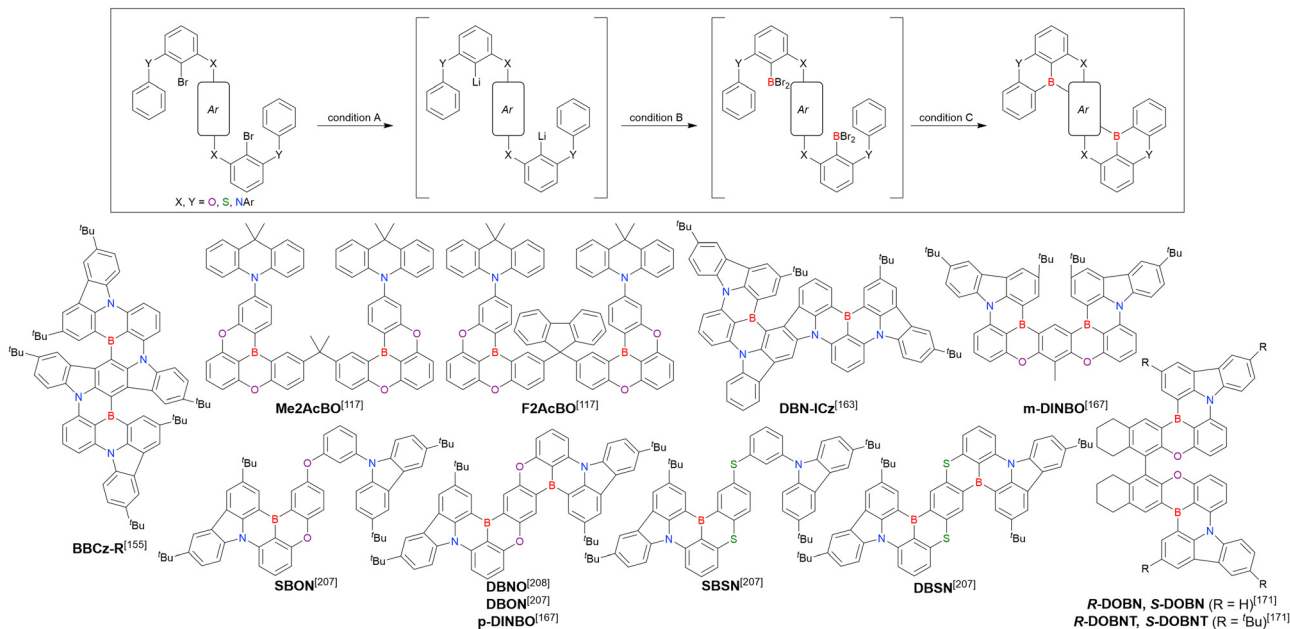*Chem. Soc. Rev.*, 2024, **53**, 1624–1692 | **1649**

Fig. 18 MR-TADF emitters synthesised by one-pot double borylation.

Table 22 Conditions used to synthesise the compounds shown in Fig. 18

Compound	Condition A[a]	Condition B[a]	Condition C[a]	Solvent	Yield [%]	Ref.
BBCz-R	^{n}BuLi (3.0)/rt, 4 h	BBr$_3$ (3.0)/rt, 12 h	NEt^{i}Pr$_2$ (4.6)/170 °C, 24 h	^{t}Bu-Benzene	5	155
Me2AcBO	^{t}BuLi (4.0)/rt, 2 h	BBr$_3$ (—)/rt, 2 h	NEt^{i}Pr$_2$ (—)/180 °C, 24 h	^{t}Bu-Benzene	8	117
F2AcBO	^{t}BuLi (4.0)/rt, 2 h	BBr$_3$ (—)/rt, 2 h	NEt^{i}Pr$_2$ (—)/180 °C, 24 h	^{t}Bu-Benzene	16	117
DBN-ICz	^{n}BuLi (6.0)/60 °C, 24 h	BBr$_3$ (6.0)/rt, 0.5 h	NEt^{i}Pr$_2$ (9.0)/120 °C, 5 h	^{t}Bu-Benzene	36	163
m-DINBO	^{n}BuLi (2.3)/60 °C, 2 h	BBr$_3$ (3.1)/rt, 2 h	NEt^{i}Pr$_2$ (4.1)/170 °C, 24 h	^{t}Bu-Benzene	22	167
SBON	^{n}BuLi (3.9)/80 °C, 5 h	BBr$_3$ (7.8)/rt, 3 h	NEt^{i}Pr$_2$ (6.1)/190 °C, 16 h	^{t}Bu-Benzene	16	207
DBNO	^{t}BuLi (4.0)/0 °C, 6 h	BBr$_3$ (2.1)/rt, 2 h	NEt^{i}Pr$_2$ (5.0)/120 °C, 24 h	^{t}Bu-Benzene	16	208
	^{n}BuLi (3.9)/80 °C, 5 h	BBr$_3$ (7.8)/rt, 3 h	NEt^{i}Pr$_2$ (6.1)/190 °C, 16 h	^{t}Bu-Benzene	10	207
	^{n}BuLi (2.3)/60 °C, 2 h	BBr$_3$ (3.1)/rt, 2 h	NEt^{i}Pr$_2$ (4.1)/170 °C, 48 h	^{t}Bu-Benzene	2	167
SBSN	^{n}BuLi (4.0)/80 °C, 5 h	BBr$_3$ (8.1)/rt, 3 h	NEt^{i}Pr$_2$ (6.4)/190 °C, 16 h	^{t}Bu-Benzene	24	207
DBSN	^{n}BuLi (4.0)/80 °C, 5 h	BBr$_3$ (8.1)/rt, 3 h	NEt^{i}Pr$_2$ (6.4)/190 °C, 16 h	^{t}Bu-Benzene	12	207
S-DOBN	^{n}BuLi (4.0)/90 °C, 2 h	BBr$_3$ (4.0)/rt, 1 h	NEt^{i}Pr$_2$ (11)/120 °C, 12 h	^{t}Bu-Benzene	10	171
S-DOBNT	^{n}BuLi (4.0)/90 °C, 2 h	BBr$_3$ (4.0)/rt, 1 h	NEt^{i}Pr$_2$ (11)/120 °C, 12 h	^{t}Bu-Benzene	12	171

[a] Numbers in parentheses refer to reagent loadings (equivalents).
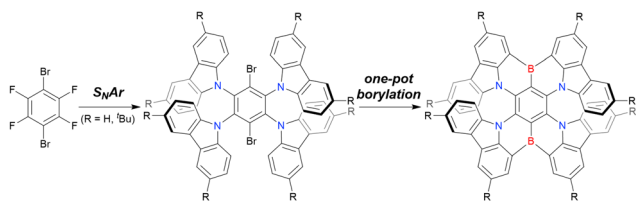
Scheme 17 Synthesis of a doubly borylated compound from 1,4-dibromo-2,3,5,6-tetrafluorobenzene.

k_{RISC} ($<1.0 \times 10^5$ s^{-1}) remain moderate. In particular, **BNO1**, **BNO2**, and **BNO3** showed a very weak TADF character owing to the *para*-positioned boron atoms and highly planar structures.[211]

2.6 Summary

Numerous MR-TADF compounds have been synthesised since the first report of one-pot borylation in 2015. Although the

basic protocol for one-pot borylation has been established, the synthesis route for borylation precursors needs to be tailored according to their structures. The obtained compounds usually show TADF properties and small FWHMs, benefiting from the MR effect. In addition, the results shown in Fig. 21 induce strong interest in introducing two or more boron atoms into MR-TADF frameworks. However, as discussed above, the simultaneous introduction of multiple boron atoms using one-pot protocols remains challenging. The further development of multiple borylation methodologies should enable the development of superior materials with MR-TADF characteristics.

3. One-shot borylation

Since Hatakeyama *et al.* proposed the molecular design of boron-embedded MR compounds with DOBNA and DABNA frameworks and their synthesis protocol (one-pot borylation),
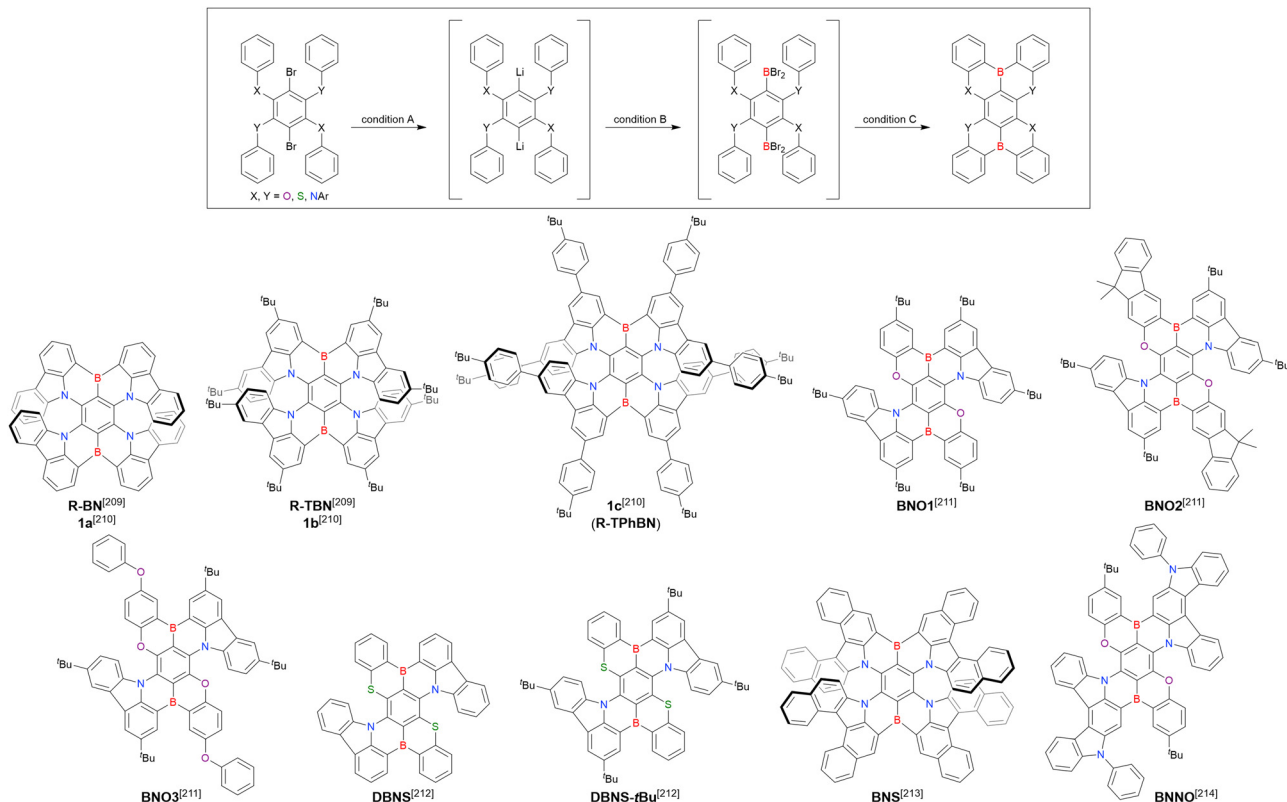
1650 | *Chem. Soc. Rev.*, 2024, **53**, 1624–1692

This journal is © The Royal Society of Chemistry 2024

Fig. 19 Double-borylated MR-TADF emitters synthesised from hexa-substituted benzene.

Table 23 Conditions used to synthesise the compounds shown in Fig. 19

Compound	Condition A[a]	Condition B[a]	Condition C[a]	Solvent	Yield [%]	Ref.
R-BN	[n]BuLi (6.1)/60 °C, 24 h	BBr$_3$ (12)/rt, 0.5 h	NEt[i]Pr$_2$ (18)/120 °C, 5 h	[t]Bu-Benzene	38	209
	[n]BuLi (4.0)/rt, 12 h	BBr$_3$ (4.0)/rt, 24 h	NEt[i]Pr$_2$ (4.0)/180 °C, 72 h	o-Dichlorobenzene	53	210
R-TBN	[n]BuLi (6.1)/60 °C, 24 h	BBr$_3$ (12)/rt, 0.5 h	NEt[i]Pr$_2$ (18)/120 °C, 5 h	[t]Bu-Benzene	40	209
	[n]BuLi (4.0)/rt, 12 h	BBr$_3$ (4.0)/rt, 24 h	NEt[i]Pr$_2$ (4.0)/180 °C, 72 h	o-Dichlorobenzene	25	210
R-TPhBN	[n]BuLi (4.0)/rt, 12 h	BBr$_3$ (4.0)/rt, 24 h	NEt[i]Pr$_2$ (4.0)/180 °C, 72 h	o-Dichlorobenzene	23	210
BNO1	[n]BuLi (—)/60 °C, 8 h	BBr$_3$ (—)/rt, 1 h	NEt[i]Pr$_2$ (—)/170 °C, 24 h	Mesitylene	34	211
BNO2	[n]BuLi (—)/60 °C, 8 h	BBr$_3$ (—)/rt, 1 h	NEt[i]Pr$_2$ (—)/170 °C, 24 h	Mesitylene	38	211
BNO3	[n]BuLi (—)/60 °C, 8 h	BBr$_3$ (—)/rt, 1 h	NEt[i]Pr$_2$ (—)/170 °C, 24 h	Mesitylene	31	211
DBNS	[n]BuLi (2.5)/rt, 4 h	BBr$_3$ (2.5)/rt, 2 h	NEt[i]Pr$_2$ (3.9)/170 °C, 24 h	[t]Bu-Benzene	30	212
DBNS-tBu	[n]BuLi (2.5)/rt, 4 h	BBr$_3$ (2.5)/rt, 2 h	NEt[i]Pr$_2$ (3.5)/170 °C, 24 h	[t]Bu-Benzene	16	212
BNS	[n]BuLi (4.0)/60 °C, 2 h	BBr$_3$ (4.0)/rt, 6 h	NEt[i]Pr$_2$ (4.0)/180 °C, 48 h	o-Dichlorobenzene	22	213
BNNO	[n]BuLi (6.0)/60 °C, 2 h	BBr$_3$ (6.0)/rt, 0.5 h	NEt[i]Pr$_2$ (10)/135 °C, 8 h	Xylene	30	214

[a] Numbers in parentheses refer to reagent loadings (equivalents).

numerous corresponding derivatives have been prepared using the same methodology, as described in Section 2. One-pot borylation generally relies on metal–boron exchange followed by intramolecular tandem bora-Friedel–Crafts reactions. Therefore, in many cases, the borylation precursor should possess a halogen (Cl, Br, or I) atom at the desired borylation position to provide a scaffold for metal–halogen exchange. However, the ability of halogen groups to engage in cross-couplings often interferes with the desired reactions or increases the number of steps in precursor synthesis. In addition, molecules with multiple boron atoms are difficult to synthesise because one-pot borylation proceeds *via* organometallic species. Indeed, MR compounds containing more than three boron atoms have

not been synthesised by one-pot borylation. Thus, despite its power for the synthesis of boron-embedded MR compounds, one-pot borylation is by no means a panacea.

This section focuses on one-shot borylation, which has been established in the last five years as a complementary method to one-pot borylation and involves successive intra- and intermolecular bora-Friedel–Crafts reactions converting multiple C–H bonds into C–B bonds in one shot. Unlike the one-pot borylation protocol, the one-shot borylation does not require functional groups such as halogens and features easier precursor synthesis, enabling the synthesis of MR compounds containing multiple (up to eight) boron atoms. This section overviews the one-shot borylation protocol and discusses its selectivity and the optical properties of
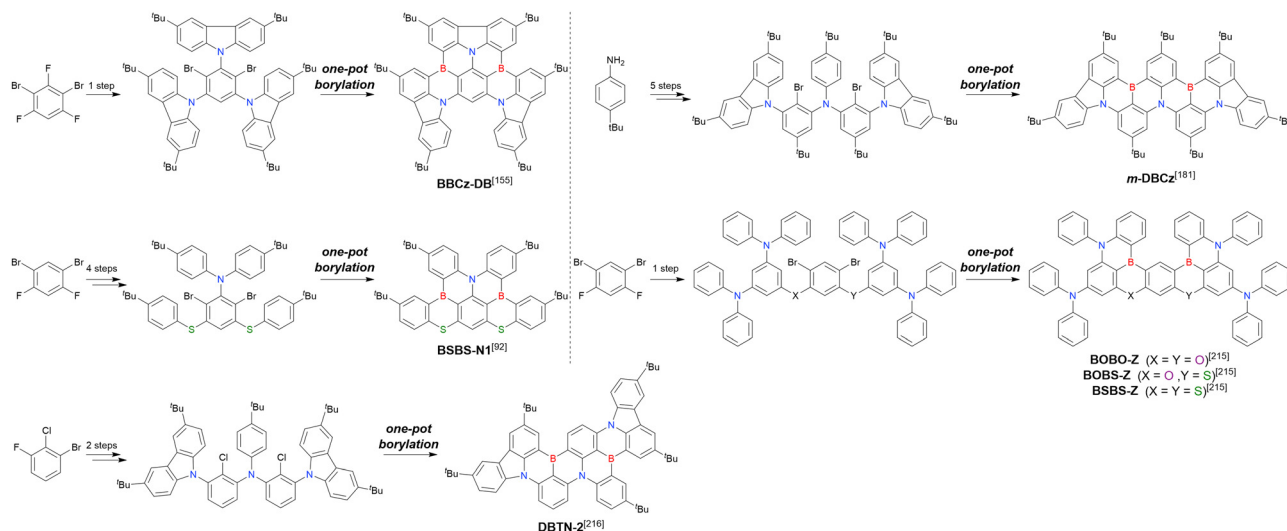
This journal is © The Royal Society of Chemistry 2024

Chem. Soc. Rev., 2024, **53**, 1624–1692 | **1651**

Fig. 20 Double-borylated MR-TADF emitters not included in Fig. 18 and 19.

Table 24 Conditions used to synthesise the compounds shown in Fig. 20

Compound	Condition A[a]	Condition B[a]	Condition C[a]	Solvent	Yield [%]	Ref.
BBCz-DB	^{n}BuLi (2.5)/rt, 4 h	BBr$_3$ (2.5)/rt, 12 h	NEt^{i}Pr$_2$ (3.8)/170 °C, 24 h	^{t}Bu-Benzene	36	155
m-DBCz	^{t}BuLi (4.0)/0 °C, 12 h	BBr$_3$ (3.0)/rt, 6 h	PMP (6.0)/160 °C, 24 h	^{t}Bu-Benzene	13	181
BSBS-N1	^{t}BuLi (4.8)/rt, 4 h	BBr$_3$ (3.0)/rt, 12 h	PMP (4.0)/170 °C, 24 h	^{t}Bu-Benzene	18	92
BOBO-Z	^{n}BuLi (3.0)/60 °C, 2 h	BBr$_3$ (3.0)/rt, 2 h	PMP (4.5)/160 °C, 24 h	^{t}Bu-Benzene	20	215
BOBS-Z	^{n}BuLi (4.4)/60 °C, 2 h	BBr$_3$ (2.4)/rt, 2 h	PMP (4.0)/160 °C, 24 h	^{t}Bu-Benzene	20	215
BSBS-Z	^{n}BuLi (4.4)/60 °C, 2 h	BBr$_3$ (2.4)/rt, 2 h	PMP (4.0)/160 °C, 24 h	^{t}Bu-Benzene	14	215
DBTN-2	^{t}BuLi (2.5)/60 °C, 6 h	BBr$_3$ (2.5)/rt, 6 h	NEt^{i}Pr$_2$ (2.5)/120 °C, 12 h	^{t}Bu-Benzene	5	216

[a] Numbers in parentheses refer to reagent loadings (equivalents).

the resulting compounds. In addition, synthesis protocols involving not only C–H but also N–H borylation and a recently reported sequential one-pot/one-shot borylation protocol are presented.

3.1 One-shot (C–H) borylation

In 2018, Hatakeyama et al. demonstrated the potential utility of one-shot borylation protocols.[217] In the two-step synthesis of B$_4$N$_3$-doped nanographene B4, the crucial step is the quadruple borylation of triarylamines that converts 11 C–H bonds into C–B bonds in one shot. In addition, the judicious choice of the Brønsted base enables the selective double and triple borylation of triarylamines. The borylation precursor, $N^1,N^1,N^3,$-N^3,N^5,N^5-hexakis(4-methylphenyl)-1,3,5-benzenetriamine, was obtained from 1,3,5-tribromobenzene by Buchwald–Hartwig coupling in 98% yield, and the subsequent one-shot quadruple borylation proceeded in the presence of 12 equiv. of boron triiodide (BI$_3$) under reflux conditions (bath temperature = 200 °C) to afford the target compound B4 in 35% isolated yield and a small amount of B3 as a byproduct (Scheme 18). Notably, B4 was synthesised using only the highly reactive BI$_3$ and not other boron sources such as boron trichloride (BCl$_3$) and BBr$_3$. Selective double and triple borylations were also achieved under optimal conditions. In the presence of 5.0 equiv. of BI$_3$ and 2.0 equiv. of Ph$_3$B, selective double borylation occurred under reflux conditions (bath temperature = 190 °C) to afford B2 in 76% yield.

In contrast, triple borylation occurred at elevated temperatures (bath temperature = 200 °C) in 1,2,4-trichlorobenzene as a high-boiling-point solvent to afford B3 in 45% yield. In addition, the double one-shot borylation of a fluorine-bearing triarylamine proceeded under similar conditions to afford B2-F in 58% yield (Scheme 18). Notably, the use of Ph$_3$B as a Brønsted base was crucial for B3 formation. The addition of Ph$_3$B reduced the concentration of HI via its retro-Friedel–Crafts reaction. As a result, adequate HI concentrations were maintained in situ, and the Friedel–Crafts/retro-Friedel–Crafts reaction of the products was not inhibited to selectively give the thermodynamic product, i.e., B3. The reduction in HI concentration simultaneously increased the yield by suppressing competitive C–N bond cleavage. Indeed, the reaction in the absence of Ph$_3$B selectively afforded B3 in significantly reduced yield (13%). In contrast, other Brønsted bases such as NEt^{i}Pr$_2$ and N,N-dimethyltoluidine did not induce the formation of B3. Amine-type Brønsted bases effectively captured HI and therefore hindered the Friedel–Crafts/retro-Friedel–Crafts reaction of the products to afford only B2 as the kinetic product (44–54%). Hence, the trapping of Brønsted acids (e.g., HBr and HI) generated during the reaction is one of the general strategies for suppressing side reactions and controlling the selectivity of one-shot borylation. The resulting B,N-doped nanographenes (B2–B4 and B2-F) showed pure deep blue fluorescence and small ΔE_{ST} values (0.14–0.18 eV) (Table 26).

1652 | Chem. Soc. Rev., 2024, 53, 1624–1692

This journal is © The Royal Society of Chemistry 2024

Table 25 Photophysical properties of the compounds shown in Fig. 17–20

Compound	Condition	λ_{PL}^{max} [nm]	FWHM [nm]	Φ_{PL} [—]	ΔE_{ST} [eV]	k_{RISC} [s^{-1}]	Ref.
ADBNA-Me-Mes	CH$_2$Cl$_2$/1 wt%-DOBNA-OAr[b]	484/482	38/33	0.79/0.89	—/0.19	—/7.58 × 10^3	205
	CH$_2$Cl$_2$/1 wt%-PMMA[a]	482/485	—/—	0.71/0.84	—/0.18	—/—	206
ADBNA-Me-Tip	CH$_2$Cl$_2$/1 wt%-DOBNA-OAr[b]	482/479	36/34	0.76/0.88	—/0.20	—/8.98 × 10^3	205
ADBNA-Me-Mes-Mes^F	CH$_2$Cl$_2$/1 wt%-PMMA[a]	485/488	—/—	0.88/0.91	—/0.19	—/—	206
ADBNA-Me-Mes-CzAr	CH$_2$Cl$_2$/1 wt%-PMMA[a]	483/485	—/—	0.82/0.91	—/0.18	—/—	206
ADBNA-Me-Mes-Me$_4$N	CH$_2$Cl$_2$/1 wt%-PMMA[a]	477·609/487	—/—	0.19/0.26	—/0.17	—/—	206
ADBNA-Me-Mes^F	CH$_2$Cl$_2$/1 wt%-PMMA[a]	487/491	—/—	0.85/0.93	—/0.19	—/—	206
ADBNA-Me-CzAr	CH$_2$Cl$_2$/1 wt%-PMMA[a]	486/487	—/—	0.81/0.86	—/0.17	—/—	206
ADBNA-Me-Me$_4$N	CH$_2$Cl$_2$/1 wt%-PMMA[a]	481·601/495	—/—	0.18/0.24	—/0.13	—/—	206
BBCz-R	Toluene/2 wt%-mCBP[a]	615/619	21/27	0.89/0.79	0.19/—	1.2 × 10^4/1.2 × 10^4	155
Me2AcBO	Toluene/5 wt%-mCP[a]	474/470	—/57	—/0.99	—/0.05	—/1.13 × 10^6	117
F2AcBO	Toluene/5 wt%-mCP[a]	478/467	—/59	—/0.97	—/0.05	—/1.38 × 10^6	117
DBN-ICz	Toluene/3 wt%-mCBP[a]	542/545	18/23	0.986/—	0.20/—	0.7 × 10^4/—	163
m-DINBO	Toluene/3 wt%-mCBP[a]	456/466	17/22	—/0.94	—/0.060	—/3.1 × 10^4	167
p-DINBO[c]	Toluene/3 wt%-mCBP[a]	500/512	19/45	—/0.96	—/0.061	—/1.4 × 10^4	167
DBON[c]	Toluene/4 wt%-mCBP[a]	505/—	20/—	—/0.98	0.13/—	—/0.8 × 10^5	207
DBNO[c]	Toluene/1 wt%-PhCzBCz[a]	500/508	19/28	0.96/0.84	0.17/—	—/3.0 × 10^4	208
SBON	Toluene/4 wt%-mCBP[a]	463/—	24/—	—/0.74	0.16/—	—/0.5 × 10^5	207
SBSN	Toluene/4 wt%-mCBP[a]	489/—	27/—	—/0.76	0.10/—	—/1.5 × 10^5	207
DBSN	Toluene/4 wt%-mCBP[a]	553/—	28/—	—/0.98	0.13/—	—/1.9 × 10^5	207
R-DOBN	Toluene/5 wt%-26DCzPPy[a]	453/—	21/—	0.83/0.91	0.14/—	—/1.6 × 10^4	171
R-DOBNT	Toluene/5 wt%-26DCzPPy[a]	459/—	21/—	0.89/0.96	0.12/—	—/0.8 × 10^4	171
R-BN	Toluene	662	38	1.00	0.18	6.7 × 10^4	209
	Toluene	660	—	1.00	0.22	7.3 × 10^4	210
R-TBN	Toluene	692	38	1.00	0.16	2.5 × 10^4	209
	Toluene	684	—	0.99	0.21	2.3 × 10^4	210
R-TPhBN	Toluene	696	—	0.90	0.18	3.0 × 10^4	210
BNO1	Toluene/1 wt%-DMIC-TRZ[a]	605/610	32/35	0.96/—	—/0.25	—/—	211
BNO2	Toluene/1 wt%-DMIC-TRZ[a]	609/618	32/37	0.95/—	—/0.27	—/—	211
BNO3	Toluene/1 wt%-DMIC-TRZ[a]	616/624	33/38	0.96/—	—/0.26	—/—	211
DBNS	CH$_2$Cl$_2$	631	40	0.80	0.20	2.1 × 10^5	212
DBNS-tBu	CH$_2$Cl$_2$	641	39	0.85	0.19	2.2 × 10^5	212
BNS	Toluene	737	—	0.82	0.14	8.1 × 10^3	213
BNNO	Toluene	637	32	0.95	0.09	1.4 × 10^4	214
BBCz-DB	Toluene/2 wt%-mCBP[a]	466/471	16/26	0.93/0.91	0.15/—	1.9 × 10^4/2.2 × 10^4	155
m-DBCz	Toluene/1 wt%- PhCzBCz[a]	541/547	32/35	0.95/0.97	0.04/—	—/1.65 × 10^5	181
BSBS-N1	Toluene/2 wt%-mCBP[a]	473/478	21/24	0.59/0.89	0.13/0.14	1.5 × 10^6/1.9 × 10^6	92
BOBO-Z	Toluene/3 wt%-mCBP[a]	441/445	15/18	0.76/0.64	0.15/0.10	0.7 × 10^5/0.7 × 10^5	215
BOBS-Z	Toluene/3 wt%-mCBP[a]	453/457	21/24	0.94/0.93	0.16/0.12	4.3 × 10^5/8.6 × 10^5	215
BSBS-Z	Toluene/3 wt%-mCBP[a]	460/464	20/22	0.93/0.88	0.14/0.12	8.8 × 10^5/1.6 × 10^6	215
DBTN-2	Toluene/2.5 wt%-SF3TRZ[a]	512/—	20/—	—/1.00	—/0.06	—/1.7 × 10^5	216

[a] See Table 2 for the full compound name. [b] See Scheme 27. [c] Same compound named differently.
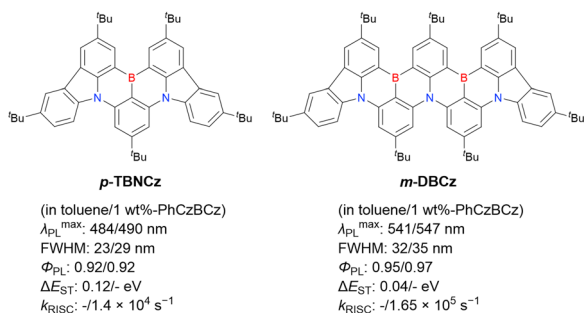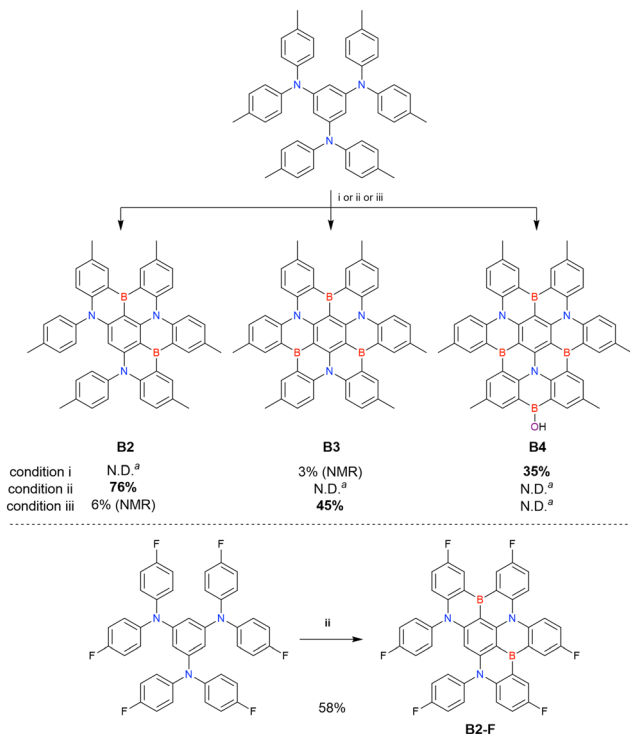

Fig. 21 Photophysical parameters of **p-TBNCz** and **m-DBCz** reported in ref. 181.

The selectivity of one-shot borylation can be attributed to several factors, as discussed below. Hatakeyama *et al.* reported the synthesis of carbazole-based DABNA analogues using one-shot borylation (Scheme 19).[111] The one-shot borylation of the precursor bearing one carbazolyl and two di-*p*-tolylamino groups proceeded at 120 °C in the presence of 2.0 equiv. of BBr$_3$ to afford **CzDABNA-NP-M/TB** in 63% yield. Notably, no regioisomers were observed. Moreover, the double borylation of the same substrate was achieved at 140 °C using 4.0 equiv. of BBr$_3$. Two boron atoms were selectively introduced at *ortho*-positions with respect to the carbazolyl group to afford **CzB2-M/TB** in 72% yield. According to density functional theory (DFT) calculations, the HOMO energy levels of the borylation precursor, **CzDABNA-NP-M/TB**, and **CzB2-M/TB** (−4.84, −4.77, and −4.73 eV, respectively) are sufficiently high for electrophilic C–H borylation. The HOMO of the borylation precursor is mostly localised at *para*-positions relative to the di-*p*-tolylamino groups (red circles, Fig. 22), which is attributed to their stronger electron-donating nature compared to that of the carbazolyl group. This indicates that the initial borylation predominantly occurs at the carbon atom between the 9-carbazolyl and di-*p*-tolylamino groups to afford **CzDABNA-NP-M/TB**. In other

This journal is © The Royal Society of Chemistry 2024

Chem. Soc. Rev., 2024, **53**, 1624–1692 | **1653**

Scheme 18 Synthesis of **B2**, **B3**, **B4**, and **B2-F**. Conditions and reagents: (i) BI₃ (12 equiv.), *o*-dichlorobenzene, reflux (bath temperature: 200 °C), 12 h, (ii) BI₃ (5.0 equiv.), Ph₃B (2.0 equiv.), *o*-dichlorobenzene, reflux (bath temperature: 190 °C), 20 h, (iii) BI₃ (5.0 equiv.), Ph₃B (2.0 equiv.), 1,2,4-trichlorobenzene, 200 °C, 20 h. *ᵃ* Not detected in ref. 217.

words, the initial borylation of the one-shot borylation protocol occurs at the *para*-position with respect to the most electron-donating substituent and is followed by tandem bora-Friedel–Crafts reactions affording the kinetic product. The second borylation of **CzDABNA-NP-M/TB** can proceed at two sites, namely the *ortho*-positions relative to the di-*p*-tolylamino group. However, the *p*-tolyl groups (blue circles, Fig. 22) perpendicular to the central benzene ring prevent BBr₃ from approaching the reactive carbon owing to steric hindrance.

In contrast, the carbazolyl group is positioned horizontally relative to the central benzene ring, allowing for easy access by BBr₃. Consequently, the second borylation predominantly occurs at the carbon atom located between the 9-carbazolyl and di-*p*-tolylamino groups to afford **CzB2-M/TB**. In brief, the selectivity of one-shot borylation is determined by both electronic and steric factors.

The synthesis of narrowband deep-blue emissive compounds **BN1**–**BN3** by Yang *et al.* are a good example illustrating the kinetic and thermodynamic selectivity of one-shot borylation (Scheme 20
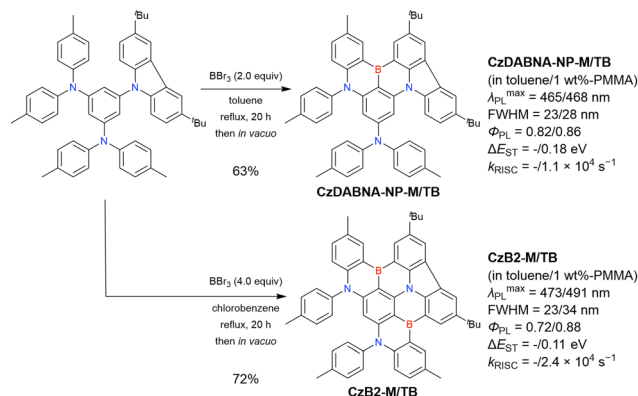
Scheme 19 Synthesis of **CzDABNA-NP-M/TB** and **CzB2-M/TB** reported in ref. 111.
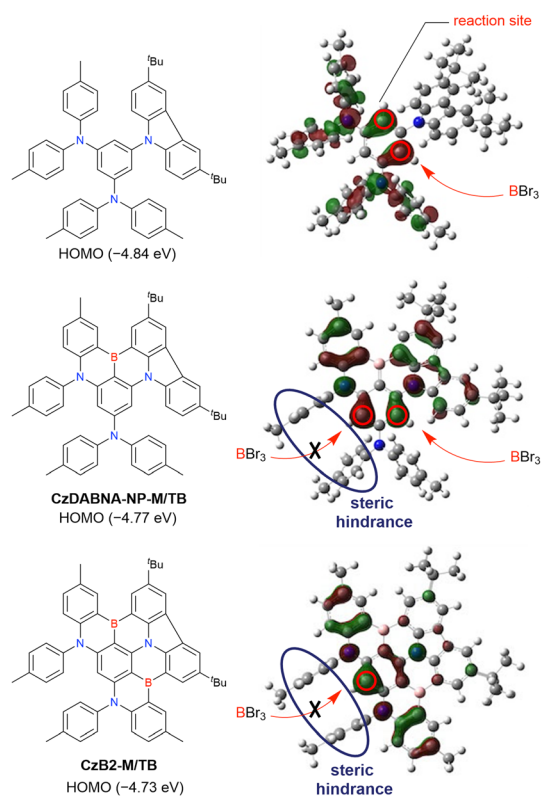
Fig. 22 Highest occupied Kohn–Sham orbitals (HOMOs) of the compounds shown in Scheme 19 calculated at the B3LYP/6-31G(d) level of theory.
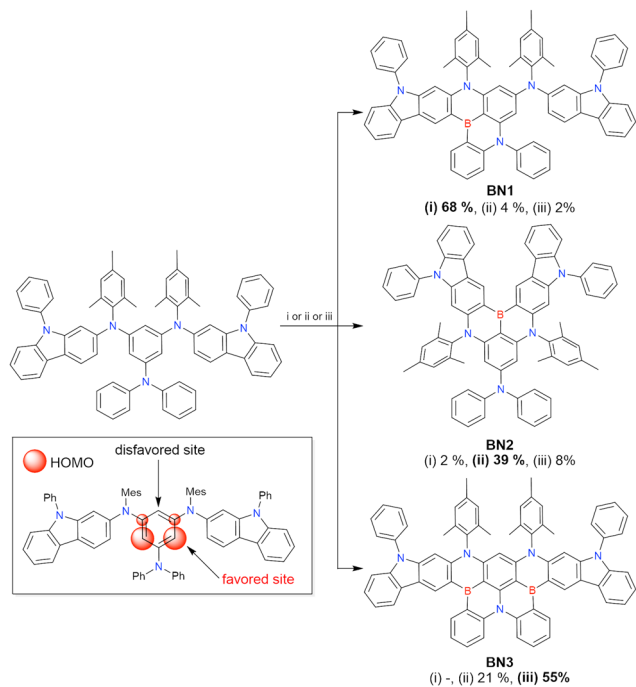
and Table 27).[218] The one-shot borylation was performed with 12 equiv. of BBr₃ at 180 °C and mainly occurred at the carbon

Table 26 Photophysical properties of the compounds shown in Scheme 18

Compound	Condition	λ_{PL}^{max} [nm]	FWHM [nm]	Φ_{PL}	ΔE_{ST} [eV]	k_{RISC} [s^{-1}]
B2	CH₂Cl₂/1 wt%-PMMA*ᵃ*	461/455	39/32	0.19/0.68	0.12/0.18	—/4.1 × 10⁴
B3	CH₂Cl₂/1 wt%-PMMA*ᵃ*	442/441	50/34	0.13/0.47	0.31/0.15	—/—
B4	CH₂Cl₂/1 wt%-PMMA*ᵃ*	449/450	22/38	0.21/0.61	0.19/0.15	—/—
B2-F	1 wt%-PMMA*ᵃ*	467	44	0.57	0.15	—/—

ᵃ See Table 2 for the full compound name.

1654 | *Chem. Soc. Rev.*, 2024, **53**, 1624–1692

This journal is © The Royal Society of Chemistry 2024
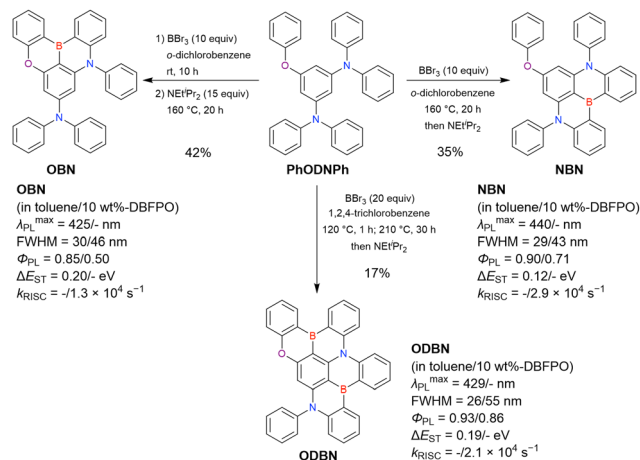
Scheme 20 Synthesis of **BN1–BN3**. Conditions and reagents: (i) BBr$_3$ (12 equiv.), *o*-dichlorobenzene, 180 °C, 20 h; then NEt^{i}Pr$_2$, (ii) BBr$_3$ (12 equiv.), *o*-dichlorobenzene, 210 °C, 20 h; then NEt^{i}Pr$_2$, (iii) BBr$_3$ (24 equiv.), *o*-dichlorobenzene, 210 °C, 20 h; then NEt^{i}Pr$_2$ (ref. 218).

Scheme 21 Synthesis of **OBN**, **NBN**, and **ODBN** in ref. 219.

atom in the central benzene ring at the *para*-position with respect to the 2-carbazolylmesitylamino group (where the HOMO was primarily localised) to afford mono-borylated **BN1** in 68% yield. In contrast, the mono-borylated regioisomer **BN2** was obtained in 39% yield as the major product at a higher reaction temperature (210 °C).

Although the borylated position of **BN2** does not contribute to the precursor HOMO and is therefore a disfavoured site, DFT calculations suggest that **BN2** is 2.2 kcal mol^{-1} more stable than **BN1**. Hence, initial borylation is assumed to occur at the same position as in the case of **BN1**, with a subsequent retro-Friedel–Crafts reaction involving *in situ* generated HBr affording **BN2** as the thermodynamic product. In addition, double one-shot borylation proceeded in the presence of an elevated amount of BBr$_3$ (24 equiv.) at 210 °C to give **BN3** in 55% yield as the kinetic product.

The synthesis of O,B,N-embedded MR compounds by Wong *et al.* also describe the selectivity of one-shot borylation (Scheme 21).[219] Based on the above description, initial borylation should occur at the *para*-position relative to the diphenylamino group. Indeed, the one-shot borylation performed using 10 equiv. of BBr$_3$ at room temperature occurred at this position,

and the subsequent intramolecular bora-Friedel–Crafts reaction in the presence of NEt^{i}Pr$_2$ as a Brønsted base afforded **OBN** in 42% yield. The base reduced the concentration of *in situ* generated HBr and prevented the retro-Friedel–Crafts reaction to promote the formation of the kinetic product **OBN**. In contrast, one-shot borylation performed at higher temperature (160 °C) using 10 equiv. of BBr$_3$ selectively furnished **NBN** in 35% yield, *i.e.*, boron was introduced at the *para*-position with respect to the phenoxy group. Given that this group is a weaker electron donor than the diphenylamine group and the *para*-position relative to this group is therefore unfavourable for borylation, **NBN** was concluded to be the thermodynamic product. In addition, double one-shot borylation affording **ODBN** in 17% yield was achieved by increasing the amount of BBr$_3$ (to 20 equiv.) and the reaction temperature (to 210 °C). Importantly, controlling the borylation temperature, number of boron equivalents, and/or Brønsted base addition enables the highly selective synthesis of kinetic/thermodynamic products.
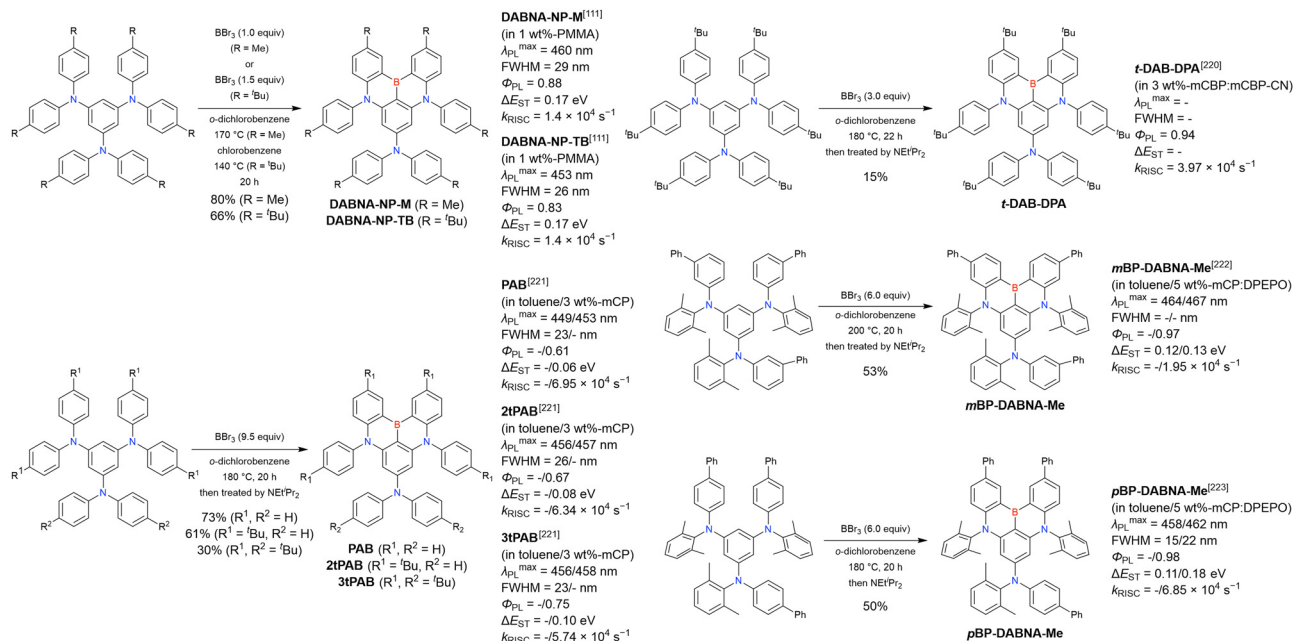
Various MR emitters have been synthesised based on the abovementioned selectivity. One-shot borylation has also been applied to the synthesis of DABNA-type compounds (Scheme 22).[111,220–223] An overview of these compounds and their borylation precursors shows that 1,3,5-trisubstituted benzenes are the preferred substrates, as they help to prevent undesired reactions. As mentioned above, one-shot borylation prefers to proceed at carbons where the HOMO is localised (*ortho*- and *para*-positions relative to the electron-donating group). However, in the case of 1,3-disubstituted benzene-type substrates, the borylation proceeds at the 4- or 6-positions rather than the sterically hindered 2-position. BBr$_3$ is the preferred boron source for their one-shot borylation, with no

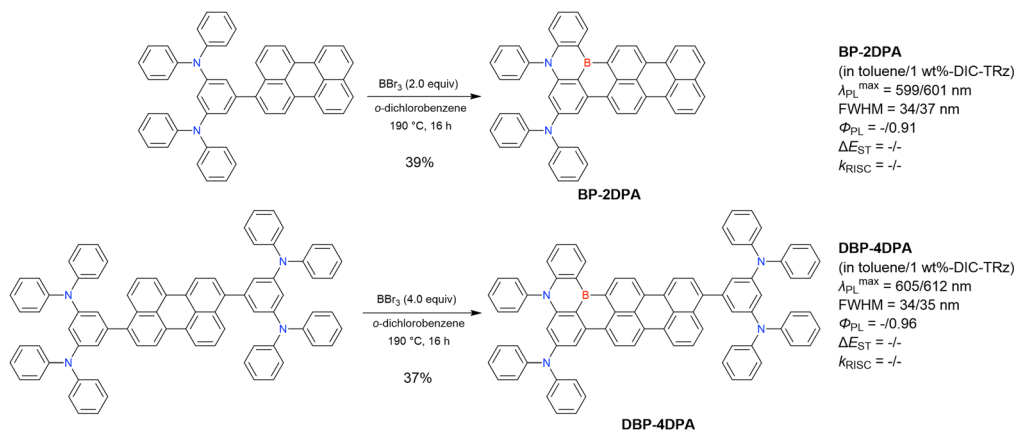Table 27 Photophysical properties of the compounds shown in Scheme 20

Compound	Condition	λ_{PL}^{max} [nm]	FWHM [nm]	Φ_{PL}	ΔE_{ST} [eV]	k_{RISC} [s^{-1}]
BN1	Toluene/1 wt%-DBFPO^a	454/458	18/22	—/0.91	0.20/0.15	—/1.3 × 10^4
BN2	Toluene/1 wt%-DBFPO^a	464/467	15/22	—/0.93	0.16/0.13	—/2.6 × 10^4
BN3	Toluene/1 wt%-DBFPO^a	456/458	17/21	—/0.98	0.15/0.12	—/2.55 × 10^5

^{a} See Table 2 for the full compound name.

This journal is © The Royal Society of Chemistry 2024

Chem. Soc. Rev., 2024, **53**, 1624–1692 | 1655

Scheme 22 Synthesis of DABNA analogues by one-shot borylation.

**Scheme 23** Synthesis of the perylene-fused BN compounds by one-shot borylation reported in ref. 224.

uses of BCl$_3$ and BI$_3$ reported to date. The synthesis of hexa-^{t}Bu-substituted DABNA (**DABNA-NP-TB**, *t*-**DAB-DPA**, or **3tPAB**) has been independently reported by Hatakeyama *et al.*,[111] Lee *et al.*,[220] and Wang *et al.*[221] However, the corresponding yields varied widely. In the last two reports, the high reaction temperature was believed to facilitate the retro-Friedel–Crafts reaction involving the *in situ* generated HBr and induce deborylation and ^{t}Bu group cleavage. In addition, all three substituents on the central benzene ring need not be electron-donating (*e.g.*, amino and phenoxy) groups; for example, one of them can be a PAH.

The MR compounds **BP-2DPA** and **DBP-4DPA**, which have a perylene moiety instead of one diphenylamino group in the **DABNA-NP** core, were synthesised by Kwon *et al.* in yields of 39% and 37%, respectively, using one-shot borylation

(Scheme 23).[224] Although many DABNA derivatives exhibit blue MR-TADF (*e.g.*, **PAB**: λ_{PL}^{max} = 449 nm in toluene),[221] **BP-2DPA** and **DBP-4DPA** feature significantly red-shifted emission (λ_{PL}^{max} = 599 nm and 605 nm in toluene, respectively), as perylene is a highly conjugated planar polycyclic aromatic system. On the other hand, **BP-2DPA** and **DBP-4DPA** do not exhibit TADF character due to the weak MR effect attributed to the non-MR perylene skeleton. Hence, **BP-2DPA** and **DBP-4DPA** were utilised as TEs for hyperfluorescence devices. The bonding/anti-bonding character of the FMOs of perylene remained, although weakened due to the fusion with the DABNA skeleton, and the shoulder peaks originating from the vibronic coupling between the S$_1$–S$_0$ electronic transition and stretching vibrations were observed in the PL and EL spectra.

Electron-donating groups other than diarylamino moieties are also available, including carbazolyl, acridyl, azetidyl, and

1656 | *Chem. Soc. Rev.*, 2024, **53**, 1624–1692

This journal is © The Royal Society of Chemistry 2024
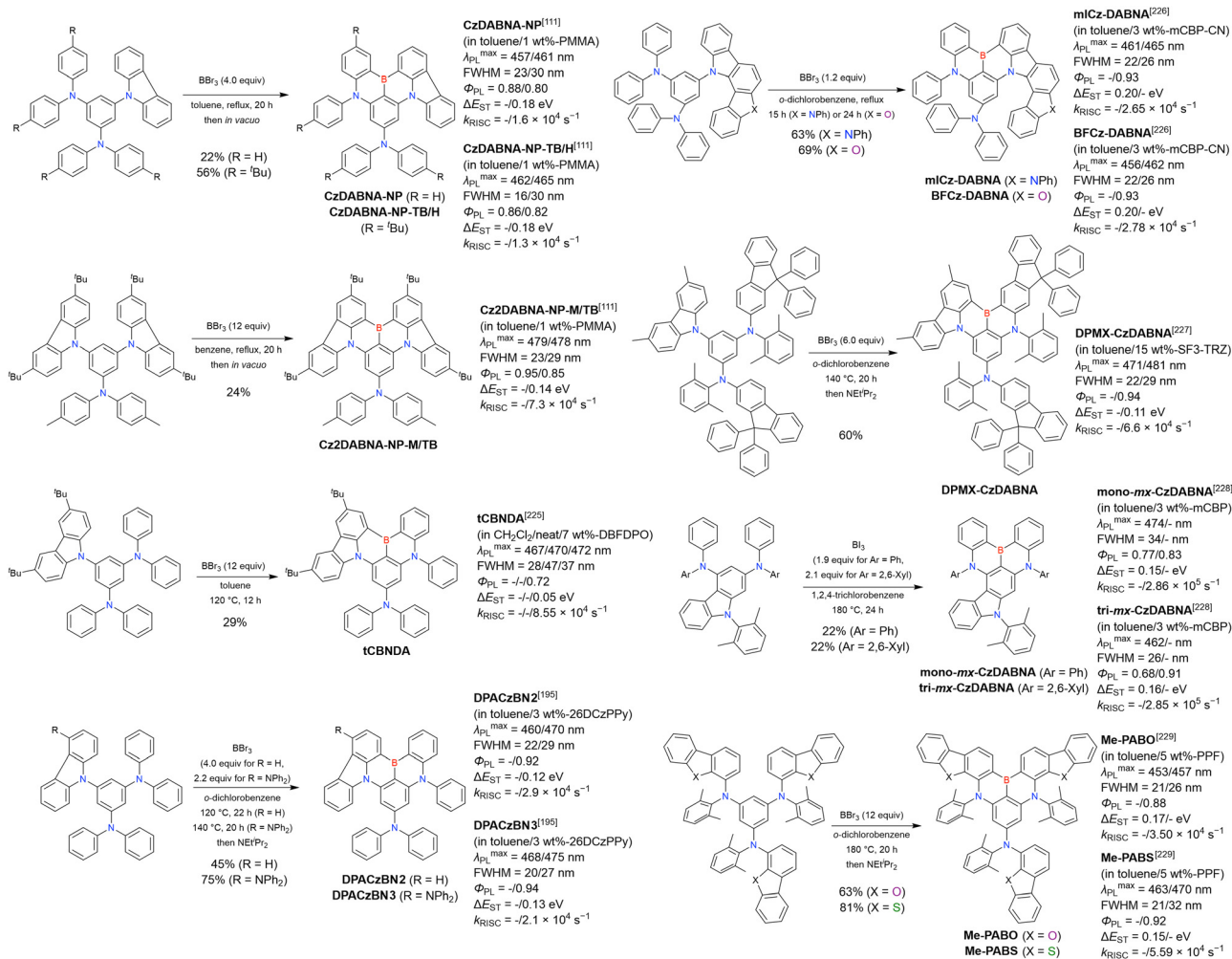
Scheme 24 Synthesis of carbazole-based DABNA analogues by one-shot borylation.

ether groups. In particular, numerous carbazole-fused CzDABNA analogues were synthesised by one-shot borylation (Scheme 24).[111,195,225–229] When the 9-carbazolyl group is used as an electron-donating group, one-shot borylation proceeds based on the selectivity described above, as this group is a weaker electron donor than the diarylamino group. BBr$_3$ is used as the boron source in most cases, but BI$_3$ is also available. Carbazole ring incorporation is often used for emission wavelength tuning, as it results in the extension of the π-conjugated system and, hence, in red-shifted emission.

According to Wang *et al.*, the one-shot borylation of a 9,10-dihydro-9,9-dimethylacridine-substituted substrate with 4.0 equiv. of BBr$_3$ proceeded at the *para*-position relative to the diarylamino group to give **tDMAC-BN** in 32% yield, whereas that of a 9,10-dihydro-9,9-diphenylacridine-substituted substrate proceeded at the *para*-position relative to the acridine moiety to afford **tDPAC-BN** in 41% yield (Scheme 25).[230] Similarly, Wang *et al.* reported that the 9,10-dihydro-9,9-dimethylacridine moiety-containing borylated compound **Ph-DMAC-BN** was obtained in 44% yield and with similar selectivity under almost identical conditions.[231] When the 9,10-dihydroacridine moiety is used as

an electron-donating group, the substituent at its 9-position seems to determine the selectivity of one-shot borylation.

Yang *et al.* attempted the one-shot borylation of the phenothiazine 5,5-dioxide-substituted substrate.[196] The one-shot borylation proceeded in the presence of 5.0 equiv. of BBr$_3$ to afford the borylation product **PTZBN3** in 11% yield and the deoxygenated product **PTZBN2** was obtained in 15% yield (Scheme 26). Although some S=O bond cleavage was observed, the sulfone moiety was found to be tolerant to one-shot borylation conditions to some extent.
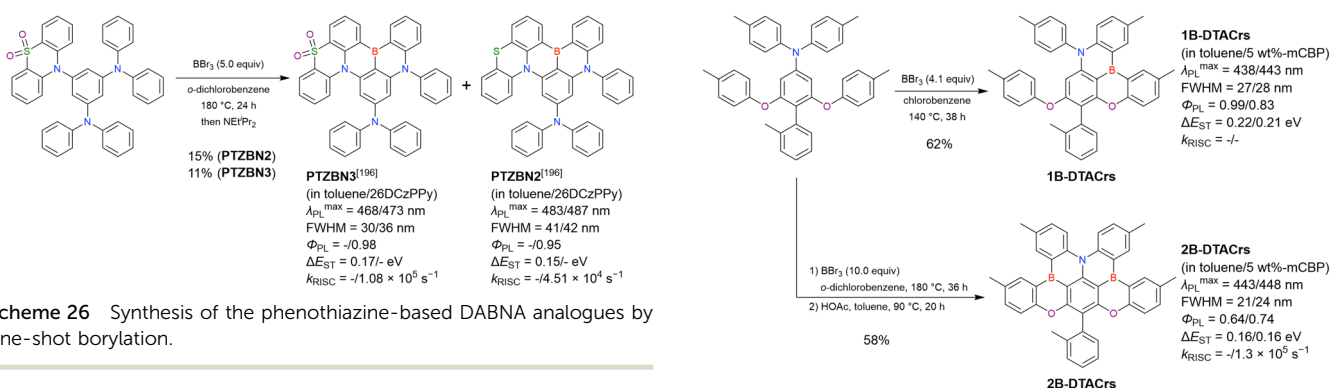
One-shot borylation is also feasible for precursors bearing oxygenated electron-donating groups (*e.g.*, aryloxy). In most cases, DOBNA derivatives are synthesised by one-pot borylation, but can also be prepared using the one-shot borylation of 1,3,5-trisubstituted benzene-type substrates. Hatakeyama *et al.* synthesised **DOBNA-OAr** in 91% yield as a host material for blue OLEDs by the one-shot borylation of three-fold symmetric 1,3,5-triaryloxybenzene in the presence of 4.0 equiv. of BI$_3$ followed by heat treatment in acetic acid (HOAc) (Scheme 27).[60]

Heat treatment in acetic acid is an important procedure for increasing the yield of borylation reactions, especially when

This journal is © The Royal Society of Chemistry 2024

Chem. Soc. Rev., 2024, **53**, 1624–1692 | 1657
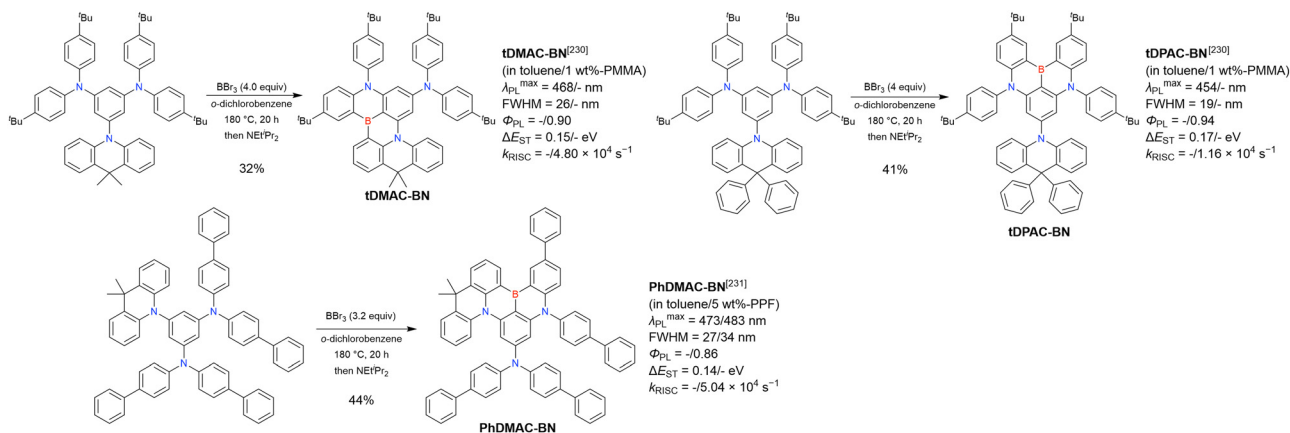
Scheme 25 Synthesis of acridine-based DABNA analogues by one-shot borylation.

Scheme 26 Synthesis of the phenothiazine-based DABNA analogues by one-shot borylation.

Scheme 28 Synthesis of **1B-DTACrs** and **2B-DTACrs** reported in ref. 232.

using a large excess of the boron source. As one-shot borylation proceeds at carbons contributing to the HOMO (often at the *para*-position relative to the electron-donating group), borylation at undesired peripheral positions may occur as a side reaction. Heat treatment in acetic acid removes the non-fused boron introduced at the periphery by excess BI_3. This technique was used to synthesise **2B-DTACrs** by Zysman-Colman et al.[232] In contrast to the mono-borylated **1B-DTACrs**, which was synthesised using 4.1 equiv. of BBr_3, the di-borylated **2B-DTACrs** was synthesised using 10 equiv. of BBr_3 followed by acetic acid treatment (Scheme 28).

Furthermore, the conditions of one-shot borylation allow for the retention of convertible halogens such as chlorine and bromine as well as for late modification (Scheme 29). Lee and Hong reported that six chlorine or bromine atoms were maintained even upon treatment with 36 equiv. of BBr_3 in *o*-dichlorobenzene at 200 °C, which afforded mono-borylated
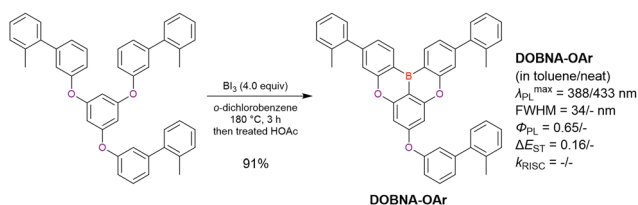

**Scheme 27** Synthesis of **DOBNA-OAr** by one-shot borylation in ref. 60.

compounds **Cl-MR** and **Br-MR** in yields of 56% and 63%, respectively.[233] In the synthesis of **DBT-BN**, **DBF-DBN**, and **DBT-DBN** by Wu and Lan et al., the chlorine atoms in the borylation precursor were partially exchanged for bromine during one-shot borylation with BBr_3. However, this did not present a problem, as these halogen atoms were consumed in the subsequent Suzuki–Miyaura coupling.[234]

One-shot borylation is also a powerful method for achieving double borylation (Scheme 30). For example, the one-shot double borylation of a precursor synthesised from a commercially available compound in three steps was carried out in the presence of 6.0 equiv. of BI_3 at 180 °C to afford the sterically protected **OAB-ABP-1** in 18% yield.[235] Note that the mesityl and methyl groups suppressed the undesirable borylation at the carbon atom contributing to the HOMO. Duan et al. used one-shot double borylation to prepare DABNA-incorporated calix[4]arene **C-BN** in 30% yield.[236] Furthermore, You et al. used one-shot double borylation at 190 °C in the presence of 26 equiv. of BBr_3 to synthesise **DTBA-B2N3** in 26% yield as an MR emitter by introducing a medium (azepine) ring to suppress aggregation-caused quenching (ACQ).[152] Kwon et al. amalgamated the conventional DOBNA and DABNA structures, synthesising **TPD4PA** and **tBu-TPD4PA** in yields of 23% and 26%, respectively, *via* one-shot double borylation in the presence of
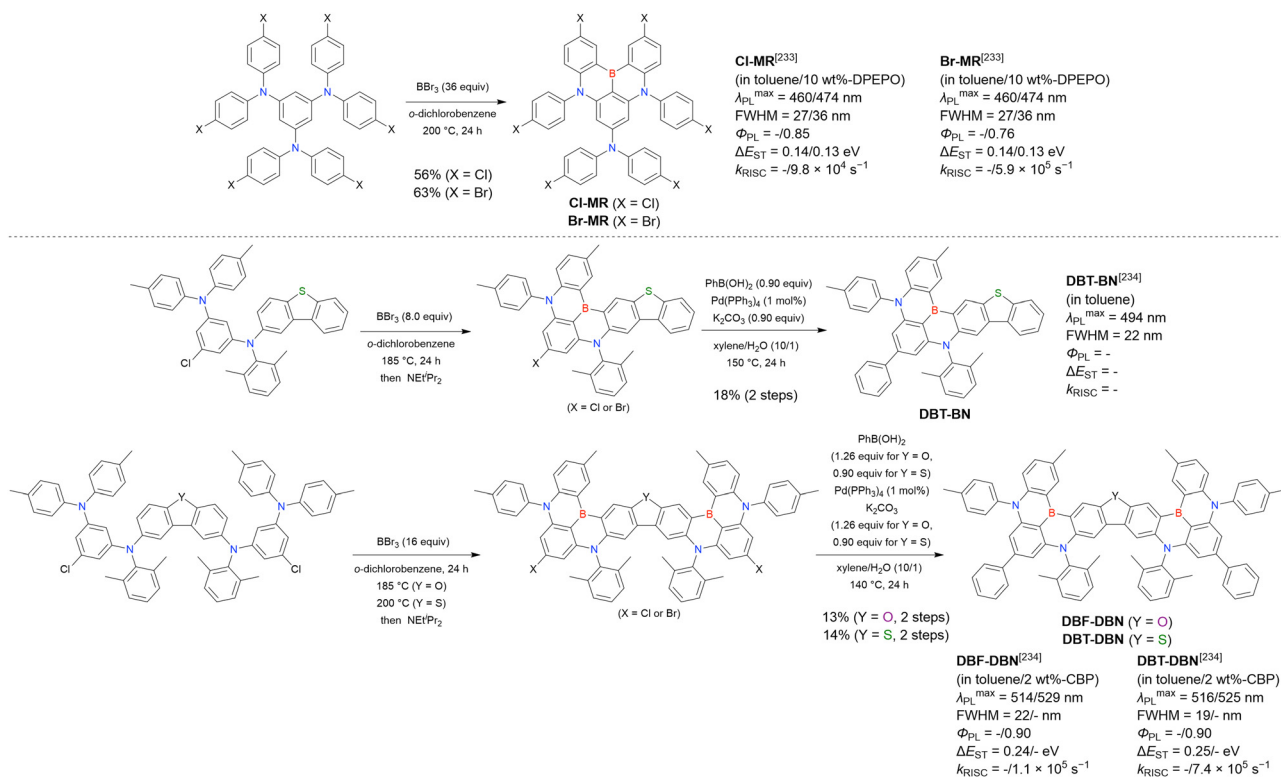
Scheme 29 Synthesis of BN compounds bearing halogen atoms by one-shot borylation.
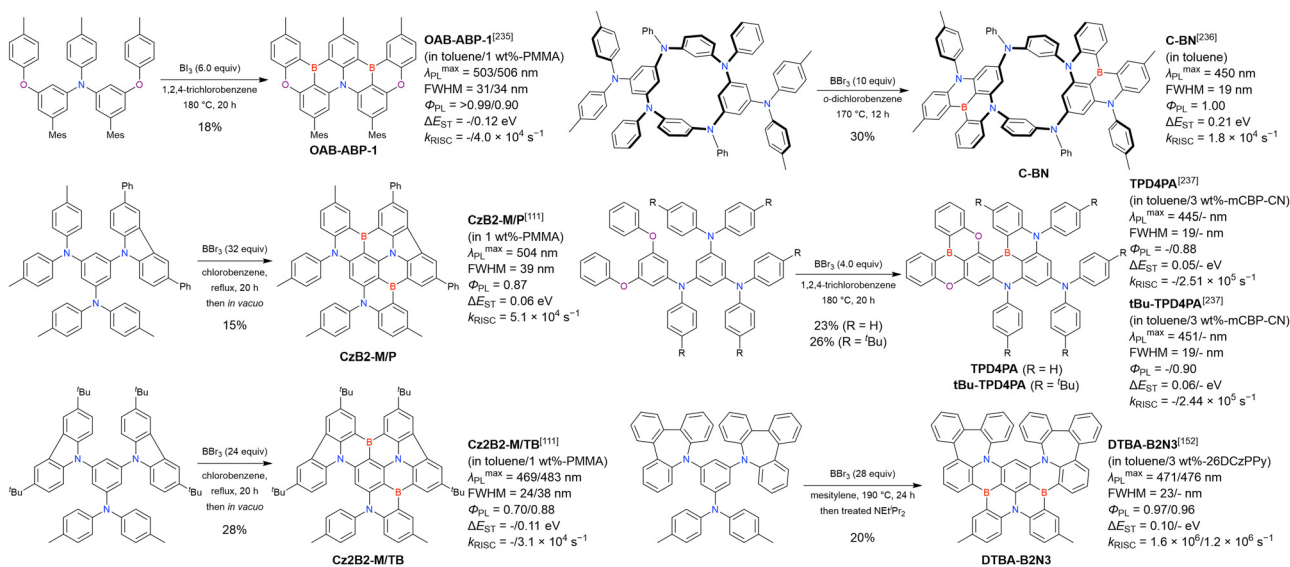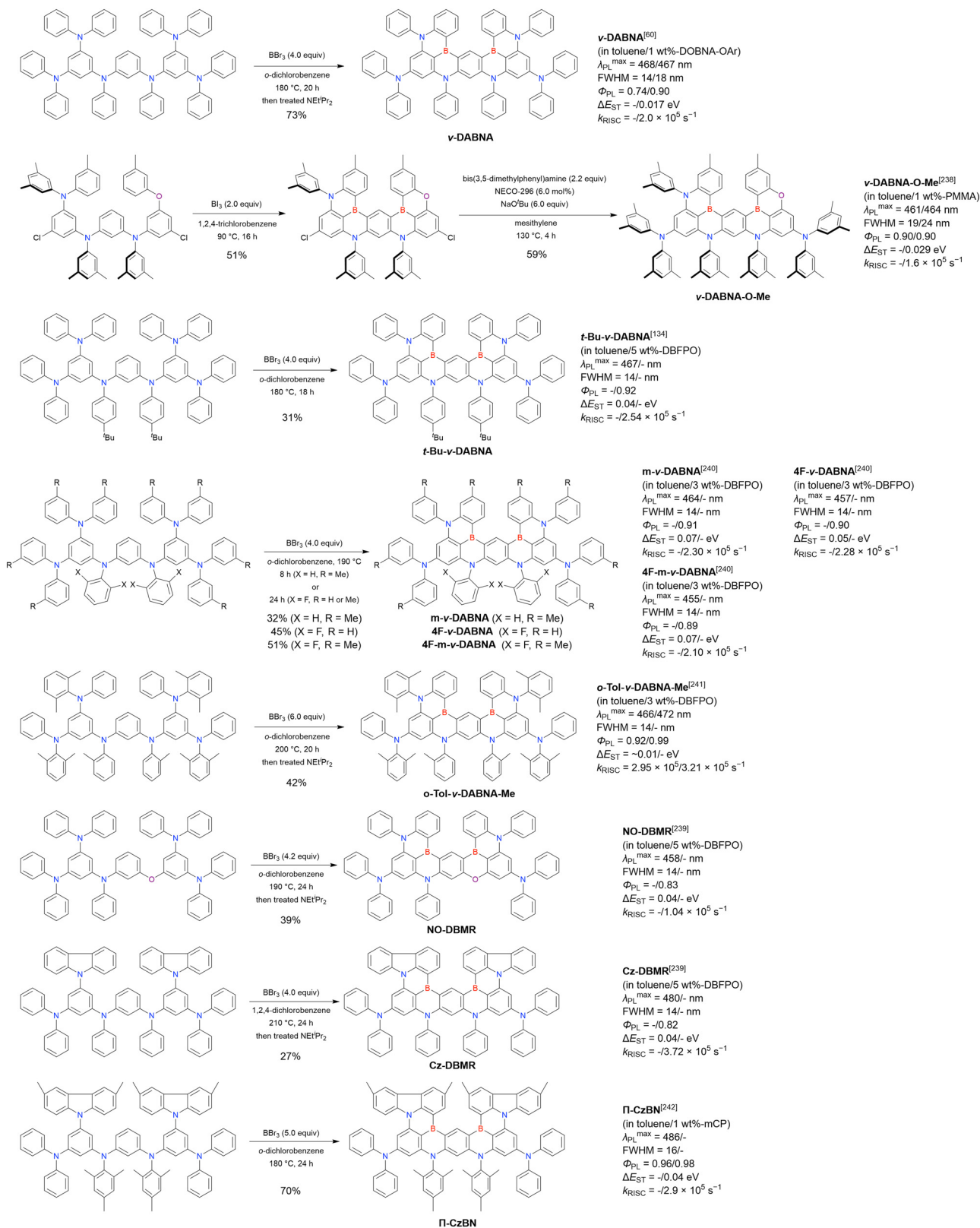

Scheme 30 Double one-shot borylation reactions.

4.0 equiv. of BBr$_3$.[237] One-shot double borylation is often performed using a large excess of BBr$_3$ or BI$_3$. The thus obtained B2 compounds are expected to exhibit enhanced MR effects and smaller ΔE_{ST} than B1 MR compounds because of the highly extended π-skeleton of the former.

In 2019, Hatakeyama *et al.* reported **ν-DABNA** as a new scaffold for narrowband MR-TADF emitters.[60] **ν-DABNA** was

synthesised from commercially available compounds in three steps including palladium-catalysed C–N coupling and one-shot borylation. The one-shot borylation of the precursor with 4.0 equiv. of BBr$_3$ at 180 °C afforded **ν-DABNA** in 36% yield (Scheme 31). According to DFT calculations, the boron atoms were selectively introduced at the carbon atoms primarily contributing to the HOMO. Additionally, the small number of

This journal is © The Royal Society of Chemistry 2024

Chem. Soc. Rev., 2024, **53**, 1624–1692 | 1659

v-DABNA[60]
(in toluene/1 wt%-DOBNA-OAr)
λ_{PL}^{max} = 468/467 nm
FWHM = 14/18 nm
Φ_{PL} = 0.74/0.90
ΔE_{ST} = -/0.017 eV
k_{RISC} = -/2.0 × 10^5 s^{-1}

v-DABNA-O-Me[238]
(in toluene/1 wt%-PMMA)
λ_{PL}^{max} = 461/464 nm
FWHM = 19/24 nm
Φ_{PL} = 0.90/0.90
ΔE_{ST} = -/0.029 eV
k_{RISC} = -/1.6 × 10^5 s^{-1}

t-Bu-v-DABNA[134]
(in toluene/5 wt%-DBFPO)
λ_{PL}^{max} = 467/- nm
FWHM = 14/- nm
Φ_{PL} = -/0.92
ΔE_{ST} = 0.04/- eV
k_{RISC} = -/2.54 × 10^5 s^{-1}

m-v-DABNA[240]
(in toluene/3 wt%-DBFPO)
λ_{PL}^{max} = 464/- nm
FWHM = 14/- nm
Φ_{PL} = -/0.91
ΔE_{ST} = 0.07/- eV
k_{RISC} = -/2.30 × 10^5 s^{-1}

4F-v-DABNA[240]
(in toluene/3 wt%-DBFPO)
λ_{PL}^{max} = 457/- nm
FWHM = 14/- nm
Φ_{PL} = -/0.90
ΔE_{ST} = 0.05/- eV
k_{RISC} = -/2.28 × 10^5 s^{-1}

4F-m-v-DABNA[240]
(in toluene/3 wt%-DBFPO)
λ_{PL}^{max} = 455/- nm
FWHM = 14/- nm
Φ_{PL} = -/0.89
ΔE_{ST} = 0.07/- eV
k_{RISC} = -/2.10 × 10^5 s^{-1}

o-Tol-v-DABNA-Me[241]
(in toluene/3 wt%-DBFPO)
λ_{PL}^{max} = 466/472 nm
FWHM = 14/- nm
Φ_{PL} = 0.92/0.99
ΔE_{ST} = ~0.01/- eV
k_{RISC} = 2.95 × 10^5/3.21 × 10^5 s^{-1}

NO-DBMR[239]
(in toluene/5 wt%-DBFPO)
λ_{PL}^{max} = 458/- nm
FWHM = 14/- nm
Φ_{PL} = -/0.83
ΔE_{ST} = 0.04/- eV
k_{RISC} = -/1.04 × 10^5 s^{-1}

Cz-DBMR[239]
(in toluene/5 wt%-DBFPO)
λ_{PL}^{max} = 480/- nm
FWHM = 14/- nm
Φ_{PL} = -/0.82
ΔE_{ST} = 0.04/- eV
k_{RISC} = -/3.72 × 10^5 s^{-1}

Π-CzBN[242]
(in toluene/1 wt%-mCP)
λ_{PL}^{max} = 486/- nm
FWHM = 16/-
Φ_{PL} = 0.96/0.98
ΔE_{ST} = -/0.04 eV
k_{RISC} = -/2.9 × 10^5 s^{-1}

Scheme 31 Synthesis of **ν-DABNA** and its analogues by one-shot borylation.

substituents at the central benzene ring and its steric accessibility are important for achieving highly selective borylation. Compared to **DABNA-1**,[38] **ν-DABNA** exhibited a substantially

higher k_{RISC} (2.0 × 10^5 s^{-1}) and was used to realise an OLED with an excellent EQE, minimum efficiency roll-off (34.4/32.8/26.0% at 15/100/1000 cd m^{-2}, respectively), and ultrapure blue
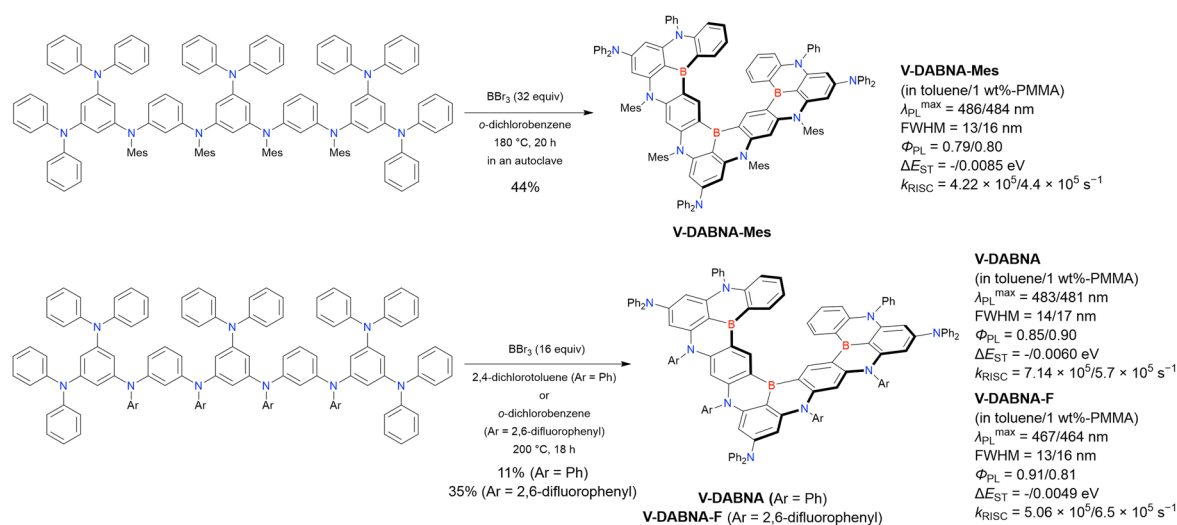
1660 | Chem. Soc. Rev., 2024, **53**, 1624–1692

This journal is © The Royal Society of Chemistry 2024

emission (FWHM = 18 nm). Therefore, ν-DABNA would replace **DABNA** as the benchmark for MR compounds. Following the success of ν-DABNA, various related derivatives have been synthesised. Hatakeyama *et al.* reported ν-DABNA-O-Me, which can be viewed as ν-DABNA with an oxygen atom instead of the nitrogen atom.[238] The one-shot double borylation of a chlorine-bearing precursor was carried out with a stoichiometric amount of BI$_3$ at 90 °C to obtain the desired intermediate in 51% yield, and the subsequent cross-coupling with bis(3,5-dimethyl-phenyl)amine at 130 °C afforded ν-DABNA-O-Me in 59% yield. In view of its lower atomic orbital energy, the oxygen atom restricts the π-conjugation of the HOMO rather than that of the LUMO. The replacement of nitrogen with oxygen affects the HOMO energy level more than it does the LUMO energy level. As a result, ν-DABNA-O-Me exhibits a larger HOMO–LUMO gap and displays a deeper blue emission (465 nm) than ν-DABNA. The emission maximum of ν-DABNA (469 nm) is slightly red-shifted relative to that of **DABNA-1** (459 nm) because of π-extension. As a result, the Commission Internationale de l'Eclairage (CIE) coordinates (0.12, 0.11) deviated from the requirements defined by the National Television System Committee (0.14, 0.08). Therefore, the replacement of nitrogen by oxygen is a powerful strategy for achieving optimal emission wavelengths. Kwon *et al.* used a similar concept to synthesise **NO-DBMR**, where the different nitrogen position in ν-DABNA was replaced by oxygen.[239] The final double one-shot borylation was carried out using 4.2 equiv. of BBr$_3$ to afford **NO-DBMR** in 39% yield. Fluorination and methylation are also used to realise blue-shifted emission. Kwon *et al.* also obtained **m-ν-DABNA**, **4F-ν-DABNA**, and **4F-m-ν-DABNA** in yields of 32%, 45%, and 51%, respectively, by one-shot borylation with 4.0 equiv. of BBr$_3$ from a substrate with a fluorinated or methylated benzene ring-substituted nitrogen.[240] Other approaches to derivative design involve the introduction of bulky substituents to prevent luminescence peak broadening due to excimer formation in the aggregated state and enhance the horizontal orientation. Based

on this strategy, Kwon *et al.* synthesised **tBu-ν-DABNA** in 31% yield by introducing ^{t}Bu groups into ν-DABNA,[134] while Yoo *et al.* synthesised **o-Tol-ν-DABNA-Me** in 42% yield *via* one-shot borylation with BBr$_3$ by changing the substituent on the nitrogen to o-tolyl or xylyl.[241] As mentioned above, the introduction of the carbazole scaffold extends the π-conjugated system and leads to red-shifted emission. The same is true for ν-DABNA derivatives, as exemplified by carbazole-fused **Cz-DBMR** and **Π-CzBN** synthesised by Kwon *et al.* and Zhang *et al.*, respectively.[239,242]

In 2022, Hatakeyama *et al.* synthesised an expanded B,N-embedded heterohelicene, **V-DABNA-Mes**, as a representative new member of the DABNA series by triple one-shot borylation.[243] The one-shot triple borylation was achieved using 32 equiv. of BBr$_3$ in an autoclave at 180 °C to afford **V-DABNA-Mes** in 44% yield (Scheme 32). The steric protection provided by the mesityl groups suppresses both overborylation and borylation at undesired reactive sites. Notably, a significant drop in the yield of **V-DABNA-Mes** (3%) was observed under standard reflux conditions in a flask because of the decreased concentration of BBr$_3$ in the reaction mixture. The one-step construction of such giant helix structures is not only synthetically useful but also an important as a design strategy for the emitters of high-performance OLEDs, as the enhanced MR effect and extended π-helix structure led to small FWHM (13 nm) and large k_{RISC} (4.22×10^5 s^{-1}) in toluene. This facile and scalable method was applied to unsubstituted and fluorine-substituted compounds, and triple one-shot borylation with 16 equiv. of BBr$_3$ gave **V-DABNA** and **V-DABNA-F** in 11% and 35% yields, respectively.[244]

Hatakeyama *et al.* achieved quadruple, sextuple, and octuple borylation to construct the largest MR-core structures, which comprised B,N-embedded nonacene (**CzB4**), tridecacene (**CzB6**), and heptadecacene (**CzB8**) frameworks, respectively.[245] The key to success was the judicious choice of the borylating reagent, namely BI$_3$ combined with 2,6-di-*tert*-butylpyridine (DTBPY), and

Scheme 32 Synthesis of the V-DABNA series reported in ref. 243 and 244.

This journal is © The Royal Society of Chemistry 2024

Chem. Soc. Rev., 2024, **53**, 1624–1692 | **1661**

long alkyl-substituted carbazolyl groups as boron-trapping groups, which suppressed the decrease in HOMO energy and insolubilisation associated with borylation. The one-shot multiple borylation with 16–32 equiv. of BI_3 and 12–24 equiv. of DTBPY (as a bulky Brønsted base) proceeded at 150 °C to afford **CzB4**, **CzB6**, and **CzB8** in yields of 90%, 86%, and 83%, respectively. Thus, each electrophilic C–H borylation proceeded in >99% yield, which is the highest efficiency reported to date for C–H borylation reactions (Scheme 33). The thus obtained large MR compounds exhibited ultra-narrowband green TADF with FWHM = 12–16 nm. This achievement suggests that carbazolyl groups may enable the construction of larger acene frameworks by multiple borylation.

Thus, one-shot borylation is a powerful synthesis method for developing boron-embedded MR compounds, especially for the introduction of multiple boron atoms, and is complementary to one-pot borylation. The selectivity of this reaction is mainly determined by electronic and steric requirements; therefore, a deep understanding of these requirements is useful for MR emitter design. It should be noted that one-shot borylation is not a panacea, allowing the synthesis of only a small fraction of the vast chemical space of MR compounds.

3.2 One-shot (N–H) borylation

This subsection focuses on MR compounds with B–N bonds synthesised by amine-directed one-shot borylation (N–H borylation). B–N covalent bonds were first used to formally replace the isoelectronic C=C bonds by Dewar in 1958.[25] Although the corresponding B,N-doped PAHs are being intensively researched because of the unique optical and electronic properties imparted by dipole B–N bonds,[26–33] highly B–N-doped PAHs do not exhibit MR-TADF and exhibit relatively large FWHMs.[246,247] In 2022, Duan *et al.* used the amine-directed formation of B–N bonds to demonstrate the preparation of MR compounds **m[B-N]N1** and **m[B-N]N2**.[248] Amine-directed
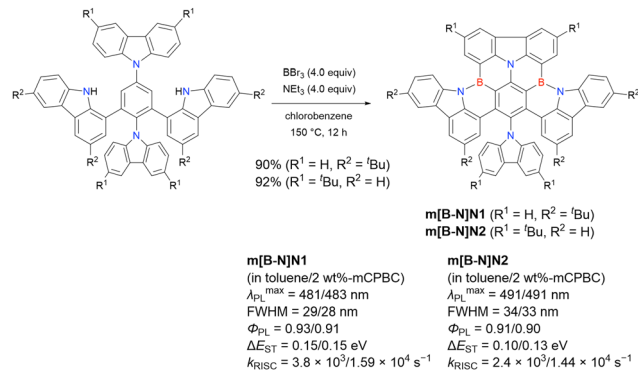
Scheme 34 Synthesis of **m[B-N]N1** and **m[B-N]N2** by the amine-directed one-shot borylation reported in ref. 248.
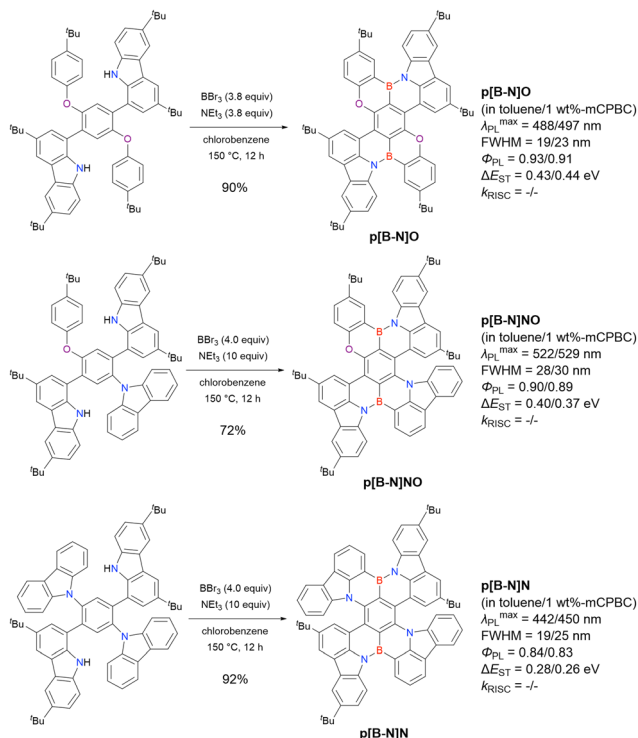
double borylation[106] occurred in chlorobenzene at 150 °C in the presence of 4.0 equiv. of BBr_3 and 4.0 equiv. of base to produce **m[B-N]N1** and **m[B-N]N2** in yields of 90% and 92%, respectively (Scheme 34). Notably, the two boron atoms were introduced at *ortho*-positions relative to the nitrogen atoms, and other byproducts including regioisomers and monoborylated compounds were not detected. While **m[B-N]N1** and **m[B-N]N2** displayed narrowband pure emission with FWHM = 26–32 nm and Φ_{PL} >90% but exhibited slightly larger ΔE_{ST} (0.13–0.15 eV) and smaller k_{RISC} compared with other B2 compounds. This indicated that the MR effect was weakened because of carbazole moieties connecting the central benzene ring *via* C–C bonds.

The same group used this facile and scalable amine-directed double borylation method to prepare a standard *para*-B–π–B skeleton modified by the stepwise replacement of nitrogen atoms with oxygen atoms (Scheme 35).[249] The resulting compounds featured a wide λ_{PL}^{max} range of 442–545 nm while maintaining narrow FWHM (19–26 nm) and high luminescence efficiency ($\Phi > 0.84$). On the other hand, these *para*-B–π–B
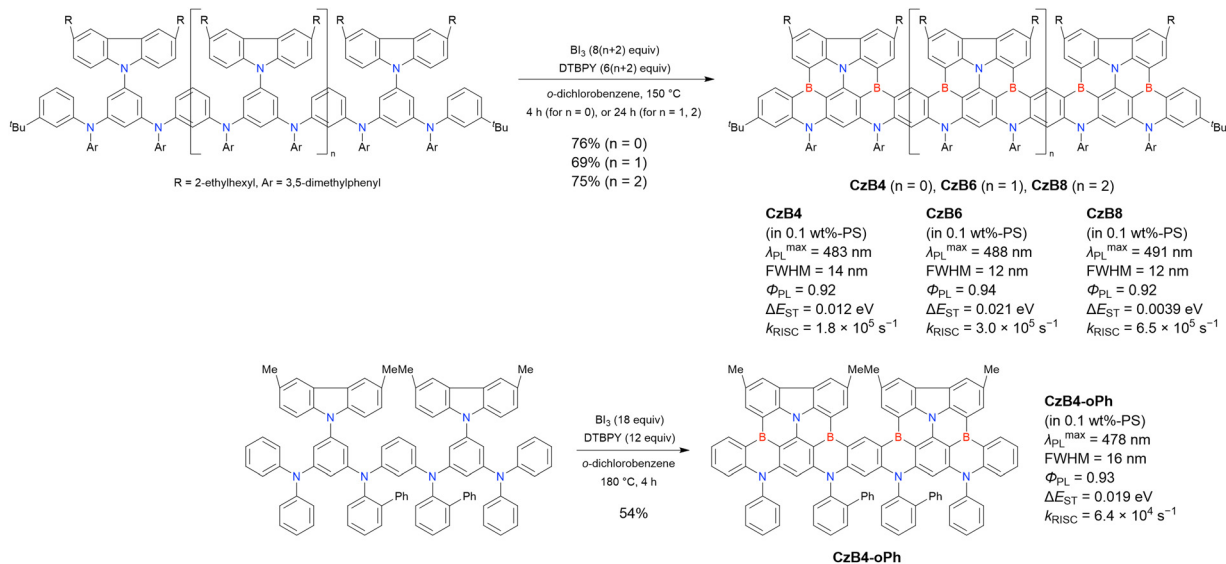
Scheme 33 Synthesis of **CzB4–CzB8** and **CzB4-oPh** by one-shot quadruple, sextuple, and octuple borylation reported in ref. 245.

1662 | *Chem. Soc. Rev.*, 2024, **53**, 1624–1692

This journal is © The Royal Society of Chemistry 2024

Scheme 35 Synthesis of B–N bond-embedded MR compounds reported in ref. 249.

compounds exhibited large ΔE_{ST} (0.26–0.44 eV) among the B2 compounds and did not show TADF behaviour because the MR effect is weakened when the two boron atoms are in the *para*-position with respect to each other, and also because the carbazole moiety, which forms a C–C bond with the central benzene ring, has a weak MR effect.

Not only the synthesis of tricoordinate boron-based MR-TADF compounds, but also those of tetracoordinate boron-based MR-TADF compounds containing B–N bonds have been achieved using amine-directed one-shot borylation. Wang *et al.* reported tetracoordinate boron-containing MR-TADF emitters
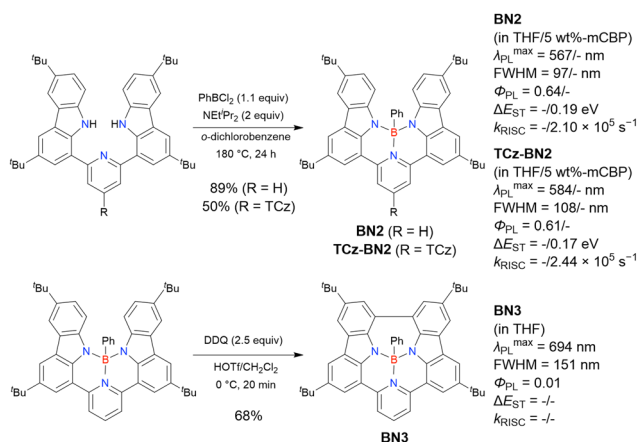
based on a C,N,C- or N,N,N-chelating pincer ligand.[250] Among them, N,N,N-chelating compounds **BN2**, **Tcz-BN2**, and **BN3** were synthesised using amine-directed one-shot borylation (Scheme 36). The amine-directed one-shot borylation of the N,N,N-ligand bearing one pyridine moiety and two N–H bonds occurred in the presence of dichlorophenylborane (PhBCl$_2$) as a boron source to afford **BN2** and **TCz-BN2**, while the subsequent Scholl reaction of **BN2** gave **BN3**. Unlike the emission spectra of conventional MR-compounds, the emission spectra of **BN2** and **TCz-BN2** were broad (FWHM = 97 and 108 nm, respectively) because of the large structural differences between the ground and excited states derived from tetracoordinate boron. In addition, **BN2** and **TCz-BN2** exhibited TADF character, although the boron orbitals are not involved in the MR structure and the MR effect is derived from the pyridine-containing skeleton.

In brief, amine-directed borylation is a facile and scalable method for synthesising B–N bond-bearing PAHs, although they often display no MR effects. The study of MR compounds bearing B–N bonds is currently in its early stage.

3.3 Sequential multiple borylation

One-shot borylation is a facile method for developing π-extended MR compounds containing multiple boron atoms. However, because this reaction proceeds at the most sterically accessible carbon atom contributing to the HOMO,[251] the chemical space of boron-based MR compounds remains largely unexplored. To address this issue, Hatakeyama *et al.* proposed a new synthesis method for boron-based MR compounds, namely sequential multiple borylation, which involves one-pot borylation, Buchwald–Hartwig coupling, and one-shot borylation.[252] This method was used to synthesise an ultrapure green MR emitter (**ω-DABNA**) as a proof-of-concept (Scheme 37). The omega-shaped MR framework containing


Scheme 36 Synthesis of tetracoordinate boron-containing MR compounds by one-shot borylation reported in ref. 250.
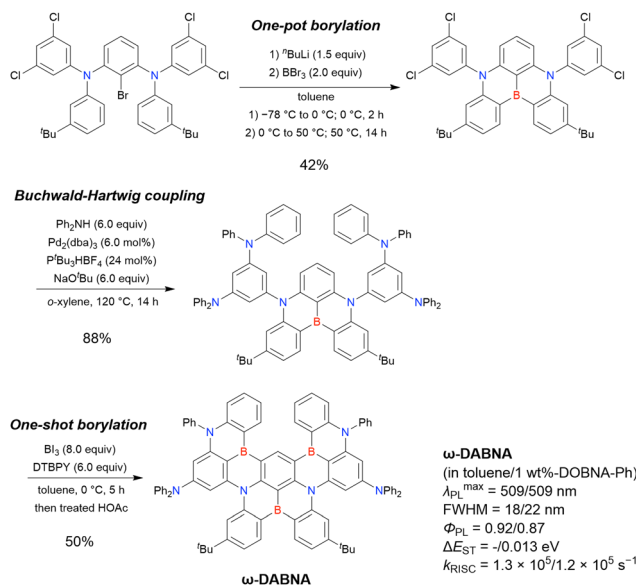
Scheme 37 Synthesis of **ω-DABNA** by sequential multiple borylation reported in ref. 252.

This journal is © The Royal Society of Chemistry 2024

Chem. Soc. Rev., 2024, **53**, 1624–1692 | **1663**

three boron atoms and four nitrogen atoms could not be accessed using conventional borylation protocols such as one-pot or one-shot borylation. This structure, featuring three boron atoms introduced into the same benzene ring, could not be synthesised by one-pot borylation because electron repulsion destabilises the trilithiated intermediate formed in the course of this reaction. In the case of one-shot borylation, triple borylation could not proceed because the HOMO is not localised at the third borylation position after the introduction of two boron atoms. The initial precursor, which has four chlorine atoms and one bromine atom, was prepared in two steps from a commercially available compound through iterative Buchwald–Hartwig coupling. The first key step in sequential multiple borylation, *i.e.*, the one-pot borylation of the initial precursor, was the construction of a DABNA skeleton retaining four chlorine atoms. Lithium–bromine exchange was followed by a bora-Friedel–Crafts reaction in the presence of 2.0 equiv. of BBr_3, which afforded a DABNA derivative bearing four chlorine atoms in 42% yield. The second key step, *i.e.*, the introduction of four diphenylamino groups into the DABNA derivative, was achieved by Buchwald–Hartwig coupling with diphenylamine, which afforded the final borylation precursor in 88% yield. The third key step was the one-shot borylation. Importantly, the HOMO of the final borylation precursor was mainly localised on the DABNA skeleton, and regioselective borylation reactions were therefore expected. Indeed, in the presence of DTBPY, the one-shot double borylation with 8.0 equiv. of BI_3 afforded **ω-DABNA** in 50% yield. In the absence of DTBPY, a significant drop in yield (4%) was observed, and a considerable amount of the precursor (80%) was recovered. This indicated that the sterically hindered DTBPY selectively captured the *in situ* generated HI to promote borylation and suppress deborylation *via* the retro-bora-Friedel–Crafts reaction. In addition, the final one-shot borylation with BBr_3 was carried out at 180 °C to afford **ω-DABNA** in a yield of 23%, which is lower than that obtained with BI_3 as the boron source (50%) because of the lower reactivity of BBr_3.

At about the same time as Hatakeyama *et al.*, Zysman-Calman *et al.* independently reported the synthesis of ladder-type deep-blue MR compounds **NBONacene** and **MesBDIDOBNA-N** using a protocol which can be categorized as sequential multiple borylations (Scheme 38).[253,254] One-pot borylation afforded ***p*MDBA-Br** in 73% yield, with subsequent coupling giving the final borylation precursors in 47% and 57% yields, respectively. One-shot borylation was performed with excess BBr_3, and the R2BBr species generated *in situ* were trapped with a Grignard reagent to afford the target compounds, **NBONacene** and **MesB-DIDOBNA-N**, in 45% and 74% yields, respectively. Although the final borylation step does not construct a fully fused structure around the introduced boron atom, these synthesis methods also seem to be sequential multiple borylation protocols.

Sequential multiple borylation can be useful for the synthesising MR-TADF materials, especially those bearing multiple boron atoms at the same aromatic ring, and thus has the potential to become a new standard protocol for MR emitter synthesis.
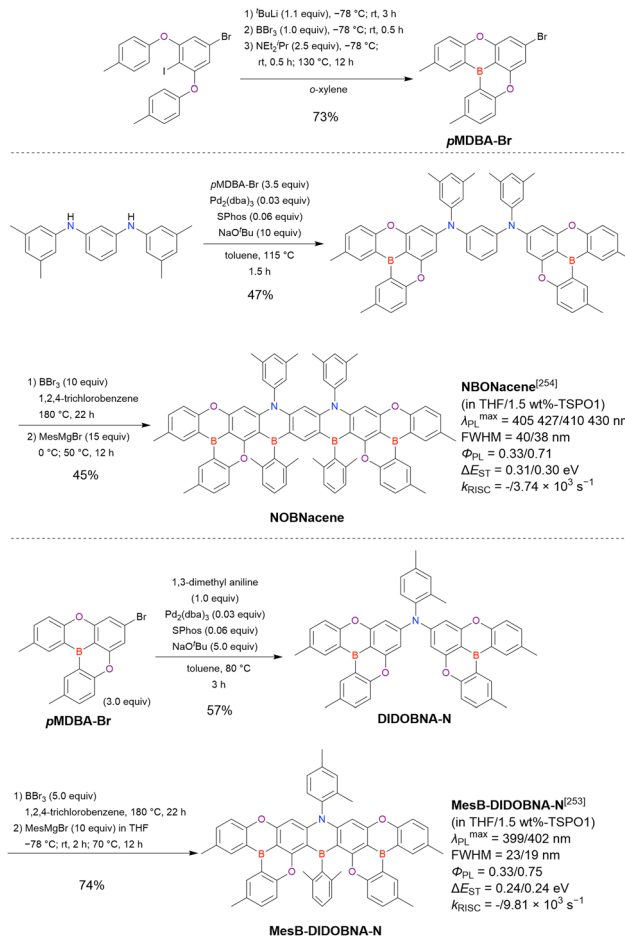
Scheme 38 Synthesis of **NOBNacene** and **MesB-DIDOBNA-N** by sequential multiple borylation.

3.4 Summary

One-shot borylation converts multiple C–H/N–H bonds into C–B/N–B bonds to construct the boron-embedded π-conjugated skeletons in one shot. This is a powerful synthesis method for producing π-extended MR compounds. Furthermore, a sequential multiple borylation protocol that elaborately combines one-shot borylation and one-pot borylation was recently developed to expand the chemical space of MR compounds. Since detailed discussion of the photophysical properties of each obtained compound is beyond the scope of this review, we summarise the photophysical data for the related compounds in Table 28, and provide brief structure–property correlations. Basic relationships, such as the dependence of the maximum emission wavelength on the electron-donating abilities of the substituents, can be explained in a similar way to that of compounds obtained by one-pot borylation (see Sections 2.2.2 and 2.3.2). Most π-extended MR compounds with multiple boron atoms obtained by one-shot borylation show a small ΔE_{ST} and large k_{RISC} because of enhanced short-range CT and long-range electronic delocalisation in the excited states.[74] Although π-extensions with 1,2-azaborine, heterole, and perylene result in materials with poor TADF properties because of the partial cancelation of the MR effect, the rigid and π-extended

Table 28 Photophysical properties of the compounds shown in Section 3

Compound	Condition	λ_{PL}^{max} [nm]	FWHM [nm]	Φ_{PL} [—]	ΔE_{ST} [eV]	k_{RISC} [s^{-1}]	Ref.
B2	CH$_2$Cl$_2$/1 wt%-PMMA[a]	461/455	39/32	0.19/0.68	0.12/0.18	—/4.1 × 10^4	217
B3	CH$_2$Cl$_2$/1 wt%-PMMA[a]	442/441	50/34	0.13/0.47	0.31/0.15	—/—	217
B4	CH$_2$Cl$_2$/1 wt%-PMMA[a]	449/450	22/38	0.21/0.61	0.19/0.15	—/—	217
B2-F	1 wt%-PMMA[a]	467	44	0.57	0.15	—	217
CzDABNA-NP-M/TB	Toluene/1 wt%-PMMA[a]	465/468	23/28	0.82/0.86	—/0.18	—/1.1 × 10^4	111
CzB2-M/TB	Toluene/1 wt%-PMMA[a]	473/491	23/34	0.72/0.88	—/0.11	—/2.4 × 10^4	111
BN1	Toluene/1 wt%-DBFPO[a]	454/458	18/22	—/0.91	0.20/0.15	—/1.3 × 10^4	218
BN2	Toluene/1 wt%-DBFPO[a]	464/467	15/22	—/0.93	0.16/0.13	—/2.6 × 10^4	218
BN3	Toluene/1 wt%-DBFPO[a]	456/458	17/21	—/0.98	0.15/0.12	—/2.55 × 10^5	218
OBN	Toluene/10 wt%-DBFPO[a]	425/—	30/46	0.85/0.50	0.20/—	—/1.3 × 10^4	219
NBN	Toluene/10 wt%-DBFPO[a]	440/—	29/43	0.90/0.71	0.12/—	—/2.9 × 10^4	219
ODBN	Toluene/10 wt%-DBFPO[a]	429/—	26/55	0.93/0.86	0.19/—	—/2.1 × 10^4	219
DABNA-NP-M	1 wt%-PMMA[a]	460	29	0.88	0.17	1.4 × 10^4	111
DABNA-NP-TB[b]	1 wt%-PMMA[a]	453	26	0.83	0.17	1.4 × 10^4	111
t-DAB-DPA[b]	3 wt%-mCBP:mCBP-CN[a]	—	—	0.94	—	3.97 × 10^4	220
PAB	Toluene/3 wt%-mCP[a]	449/453	23/—	—/0.61	—/0.06	—/6.95 × 10^4	221
2tPAB	Toluene/3 wt%-mCP[a]	456/457	26/—	—/0.67	—/0.08	—/6.34 × 10^4	221
3tPAB[b]	Toluene/3 wt%-mCP[a]	456/458	23/—	—/0.75	—/0.10	—/5.74 × 10^4	221
mBP-DABNA-Me	Toluene/5 wt%-mCP:DPEPO[a]	464/467	—/—	—/0.97	0.12/0.13	—/1.95 × 10^4	222
pBP-DABNA-Me	Toluene/5 wt%-mCP:DPEPO[a]	458/462	15/22	—/0.98	0.11/0.18	—/6.85 × 10^4	223
BP-2DPA	Toluene/1 wt%-DIC-TRz[a]	599/601	34/37	—/0.91	—/—	—/—	224
DBP-4DPA	Toluene/1 wt%-DIC-TRz[a]	605/612	34/35	—/0.96	—/—	—/—	224
CzDABNA-NP	Toluene/1 wt%-PMMA[a]	457/461	23/30	0.88/0.80	—/0.18	—/1.6 × 10^4	111
CzDABNA-NP-TB/H	Toluene/1 wt%-PMMA[a]	462/465	16/30	0.86/0.82	—/0.18	—/1.3 × 10^4	111
Cz2DABNA-NP-M/TB	Toluene/1 wt%-PMMA[a]	479/478	23/29	0.95/0.85	—/0.14	—/7.3 × 10^4	111
tCBNDA	CH$_2$Cl$_2$/neat/7 wt%-DBFDPO[a]	467/470/472	28/47/37	—/—/0.72	—/—/0.05	—/—/8.55 × 10^4	225
DPACzBN2	Toluene/3 wt%-26DCzPPy[a]	460/470	22/29	—/0.92	—/0.12	—/2.9 × 10^4	195
DPACzBN3	Toluene/3 wt%-26DCzPPy[a]	468/475	20/27	—/0.94	—/0.13	—/2.1 × 10^4	195
mICz-DABNA	Toluene/3 wt%-mCBP-CN[a]	461/465	22/26	—/0.93	0.20/—	—/2.65 × 10^4	226
BFCz-DABNA	Toluene/3 wt%-mCBP-CN[a]	456/462	22/26	—/0.93	0.20/—	—/2.78 × 10^4	226
DPMX-CzDABNA	Toluene/15 wt%-SF3-TRZ[a]	471/481	22/29	—/0.94	—/0.11	—/6.6 × 10^4	227
mono-mx-CzDABNA	Toluene/3 wt%-mCBP[a]	474/—	34/—	0.77/0.83	0.15/—	—/2.86 × 10^5	228
tri-mx-CzDABNA	Toluene/3 wt%-mCBP[a]	462/—	26/—	0.68/0.91	0.16/—	—/2.85 × 10^5	228
Me-PABO	Toluene/5 wt%-PPF[a]	453/457	21/26	—/0.88	0.17/—	—/3.50 × 10^4	229
Me-PABS	Toluene/5 wt%-PPF[a]	463/470	21/32	—/0.92	0.15/—	—/5.59 × 10^4	229
tDMAC-BN	Toluene/1 wt%-PMMA[a]	468/—	26/—	—/0.90	0.15/—	—/4.80 × 10^4	230
tDPAC-BN	Toluene/1 wt%-PMMA[a]	454/—	19/—	—/0.94	0.17/—	—/1.16 × 10^4	230
PhDMAC-BN	Toluene/5 wt%-PPF[a]	473/483	27/34	—/0.86	0.14/—	—/5.04 ×10^4	231
PTZBN3	Toluene/26DCzPPy[a]	468/473	30/36	—/0.98	0.17/—	—/1.08 × 10^5	196
PTZBN2	Toluene/26DCzPPy[a]	483/487	41/42	—/0.95	0.15/—	—/4.51 × 10^4	196
DOBNA-Oar	Toluene/neat	388/433	34/—	0.65/—	0.16/—	—/—	60
1B-DTACrs	Toluene/5 wt%-mCBP[a]	438/443	27/28	0.99/0.83	0.22/0.21	—/—	232
2B-DTACrs	Toluene/5 wt%-mCBP[a]	443/448	21/24	0.64/0.74	0.16/0.16	—/1.3 × 10^5	232
Cl-MR	Toluene/10 wt%-DPEPO[a]	460/474	27/36	—/0.85	0.14/0.13	—/9.8 × 10^4	233
Br-MR	Toluene/10 wt%-DPEPO[a]	460/474	27/36	—/0.76	0.14/0.13	—/5.9 × 10^5	233
DBT-BN	Toluene	494	22	—	—	—	234
DBF-DBN	Toluene/2 wt%-CBP[a]	514/529	22/—	—/0.90	0.24/—	—/1.1 × 10^5	234
DBT-DBN	Toluene/2 wt%-CBP[a]	516/525	19/—	—/0.90	0.25/—	—/7.4 × 10^5	234
OAB-ABP-1	Toluene/1 wt%-PMMA[a]	503/506	31/34	>0.99/0.90	—/0.12	—/4.0 × 10^4	235
CzB2-M/P	1 wt%-PMMA[a]	504	39	0.87	0.06	5.1 × 10^4	111
Cz2B2-M/TB	Toluene/1 wt%-PMMA[a]	469/483	24/38	0.70/0.88	—/0.11	—/3.1 × 10^4	111
C-BN	Toluene	450	19	1.00	0.21	1.8 × 10^4	236
TPD4PA	Toluene/3 wt%-mCBP-CN[a]	445/—	19/—	—/0.88	0.05/—	—/2.51 × 10^5	237
tBu-TPD4PA	Toluene/3 wt%-mCBP-CN[a]	451/—	19/—	—/0.90	0.06/—	—/2.44 × 10^5	237
DTBN-B2N3	Toluene/3 wt%-26DCzPPy[a]	471/475	23/—	0.97/0.96	0.10/—	1.6 × 10^6/1.2 × 10^6	152
ν-DABNA	Toluene/1 wt%-DOBNA-Oar	468/467	14/18	0.74/0.90	—/0.017	—/2.0 × 10^5	60
ν-DABNA-O-Me	Toluene/1 wt%-PMMA[a]	461/464	19/24	0.90/0.90	—/0.029	—/1.6 × 10^5	238
t-Bu-ν-DABNA	Toluene/5 wt%-DBFPO[a]	467/—	14/—	—/0.92	0.04/—	—/2.54 × 10^5	134
m-ν-DABNA	Toluene/3 wt%-DBFPO[a]	464/—	14/—	—/0.91	0.07/—	—/2.30 × 10^5	240
4F-ν-DABNA	Toluene/3 wt%-DBFPO[a]	457/—	14/—	—/0.90	0.05/—	—/2.28 × 10^5	240
4F-m-ν-DABNA	Toluene/3 wt%-DBFPO[a]	455/—	14/—	—/0.89	0.07/—	—/2.10 × 10^5	240
o-Tol-ν-DABNA-Me	Toluene/3 wt%-DBFPO[a]	466/472	14/—	0.92/0.99	∼0.01/—	2.95 × 10^5/3.21 × 10^5	241
NO-DBMR	Toluene/5 wt%-DBFPO[a]	458/—	14/—	—/0.83	0.04/—	—/1.04 × 10^5	239
Cz-DBMR	Toluene/5 wt%-DBFPO[a]	480/—	14/—	—/0.82	0.04/—	—/3.72 × 10^5	239
Π-CzBN	Toluene/1 wt%-mCP[a]	486/—	16/—	0.96/0.98	—/0.04	—/2.9 × 10^5	242
V-DABNA-Mes	Toluene/1 wt%-PMMA[a]	486/484	13/16	0.79/0.80	—/0.0085	4.22 × 10^5/4.4 × 10^5	243
V-DABNA	Toluene/1 wt%-PMMA[a]	483/481	14/17	0.85/0.90	—/0.0060	7.14 × 10^5/5.7 × 10^5	244
V-DABNA-F	Toluene/1 wt%-PMMA[a]	467/464	13/16	0.91/0.81	—/0.0049	5.06 × 10^5/6.5 × 10^5	244
CzB4	0.1 wt%-PS[a]	483	14	0.92	0.012	1.8 × 10^5	245
CzB6	0.1 wt%-PS[a]	488	12	0.94	0.021	3.0 × 10^5	245

This journal is © The Royal Society of Chemistry 2024

Chem. Soc. Rev., 2024, **53**, 1624–1692 | **1665**

Table 28 (*continued*)

Compound	Condition	λ_{PL}^{max} [nm]	FWHM [nm]	Φ_{PL} [—]	ΔE_{ST} [eV]	k_{RISC} [s^{-1}]	Ref.
CzB8	0.1 wt%-PS[a]	491	12	0.92	0.0039	6.5×10^5	245
CzB4-oPh	0.1 wt%-PS[a]	478	16	0.93	0.019	6.4×10^4	245
m[B-N]N1	Toluene/2 wt%-mCPBC[a]	481/483	29/28	0.93/0.91	0.15/0.15	$3.8 \times 10^3/1.59 \times 10^4$	248
m[B-N]N2	Toluene/2 wt%-mCPBC[a]	491/491	34/33	0.91/0.90	0.10/0.13	$2.4 \times 10^3/1.44 \times 10^4$	248
p[B-N]O	Toluene/1 wt%-mCPBC[a]	488/497	19/23	0.93/0.91	0.43/0.44	—/—	249
p[B-N]NO	Toluene/1 wt%-mCPBC[a]	522/529	28/30	0.90/0.89	0.40/0.37	—/—	249
p[B-N]N	Toluene/1 wt%-mCPBC[a]	442/450	19/25	0.84/0.83	0.28/0.26	—/—	249
BN2	THF/5 wt%-mCBP[a]	567/—	97/—	0.64/—	—/0.19	—/2.10×10^5	250
TCz-BN2	THF/5 wt%-mCBP[a]	584/—	108/—	0.61/—	—/0.17	—/2.44×10^5	250
BN3	THF	694	151	0.01	—/—	—/—	250
ω-DABNA	Toluene/1 wt%-DOBNA-Ph[c]	509/509	18/22	0.92/0.87	—/0.013	$1.3 \times 10^5/1.2 \times 10^5$	252
NBONacene	THF/1.5 wt%-TSPO1[a]	305 427/410 430	40/38	0.33/0.71	0.31/0.30	—/3.74×10^3	254
MesB-DIDOBNA-N	THF/1.5 wt%-TSPO1[a]	399/402	23/19	0.33/0.75	0.24/0.24	—/9.81×10^3	253

[a] See Table 2 for the full compound name. [b] Same compound named differently. [c] See Scheme 3.

framework provides a narrow FWHM, which is suitable for use as a TE for hyperfluorescence or PSF OLEDs. Thus, one-shot borylation has contributed significantly to the development of excellent emitters for OLEDs. However, the accessible chemical space is still limited because this reaction can only proceed at sterically unhindered carbons with a certain HOMO distributions. Therefore, it is desirable to develop new methodologies to further expand the chemical space.

4. Late-stage functionalisation

As shown in previous sections, the photophysical properties of MR compounds, including their TADF characteristics, can be tuned over a wide range through the introduction of appropriate substituents. The routes to compounds with planar tricoordinate boron can be classified into those with early- and late-stage functionalisation relative to borylation–cyclisation. The embedded boron centre sometimes limits certain types of post-reactions, *e.g.*, some nucleophiles form tetra-coordinated species while strongly acidic conditions promote retro-Friedel–Crafts reactions. Moreover, certain functional groups inhibit borylation, *e.g.*, Lewis bases such as pyridyl groups can coordinate borylation reagents such as BBr$_3$, especially in the case of one-shot borylation. Thus, compounds with certain functional groups require appropriate synthesis approaches. In addition, late-stage functionalisation is advantageous for developing a series of derivatives and comparing their properties, even if these compounds can be synthesised using both schemes. Indeed, the first example of donor-functionalised DOBNA (**DOBNA-Phenox**) was synthesised by one-pot borylation (Fig. 6),[37,105] while a wide variety of donor units have recently been developed using late-stage functionalisation. This section discusses compounds prepared using post-borylation functionalisation to understand the factors determining the success of a given approach and therefore covers a wide variety of properties and structures. In particular, the DOBNA scaffold, which holds some distinct merits besides the MR effect with short-range CT, is frequently incorporated as an acceptor unit into D–A-type TADF molecules showing long-range CT. Furthermore, this relatively stable scaffold can be used to synthesise B-doped PAHs

with electronic structures largely modulated by heterocycle fusion. In contrast, the functionalisation of the N,B,N-embedded CzBN structure mainly aims to improve the MR effect and OLED performances. The general synthesis procedures are summarised in Schemes 39–41 and 45, which cover most of the compounds appearing in this section. Thus, the structures and properties of these compounds are separately summarised in the following figures and tables. Meanwhile, certain reaction types such as nucleophilic addition and oxidation are discussed in additional schemes in each case.

4.1 Preparation of key intermediates bearing Br and Bpin groups

In the case of DOBNA, late-stage substitution is possible at 2, 3, 4, 6, and 7-positions *via* bromo-functionalisation (Fig. 23). In
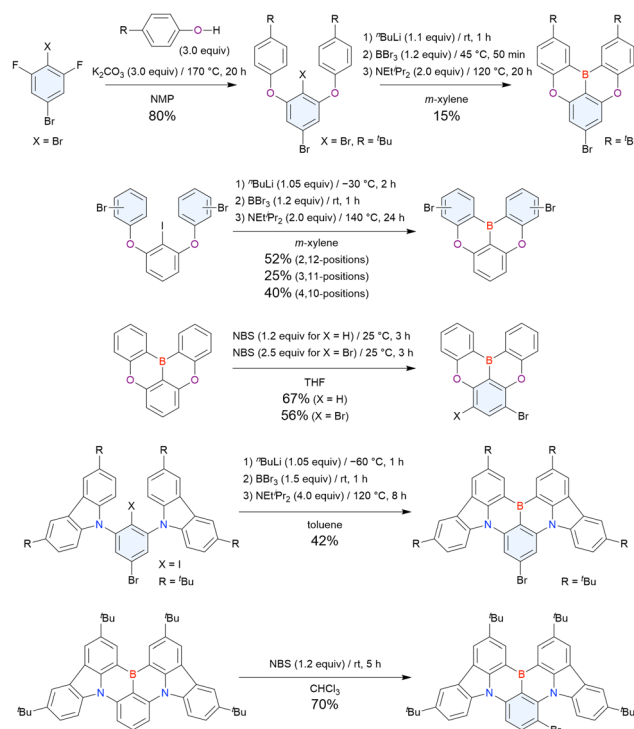
Scheme 39 Synthesis of bromo-substituted DOBNA and CzBN. The reaction conditions are reported in ref. 122, 119, 256, 184 and 258.

1666 | *Chem. Soc. Rev.*, 2024, **53**, 1624–1692

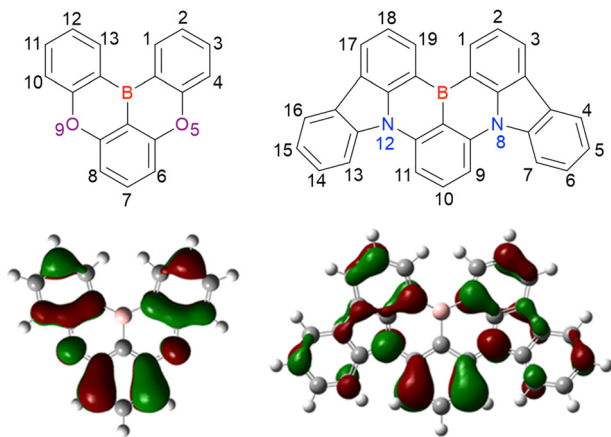This journal is © The Royal Society of Chemistry 2024

Fig. 23 Atomic position numbers and HOMO distribution for DOBNA and CzBN.

particular, 7-bromo DOBNA derivatives, which can be prepared as shown in Scheme 39, are often subjected to Buchwald–Hartwig coupling to introduce arylamine electron donors.[122] The ^{t}Bu groups at the peripheral 2,12-positions of the terminal phenyl rings reduce aggregation in the solid state. In addition, alkyl groups result in acceptor strengths lower than that of the unsubstituted DOBNA core (R = H), thus inducing a blue shift of the emission spectrum while increasing ΔE_{ST} when a donor unit is connected to 7-position.[202,255] Regarding borylation, lithium–halogen exchange might preferentially occur at the *ortho*-bromo atom with respect to the oxygen atoms despite the presence of two bromo atoms. Compounds prepared *via* lithium–bromine exchange were obtained in yields of up to ∼50%,[127,129] and the yields were not improved with lithium–iodine exchange using iodine compounds (X = I).[120,124] Dibromo derivatives substituted at the terminal phenyl rings were synthesised in a similar manner in moderate yields.[119] On the other hand, 6-monobromo and 6,8-dibromo derivatives were prepared by the bromination of **DOBNA** with NBS because of the large HOMO coefficients at 6- and 8-positions (Fig. 23).[256] The HOMO distribution also indicated the difficulty of brominating DOBNA at 7-position after borylation, which explains the different synthesis strategy depicted in Scheme 39. Most CzBN derivatives used for late-stage reactions bear four ^{t}Bu groups at 2,5,15,18-positions except for a very limited number of examples because these substituents hinder side reactions and increase the solubility of products.[162,257] CzBN derivatives mono-brominated at 10- and 9-positions were obtained using the approach employed to access brominated DOBNA derivatives.[184,258] Similarly, intermediates with various cyclised
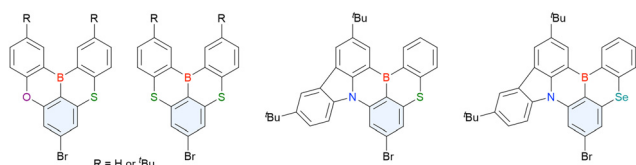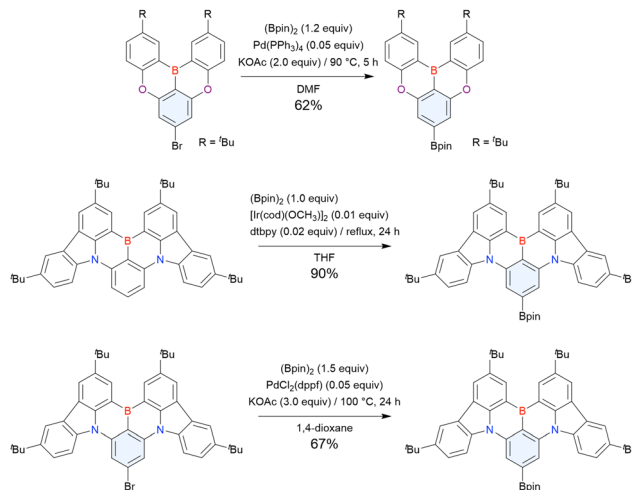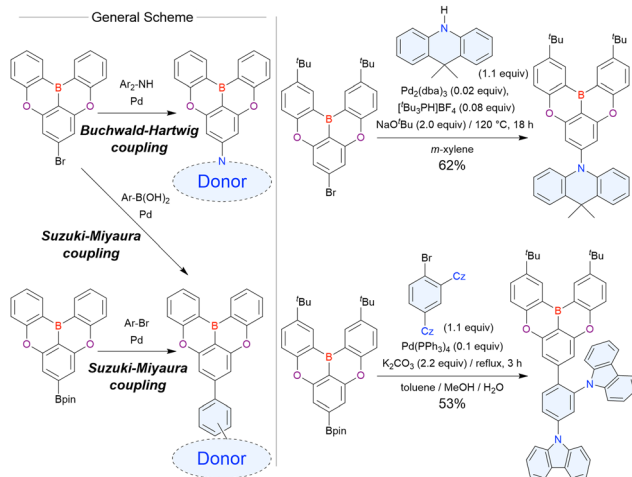

Fig. 24 Brominated derivatives with S- and Se-bridged structures.

Scheme 40 Synthesis of Bpin-substituted DOBNA and CzBN. The reaction conditions are reported in ref. 259, 260, and 185.

Scheme 41 Late-stage introduction of donor groups into DOBNA. The right panel shows the specific reaction conditions appearing in ref. 122 and 259.

configurations and heteroatom bridges used for late-stage reactions were obtained by essentially identical methods (Fig. 24).[116,130,131,133,168,169] DOBNA and CzBN derivatives bearing boronic ester groups, which engage in Suzuki–Miyaura coupling with aryl halides, can be synthesised from brominated derivatives *via* Miyaura–Ishiyama borylation or iridium-catalysed direct aromatic C–H (Hartwig–Miyaura) borylation (Scheme 40).[118,135,185,259–261] An asymmetric bridge with N and O atoms was also demonstrated.[95]

4.2 Donor-functionalised DOBNA-based materials

The DOBNA structure is useful for developing OLED host materials with high triplet energies as well as D–A-type TADF molecules with efficient spin–flip processes.[37,112] The introduction of arylamine (*e.g.*, carbazole-, diphenylamine-, 9,10-dihydroacridine- and
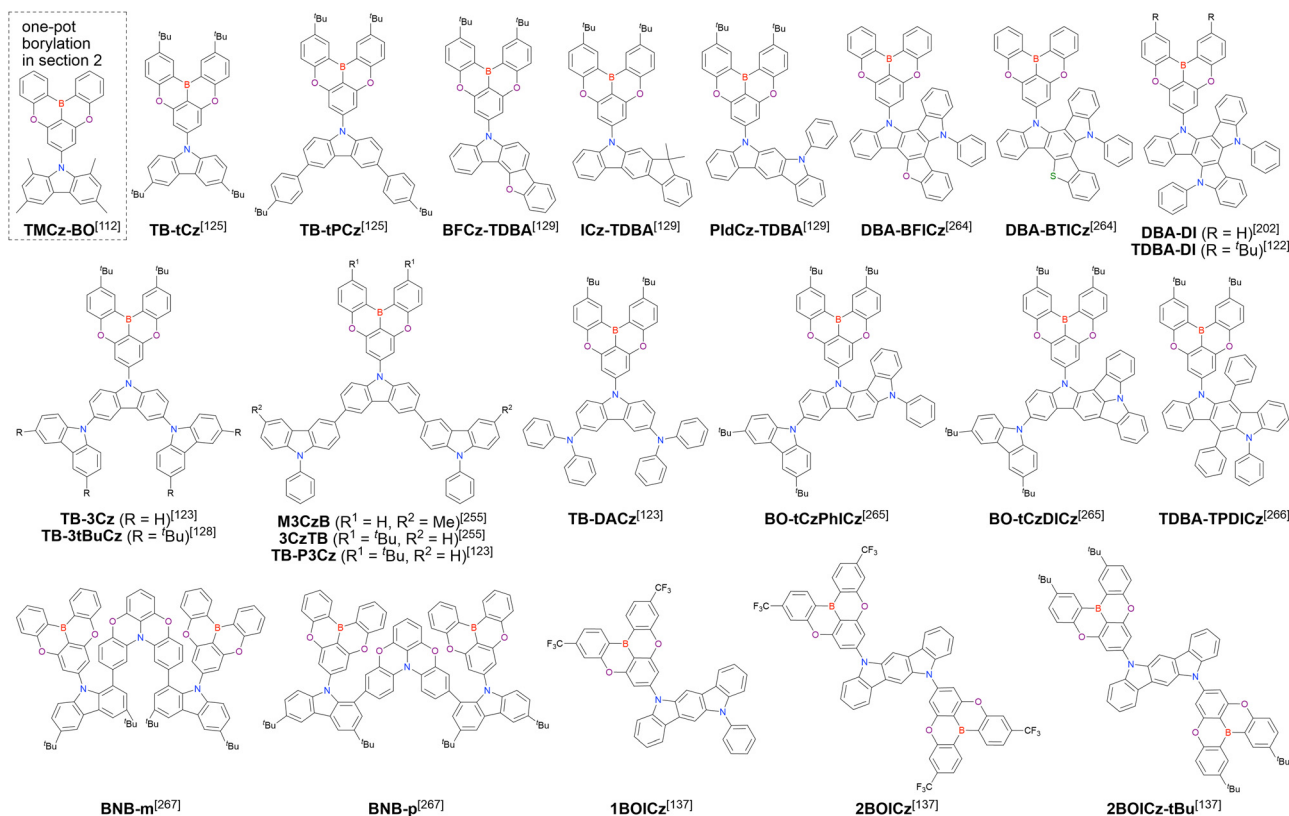
Fig. 25 DOBNA-based D–A-type TADF materials with carbazole-based donors at 7-position synthesised by late-stage functionalisation except **TMCz-BO**.

phenoxazine-based) donors by Buchwald–Hartwig coupling affords highly efficient D–A-type TADF emitters (Scheme 41). We emphasise that one-pot borylation is also useful for developing simple donor-functionalised DOBNA derivatives (Fig. 25 and 26). As mentioned above, the advantages of utilising DOBNA structures are the easy derivation of deep blue and relatively sharp emission owing to the high excited-state energies and rigid structures compared to those of acceptors such as sulfones used

in other deep blue emitters, although the emission colour can be tuned to orange-red by changing donor strength. The combination of the DOBNA structure and donors featuring spacers, such as the phenyl group, synthesised by Suzuki–Miyaura coupling leads to weak D–A interactions including through-space CT interactions and results in ultradeep blue (<450 nm) emitter and host materials.[259,262,263] The Buchwald–Hartwig amination of DOBNA derivatives typically proceeds in the presence of $Pd_2(dba)_3$
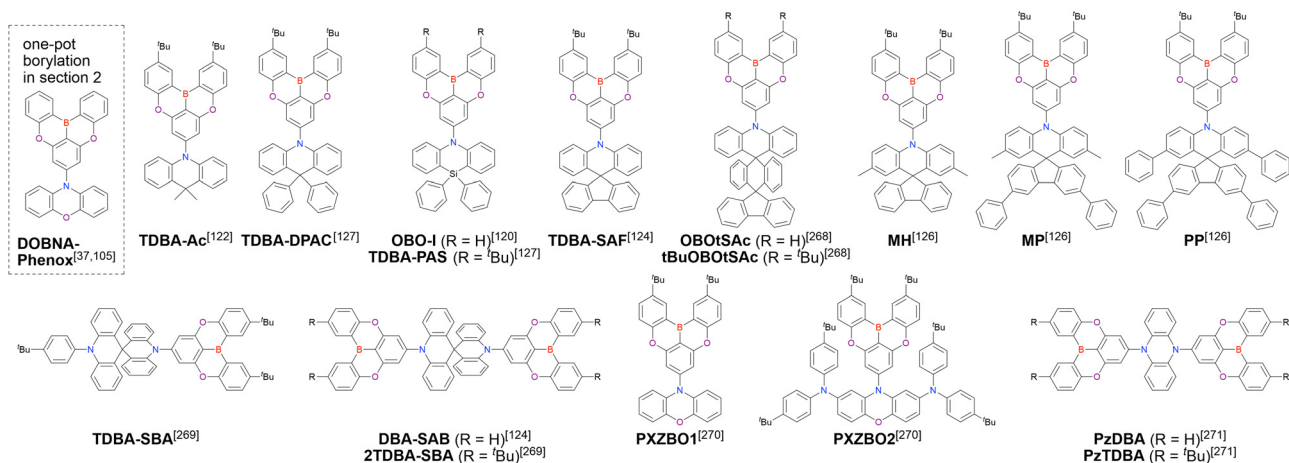
Fig. 26 DOBNA-based D–A-type TADF materials with 9,10-dihydroacridine-, phenoxazine- and 5,10-dihydrophenazine-based donors at 7-position synthesised by late-stage functionalisation except **DOBNA-Phenox**.

1668 | *Chem. Soc. Rev.*, 2024, **53**, 1624–1692

This journal is © The Royal Society of Chemistry 2024

Table 29 Photophysical properties of the materials shown in Fig. 25

Compound	Condition	λ_{PL}^{max} [nm]	FWHM [nm]	Φ_{PL} [—]	ΔE_{ST} [eV]	k_{RISC} [s^{-1}]	Ref.
TMCz-BO	Toluene/30 wt%-PPF[b]	446/467	—/—	0.81/0.98	—/0.020	—/1.9 × 10^6	112
TB-tCz	Toluene/neat-film	415/433	45/44[b]	0.53/0.41	0.23/0.20	—/0.85 × 10^6	125
TB-tPCz	Toluene/neat-film	422/445	46/42[b]	0.56/0.52	0.17/0.15	—/1.05 × 10^6	125
BFCz-TDBA	Toluene/20 wt%-mCP[a]	393/424[b]	36/41[b]	0.84/0.58	0.24/—	—/0.91 × 10^6	129
ICz-TDBA	Toluene/20 wt%-mCP[a]	416/431[b]	49/45[b]	0.84/0.63	0.19/—	—/1.27 × 10^6	129
PIdCz-TDBA	Toluene/20 wt%-mCP[a]	424/433[b]	43/43[b]	0.88/0.55	0.20/—	—/1.14 × 10^6	129
DBA-BFICz	Toluene/25 wt%-DBFPO[a]	446/476[b]	—/64[b]	—/0.97	0.17/—	—/3.50 × 10^5	264
DBA-BTICz	Toluene/25 wt%-DBFPO[a]	445/476[b]	—/64[b]	—/0.95	0.29/—	—/6.30 × 10^5	264
DBA-DI	Toluene/30 wt%-mCBP-can	467/—	—/—	—/0.95	0.03/—	—/6.21 × 10^6	202
TDBA-DI	Toluene/20 wt%-DBFPO[a]	456/—	55/65[b]	—/0.99	0.11/0.05	—/1.08 × 10^6	122
TB-3Cz	Toluene/neat-film	413/433	—/—	0.52/0.97	—/—	—/2.54 × 10^5	123
TB-3tBuCz	Toluene/10 wt%-26DCzPPy[a]	425/425[b]	46/46[b]	—/1.00	0.05/—	—/2.70 × 10^5	128
M3CzB	Toluene/20 wt%-DBFPO[a]	445/478[b]	—/—	—/0.93	0.14/—	—/1.40 × 10^5	255
3CzTB	Toluene/20 wt%-DBFPO[a]	433/470[b]	—/—	—/0.88	0.23/—	—/1.02 × 10^5	255
TB-P3Cz	Toluene/neat-film	433/460	—/—	0.51/0.92	—/—	—/2.46 × 10^5	123
TB-DACz	Toluene/neat-film	493/494	—/—	0.52/0.89	—/—	—/1.35 × 10^5	123
BO-tCzPhICz	Toluene/30 wt%-mCP[a]	440/444	52/54	—/0.93	—/0.08	—/3.44 × 10^6	265
BO-tCzDICz	Toluene/30 wt%-mCP[a]	438/451	50/50	—/0.77	—/0.15	—/2.09 × 10^6	265
TDBA-TPDICz	Toluene/20 wt%-DBFPO[a]	447/462[b]	—/58[b]	—/0.86	0.41/—	—/1.15 × 10^5	266
BNB-m	Toluene/10 wt%-mCP[a]	504/502	60/72[b]	—/1.00	—/0.03	—/1.60 × 10^5	267
BNB-p	Toluene/10 wt%-mCP[a]	529/518	64/74[b]	—/0.86	—/0.11	—/9.88 × 10^4	267
1BOICz	Toluene/20 wt%-mCPBC[a]	527/534	85/101[b]	0.90/1.00	—/0.05	—/1.12 × 10^6	137
2BOICz	Toluene/20 wt%-mCPBC[a]	518/528	83/91[b]	0.89/1.00	—/0.06	—/1.18 × 10^6	137
2BOICz-tBu	Toluene/20 wt%-mCPBC[a]	—/467[b]	—/—	—/—	—/0.25	—/—	137

[a] See Table 2 for the full compound name. [b] Taken from the EL spectrum.

(0.01–0.2 equiv.), [^{t}Bu$_3$PH]BF$_4$ (0.015–0.3 equiv.), and NaO^{t}Bu (1–4 equiv.) in aromatic solvents at >100 °C, although SPhos and XPhos are sometimes used as ligands. Suzuki–Miyaura coupling typically proceeds under the standard conditions of Pd(PPh$_3$)$_4$ (0.02–0.1 equiv.) and aqueous K$_2$CO$_3$ (2–3 equiv.). The yields of these reactions are generally sufficiently high (40–80%).

The HOMO and LUMO energies of **DOBNA** (about −6.0 and −3.0 eV, respectively) are deeper than those of standard donor units such as di-^{t}Bu-carbazole and 9,10-dihydro-9,9-dimethylacridine. Hence, the functionalised DOBNA derivatives in Fig. 25 and 26 show CT excited states where the HOMO and LUMO are well separated in the substituted donor and DOBNA

moieties, respectively, as is commonly supported by DFT calculations. However, according to Tables 29 and 30, the FWHMs of these compounds are smaller than those typically observed for D–A-type TADF materials, probably because of a certain contribution of the MR effect. In addition, a markedly high Φ_{PL}, small ΔE_{ST}, and high k_{RISC} were simultaneously achieved.

The seminal work on this series of compounds was reported by Kwon *et al.* in 2019,[122] and numerous following papers described a wide variety of donor units. The emission wavelengths seemed to be linearly correlated with the strength of the D–A interactions. For example, the emission of **DBA-BFICz** was blue-shifted relative to that of **DBA-DI** with a stronger

Table 30 Photophysical properties of the materials shown in Fig. 26

Compound	Condition	λ_{PL}^{max} [nm]	FWHM [nm]	Φ_{PL} [—]	ΔE_{ST} [eV]	k_{RISC} [s^{-1}]	Ref.
DOBNA-Phenox	1 wt%-PMMA[b]/20 wt%-CBP[a]	492/504[b]	/—	0.92/—	0.06/—	—/—	37
TDBA-Ac	Toluene/20 wt%-DBFPO[a]	458/—	50/55[b]	—/0.93	0.06/—	—/0.99 × 10^6	122
TDBA-DPAC	Toluene/20 wt%-DPEPO[a]	444/450[b]	52/60[b]	0.88/0.88	0.04/0.02	—/1.23 × 10^6	127
OBO-I	Toluene/20 wt%-PPF[a]	439/451	51/60[b]	0.47/0.81	—/—	—/1.1 × 10^6	120
DTBA-PAS	Toluene/20 wt%-DPEPO[a]	427/435[b]	50/54	0.35/0.92	—/—	—/1.70 × 10^6	127
TDBA-SAF	Toluene/20 wt%-DPEPO[a]	450/456[b]	47/55[b]	—/0.90	—/0.11	—/2.1 × 10^6	124
OBOtSAc	Toluene/10 wt%-DPEPO[a]	452/454	50/50[b]	—/0.97	—/0.06	—/5.59 × 10^5	268
tBuOBOtSAc	Toluene/10 wt%-DPEPO[a]	446/450	48/48[b]	—/0.90	—/0.08	—/4.74 × 10^5	268
MH	Toluene/10 wt%-PPF[a]	477/473[b]	—/58[b]	—/0.99	−0.01/—	—/1.52 × 10^6	126
MP	Toluene/10 wt%-PPF[a]	472/470[b]	—/57[b]	—/0.98	0.02/—	—/0.58 × 10^6	126
PP	Toluene/10 wt%-PPF[a]	475/471[b]	—/57[b]	—/0.80	0.20/—	—/—	126
TDBA-SBA	Toluene/20 wt%-DBFPO[a]	450/467[b]	—/55[b]	—/0.89	0.01/—	—/1.37 × 10^6	269
DBA-SAB	Toluene/20 wt%-DPEPO[a]	460/472[b]	52/62[b]	—/0.87	—/0.07	—/1.9 × 10^6	124
2TDBA-SBA	Toluene/20 wt%-DBFPO[a]	448/475[b]	—/56[b]	—/0.87	0.01/—	—/1.35 × 10^6	269
PXZBO1	Toluene/20 wt%-DBFPO[a]	506/507	—/—	—/0.94	0.01/—	—/2.42 × 10^6	270
PXZBO2	Toluene/20 wt%-DBFPO[a]	572/552	—/—	—/0.97	0.01/—	—/1.49 × 10^6	270
PzDBA	Toluene/5 wt%-TCTA[a]:Bepp$_2$[a]	610/595[b]	—/—	—/0.85	—/0.05	—/0.84 × 10^6	271
PzTDBA	Toluene/5 wt%-TCTA[a]:Bepp$_2$[a]	599/576[b]	—/—	—/1.00	—/0.06	—/1.19 × 10^6	271

[a] See Table 2 for the full compound name. [b] Taken from the EL spectrum.

This journal is © The Royal Society of Chemistry 2024

Chem. Soc. Rev., 2024, **53**, 1624–1692 | **1669**

donor,[202,264] which enabled the fabrication of hyperfluorescence devices using **ν-DABNA**.[60] In addition, the emission of di-*t*Bu-substituted DOBNA derivatives was blue-shifted by ~10 nm relative to that of unsubstituted DOBNA derivatives, as represented by the **TDBA-DI** versus **DBA-DI** case in Table 29 and the **OBO-I** versus **DTBA-PAS** case in Table 30 despite the reports from different research groups.[120,122,127,202] Stronger D–A interactions also seem to reduce ΔE_{ST}, as shown by the comparison between **M3CzB** and **3CzTB**,[255] although comparing materials reported by different research groups may be more difficult because of the different criteria used to extract S_1 and T_1 energies from the spectra. Compounds having relatively strong donors with phenoxazine subunits (**DOBNA-Phenox**, **BNB-m**, **BNB-p**, **PXZBO1**, and **PXZBO2**) or strong electron-withdrawing CF_3 groups attached to the DOBNA structure (**1BOICz** and **2BOICz**) showed emission peaks at >500 nm,[137,267,270] *i.e.*, in the region where the hyperfluorescence system using green MR emitters is also operational.[163] In addition, A–D–A-type TADF compounds, **PzDBA** and **PzTDBA**, which represent a very rare configuration in the TADF family of materials, were developed using a 5,10-dihydrophenazine unit and showed orange to red emission.[271] However, these green to red emitters have relatively large FWHM values.

The distinct photophysical features of these materials are their quite short delayed-fluorescence lifetime (τ_d), weak concentration quenching, good solubility, and high molecular orientational factor. For D–A-type TADF materials, τ_d typically ranges from several to a few hundred microseconds and is generally shorter than that of MR-type TADF materials. In contrast, some of the materials in Fig. 25 and 26, *e.g.*, **TMCz-BO**, **ICz-TDBA**, **DBA-BFICz**, **TDBA-DI**, **DBA-DI**, **BO-tCzPhICz**, **BO-tCzDICz**, **1BOICz**, **2BOICz**, **TDBA-Ac**, **TDBA-SBA**, **DBA-SAB**, and **2TDBA-SBA**, showed nanosecond-scale τ_d values.[112,122,124,129,137,202,264,265,269] As shown in Tables 29 and 30, relatively high doping concentrations are generally selected for these compounds. In particular, **TB-3Cz**, **TB-P3Cz**, and **TB-DACz** showed very high Φ_{PL} values of >80% in the neat-film state.[123] As a result, aggregation-induced emission (AIE) properties were also investigated for these compounds as well as for

TB-tCz and **TB-tPCz**.[123,125] Meanwhile, the introduction of silicon suppressed the broadening of the emission spectra at high doping concentrations.[127] The solubility was also good despite the relatively planar nature of the DOBNA structure. For some compounds, namely **TB-tCz**, **TB-tPCz**, **BFCz-TDBA**, **ICz-TDBA**, **PIdCz-TDBA**, **TB-3Cz**, **TB-3tBuCz**, **TB-P3Cz**, **TB-DACz**, **BO-tCzPhICz**, and **BO-tCzDICz**, solution-processed OLEDs were fabricated, and high EQEs (>10%) and excellent CIE_y values (<0.1) were achieved.[123,125,128,129,265] The high EQEs of these compounds were ascribed to not only the high Φ_{PL} but also high degree of horizontal dipole orientation. In general, rigid and linear molecular shapes are favourable for increasing horizontal molecular orientation during vacuum deposition.[272] Therefore, linear molecules such as **TDBA-DI**, **3CzTB**, **BNB-m**, **1BOICz**, **2BOICz**, **TDBA-SAF**, **DBA-SAB**, **OBOtSAc**, **tBuOBOtSAc**, **TDBA-SBA**, **2TDBA-SBA**, **PzDBA**, and **PzTDBA** are oriented horizontally, as the high aspect ratios of the molecular-shape result in high orientation factors, which follow the order of **TDBA-SAF** < **DBA-SAB**, **1BOICz** < **2BOICz**, **OBOtSAc** < **tBuOBOtSAc**, and **TDBA-SBA** < **2TDBA-SBA**.[122,124,137,255,267–269,271]

The compounds shown in Fig. 27 are slightly different from those in Fig. 25 and 26. Although **BCz**, **BBFCz**, and **BICz** have CT excited states between donor and acceptor units, **BCz** also has an LE feature within the MR core according to the calculated S_1, while the emission spectrum of **BICz** has a vibrational shoulder.[259] Although the donor strength is higher for **BICz** than for **BBFCz**, the related emission maxima are similar (Table 31). This behaviour is different from that in the **BFCz-TDBA** versus **ICz-TDBA** case (Fig. 25), indicating a different nature of D–A interactions. However, these compounds also have the advantages of short τ_d (~1 μs), weak concentration quenching with high Φ_{PL} in the neat film, AIE, and solution processability. **BCzTC** features a D–A interaction through a σ-linker, which results in a very weak CT interaction. Therefore, this compound was used as a bipolar host for a basic TADF material (**t4CzIPN**), with **BDTC** adopted as a reference unipolar host.[262] **AC-BO**, **QAC-BO**, and **Cz-BO** were synthesised as shown in Scheme 42.[263] Although the organoboron atom generally acts as a Lewis acid, the Lewis acidity of the boron centre in the
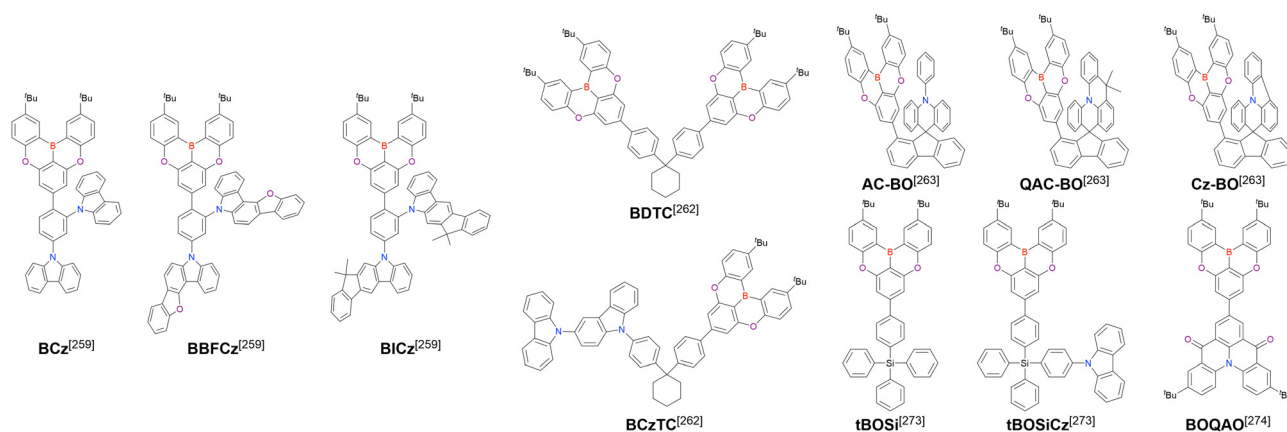

Fig. 27 DOBNA derivatives with substituents at 7-position synthesised by late-stage functionalisation.

1670 | *Chem. Soc. Rev.*, 2024, **53**, 1624–1692

This journal is © The Royal Society of Chemistry 2024

Table 31 Photophysical properties of the materials shown in Fig. 27

Compound	Condition	λ_{PL}^{max} [nm]	FWHM [nm]	Φ_{PL} [—]	ΔE_{ST} [eV]	k_{RISC} [s^{-1}]	Ref.
BCz	Toluene/neat-film	405/414	25/37	0.26/0.61	—/0.40	—/—	259
BBFCz	Toluene/neat-film	405/423	25/51	0.44/0.86	0.26/0.32	—/0.90 × 10^6	259
BICz	Toluene/neat-film	407/431	49/53	0.21/0.76	0.15/0.18	—/1.10 × 10^6	259
BDTC	Toluene/neat-film	403/416, 439	—/—	—/—	0.28/—	—/—	262
BCzTC	Toluene/neat-film	368, 404/414	—/—	—/—	0.24/—	—/—	262
AC-BO	Toluene/10 wt%-PMMA^a	—/446	—/57	—/0.77	0.13/—	—/0.23 × 10^6	263
QAC-BO	Toluene/10 wt%-PMMA^a	—/428	—/49	—/0.83	0.20/—	—/1.61 × 10^7	263
Cz-BO	Toluene/10 wt%-PMMA^a	—/411	—/35	—/0.89	0.29/—	—/—	263
tBOSi	Toluene/5 wt%-mCPCN^a	408/414	28/28	0.51/0.81	0.26/—	—/—	273
tBOSiCz	Toluene/5 wt%-mCPCN^a	408/414	28/28	0.52/0.85	0.21/—	—/—	273
BOQAO	Toluene/5 wt%-CBP^a	474/487	28/33	—/0.99	0.22/—	—/2.4 × 10^4	274

^{a} See Table 2 for the full compound name.
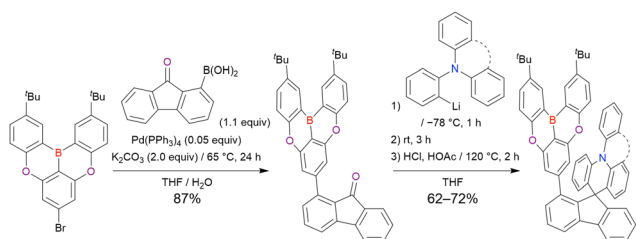
Scheme 42 Late-stage introduction of donor groups for through-space CT.

DOBNA scaffold might be decreased by the π-electrons of co-planar oxygen and become weaker than that of the carbonyl group. These compounds have through-space CT and thus exhibit deep blue emission. The emission properties of **tBOSi** and **tBOSiCz** should be similar to that of 7-phenyl-substituted DOBNA; moreover, the triphenylsilane moiety inhibits intermolecular interactions and thus helps to preserve the deep blue emission in the solid state.[273] The combination of a carbonyl-based MR structure (**QAO**) and DOBNA, named **BOQAO** and synthesised by Suzuki–Miyaura coupling (Scheme 41), should be critically different from the other abovementioned compounds because the DOBNA structure does not function as an acceptor owing to its LUMO level being shallower than that of **QAO**.[274] Thus, the photophysical properties of **BOQAO** are similar to those of **QAO**, although a weak long-range intramolecular CT is involved.

DOBNA derivatives substituted at positions other than 7-position are summarised in Fig. 28 and Table 32. The molecules described by Wang et al. and Wu et al. were developed in 2019.[119,256] The emission of compounds with two donors at the terminal phenyl rings was red-shifted relative to that of 7-substituted compounds (**m-Ac-DBNA** versus **TDBA-Ac**; **DBA-Cz** versus **TB-tCz**).[113,119,122,125] This class of compounds also showed high Φ_{PL} in the aggregated states including neat films (>90% for **p-AC-DBNA**), short τ_d (920 ns for **DBA-DTMCz**), and highly oriented alignment (>0.8 for **DBA-DTMCz** and **OBO-II**).[119–121] Notably, the EQE of the device with a neat **OBO-II**-based emissive layer reached 23.1%. In addition, the hyperfluorescence device with **ν-DABNA** doped into a **DBA-DTMCz**-based emissive layer showed an EQE of 43.9%, which is the highest value reported to date for such devices. Meanwhile, the three isomers of **AC-DBNA** display temperature-dependent emission and mechanochromism. In a series of **OBA** derivatives, phenoxazine derivatives (**OBA-O** and **OBA-BrO**) showed better Φ_{PL} and EQE values as well as emission maxima at shorter wavelengths than phenothiazine derivatives (**OBA-S** and **OBA-BrS**).[256] However, **OBA-BrS** showed the shortest τ_d of 810 ns. Bromo-substituted derivatives showed elevated k_{RISC} values owing to the heavy-atom effect.

The synthesis and properties of DOBNA-based polymers are summarised in Scheme 43 and Table 33. After the introduction of the vinyl group by the Stille coupling of 7-brominated DOBNA derivatives with tributylvinylstannane or by their Suzuki–Miyaura coupling with (para-vinylphenyl)boronic acid
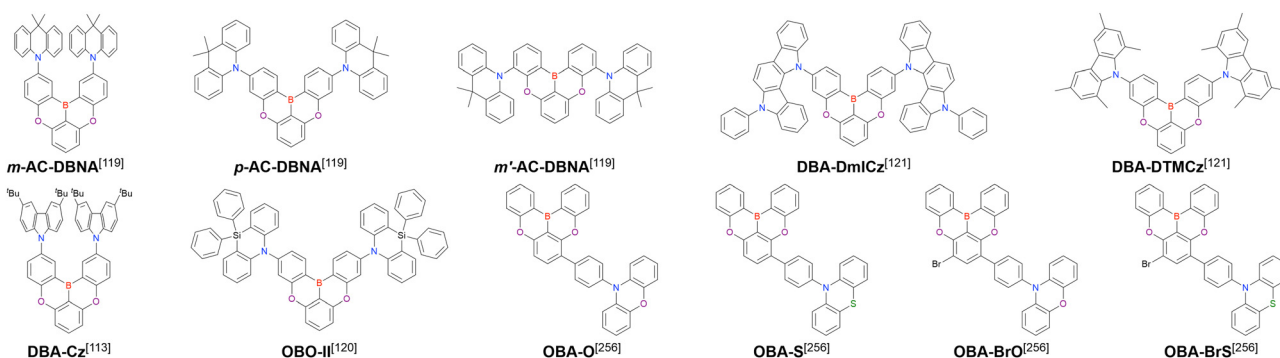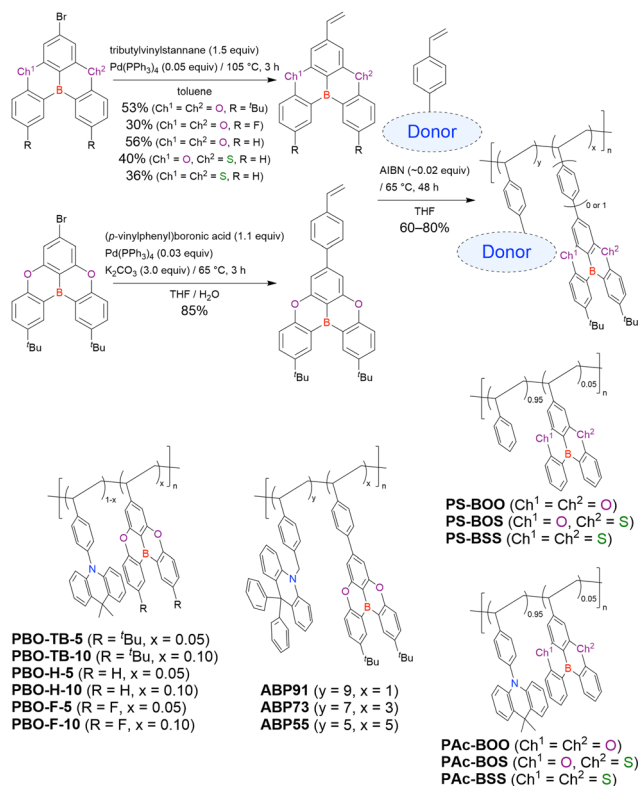

Fig. 28 DOBNA-based D–A-type TADF materials with substituents at 2, 3, 4 and 6-positions synthesised by late-stage functionalisation.

This journal is © The Royal Society of Chemistry 2024

Chem. Soc. Rev., 2024, **53**, 1624–1692 | **1671**

Table 32 Photophysical properties of the materials shown in Fig. 28

Compound	Condition	λ_{PL}^{max} [nm]	FWHM [nm]	Φ_{PL} [—]	ΔE_{ST} [eV]	k_{RISC} [s^{-1}]	Ref.
m-AC-DBNA	CH$_2$Cl$_2$/5 wt%-BCPO^a/neat-film	569/492/514	—/—/—	0.58/0.89/0.73	—/0.01/—	—/2.61 × 10^5/3.03 × 10^5	119
p-AC-DBNA	CH$_2$Cl$_2$/5 wt%-BCPO^a/neat-film	557/496/516	—/—/—	0.96/0.96/0.94	—/0.01/—	—/11.7 × 10^5/8.33 × 10^5	119
m'-AC-DBNA	CH$_2$Cl$_2$/5 wt%-BCPO^a/neat-film	568/498/518	—/—/—	0.51/0.87/0.70	—/0.03/—	—/8.44 × 10^5/3.98 × 10^5	119
DBA-DmICz	Toluene/30 wt%-DBFPO^a/neat-film	448/485^b/—	58/68^b/—	—/0.95/0.83	0.12/—/—	—/0.62 × 10^6/—	121
DBA-DTMCz	Toluene/30 wt%-DBFPO^a/neat-film	455/479^b/—	53/58^b/—	—/0.99/0.86	0.02/—/—	—/2.10 × 10^6/—	121
DBA-Cz	Toluene/10 wt%-DPEPO^a/neat-film	447/450/494	38/47/75	—/0.90/0.52	0.03/—/—	—/—/4.6 × 10^5	113
OBO-II	Toluene/20 wt%-PPF^a/neat-film	450/465/476	53/58^b/—	0.48/0.98/0.73	—/—/—	—/9.2 × 10^5/5.0 × 10^5	120
OBA-O	Toluene/10 wt%-mCP^a	444/450	—/—	0.76/0.84	—/0.09	—/4.28 × 10^5	256
OBA-S	Toluene/10 wt%-mCP^a	456/470	—/—	0.63/0.75	—/0.09	—/2.76 × 10^5	256
OBA-BrO	Toluene/10 wt%-mCP^a	470/476	—/—	0.84/0.92	—/0.04	—/8.97 × 10^5	256
OBA-BrS	Toluene/10 wt%-mCP^a	478/470	—/—	0.53/0.55	—/0.07	—/8.41 × 10^5	256

^{a} See Table 2 for the full compound name. ^{b} Taken from the EL spectrum.

Scheme 43 Synthesis of DOBNA-based polymers reported in ref. 132, 275, and 116.

Table 33 Photophysical properties of the materials shown in Scheme 43^a

Compound	Condition	λ_{PL}^{max} [nm]	FWHM [nm]	Φ_{PL} [—]	ΔE_{ST} [eV]	Ref.
PBO-TB-5	Neat-film	444	—	0.32	0.09	132
PBO-TB-10	Neat-film	453	—	0.37	0.09	132
PBO-H-5	Neat-film	448	—	0.44	0.06	132
PBO-H-10	Neat-film	455	—	0.48	0.07	132
PBO-F-5	Neat-film	471	—	0.65	0.01	132
PBO-F-10	Neat-film	480	—	0.70	0.02	132
ABP91	Neat-film	407	—	—	0.30	275
ABP73	Neat-film	412, 436	—	—	0.29	275
ABP55	Neat-film	414, 442	—	—	0.29	275
PS-BOO	Toluene	398 (LE)	33	0.73	—	116
PS-BOS	Toluene	435 (LE)	31	0.65	—	116
PS-BSS	Toluene	456 (LE)	30	0.59	—	116
PAc-BOO	Toluene	457 (CT)	63	0.44	—	116
PAc-BOS	Toluene	434 (LE), 475 (CT)	62	0.56	—	116
PAc-BSS	Toluene	455 (LE)	30	0.60	—	116

^{a} k_{RISC} values were not reported.

wavelengths (by ~10 nm) with increasing DOBNA molar fraction. On the other hand, the effect of this parameter on the emission spectra is more obvious for the **ABP** series.[275] In view of the absence of intramolecular through-space CT, which was confirmed in solution-phase emission spectra, the intermolecular D–A interactions in the film state caused the appearance of a new CT emission peak, resulting in a large variation of the CT/LE ratio upon going from **ABP91** to **ABP55**. Solution-processed OLEDs were fabricated using **PBO** derivatives as the emitter or **ABP** derivatives as the host for **t4CzIPN**, and EQEs of up to 15.0 and 22.2%, respectively, were achieved.

Wang *et al.* developed S-bridged DOBNA analogues (**BOS** and **BSS**) and investigated the photophysical properties of the parent structures and their polymers.[116] The introduction of sulphur reduced the energy gap by increasing HOMO and decreasing LUMO energies, thus resulting in deep blue emission with emission maxima of 434 nm (**BOS**) and 457 nm (**BSS**) without any substitutions. These maxima were red-shifted by 38–61 nm relative to that of unsubstituted **DOBNA** (**BOO**) at 396 nm. Importantly, the S-bridged structure preserved the narrow FWHMs (30, 29, and 27 nm for **BOO**, **BOS** and **BSS**, respectively). Moreover, k_{RISC} increased by one order of magnitude because of the enhancement of SOC *via* the heavy-atom
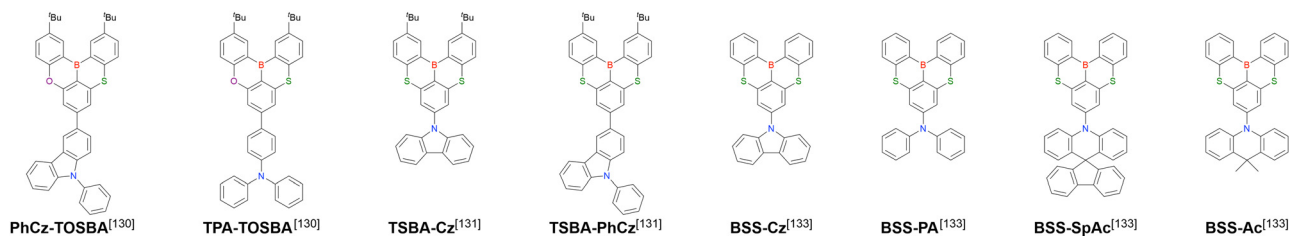
under palladium catalysis, co-polymers with donor units were synthesised by free radical polymerisation using 2,2′-azobis(isobutyronitrile) (AIBN) as an initiator.[116,132,275] Compounds of the **PBO** series showed through-space D–A interactions, which resulted in **PBO-TB-5** and **AC-BO** showing similar emission maxima (Fig. 27).[132,263] Although the Φ_{PL} values of the polymers were lower than those of small molecules, sufficiently small ΔE_{ST} values were achieved. The electron-donating ^{t}Bu and electron-withdrawing F groups attached to the DOBNA scaffold modulated D–A interactions in a similar manner to that observed for small molecules in Fig. 25 and 26. The emission maxima of **PBO** derivatives shifted to longer

1672 | *Chem. Soc. Rev.*, 2024, **53**, 1624–1692

This journal is © The Royal Society of Chemistry 2024

Fig. 29 S-Bridged DOBNA analogues synthesised by late-stage functionalisation.

effect of sulphur.[55] As a result, the delayed fluorescence ratio in total emission increased from 4% for **BOO** to 81% and 90% for **BOS** and **BSS**, respectively. Polystyrene (PS)-based polymers (**PS-BOO, PS-BOS,** and **PS-BSS**) showed emission similar to that of their parent DOBNA analogues. Interestingly, donor-based polymers showed different emission profiles because of the formation of CT excited states. The emission of **PAc-BOO** was broad, dependent on solvent polarity, and red-shifted by 59 nm compared to that of **PS-BOO**, which was assigned to long-range CT. In contrast, **PAc-BSS** showed only one narrow emission peak corresponding to the LE emission of MR **BSS** with short-range CT. **PAc-BOS** showed two (LE and CT) emission bands. This feature was clearly correlated with the increase in the HOMO energy of **BOO, BOS,** and **BSS**, and the small offset of HOMO levels between donor and acceptor units hindered CT formation. The OLED with **PAc-BSS** showed the highest EQE of 13.1% for blue TADF polymers with a CIE_y of < 0.15.

Small molecules with S-bridged DOBNA analogues and donor units connected at 7-position were subsequently developed (Fig. 29 and Table 34). Similar to the polymer case mentioned above, the higher HOMO levels of S-bridged structures resulted in red-shifted and LE-dominated emission. **PhCz-TOSBA** and **TPA-TOSBA** showed similar emission spectra in toluene, whereas the emission of **TPA-TOSBA** with a stronger donor exhibited partial long-range CT character.[130] For **TSBA-Cz** and **TSBA-PhCz**, both S_1 and T_1 states were LE-dominant, resulting in substantially similar photophysical properties based on the MR effect.[131] In **BSS-Cz, BSS-PA, BSS-SpAc,** and **BSS-Ac**, the HOMO levels of donor units become shallower in the order of Cz < PA < SpAc < Ac.[133] Similar to **TSBA-Cz, BSS-Cz** showed LE-dominated emission with a narrow FWHM of 28 nm because of the small HOMO offset. Notably, the emission wavelength was red-shifted by the incorporation of ^tBu

groups, which differed from the CT emission in D–A-type molecules in Fig. 25 and 26, suggesting pure MR emission. Although no CT between **BSS** and 9,10-dihydro-9,9-dimethyla-cridine was observed in the **PAc-BSS** polymer, **BSS-SpAc** and **BSS-Ac** showed long-range CT emission in addition to LE emission.

Scheme 44 shows some examples of the fused π-extension of DOBNA derivatives. The synthesis of **Ph-OBNA** involved Suzuki–Miyaura coupling followed by cyclisation and *N*-aryl coupling reactions.[276] Although **Ph-OBNA** showed TADF properties, its planar structure led to excimer formation at high concentrations and ACQ. Another fused DOBNA derivative, **DOBDiKTa**, has a carbonyl-based MR structure (**QAO**, here called **DiKTa**) composed of two merged MR fragments.[277] Although **DOB-DiKTa** is composed of the same units as **BOQAO** in Fig. 27, the fused benzene is substituted by the electron-withdrawing boron atom and carbonyl group in a *meta* relationship as well as the electron-donating nitrogen and oxygen atoms in the same relationship, effectively merging the MR effect. The synthesis of **DOBDiKTa** involved two coupling reactions followed by saponification and two-fold intramolecular Friedel–Crafts acrylation promoted by $SnCl_2$ as a Lewis acid. The emission maximum of **DOBDiKTa** was slightly blue-shifted relative to that of **QAO**. In addition, the TADF properties including Φ_{PL}, ΔE_{ST}, and k_{RISC} were superior to those of each individual MR unit.
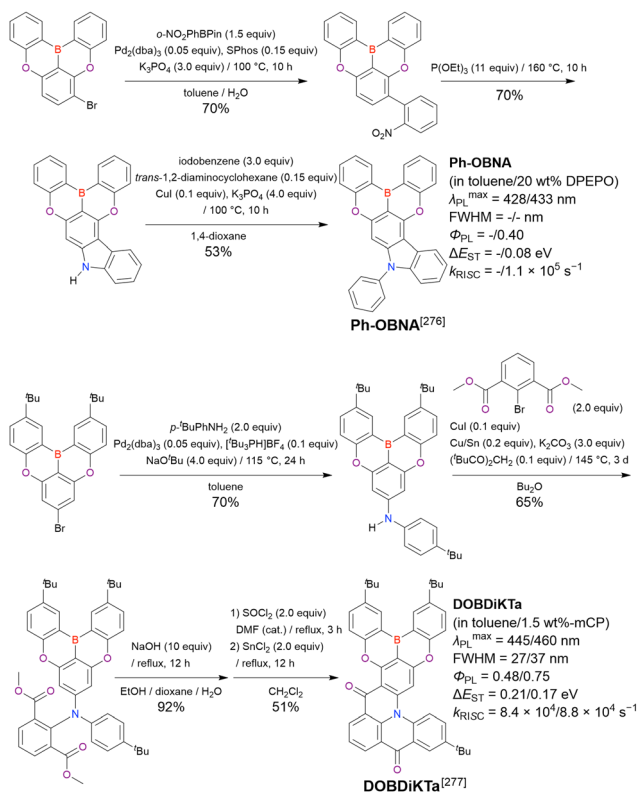
4.3 Functionalised CzBN

The late-stage synthesis strategies for CzBN derivatives are fundamentally identical to those for DOBNA derivatives, as shown in Scheme 45 corresponding to Scheme 41. Similar to the DOBNA case, one-pot borylation is seldom selected for synthesising some donor-substituted CzBN derivatives but may still be useful given the reports of exactly the same

Table 34 Photophysical properties of the materials shown in Fig. 29

Compound	Condition	λ_{PL}^{max} [nm]	FWHM [nm]	Φ_{PL} [—]	ΔE_{ST} [eV]	k_{RISC} [s⁻¹]	Ref.
PhCz-TOSBA	Toluene/10 wt%-26DCzPPy^a	444/454	32/41	—/0.61	0.23/—	—/4.08 × 10⁴	130
TPA-TOSBA	Toluene/10 wt%-26DCzPPy^a	447/467	34/67	—/0.62	0.36/—	—/1.91 × 10⁴	130
TSBA-Cz	Toluene/10 wt%-26DCzPPy^a	463/469	30/40	—/0.80	0.21/—	—/5.29 × 10⁴	131
TSBA-PhCz	Toluene/10 wt%-26DCzPPy^a	470/478	36/40	—/0.80	0.18/—	—/7.62 × 10⁴	131
BSS-Cz	Toluene/1 wt%-PS^a	455/457	28/29	0.86/—	0.14/—	—/1.5 × 10⁵	133
BSS-PA	Toluene/1 wt%-PS^a	454/—	35/—	0.66/—	0.13/—	—/1.6 × 10⁵	133
BSS-SpAc	Toluene/1 wt%-PS^a	456, 505/—	101/—	0.89/—	0.07/—	—/1.5 × 10⁵, 3.0 × 10⁵	133
BSS-Ac	Toluene/1 wt%-PS^a	456, 513/—	105/—	0.90/—	0.04/—	—/1.5 × 10⁵, 5.2 × 10⁵	133

^{a} See Table 2 for the full compound name.

This journal is © The Royal Society of Chemistry 2024

Chem. Soc. Rev., 2024, **53**, 1624–1692 | **1673**

Scheme 44 Late-stage ring-fusion of DOBNA derivatives.

compounds prepared by both methods (*vide infra*). The standard reaction conditions for the Buchwald–Hartwig amination of CzBN derivatives are Pd$_2$(dba)$_3$ (0.02–0.08 equiv.), [^{t}Bu$_3$PH]BF$_4$ (0.08–0.32 equiv.), and NaO^{t}Bu (2–4 equiv.) in aromatic solvents at >80 °C. The Suzuki–Miyaura coupling conditions are broadly variable, with a representative example being Pd(PPh$_3$)$_4$ (~0.05 equiv.) and K$_2$CO$_3$ (~2 equiv.) in THF/H$_2$O at reflux. As most materials discussed here are based on 3,6-di-*tert*-butyl-9*H*-carbazole, the photophysical properties of the tetra-^{t}Bu CzBN skeleton (originally named **DtBuCzB**, but referred to here as **BCzBN** to correspond to the substituted CzBN) are the basis for evaluating substitution effects. Typical
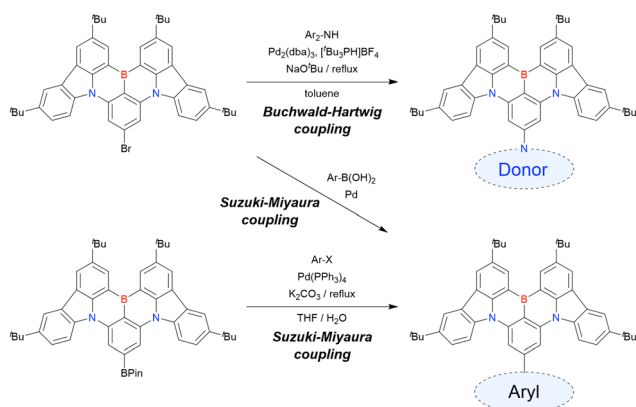
Scheme 45 General scheme for the late-stage functionalisation of CzBN by Buchwald–Hartwig and Suzuki–Miyaura couplings.

emission maximum, FWHM, Φ_{PL}, ΔE_{ST}, and k_{RISC} values for **BCzBN** in toluene are 481–484 nm, 22–23 nm, 91–98%, 0.13–0.15 eV, and 1.4–3.0 × 10^4 s^{-1}, respectively.[154,257,278] In general, the MR effect with narrow emission is maintained even for relatively strong donor substituents because the HOMO of **CzBN** is shallower than that of **DOBNA**. Changes in the excited-state nature upon going from MR with short-range CT to long-range D–A-type CT could be observed by comparing phenoxazine-substituted derivatives, with the HOMO levels of the CzBN moiety slightly decreasing upon going from **CzBN3** to **CzBN1** (Fig. 30 and Table 35).[257] Thus, **CzBN1** showed two emission bands, namely a sharp band at 471 nm and a broad band at 533 nm. Although **CzBN3** (aka **BN-PXZ**[176] in Section 2 and **BNCz-PXZ**) exhibited a small FWHM comparable to that of **BCzBN** in toluene, a new broad band at ~600 nm emerged in polar solvents.[187] In contrast, **BNCz-DMAC** (aka **BN-AC** in Section 2)[176] and **BNCz-SAF** with weaker donors showed a single narrow emission band even in polar solvents with a small positive solvatochromic effect, which is a common feature of MR materials. These results indicate that the HOMO of **BCzBN** was very slightly shallower than that of the phenoxazine moiety. Despite the negligible change in the shape of the emission spectrum upon the introduction of diarylamine donors, these substituents affected the HOMO–LUMO gap of the CzBN core and the electronic properties of the related derivatives. The HOMO of **CzBN** has no coefficient on the atom in 10-position (Fig. 23), unlike the corresponding LUMO. The opposite HOMO–LUMO behaviour is observed at 9- and 11-positions. Thus, the introduction of electron-donating substituents such as arylamines directly at 10-position, which is *para*-position with respect to the B atom, increases the energy gap. In fact, the emission spectra of **CzBN3**, **BNCz-DMAC**, **BNCz-SAF**, and **SPBAC-tCzBN** were slightly blue-shifted relative to that of **BCzBN**.[187,257,279] In contrast, the emission spectra were slightly red-shifted upon the introduction of electron-withdrawing substituents (Fig. 31 and Table 36). Note that the introduction of electron-donating arylamines with a phenyl spacer caused a red shift because of the contribution of long-range CT characteristics (*vide infra*, *e.g.*, **o-SPAC-tCzBN**).[279] The important advantage of introducing substituents is the incorporation of intersegmental CT triplet states such as the T$_2$ level, which accelerates RISC. This level is silently induced without perturbing the lowest excited singlet states. Thus, the emission properties of, *e.g.*, **CzBN3** and **SPAC-tCzBN** are substantially similar to those of **BCzBN**, while the k_{RISC} values of these two compounds exceed that of **BCzBN** by about one order of magnitude. The emission of a heptagonal tribenzo[*b,d,f*]azepine derivative, **TBA-BCz-BN**, is further blue-shifted relative to that of carbazole and diphenylamine derivatives.[111,172,186] **DCz-BSN** and **DCz-BSeN** synthesised based on this strategy and featuring asymmetric S- and Se-bridged CzBN structures, respectively, exhibit high-colour-purity emission in the deep blue region and large k_{risc}.[168,169] Compounds bearing electron-donating groups with a phenyl spacer, namely **BNCz-pTPA**, **BNCz-mTPA**, **o-SPAC-tCzBN**, **S-Cz-BN**, **D-Cz-BN**, **BN-CP1**, **BN-CP2**, **BN-PhOH**, and **BN-PhOCH$_3$**, showed slightly red-shifted emission, while some compounds with relatively strong donors,

1674 | *Chem. Soc. Rev.*, 2024, **53**, 1624–1692

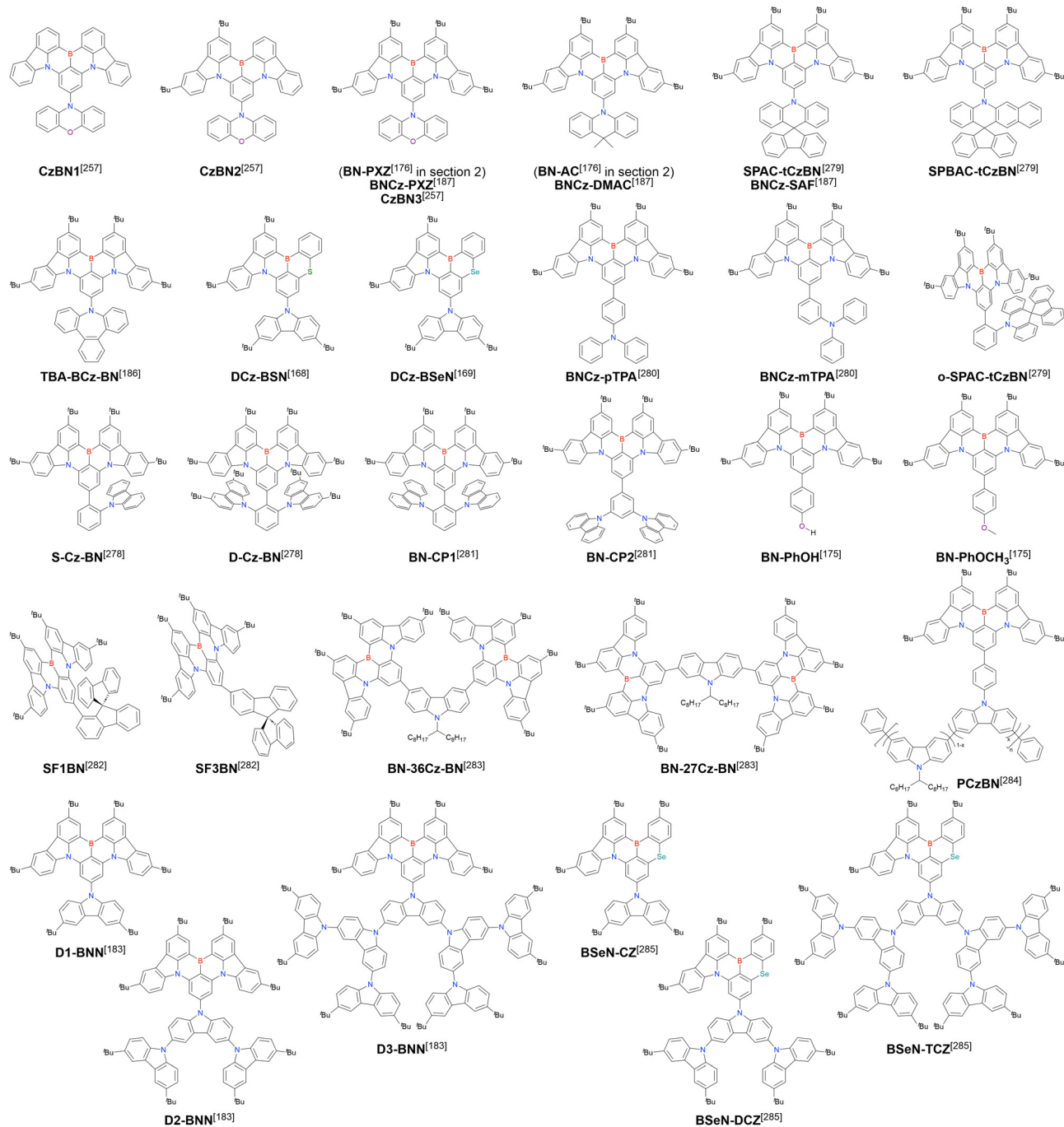This journal is © The Royal Society of Chemistry 2024

Fig. 30 CzBN derivatives with donor substituents at the 10-position and related chalcogen-bridged compounds synthesised by late-stage functionalisation.

namely **BNCz-pTPA**, **BNCz-mTPA**, and **o-SPAC-tCzBN**, exhibited higher k_{RISC} because of the distinct contribution of the long-range CT triplet state.[175,278–281] Although the basic photophysical properties of **BN-PhOH** and **BN-PhOCH₃** are not significantly different, the synthesis of methoxy-substituted compounds might not be straightforward because of demethylation by BBr₃; however, the SMe group can be preserved.[175,178] Thus, the methoxy derivative was synthesised using the Williamson ether synthesis in the presence of sodium hydride (Scheme 46).[175]

MR emitters generally suffer from strong molecular aggregation owing to their planar structures and thus experience substantial deterioration of emission properties at high doping concentrations. In particular, concentration quenching-induced decreases in Φ_{PL} and Dexter energy transfer-induced triplet loss are serious issues in the corresponding OLEDs. Thus, MR emitter-based OLEDs are usually fabricated using very low doping concentrations such as 1 wt%. The structural modifications of MR emitters also aim to suppress aggregation.

This journal is © The Royal Society of Chemistry 2024

Chem. Soc. Rev., 2024, **53**, 1624–1692 | 1675

Table 35 Photophysical properties of the compounds shown in Fig. 30

Compound	Condition	λ_{PL}^{max} [nm]	FWHM [nm]	Φ_{PL} [—]	ΔE_{ST} [eV]	k_{RISC} [s^{-1}]	Ref.
CzBN1	Toluene/5 wt%-DMIC-TRZ^a	471, 533/523^b	78/75^b	0.95/0.95	0.13/—	2.06×10^6/1.3×10^6	257
CzBN2	Toluene/5 wt%-DMIC-TRZ^a	477, 522/481^b	75/75^b	0.97/0.97	0.14/—	7.82×10^5/4.4×10^5	257
CzBN3	Toluene/5 wt%-DMIC-TRZ^a	478/487^b	21/27^b	0.99/0.98	0.15/—	3.27×10^5/2.8×10^5	257
BNCz-PXZ	Toluene/3 wt%-mCBP^a	477/482	23/34	—/0.84	0.12/—	—/3.11×10^5	187
BNCz-DMAC	Toluene/3 wt%-mCBP^a	478/484	22/26	—/0.83	0.13/—	—/1.20×10^6	187
BNCz-SAF	Toluene/3 wt%-mCBP^a	478/484	23/25	—/0.86	0.15/—	—/7.4×10^5	187
SPAC-tCzBN	Toluene/10 wt%-PhCzBCz^a	481/480^b	20/24^b	—/0.83	0.13/—	—/0.9×10^5	279
SPBAC-tCzBN	Toluene/10 wt%-PhCzBCz^a	480/480^b	20/25^b	—/0.89	0.13/—	—/1.2×10^5	279
TBA-BCz-BN	Toluene/3 wt%-mCBP^a	468/472	22/28	—/0.86	0.14/—	—/—	186
DCz-BSN	Toluene/1 wt%-PS^a	463/462	26/—	—/0.88	0.12/—	—/1.04×10^5	168
DCz-BSeN	Toluene/1 wt%-PS^a	472/467	28/—	—/0.93	0.14/—	—/8.8×10^6	169
BNCz-pTPA	Toluene/1 wt%-mCBP^a	487/490^b	22/29^b	0.95/—	0.11/—	—/4.45×10^5	280
BNCz-mTPA	Toluene/1 wt%-mCBP^a	489/490^b	22/30^b	0.92/—	0.12/—	—/2.29×10^5	280
o-SPAC-tCzBN	Toluene/10 wt%-PhCzBCz^a	490/492^b	21/26^b	—/0.86	0.11/—	—/1.1×10^5	279
S-Cz-BN	Toluene/1 wt%-mCBP^a/neat-film	490/488^b/—	23/26^b/40	0.94/0.95/0.47	0.16/—/—	1.8×10^4/2.9×10^4/—	278
D-Cz-BN	Toluene/1 wt%-mCBP^a/neat-film	490/488^b/—	22/24^b/26	0.98/0.98/0.54	0.14/—/—	1.8×10^4/3.0×10^4/—	278
BN-CP1	Toluene/1 wt%-mCBP^a/neat-film	490/496/502	23/25/28	—/0.93/0.40	0.12/—/—	—/1.56×10^4/—	281
BN-CP2	Toluene/1 wt%-mCBP^a/neat-film	490/496/521	23/26/48	—/0.91/0.25	0.13/—/—	—/1.43×10^4/—	281
BN-PhOH	Toluene/3 wt%-mCBP^a	485/494	26/32^b	0.80/—	0.14/—	—/2.85×10^4	175
BN-PhOCH$_3$	Toluene/3 wt%-mCBP^a	485/494	26/29^b	0.78/—	0.15/—	—/2.98×10^4	175
SF1BN	Toluene/2 wt%-mCBP^a	493/492^b	23/28^b	0.90/0.93	0.13/—	—/9.12×10^4	282
SF3BN	Toluene/2 wt%-mCBP^a	493/492^b	25/28^b	0.86/0.90	0.15/—	—/3.31×10^4	282
BN-36Cz-BN	Toluene/5 wt%-DMIC-TRZ^a	488/497	22/33	—/0.65	0.125/—	—/1.6×10^5	283
BN-27Cz-BN	Toluene/5 wt%-DMIC-TRZ^a	489/499	22/32	—/0.66	0.124/—	—/0.80×10^5	283
PCzBN1	Toluene/neat-film	421, 487/430, 452, 491	25/33	—/0.58	—/0.14	—/8.2×10^4	284
PCzBN3	Toluene/neat-film	421, 487/423, 451, 496	25/42	—/0.51	—/0.13	—/8.6×10^4	284
PCzBN5	Toluene/neat-film	421, 488/501	25/43	—/0.43	—/0.13	—/2.18×10^5	284
D1-BNN	Toluene/10 wt%-mCP^a	474/483^b	21/26	—/0.68	0.15/—	—/1.55×10^3	183
D2-BNN	Toluene/10 wt%-mCP^a	473/478^b	21/24	—/0.80	0.16/—	—/2.35×10^3	183
D3-BNN	Toluene/10 wt%-mCP^a	473/477^b	21/24	—/0.92	0.17/—	—/3.94×10^3	183
BSeN-CZ	Toluene/1 wt%-PS^a	476/—	26/30	—/0.76	0.12/—	—/8.5×10^6	285
BSeN-DCZ	Toluene/1 wt%-PS^a	475/—	26/29	—/0.79	0.12/—	—/9.0×10^6	285
BSeN-TCZ	Toluene/1 wt%-PS^a	474/—	26/30	—/0.85	0.12/—	—/9.1×10^6	285

^{a} See Table 2 for the full compound name. ^{b} Taken from the EL spectrum.
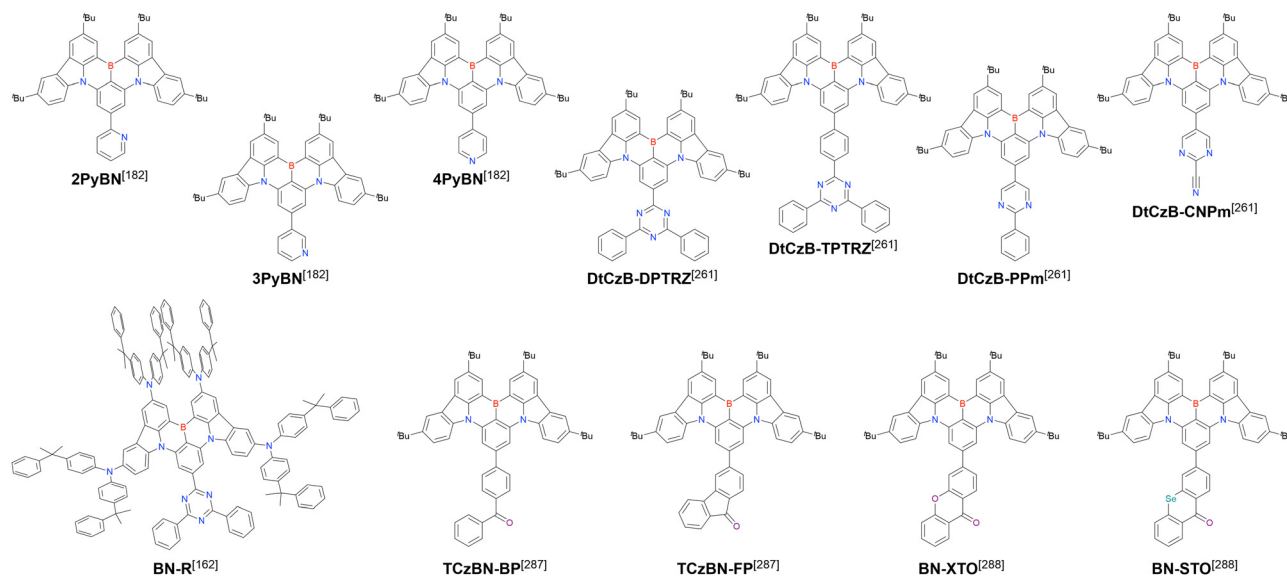

Fig. 31 CzBN derivatives with acceptor substituents at 10-position synthesised by late-stage functionalisation.

Among the available methods, the steric wrapping strategy is particularly efficient. For example, the Φ_{PL} of a 30 wt% BCzBN-doped film was less than 50%, while doping with 30 wt% S-Cz-BN and D-Cz-BN maintained high Φ_{PL} values of >80–90%.[278] In addition, spectral broadening was found to be negligible for D-Cz-BN even in the neat-film. This trend was also confirmed by

1676 | Chem. Soc. Rev., 2024, 53, 1624–1692

This journal is © The Royal Society of Chemistry 2024

Table 36 Photophysical properties of the materials shown in Fig. 31

Compound	Condition	λ_{PL}^{max} [nm]	FWHM [nm]	Φ_{PL} [—]	ΔE_{ST} [eV]	k_{RISC} [s^{-1}]	Ref.
2PyBN	Toluene/1 wt%-DMIC-TRZ^a	499/507	21/26^b	—/0.94	—/0.02	—/7.7 × 10^4	182
3PyBN	Toluene/1 wt%-DMIC-TRZ^a	490/497	23/27^b	—/0.90	—/0.03	—/8.7 × 10^4	182
4PyBN	Toluene/1 wt%-DMIC-TRZ^a	495/506	24/27^b	—/0.86	—/0.02	—/9.5 × 10^4	182
DtCzB-DPTRZ	Toluene/3 wt%-PhCzBCz^a	521/536	24/43	0.94/0.87	0.18/—	—/0.10 × 10^4	261
DtCzB-TPTRZ	Toluene/3 wt%-PhCzBCz^a	501/520	27/41	0.97/0.95	0.11/—	—/1.08 × 10^4	261
DtCzB-PPm	Toluene/3 wt%-PhCzBCz^a	499/510	25/36	0.96/0.94	0.11/—	—/1.02 × 10^4	261
DtCzB-CNPm	Toluene/3 wt%-PhCzBCz^a	515/540	36/45	0.93/0.87	0.15/—	—/0.14 × 10^4	261
BN-R	Toluene/1 wt%-NPB^a:DMFBD-TRZ^a	624/620	46/49	0.94/0.90	0.11/—	—/1.1 × 10^4	162
TCzBN-BP	Toluene/3 wt%-SF3TRZ^a	497/508	29/33	—/0.98	0.14/0.09	—/7.7 × 10^4	287
TCzBN-FP	Toluene/5 wt%-SF3TRZ^a	516/542	37/56	—/0.75	0.17/0.14	—/5.1 × 10^4	287
BN-XTO	Toluene/5 wt%-DMIC-TRZ^a	—/515	26/33	—/0.93	—/0.08	—/3.0 × 10^4	288
BN-STO	Toluene/5 wt%-DMIC-TRZ^a	—/517	29/34	—/0.96	—/0.13	—/1.2 × 10^5	288

^{a} See Table 2 for the full compound name. ^{b} Taken from the EL spectrum.
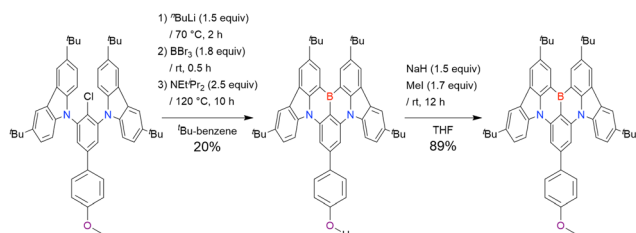
Scheme 46 Synthesis of a methoxy-substituted compound.

the comparison between **BN-CP1** and **BN-CP2** simultaneously reported by different groups.[281] Two derivatives with the more electrically neutral spiro-9,9′-bifluorene moiety, namely **SF1BN** and **SF3BN**, were examined to prove the influence of steric hindrance on photophysical properties.[282] Although **SF3BN**, **D-Cz-BN**, and **BN-CP1** were synthesised by routine Suzuki–Miyaura coupling (Scheme 45), **SF1BN** had to be synthesised by a different method (Scheme 47) because the bulky fluorene moiety prevented the catalytic cycle of this coupling.

Solution-processable **BCzBN** derivatives were developed using N-branched-alkyl carbazoles. Small molecules with two **BCzBN** moieties, **BN-36Cz-BN** and **BN-27Cz-BN**, showed relatively weak ACQ.[283] A polycarbazole-based MR polymer (**PCzBN**) was prepared by grafting the **BCzBN** moiety as a pendant (Scheme 47).[284] MR dendrimers were also developed by introducing up to third-generation carbazole dendrons at the periphery of the **BCzBN** skeleton.[183,285] Compounds based on a third-generation carbazole dendron (**D3-BNN** and **BSeN-TCZ**) showed higher Φ_{PL} than those based on a first-generation dendron (**D1-BNN** and **BSeN-Cz**). Concentration quenching and emission spectrum broadening were also suppressed when the third-generation dendron was used at high doping concentrations.

Compounds with acceptor moieties at 10-position are summarised in Fig. 31 and Table 36. The presence of pyridine-type substructures may disorder the tandem lithiation-borylation-annulation and one-shot electrophilic C–H borylation. Some works also reported these attempts and the failure of the corresponding reactions.[182,261] Thus, compounds **2PyBN**, **3PyBN**, **4PyBN**, **DtCzB-DPTRZ**, **DtCzB-TPTRZ**, **DtCzB-PPm**, and **DtCzB-CNPm** were prepared by late-stage reactions, with the
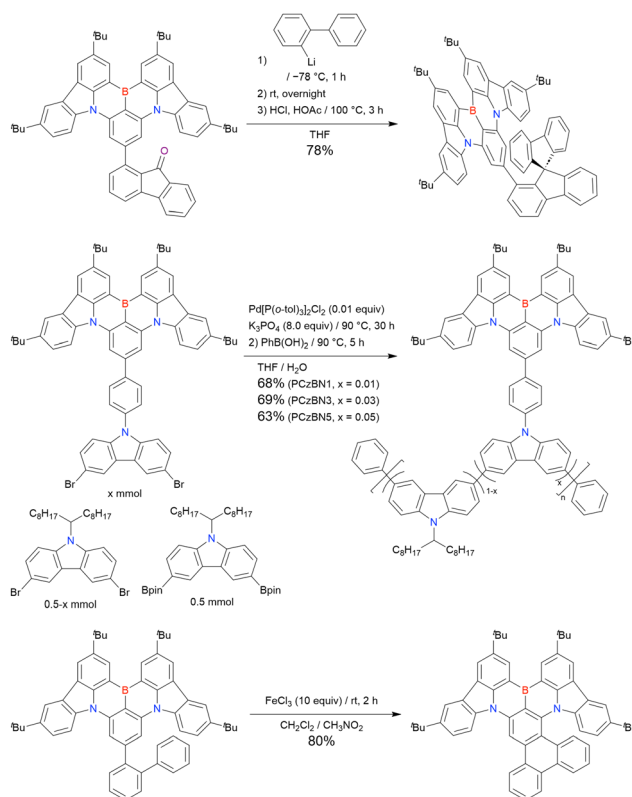
Scheme 47 Sequential synthesis of CzBN derivatives involving Suzuki–Miyaura coupling in Scheme 45. Top: Nucleophilic addition of 2-lithio-1,1′-biphenyl to a carbonyl group followed by intramolecular condensation-cyclisation. Middle: Polymerisation reaction. The dibromo precursor was prepared from CzBN-Bpin and 3,6-dibromo-9-(4-iodophenyl)-9H-carbazole. Bottom: Oxidative Scholl coupling.

synthesis of the PyBN series involving CuCl-assisted Suzuki–Miyaura coupling.[286] Note that in pyridyl DOBNA synthesis, the pyridine-functionalised precursor underwent lithiation-borylation to afford the desired product in good yield.[139] Although all of these pyridine-based BCzBN derivatives exhibited red-shifted emission compared to that of the parent **BCzBN**, the intramolecular hydrogen-bonding in **2PyBN** and **DtCzB-DPTRZ** caused molecular rigidity, enhanced
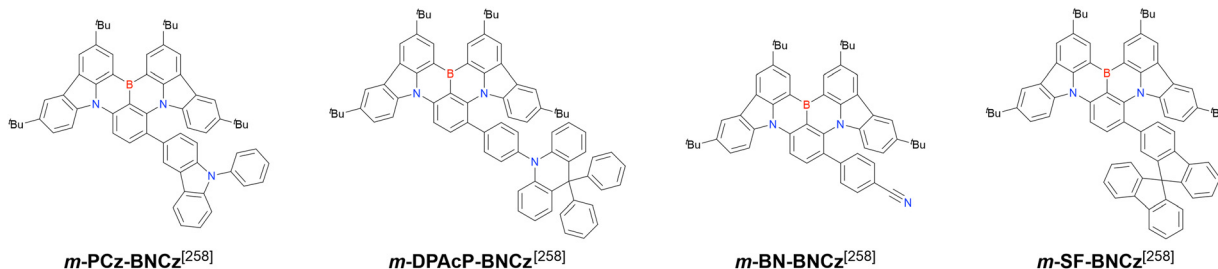
This journal is © The Royal Society of Chemistry 2024

Chem. Soc. Rev., 2024, **53**, 1624–1692 | **1677**

Fig. 32 CzBN derivatives with substituents at 9-position synthesised by late-stage functionalisation.

conjugation, and more strongly red-shifted emission. The replacement of the ^{t}Bu group by a bis[4-(2-phenyl-2-propyl)phenyl]amine unit in **BN-R** substantially increased the HOMO energy, affording a red emitter with a narrow spectrum.[162] The bulky donor moiety also helps to suppress aggregation and enhance solubility. The carbonyl moiety may also cause unpredictable side reactions during borylation. Thus, some compounds have been developed using late-stage reactions. Similar to the case of relatively strong donors as substituents,[187] long-range CT became dominant with relatively strong acceptors (**TCzBN-BP** *versus* **TCzBN-FP**).[287] In addition to the management of intersegmental CT triplet states, the heavy-atom effect further increased k_{RISC} in **BN-STO**.[288]

BCzBN derivatives with donors and acceptors at 9-position (Fig. 32 and Table 37) were synthesised through bromination using NBS (Scheme 39) followed by Suzuki–Miyaura coupling.[258] Polycyclisation extended at 9- and 10-positions formed a triphenylene core in **BN-TP** (Fig. 33 and Table 38), which was difficult to obtain from triphenylene as the starting material. Alternatively, this species could be synthesised from **BCzBN** *via* a three-step process including the Hartwig-Miyaura C–H borylation, Suzuki–Miyaura coupling, and the Scholl reaction in the presence of FeCl$_3$ (Scheme 47).[289] The large HOMO coefficient at 9-position was conducive to intramolecular cyclisation. Nitrogen-containing compounds **BN-TP-N1–4** were synthesised using the same approach, with the construction of phenylpyridine moieties in **BT-TP-N2** and **BT-TP-N3** performed using a different sequence.[290]

The HOMO and LUMO of **BN-TP** extend to each benzene ring connected to 9- and 10-positions, respectively, and the whole molecular orbital preserves the alternating distribution characteristic of MR materials. Thus, the conventional HOMO and LUMO distributions of PAHs including triphenylene showing uniform bonding and anti-bonding between carbon atoms were effectively modulated with the help of the MR fragment. The extension of π-conjugation onto the triphenylene part in

BN-TP resulted in an emission peak that was red-shifted relative to that of **BN-DP**. In addition, nitrogen atoms anchored at positions contributing to the LUMO afforded further red-shifted emission in **BN-TP-N1** and **BN-TP-N2**. In contrast, blue-shifted (ultrapure green) emission was observed for **BN-TP-N3** and **BN-TP-N4**. The dimerisation of **BCzBN** also extended the conjugation of MR cores, resulting in green emitters.[185] As shown in Scheme 48, the synthesis of **p-CzB** involved the frequently used standard Suzuki–Miyaura coupling, while **m-CzB** was synthesised in moderate yield by oxidative coupling using Cu(ClO$_4$)$_2$·6H$_2$O as the oxidant, as this type of reaction was favoured by the large HOMO distribution at 9- and 11-positions.

The introduction of cyano groups at the *para*-position of boron resulted in a bathochromic shift to give MR materials with green to red emission (Table 39). Interestingly, several methods have been used to introduce cyano groups by substituting halogen atoms in late-stage functionalisation (Scheme 49). Treatment with CuCN in refluxing DMF (Rosenmund–von Braun reaction) is the most simple and widely used method, and has been applied for the synthesis of **CN-BCz-BN**.[184] Meanwhile, **CNCz-BNCz**, which has two additional carbazole rings, was synthesised through lithiation with ^{n}BuLi followed by transnitrilation with dimethylmalononitrile (DMMN).[291] Lithiation after the introduction of boron might cause relatively low yields. Palladium-catalysed cyanation with K$_4$[Fe(CN)$_6$] as an environmentally benign reagent was used to synthesise a DABNA derivative, where the MR core was prepared by one-shot borylation.[114] The combination of one-shot borylation and late-stage cyanation through the substitution of halogen atoms enables the further development of MR emitters over the full colour range.

The late-stage synthesis of oxidised sulphur and phosphorus species are summarised in Scheme 50. As mentioned above, **BN(p)SCH$_3$** was synthesised *via* tandem lithiation-borylation-

Table 37 Photophysical properties of the materials shown in Fig. 32

Compound	Condition	λ_{PL}^{max} [nm]	FWHM [nm]	Φ_{PL} [—]	ΔE_{ST} [eV]	k_{RISC} [s^{-1}]	Ref.
m-PCz-BNCz	Toluene/3 wt%-PhCzBCz^a	494/500	25/33	0.97/0.98	0.15/—	—/1.29 × 10^4	258
m-DPAcP-BNCz	Toluene/3 wt%-PhCzBCz^a	491/498	26/34	0.97/0.97	0.14/—	—/1.16 × 10^4	258
m-BN-BNCz	Toluene/3 wt%-PhCzBCz^a	488/496	25/32	0.93/0.95	0.16/—	—/0.93 × 10^4	258
m-SF-BNCz	Toluene/3 wt%-PhCzBCz^a	491/498	25/32	0.96/0.98	0.16/—	—/1.16 × 10^4	258

^{a} See Table 2 for the full compound name.

1678 | *Chem. Soc. Rev.*, 2024, **53**, 1624–1692

This journal is © The Royal Society of Chemistry 2024
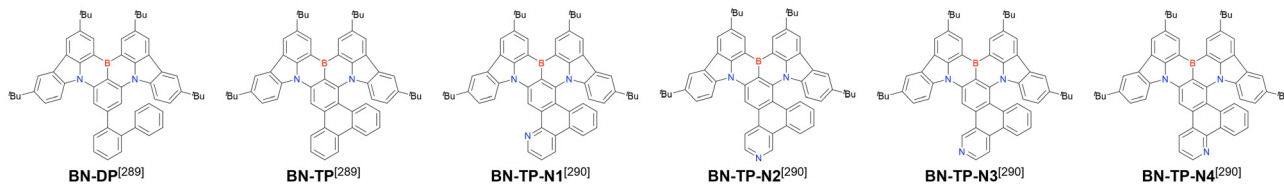
Fig. 33 CzBN derivatives with fused π-extension synthesised by late-stage functionalisation.

Table 38 Photophysical properties of the compounds shown in Fig. 33

Compound	Condition	λ_{PL}^{max} [nm]	FWHM [nm]	Φ_{PL} [—]	ΔE_{ST} [eV]	k_{RISC} [s^{-1}]	Ref.
BN-DP	Toluene	490/—	23/—	0.94/—	0.16/—	—/—	289
BN-TP	Toluene/3 wt%-/10 wt%-PhCzBCz^a	523/529/537	34/36/39	0.96/0.96/0.92	0.14/—/—	—/2.09 × 10^4/2.26 × 10^4	289
BN-TP-N1	Toluene/3 wt%-PhCzBCz^a	526/534	33/43	0.94/0.95	0.17/—	—/1.01 × 10^4	290
BN-TP-N2	Toluene/3 wt%-PhCzBCz^a	528/535	33/43	0.92/0.91	0.19/—	—/0.83 × 10^4	290
BN-TP-N3	Toluene/3 wt%-PhCzBCz^a	519/526	32/39	0.99/0.97	0.15/—	—/1.70 × 10^4	290
BN-TP-N4	Toluene/3 wt%-PhCzBCz^a	520/530	32/42	0.98/0.97	0.14/—	—/1.90 × 10^4	290

^{a} See Table 2 for the full compound name.
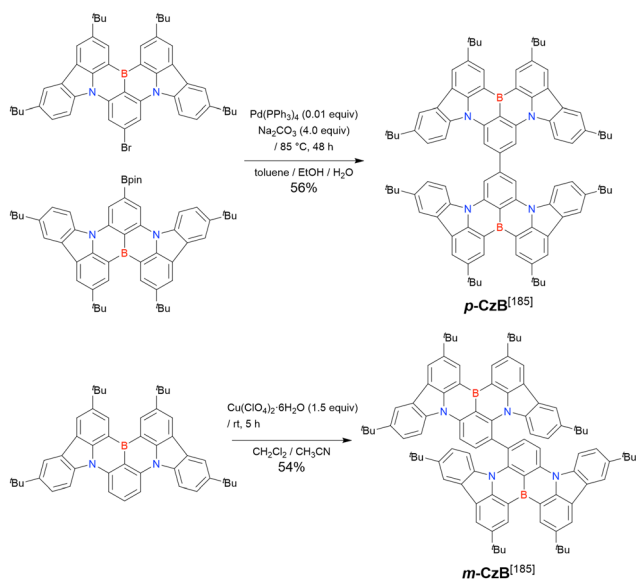
Scheme 48 Synthesis of a CzBN dimer by oxidative coupling.

annulation from a **BCzBN** precursor with a pre-installed SMe group[178] and then treated with 3-chloroperbenzoic acid (mCPBA) to afford the corresponding sulfoxide (**BN(p)SOCH₃**) and sulfone (**BN(p)SO₂CH₃**). Diphenyl sulphide and diphenyl sulfone derivatives (**TCzBN-S** and **TCzBN-SO**, respectively) were prepared by Suzuki–Miyaura coupling with the corresponding bromide.[292] The electron-donating SMe group caused blue-shifted emission, while electron-withdrawing sulfoxide and sulfone moieties yielded red-shifted emission. The k_{RISC} values of **BN(p)SCH₃** and **TCzBN-S** exceeded those of the oxidised compounds because of the differences in ΔE_{ST}. A phosphine oxide derivative, **tCBNDADPO**, was designed as an ambipolar self-host.[293] The host segments were integrated into the MR core without involving a CT excited state. The synthesis of this

compound included bromination by NBS on the diphenyla-mine unit, palladium-catalysed P–C coupling, and oxidation with H₂O₂. The Φ_{PL} of **tCBNDADPO** with a high doping concentration of 30 wt% was 99% in the doped film. The comparison of compounds with/without phosphorylation was reported in a different paper.[225]

Late-stage reactions allow for the introduction of various functionalities. The chiral MR compounds shown in Fig. 34 were synthesised using the coupling reactions presented in Scheme 45.[260,294] The effects of π-framework extension on the MR properties were basically same as those for the materials mentioned above. Additional chiral units of [2.2]paracyclo(1,4)-carbazolophane (Czp) and octahydro-binaphthol (OBN) partici-pated in the circularly polarised luminescence (CPL) process. Thus, the $|g_{PL}|$ factors of **Czp-tBuCzB** (1.6 × 10^{-3}) and **Czp-POAB** (1.4 × 10^{-3}) were similar to those of other CP-TADF molecules with the Czp moiety.[295] Similarly, the CPL properties of **OBN-2CN-BN** and **OBN-4CN-BN** were similar to those reported in the literature.[296]

4.4 Metal complexes

Phosphorescent metal complexes based on the DOBNA scaffold have been reported; e.g., a ligand based on DOBNA-pyridine was synthesised by the borylation of 2-(4-bromo-3,5-dipheno-xyphenyl)pyridine (Scheme 51 and Table 40). Phosphorescent iridium(III) complexes with the acetylacetonate (acac) ligand, [Ir(C^N)2(acac)], were prepared by well-established methods.[139] The emission maximum of **IrBBacac** having two DOBNA-based ligands (638 nm) was largely red-shifted relative to that of the corresponding complex without boron atoms (544 nm). The good rigidity and planarity of the DOBNA-based ligand contributed to the small FWHM. The combination with a N-embedded ligand (**IrBNacac**) showed a slightly blue-shifted emission maximum at 523 nm and a narrower FWHM.[297] The different types of ligands led to the T₁ level with several characters including a metal-to-ligand CT transition (³MLCT),

This journal is © The Royal Society of Chemistry 2024

Chem. Soc. Rev., 2024, **53**, 1624–1692 | **1679**

Table 39 Photophysical properties of the materials shown in Schemes 48–50

Compound	Condition	λ_{PL}^{max} [nm]	FWHM [nm]	Φ_{PL} [—]	ΔE_{ST} [eV]	k_{RISC} [s^{-1}]	Ref.
p-CzB	Toluene/1 wt%-mCBP-can	505/513	34/41	0.85/0.80	0.17/0.14	4.2×10^4/4.6×10^4	185
m-CzB	Toluene/1 wt%-mCBP-can	515/517	35/40	0.90/0.85	0.13/0.09	1.2×10^5/2.3×10^5	185
CN-BCz-BN	Toluene	496	21	—	—	—	184
CNCz-BNCz	Toluene/3 wt%-CBP^a	581/582	42/45	0.90/0.96	0.18/—	4.2×10^5/—	184
ν-DABNA-CN-Me	Toluene/1 wt%-PMMA^a	496/503	17/27	0.86/0.74	—/0.1	1.0×10^5/—	114
BN(p)SCH$_3$	Toluene/3 wt%-26DCzppy^a	479/488	24/38	—/0.92	0.12/—	—/6.4×10^4	178
BN(p)SOCH$_3$	Toluene/3 wt%-26DCzppy^a	482/490	22/33	—/0.71	0.16/—	—/3.0×10^4	178
BN(p)SO$_2$CH$_3$	Toluene/3 wt%-26DCzppy^a	490/496	21/29	—/0.99	0.20/—	—/3.5×10^4	178
TCzBN-S	Toluene/8 wt%-SF3TRZ^a	488/498	25/32	—/0.98	0.14/0.13	—/1.4×10^5	292
TCzBN-SO	Toluene/8 wt%-SF3TRZ^a	494/508	27/31	—/0.98	0.14/0.14	—/5.6×10^4	292
tCBNDADPO	CH$_2$Cl$_2$/10 wt%-/30 wt%-DBFDPO^a	466/472/472	26/38/44	—/0.79/0.99	—/———/0.04	—/1.75×10^4/2.43×10^4	293
tCBNDASPO	CH$_2$Cl$_2$/20 wt%-/30 wt%-DBFDPO^a	467/472/472	28/32/32	—/0.92/0.79	—/0.04/—	—/4.55×10^4/3.82×10^4	225

^{a} See Table 2 for the full compound name.
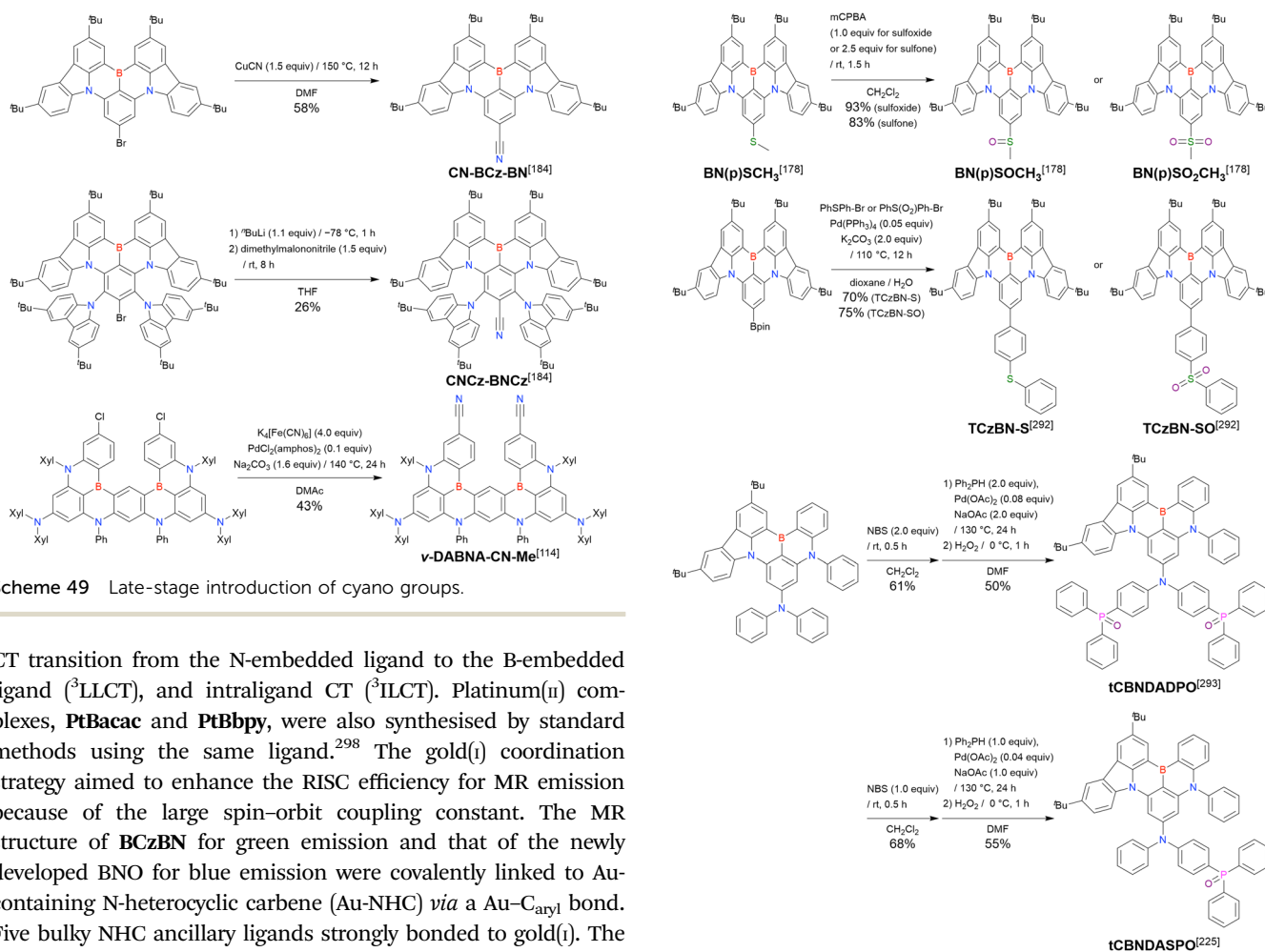
Scheme 49 Late-stage introduction of cyano groups.

Scheme 50 Late-stage introduction of sulfoxide, sulfone, and phosphine oxide groups.

CT transition from the N-embedded ligand to the B-embedded ligand (^{3}LLCT), and intraligand CT (^{3}ILCT). Platinum(II) complexes, **PtBacac** and **PtBbpy**, were also synthesised by standard methods using the same ligand.[298] The gold(I) coordination strategy aimed to enhance the RISC efficiency for MR emission because of the large spin–orbit coupling constant. The MR structure of **BCzBN** for green emission and that of the newly developed **BNO** for blue emission were covalently linked to Au-containing N-heterocyclic carbene (Au-NHC) via a Au–C$_{aryl}$ bond. Five bulky NHC ancillary ligands strongly bonded to gold(I). The complexes were synthesised by a coupling reaction between Bpin-functionalised MR cores and (NHC)AuCl (Scheme 51).[95,299] The emission wavelengths of gold complexes were slightly red-shifted compared to those without the Au-NHC functionality. The high Φ_{PL} and narrow FWHM were maintained despite the large k_{RISC}.

4.5 B-doped fused PAHs

The introduction of heteroatoms, especially boron, oxygen, and nitrogen, into fused PAHs affords novel π-conjugated systems showing dramatically different optoelectronic properties despite their structural similarities. Recent progress in the development of the bottom-up synthesis of nanographenes using solution-based techniques holds great promise for accelerating the evolution of heteroatom incorporation. Late-stage
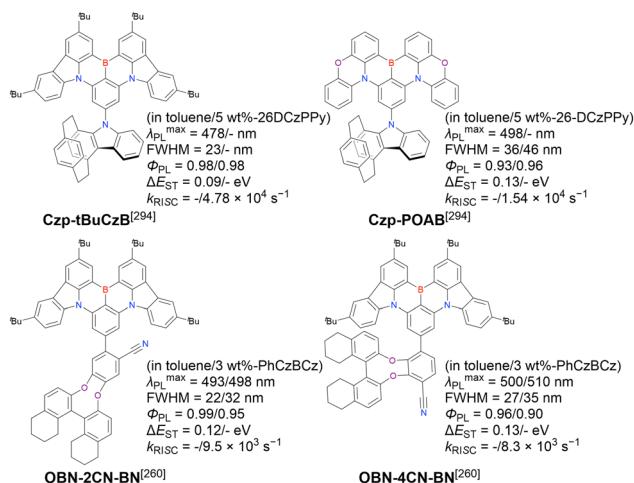
1680 | Chem. Soc. Rev., 2024, **53**, 1624–1692

This journal is © The Royal Society of Chemistry 2024

Fig. 34 CzBN derivatives showing CPL.

synthesis using pre-prepared MR structures such as **DOBNA** and **BCzBN** is advantageous for constructing extended π-conjugation in a short number of steps. We have not summarised photophysical properties for the following compounds described in Schemes 52–56 since they do not show any TADF characteristics.

Hexabenzocoronene-based molecules are examples of DOBNA-fused systems (Scheme 52).[136] Chemical structures having multiple helical regions and distorted configurations affect the electronic properties. Intermediates with alkyne moieties were synthesised by Sonogashira–Hagihara coupling using DOBNA derivatives. The subsequent cyclotrimerisation of

these alkyne derivatives catalysed by $Co_2(CO)_8$ yielded hexa-aryl precursors.

Intramolecular cyclodehydrogenation was performed using $FeCl_3$ for **HBC-3BO** and 2,3-dichloro-5,6-dicyano-1,4-benzo-quinone (DDQ) and trifluoromethanesulfonic acid (TfOH) for **HBC-6BO** to complete the reaction. For **HBC-6BO,** the branched alkyl chains were used to enhance solubility. The absorption/emission maxima of **tBu-HBC**, **HBC-3BO**, and **HBC-6BO** were located at 360/493, 438/529 and 514/602 nm, respectively, showing that the introduction of the DOBNA scaffold resulted in a substantial red-shift. Φ_{PL} also increased after the incorporation of the DOBNA moiety (from 5.8% to 18–20%).

Certain PAHs have a unique open-shell singlet biradical character. Indenofluorenes (IFs) and their π-extended derivatives show moderate-to-high biradical characters, while B-containing biradicaloids might be more challenging to synthesise because of their high reactivities. Therefore, rigid and stable DOBNA and CzBN structures were merged with IFs to afford, *e.g.*, DOBNA and CzBN-fused *s*- and *as*-indacenes. The central core structures are based on indeno[1,2-*b*]fluorene, indeno[2,1-*b*]fluorene, and fluoreno[1,2-*b*]fluorene, which are herein referred to as [1,2-*b*]IF, [2,1-*b*]IF, and [1,2-*b*]FF, respectively (Scheme 53). The corresponding synthesis process involved three steps including Suzuki–Miyaura coupling, nucleophilic addition of mesityl magnesium bromide to yield a diol, intramolecular Friedel–Crafts alkylation induced by treatment with $BF_3 \cdot Et_2O$, and oxidative dehydrogenation with DDQ.[118,135,300] The characterisation of **[1,2-*b*]IF-α-DOBNA** and **[2,1-*b*]IF-α-DOBNA** using NMR, X-ray single-crystal analysis, electron paramagnetic resonance (EPR), ultraviolet-visible
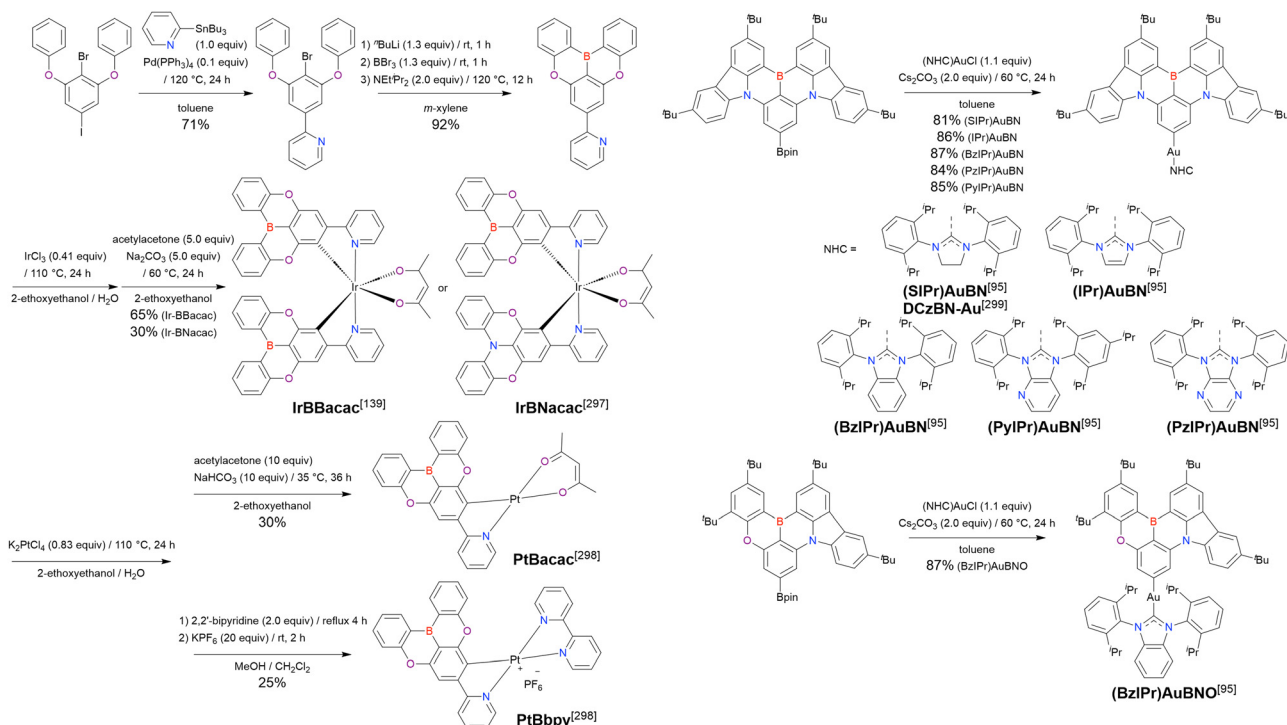

Scheme 51 Synthesis of DOBNA- and CzBN-based metal complexes.

This journal is © The Royal Society of Chemistry 2024

Chem. Soc. Rev., 2024, **53**, 1624–1692 | **1681**

Table 40 Photophysical properties of the compounds shown in Scheme 51

Compound	Condition	λ_{PL}^{max} [nm]	FWHM [nm]	Φ_{PL} [—]	ΔE_{ST} [eV]	k_{RISC} [s^{-1}]	Ref.
IrBBacac	CH$_2$Cl$_2$/10 wt%-CBP^a:mMTDATA^a	638/639	—/53	0.21/0.34	NA^b/NA^b	NA^b/NA^b	139
IrBNacac	CH$_2$Cl$_2$/1 wt%-PS^a	625/623	—/50	—/0.35	NA^b/NA^b	NA^b/NA^b	297
PtBacac	CH$_2$Cl$_2$/1 wt%-PS^a	578/578	—/—	0.30/0.45	NA^b/NA^b	NA^b/NA^b	298
PtBbpy	CH$_2$Cl$_2$/1 wt%-PS^a	—/588	—/—	—/0.12	NA^b/NA^b	NA^b/NA^b	298
(SIPr)AuBN	THF/2 wt%-PMMA^a	511/515	30/37	0.88/0.92	—/—	—/—	95
DCzBN-Au	Toluene/1 wt%-mCP^a	514/508	28/39	—/0.95	0.09/0.13	—/2.3 × 10^7	299
(IPr)AuBN	THF/MeCN/2 wt%-PMMA^a	511/—/514	31/—/37	0.83/—/0.90	—/—/—	—/3.3 × 10^4/—	95
(BzIPr)AuBN	THF/MeCN/2 wt%-PMMA^a	511/—/513	30/—/37	0.86/—/0.91	—/—/—	—/5.0 × 10^4/—	95
(PyIPr)AuBN	THF/MeCN/2 wt%-PMMA^a	511/—/514	30/—/37	0.93/—/0.88	—/—/—	—/3.2 × 10^4/—	95
(PzIPr)AuBN	THF/2 wt%-PMMA^a	510/514	30/37	0.78/0.87	—/—	—/—	95
(BzIPr)AuBNO	THF/MeCN/2 wt%-PMMA^a	471/—/473	30/—/37	0.89/—/0.84	—/—/—	—/1.1 × 10^4/—	95

^{a} See Table 2 for the full compound name. ^{b} Not applicable because of phosphorescent materials.
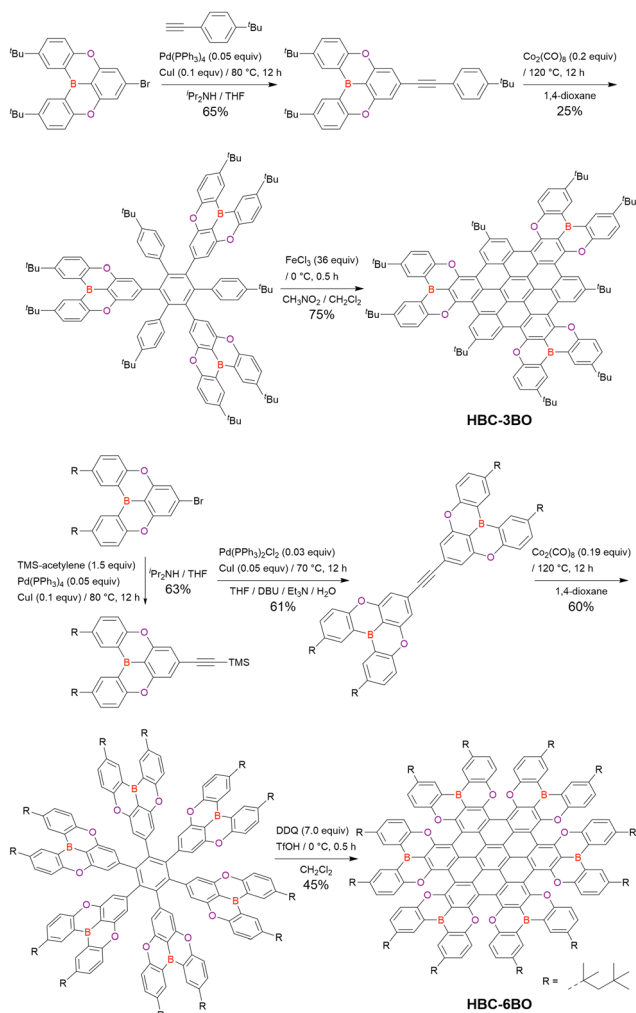
Scheme 52 Synthesis of DOBNA-based nanographene reported in ref. 136.

(UV-vis) absorption, and cyclic voltammetry measurements confirmed the significant contributions of the open-shell biradical form, which exceeded those for the corresponding indenofluorenes. The isomeric compound **[1,2-b]IF-β-DOBNA** showed clearly resolved NMR signals, a very weak EPR signal, and a wider energy gap, which indicated a much smaller biradical character. N,B,N-substituted species showed a higher biradical character than O,B,O-substituted ones according to theoretical calculations. Thus, **[1,2-b]IF-α-BCzBN** and **[1,2-b]FF-α-BCzBN** showed significantly red-shifted absorption maxima at 803 and 876 nm, respectively, as well as small energy gaps. These results demonstrate that MR structures greatly influence the open-shell biradical nature of PAHs.

4.6 Lewis acid–base adducts

The vacant p-orbital of boron is responsible for Lewis acidity, although the structural constraint of boron atoms in the planar π-conjugated systems with N,O heteroatom bridges in MR structures lowers this acidity. Indeed, DOBNA and CzBN derivatives can interact with Lewis bases such as pyridine, 4-dimethylaminopyridine (DMAP), and fluoride ions (Scheme 54). A compound with a DOBNA and N-embedded dioxygen-bridged structure, **BO-NO**, showed yellow emission in the polar CH$_2$Cl$_2$.[301] The emission intensity decreased upon the addition of pyridine, while the addition of DMAP induced the emergence of a new emission band in the blue region and decreased the intensity of the emission band in the yellow region. The binding constants of **BO-NO** towards pyridine and DMAP were estimated as 27 and 4.2 × 10^4 M^{-1}, respectively, which are much lower than those of planar fused trinaphthylboranes.[302] The phosphorescence of **IrBBacac** showed a similar behaviour.[139] The emission peak lost intensity and shifted to longer wavelengths (from 647 to 667 nm) upon the addition of pyridine. In contrast, DMAP addition caused an emission blue shift and intensity increase.

The two Lewis bases, pyridine and DMAP, coordinated at different positions, and π–π interactions between two DMAP molecules were observed in the crystal structure. As **BCzBN** shows intense emission with a narrow FWHM and high Φ_{PL}, as well as good chemical and thermal stability, it is well suited for the construction of turn-off-type fluorescent probes. The interactions between the boron centre and the fluoride ion upon the addition of tetrabutylammonium fluoride (TBAF) resulted in the formation of a non-fluorescent complex and, hence, substantial emission quenching.[303] Consequently, boron-based MR materials hold great promise for the highly sensitive, selective, and reversible sensing of fluoride ions.

1682 | *Chem. Soc. Rev.*, 2024, **53**, 1624–1692

This journal is © The Royal Society of Chemistry 2024
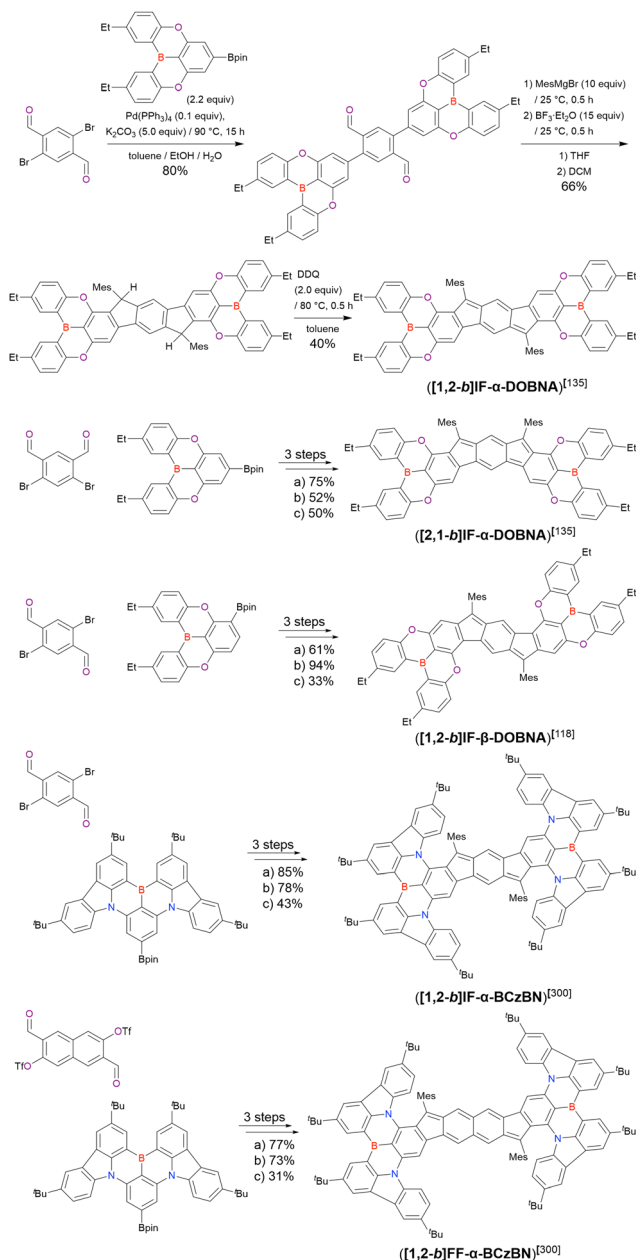
Scheme 53 Synthesis of DOBNA-based biradicaloids.

Lewis acid–base coordination not only changed optical properties, but also enhanced the open-shell biradical character[118,135]

N-Heterocycle-tethered DOBNA structures were investigated as stimuli-responsive materials.[115] Although compounds **B1** and **B3** were synthesised by one-pot borylation, the synthesis of **B2** involved an additional S_NAr reaction. The syntheses of **B4** and **B5** involved Sonogashira–Hagihara cross-coupling followed by a click reaction (Scheme 55). Compounds **B1**–**B3** having an *n*-butyl-1*H*-1,2,4-triazole scaffold exhibited emission intensity enhancement at elevated temperatures in solution, while compounds **B4** and **B5** containing an *n*-hexyl-1*H*-1,2,3-triazole scaffold showed fluorescence quenching under the same conditions. The thermally responsive emission of **B1**–**B3** was
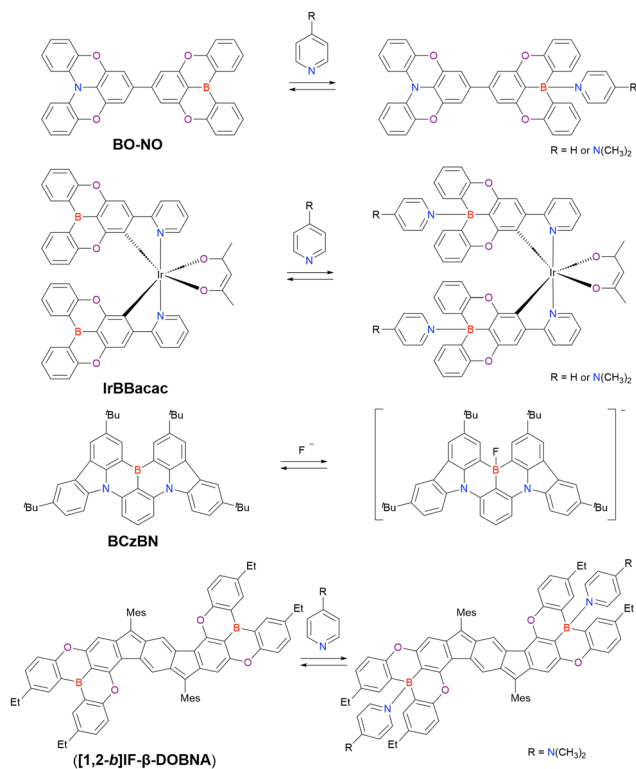
Scheme 54 Lewis acid–base adducts of DOBNA and CzBN structures.
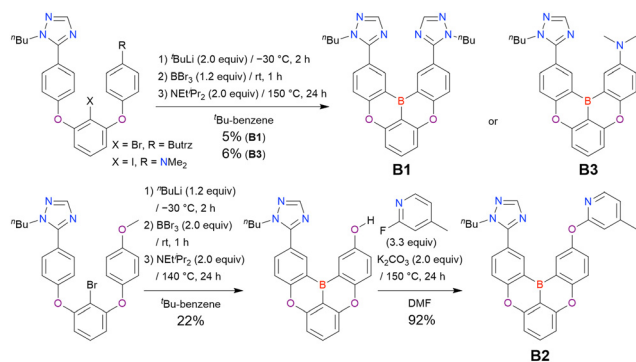
Scheme 55 Synthesis of multi-stimuli responsive materials.

caused by the dynamic switching of intermolecular B–N interactions. In addition, these compounds exhibited remarkable mechanochromism in the solid state. The formation of B–N pairs was also used to develop supramolecular copolymers.[138] The peripheries of the DOBNA core accommodated three amide units as H-bonding supramolecular motifs, which were

This journal is © The Royal Society of Chemistry 2024

Chem. Soc. Rev., 2024, **53**, 1624–1692 | **1683**
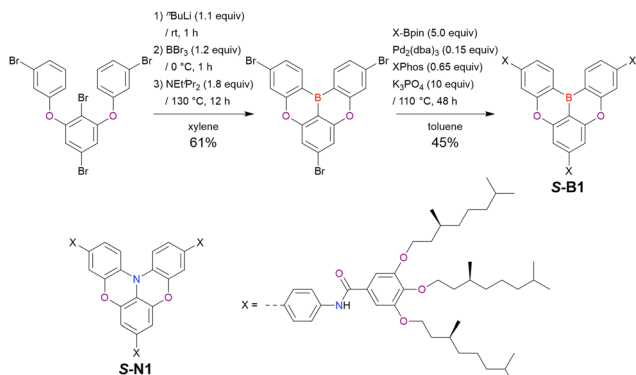
Scheme 56 Late-stage introduction of peripheral gallic amides with (*S*)-3,7-dimethyloctyl chains for supramolecular copolymers.

introduced by late-stage coupling to give **S-B1** (Scheme 56). Co-facial B–N contacts in the copolymer with **S-N1** facilitated the formation of an exciplex with TADF properties, followed by circularly polarised emission. Overall, the high stability of bridged triarylboranes is of key importance, enabling a wide variety of applications.

4.7 Summary

Late-stage functionalisation is a useful method for developing a wide variety of structures, as photophysical properties can be finely tuned by the attachment of appropriate donor and acceptor moieties. Moreover, this method enables the utilisation of MR fragments as building blocks and thus allows one to expand the application scope of MR materials by gaining additional functionality and incorporation into systems with extended π-conjugation.

5. Ladder-type boron-based MR compounds

Most boron-based MR-TADF compounds introduced in the previous sections possess boron atoms at the ring junction, featuring planarity constraints, *i.e.*, planarised triaryl boron-based compounds.[37] On the other hand, some B,N-based PAHs, in which boron atoms are not fully constrained, also exhibit MR effects. These compounds are synthesised using methods closely resembling one-pot or one-shot borylation, as discussed in the present section. The incorporation of tricoordinate boron atoms into the framework of linear acenes is an effective strategy for achieving the properties of the parent π-conjugated systems, which are inaccessible in carbon-only acenes. In 2006, Kawashima *et al.* reported a series of ladder-type fused azaborines in which the boron and nitrogen atoms are located in *para*-positions with respect to each other.[304] Zysman-Colman *et al.* reported B,N-doped heptacene **α-3BNOH**, where the boron and nitrogen atoms are located in *para*-positions with respect to each other.[305] The triple electrophilic C–H borylation of N^1-(3-(di-*p*-tolylamino)phenyl)-N^1,N^3,-N^3-tri-*p*-tolylbenzene-1,3-diamine occurred in the presence of
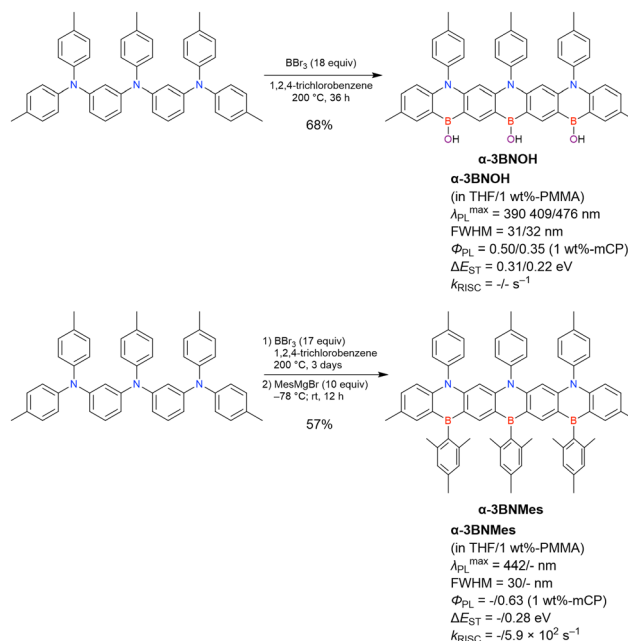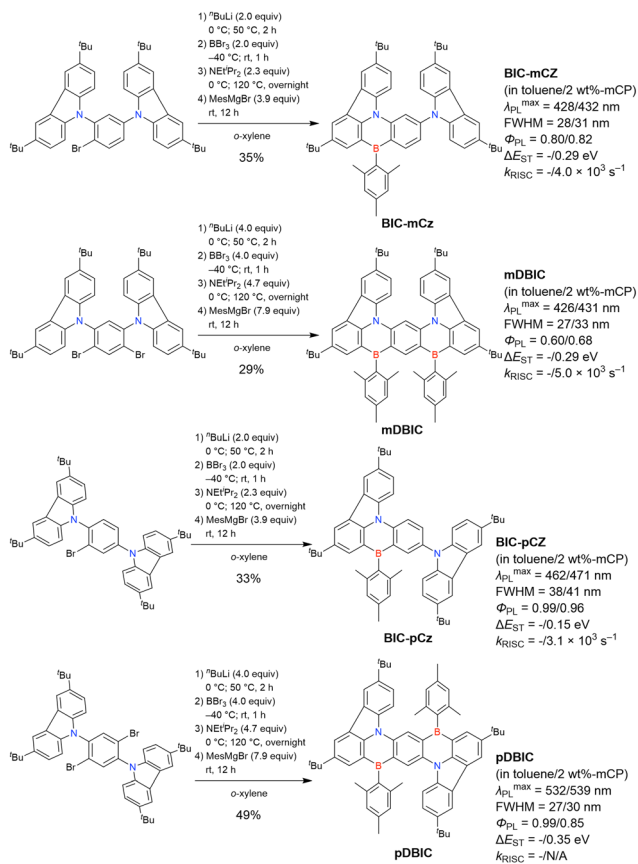

Scheme 57 Synthesis of **α-3BNOH** and **α-3BNMes** by triple electrophilic C–H borylation.

18 equiv. of BBr_3 and afforded a tri-B–Br intermediate that was subsequently hydrolysed to give **α-3BNOH** in 68% yield (Scheme 57, top). Note that the process up to the point of hydrolysis is the same as that of one-shot borylation. The thus obtained **α-3BNOH** exhibited narrow deep blue emission with CIE coordinates of (0.17, 0.01) and presented an attractive combination of TADF and TTA in a single material. **α-3BNMes** was also synthesized by trapping the tri-B–Br intermediate with a Grignard reagent instead of hydrolysing the former (Scheme 57, bottom).[306] **α-3BNMes** showed a narrow blue emission at 442 nm (FWHM = 30 nm) that was red-shifted compared with that of **α-3BNOH** because of the replacement of the strongly mesomerically electron-donating hydroxyl groups with inductively electron-withdrawing mesityl substituents. It is noteworthy that BN-doped heptacene **α-3BNMes** exhibited TADF behaviour in contrast to BN-doped pentacene reported by Kawashima *et al.*[304] due to the small ΔE_{ST} (0.28 eV) attributed to the highly π-extended structure.

Duan *et al.* prepared carbazole-fused 1,4-diazaborine type MR-TADF compounds with nonplanar boron atoms on the periphery.[307] Starting with mono-brominated bis(*N*-carbazolyl)-benzene, the one-pot sequence of lithium–bromine exchange, borylation, intramolecular bora-Friedel–Crafts reaction, and trapping with a Grignard reagent afforded mono-borylated **BIC-mCz** and **BIC-pCz** in yields of 35% and 33%, respectively (Scheme 58). In the same manner, double-borylated **mDBIC** and **pDBIC** were obtained from a dibrominated precursor in 29% and 49% yields, respectively. Notably, the process up to trapping with the Grignard reagent is identical to the one-pot borylation protocol, the only difference being the presence of a non-condensed substituent on the boron centre. The above borylated compounds displayed deep blue to pure green MR

1684 | *Chem. Soc. Rev.*, 2024, **53**, 1624–1692

This journal is © The Royal Society of Chemistry 2024

Scheme 58 Synthesis of **BIC-*m*Cz**, **BIC-*p*Cz**, ***m*DBIC**, and ***p*DBIC**.

emission at 426–532 nm with a FWHM of 27–38 nm. These ladder-type boron-based MR compounds exhibit larger ΔE_{ST} and smaller k_{RISC} due to their relatively small MR effects.

6. Conclusions

This review summarises the synthetic routes for boron-based MR emitters. For single or double borylation, one-pot borylation is the first choice because of its high regioselectivity. Commercially available polyhalobenzenes containing fluorine, chlorine, bromine, and iodine atoms are efficiently converted to one-pot borylation precursors *via* S_NAr reactions and Buchwald–Hartwig couplings with complementary site (halogen) selectivity. However, diarylamines cannot be introduced *via* S_NAr reactions, which has severely limited the chemical space of MR emitters. Moreover, double borylation is generally low-yielding and therefore impractical. For multiple borylation, one-shot borylation is an advantageous method but requires a judicious choice of precursors and reaction conditions to achieve kinetic or thermodynamic regioselectivity control. The combination of one-pot and one-shot borylations, *i.e.*, sequential multiple borylation, is a promising method for constructing novel MR skeletons with multiple boron atoms. The late-stage functionalisation of MR emitters is useful for tuning their emission wavelengths, increasing their k_{RISC} values, or imparting new functions (*e.g.*, chiroptical, sensing, and stimuli-responsive

properties). Although these protocols have achieved impressive results for the last several years, the practical application of MR emitters is still limited to their use as blue-fluorescent emitters in OLED displays. Therefore, to design MR emitters not only exhibiting specific properties but also complying with all practical requirements, especially high stability during device operation, the current chemical space needs to be well understood and further expanded by developing new synthetic protocols. Furthermore, the expansion of the chemical space will break through unconscious limits of one's imagination and pave the way for practical applications beyond OLEDs.

Conflicts of interest

There are no conflicts to declare.

Acknowledgements

Notes and references

1 F. Jäkle, *Coord. Chem. Rev.*, 2006, **250**, 1107–1121.
2 A. Wakamiya and S. Yamaguchi, *Pure Appl. Chem.*, 2006, **78**, 1413–1424.
3 Z. M. Hudson and S. Wang, *Acc. Chem. Res.*, 2009, **42**, 1584–1596.
4 C. R. Wade, A. E. J. Broomsgrove, S. Aldridge and F. P. Gabbai, *Chem. Rev.*, 2010, **110**, 3958–3984.
5 F. Jäkle, *Chem. Rev.*, 2010, **110**, 3985–4022.
6 A. Escande and M. J. Ingleson, *Chem. Commun.*, 2015, **51**, 6257–6274.
7 A. Wakamiya and S. Yamaguchi, *Bull. Chem. Soc. Jpn.*, 2015, **88**, 1357–1377.
8 Y. Ren and F. Jäkle, *Dalton Trans.*, 2016, **45**, 13996–14007.
9 L. Ji, S. Griesbeck and T. B. Marder, *Chem. Sci.*, 2017, **8**, 846–863.
10 G. Turkoglu, M. E. Cinar and T. Ozturk, *Molecules*, 2017, **22**, 1522.
11 E. von Grotthuss, A. John, T. Kaese and M. Wagner, *Asian J. Org. Chem.*, 2018, **7**, 37–53.
12 S. K. Mellerup and S. Wang, *Chem. Soc. Rev.*, 2019, **48**, 3537–3549.
13 H. Helten, *Chem. – Asian J.*, 2019, **14**, 919–935.
14 J. Huo, H. Wang, S. Li, H. Shi, Y. Tang and B. Z. Tang, *Chem. Rec.*, 2020, **20**, 556–569.
15 X. Yin, J. Liu and F. Jäkle, *Chem. – Eur. J.*, 2021, **27**, 2973–2986.
16 S. M. Berger, M. Ferger and T. B. Marder, *Chem. – Eur. J.*, 2021, **27**, 7043–7058.

This journal is © The Royal Society of Chemistry 2024

Chem. Soc. Rev., 2024, **53**, 1624–1692 | **1685**

17 J. Shi, Z. Ran, F. Peng, M. Chen, L. Li, L. Ji and W. Huang, *J. Mater. Chem. C*, 2022, **10**, 9165–9191.

18 S. M. Berger and T. B. Marder, *Mater. Horiz.*, 2022, **9**, 112–120.

19 M. Wang and C.-H. Zhao, *Chem. Rec.*, 2022, **22**, e202100199.

20 J. Han, Y. Chen, N. Li, Z. Huang and C. Yang, *Aggregate*, 2022, **3**, e182.

21 R. Wang, C.-S. Lee and Z. Lu, *J. Organomet. Chem.*, 2023, **984**, 122564.

22 J. Doty, B. Babb, P. Grisdale, M. Glogowski and J. Williams, *J. Organomet. Chem.*, 1972, **38**, 229–236.

23 C. D. Entwistle and T. B. Marder, *Angew. Chem., Int. Ed.*, 2002, **41**, 2927–2931.

24 C. D. Entwistle and T. B. Marder, *Chem. Mater.*, 2004, **16**, 4574–4585.

25 M. J. S. Dewar, V. P. Kubba and R. Pettit, *J. Chem. Soc.*, 1958, 3073–3076.

26 Z. Liu and T. B. Marder, *Angew. Chem., Int. Ed.*, 2008, **47**, 242–244.

27 M. J. D. Bosdet and W. E. Piers, *Can. J. Chem.*, 2009, **87**, 8–29.

28 P. G. Campbell, A. J. V. Marwitz and S.-Y. Liu, *Angew. Chem., Int. Ed.*, 2012, **51**, 6074–6092.

29 M. M. Morgan and W. E. Piers, *Dalton Trans.*, 2016, **45**, 5920–5924.

30 J.-Y. Wang and J. Pei, *Chin. Chem. Lett.*, 2016, **27**, 1139–1146.

31 G. Belanger-Chabot, H. Braunschweig and D. K. Roy, *Eur. J. Inorg. Chem.*, 2017, 4353–4368.

32 Z. X. Giustra and S.-Y. Liu, *J. Am. Chem. Soc.*, 2018, **140**, 1184–1194.

33 X. Chen, D. Tan and D.-T. Yang, *J. Mater. Chem. C*, 2022, **10**, 13499–13532.

34 I. Shin, H. N. Lim and W. P. Hong, *Synthesis*, 2022, 570–588.

35 Z. Zhou, A. Wakamiya, T. Kushida and S. Yamaguchi, *J. Am. Chem. Soc.*, 2012, **134**, 4529–4532.

36 M. Hirai, N. Tanaka, M. Sakai and S. Yamaguchi, *Chem. Rev.*, 2019, **119**, 8291–8331.

37 H. Hirai, K. Nakajima, S. Nakatsuka, K. Siren, J. Ni, S. Nomura, T. Ikuta and T. Hatakeyama, *Angew. Chem., Int. Ed.*, 2015, **54**, 13581–13585.

38 T. Hatakeyama, K. Shiren, K. Nakajima, S. Nomura, S. Nakatsuka, K. Kinoshita, J. Ni, Y. Ono and T. Ikuta, *Adv. Mater.*, 2016, **28**, 2777–2781.

39 C. A. Parker and C. G. Hatchard, *Trans. Faraday Soc.*, 1961, **57**, 1894–1904.

40 A. Endo, M. Ogasawara, A. Takahashi, D. Yokoyama, Y. Kato and C. Adachi, *Adv. Mater.*, 2009, **21**, 4802–4806.

41 H. Uoyama, K. Goushi, K. Shizu, H. Nomura and C. Adachi, *Nature*, 2012, **492**, 234–238.

42 C. W. Tang and S. A. Vanslyke, *Appl. Phys. Lett.*, 1987, **51**, 913–915.

43 M. A. Baldo, D. F. O'Brien, Y. You, A. Shoustikov, S. Sibley, M. E. Thompson and S. R. Forrest, *Nature*, 1998, **395**, 151–154.

44 S. M. Suresh, D. Hall, D. Beljonne, Y. Olivier and E. Zysman-Colman, *Adv. Funct. Mater.*, 2020, **30**, 1908677.

45 H. J. Kim and T. Yasuda, *Adv. Opt. Mater.*, 2022, **10**, 2201714.

46 R. K. Konidena and K. R. Naveen, *Adv. Photonics Res.*, 2022, **3**, 2200201.

47 T. Fan, Y. Zhang, D. Zhang and L. Duan, *Chem. – Eur. J.*, 2022, **28**, e202104624.

48 K. R. Naveen, H. I. Yang and J. H. Kwon, *Commun. Chem.*, 2022, **5**, 149.

49 K. R. Naveen, P. Palanisamy, M. Y. Chae and J. H. Kwon, *Chem. Commun.*, 2023, **59**, 3685–3702.

50 Y. Xu, Q. Wang, X. Song, Y. Wang and C. Li, *Chem. – Eur. J.*, 2023, **29**, e202203414.

51 L. Xiaofeng, Z. Dongdong, D. Lian and Z. Yuewei, *Front. Chem.*, 2023, **11**, 1198404.

52 H.-Z. Li, F.-M. Xie, Y.-Q. Li and J.-X. Tang, *J. Mater. Chem. C*, 2023, **11**, 6471–6511.

53 C. Lv, X. Wang, Q. Zhang and Y. Zhang, *Mater. Chem. Front.*, 2023, **7**, 2809–2827.

54 F. Santoro, A. Lami, R. Improta, J. Bloino and V. Barone, *J. Chem. Phys.*, 2008, **128**, 224311.

55 I. S. Park, K. Matsuo, N. Aizawa and T. Yasuda, *Adv. Funct. Mater.*, 2018, **28**, 1802031.

56 S. Park, Y. Xiong, R.-H. Kim, P. Elvikis, M. Meitl, D.-H. Kim, J. Wu, J. Yoon, C.-J. Yu, Z. Liu, Y. Huang, K.-C. Hwang, P. Ferreira, X. Li, K. Choquette and J. A. Rogers, *Science*, 2009, **325**, 977–981.

57 V. L. Colvin, M. C. Schlamp and A. P. Alivisatos, *Nature*, 1994, **370**, 354–357.

58 S. Coe, W. K. Woo, M. Bawendi and V. Bulovic, *Nature*, 2002, **420**, 800–803.

59 T. Sato, K. Tokunaga, N. Iwahara, K. Shizu and K. Tanaka, in *The Jahn–Teller Effect*, ed. H. Koppel, D. Yarkony and H. Barentzen, Springer, Springer Series in Chemical Physics, 2009, vol. 97, pp. 99–129.

60 Y. Kondo, K. Yoshiura, S. Kitera, H. Nishi, S. Oda, H. Gotoh, Y. Sasada, M. Yanai and T. Hatakeyama, *Nat. Photonics*, 2019, **13**, 678–682.

61 M. G. Prais, D. F. Heller and K. F. Freed, *Chem. Phys.*, 1974, **6**, 331–352.

62 Y. Lei, H. Guo, J. Wang and R. Jia, *Dalton Trans.*, 2019, **48**, 5064–5071.

63 L. Liu, Q. Wei, Y. Cheng, H. Ma, S. Xiong and X. Zhang, *J. Mater. Chem. C*, 2020, **8**, 5839–5846.

64 K. Goushi, K. Yoshida, K. Sato and C. Adachi, *Nat. Photonics*, 2012, **6**, 253–258.

65 Q. Zhang, J. Li, J. Shizu, S. Huang, S. Hirata, H. Miyazaki and C. Adachi, *J. Am. Chem. Soc.*, 2012, **134**, 14706–14709.

66 J.-L. Brédas, D. Beljonne, V. Coropceanu and J. Cornil, *Chem. Rev.*, 2004, **104**, 4971–5004.

67 M. K. Etherington, J. Gibson, H. F. Higginbotham, T. J. Penfold and A. P. Monkman, *Nat. Commun.*, 2016, **7**, 13680.

68 P. K. Samanta, D. Kim, V. Coropceanu and J.-L. Brédas, *J. Am. Chem. Soc.*, 2017, **139**, 4042–4051.

1686 | *Chem. Soc. Rev.*, 2024, **53**, 1624–1692

This journal is © The Royal Society of Chemistry 2024

69 H. Noda, X.-K. Chen, H. Nakanotani, T. Hosokai, M. Miyajima, N. Notsuka, Y. Kashima, J.-L. Brédas and C. Adachi, *Nat. Mater.*, 2019, **18**, 1084–1090.

70 B. Wex and B. R. Kaafarani, *J. Mater. Chem. C*, 2017, **5**, 8622–8653.

71 X.-K. Chen, D. Kim and J.-L. Brédas, *Acc. Chem. Res.*, 2018, **51**, 2215–2224.

72 J. Eng and T. J. Penfold, *Chem. Rec.*, 2020, **20**, 831–856.

73 H. Nakanotani, Y. Tsuchiya and C. Adachi, *Chem. Lett.*, 2021, **50**, 938–948.

74 A. Pershin, D. Hall, V. Lemaur, J.-C. Sancho-Garcia, L. Muccio-li, E. Zysman-Colman, D. Beljonne and Y. Olivier, *Nat. Commun.*, 2019, **10**, 597.

75 H. Nakanotani, T. Furukawa, T. Hosogai, T. Hatakeyama and C. Adachi, *Adv. Opt. Mater.*, 2017, **5**, 1700051.

76 C.-C. Yan, X.-D. Wang and L.-S. Liao, *Adv. Sci.*, 2022, **9**, 2200525.

77 M. Mamada, S. Maedera, S. Oda, T. B. Nguyen, H. Nakanotani, T. Hatakeyama and C. Adachi, *Mater. Chem. Front.*, 2023, **7**, 259–266.

78 D. Yokoyama, *J. Mater. Chem.*, 2011, **21**, 19187–19202.

79 J. Frischeisen, D. Yokoyama, A. Endo, C. Adachi and W. Brütting, *Org. Electron.*, 2011, **12**, 809–817.

80 W. Brütting, J. Frischeisen, T. D. Schmidt, B. J. Scholz and C. Mayr, *Phys. Status Solidi A*, 2013, **210**, 44–65.

81 T. D. Schmidt, T. Lampe, M. R. D. Sylvinson, P. I. Djurovich, M. E. Thompson and W. Brütting, *Phys. Rev. Applied.*, 2017, **8**, 037001.

82 T. Northey and T. J. Penfold, *Org. Electron.*, 2018, **59**, 45–48.

83 I. Kim, K. H. Cho, S. O. Jeon, W.-J. Son, D. Kim, Y. M. Rhee, I. Jang, H. Choi and D. S. Kim, *JACS Au*, 2021, **1**, 987–997.

84 X. Wu, B.-K. Su, D.-G. Chen, D. Liu, C.-C. Wu, Z.-X. Huang, T.-C. Lin, C.-H. Wu, M. Zhu, E. Y. Li, W.-Y. Hung, W. Zhu and P.-T. Chou, *Nat. Photonics*, 2021, **15**, 780–786.

85 K. Shizu and H. Kaji, *Commun. Chem.*, 2022, **5**, 53.

86 S. Schmidbauer, A. Hohenleutner and B. König, *Adv. Mater.*, 2013, **25**, 2114–2129.

87 J. Lee, C. Jeong, T. Batagoda, C. Coburn, M. E. Thompson and S. R. Forrest, *Nat. Commun.*, 2017, **8**, 15566.

88 H. Lim, S.-J. Woo, Y. H. Ha, Y.-H. Kim and J.-J. Kim, *Adv. Mater.*, 2022, **34**, 2100161.

89 T. B. Nguyen, H. Nakanotani and C. Adachi, *Adv. Opt. Mater.*, 2022, **10**, 2200704.

90 H. Jiang, P. Tao and W.-Y. Wong, *ACS Mater. Lett.*, 2023, **5**, 822–845.

91 X. Wang, L. Wang, G. Meng, X. Zeng, D. Zhang and L. Duan, *Sci. Adv.*, 2023, **9**, eadh1434.

92 M. Nagata, H. Min, E. Watanabe, H. Fukumoto, Y. Mizuhata, N. Tokitoh, T. Agou and T. Yasuda, *Angew. Chem., Int. Ed.*, 2021, **60**, 20280–20285.

93 S. M. Pratik, V. Coropceanu and J.-L. Brédas, *ACS Mater. Lett.*, 2022, **4**, 440–447.

94 I. S. Park, H. Min and T. Yasuda, *Angew. Chem., Int. Ed.*, 2022, **61**, e202205684.

95 S. Cai, G. S. M. Tong, L. Du, G. K.-M. So, F.-F. Hung, T.-L. Lam, G. Cheng, H. Xiao, X. Chang, Z.-X. Xu and C.-M. Che, *Angew. Chem., Int. Ed.*, 2022, **61**, e202213392.

96 H. Nakanotani, T. Higuchi, T. Furukawa, K. Masui, K. Morimoto, M. Numata, H. Tanaka, Y. Sagara, T. Yasuda and C. Adachi, *Nat. Commun.*, 2014, **5**, 4016.

97 D. Zhang, X. Song, A. J. Gillett, B. H. Drummond, S. T. E. Jones, G. Li, H. He, M. Cai, D. Credgington and L. Duan, *Adv. Mater.*, 2020, **32**, 1908355.

98 C.-Y. Chan, M. Tanaka, Y.-T. Lee, Y.-W. Wong, H. Nakanotani, T. Hatakeyama and C. Adachi, *Nat. Photonics*, 2021, **15**, 203–207.

99 S. O. Jeon, K. H. Lee, J. S. Kim, S.-G. Ihn, Y. S. Chung, J. W. Kim, H. Lee, S. Kim, H. Choi and J. Y. Lee, *Nat. Photonics*, 2021, **15**, 208–215.

100 M. Mamada, H. Katagiri, C.-Y. Chan, Y.-T. Lee, K. Goushi, H. Nakanotani, T. Hatakeyama and C. Adachi, *Adv. Funct. Mater.*, 2022, **32**, 2204352.

101 P. Heimel, A. Mondal, F. May, W. Kowalsky, C. Lennartz, D. Andrienko and R. Lovrincic, *Nat. Commun.*, 2018, **9**, 4990.

102 E. Kim, J. Park, M. Jun, H. Shin, J. Baek, T. Kim, S. Kim, J. Lee, H. Ahn and S. Kim, *Sci. Adv.*, 2022, **8**, eabq1641.

103 X. Cao, K. Pan, J. Miao, X. Lv, Z. Huang, F. Ni, X. Yin, Y. Wei and C. Yang, *J. Am. Chem. Soc.*, 2022, **144**, 22976–22984.

104 Y. X. Hu, J. Miao, T. Hua, Z. Huang, Y. Qi, Y. Zou, Y. Qiu, H. Xia, H. Liu, X. Cao and C. Yang, *Nat. Photonics*, 2022, **16**, 803–810.

105 S. Oda and T. Hatakeyama, *Bull. Chem. Soc. Jpn.*, 2021, **94**, 950–960.

106 T. Hatakeyama, S. Hashimoto, S. Seki and M. Nakamura, *J. Am. Chem. Soc.*, 2011, **133**, 18614–18617.

107 A. D. Grosso, R. G. Pritchard, C. A. Muryn and M. J. Ingleson, *Organometallics*, 2010, **29**, 241–249.

108 N. Ishida, T. Moriya, T. Goya and M. Murakami, *J. Org. Chem.*, 2010, **75**, 8709–8712.

109 S. A. Iqbal, J. Pahl, K. Yuan and M. J. Ingleson, *Chem. Soc. Rev.*, 2020, **49**, 4564–4591.

110 S. Rej and N. Chatani, *Angew. Chem., Int. Ed.*, 2022, **61**, e202209539.

111 S. Oda, W. Kumano, T. Hama, R. Kawasumi, K. Yoshiura and T. Hatakeyama, *Angew. Chem., Int. Ed.*, 2021, **60**, 2882–2886.

112 J. U. Kim, I. S. Park, C.-Y. Chan, M. Tanaka, Y. Tsuchiya, H. Nakanotani and C. Adachi, *Nat. Commun.*, 2020, **11**, 1765.

113 J. Han, Z. Huang, J. Miao, Y. Qiu, Z. Xie and C. Yang, *Chem. Sci.*, 2022, **13**, 3402–3408.

114 S. Oda, T. Sugitani, H. Tanaka, K. Tabata, R. Kawasumi and T. Hatakeyama, *Adv. Mater.*, 2022, **34**, 2201778.

115 G. Meng, T. Peng, Y. Shi, H. Li, X. Wang, X. Yin, D.-T. Yang, S. Wang and N. Wang, *J. Mater. Chem. C*, 2020, **8**, 7749–7754.

116 F. Chen, L. Zhao, X. Wang, Q. Yang, W. Li, H. Tian, S. Shao, L. Wang, X. Jing and F. Wang, *Sci. China: Chem.*, 2021, **64**, 547–551.

117 Y. Chen, N. Li, Z. Huang, G. Xie and C. Yang, *Chem. Eng. J.*, 2022, **430**, 133078.

118 X. Tian, J. Guo, W. Sun, L. Yuan, C. Dou and Y. Wang, *Chem. – Eur. J.*, 2022, **28**, e202200045.

This journal is © The Royal Society of Chemistry 2024

Chem. Soc. Rev., 2024, **53**, 1624–1692 | 1687

119 G. Meng, X. Chen, X. Wang, N. Wang, T. Peng and S. Wang, *Adv. Opt. Mater.*, 2019, **7**, 1900130.

120 I. S. Park, H. Min, J. U. Kim and T. Yasuda, *Adv. Opt. Mater.*, 2021, **9**, 2101282.

121 H. Lee, R. Braveenth, S. Muruganantham, C. Y. Jeon, H. S. Lee and J. H. Kwon, *Nat. Commun.*, 2023, **14**, 419.

122 D. H. Ahn, S. W. Kim, H. Lee, I. J. Ko, D. Karthik, J. Y. Lee and J. H. Kwon, *Nat. Photonics*, 2019, **13**, 540–546.

123 H. J. Kim, M. Godumala, S. K. Kim, J. Yoon, C. Y. Kim, H. Park, J. H. Kwon, M. J. Cho and D. H. Choi, *Adv. Opt. Mater.*, 2020, **8**, 1902175.

124 H. Lim, H. J. Cheon, S.-J. Woo, S.-K. Kwon, Y.-H. Kim and J.-J. Kim, *Adv. Mater.*, 2020, **32**, 2004083.

125 H. J. Kim, H. Kang, J.-E. Jeong, S. H. Park, C. W. Koh, C. W. Kim, H. Y. Woo, M. J. Cho, S. Park and D. H. Choi, *Adv. Funct. Mater.*, 2021, **31**, 2102588.

126 R. Pei, H. Liu, C. Zhou, J. Miao and C. Yang, *J. Mater. Chem. C*, 2021, **9**, 17136–17142.

127 H.-J. Tan, G.-X. Yang, Y.-L. Deng, C. Cao, J.-H. Tan, Z.-L. Zhu, W.-C. Chen, Y. Xiong, J.-X. Jian, C.-S. Lee and Q.-X. Tong, *Adv. Mater.*, 2022, **34**, 2200537.

128 Y. Xie, L. Hua, Z. Wang, Y. Liu, S. Ying, Y. Liu, Z. Ren and S. Yan, *Sci. China: Chem.*, 2023, **66**, 826–836.

129 B. Chen, C. Liao, D. Li, H. Liu and S. Wang, *J. Mater. Chem. C*, 2023, **11**, 8767–8775.

130 H. Gao, S. Shen, Y. Qin, G. Liu, T. Gao, X. Dong, Z. Pang, X. Xie, P. Wang and Y. Wang, *J. Phys. Chem. Lett.*, 2022, **13**, 7561–7567.

131 H. Gao, Z. Li, Z. Pang, Y. Qin, G. Liu, T. Gao, X. Dong, S. Shen, X. Xie, P. Wang, C.-S. Lee and Y. Wang, *ACS Appl. Mater. Interfaces*, 2023, **15**, 5529–5537.

132 F. Chen, J. Hu, X. Wang, S. Shao, L. Wang, X. Jing and F. Wang, *Sci. China: Chem.*, 2020, **63**, 1112–1120.

133 Y. Chang, Y. Wu, X. Wang, W. Li, Q. Yang, S. Wang, S. Shao and L. Wang, *Chem. Eng. J.*, 2023, **451**, 138545.

134 K. R. Naveen, H. Lee, R. Braveenth, D. Karthik, K. J. Yang, S. J. Hwang and J. H. Kwon, *Adv. Funct. Mater.*, 2021, **32**, 2110356.

135 J. Guo, Y. Yang, C. Dou and Y. Wang, *J. Am. Chem. Soc.*, 2021, **143**, 18272–18279.

136 J. Guo, T. Zhang, Z. Li, K. Ye, Y. Wang and C. Dou, *Chem. Commun.*, 2023, **59**, 2644–2647.

137 G. Meng, H. Dai, Q. Wang, J. Zhou, T. Fan, X. Zeng, X. Wang, Y. Zhang, D. Yang, D. Ma, D. Zhang and L. Duan, *Nat. Commun.*, 2023, **14**, 2394.

138 B. Adelizzi, P. Chidchob, N. Tanaka, B. A. G. Lamers, S. C. J. Meskers, S. Ogi, A. R. A. Palmans, S. Yamaguchi and E. W. Meijer, *J. Am. Chem. Soc.*, 2020, **142**, 16681–16689.

139 Q. Li, C. Shi, M. Huang, X. Wei, H. Yan, C. Yang and A. Yuan, *Chem. Sci.*, 2019, **10**, 3257–3263.

140 S. Nakatsuka, H. Gotoh, K. Kinoshita, N. Yasuda and T. Hatakeyama, *Angew. Chem., Int. Ed.*, 2017, **56**, 5087–5090.

141 S. H. Han, J. H. Jeong, J. W. Yoo and J. Y. Lee, *J. Mater. Chem. C*, 2019, **7**, 3082–3089.

142 P. Jiang, L. Zhan, X. Cao, X. Lv, S. Gong, Z. Chen, C. Zhou, Z. Huang, F. Ni, Y. Zou and C. Yang, *Adv. Opt. Mater.*, 2021, **9**, 2100825.

143 T. Hua, L. Zhan, N. Li, Z. Huang, X. Cao, Z. Xiao, S. Gong, C. Zhou, C. Zhong and C. Yang, *Chem. Eng. J.*, 2021, **426**, 131169.

144 X. Wu, J.-W. Huang, B.-K. Su, S. Wang, L. Yuan, W.-Q. Zheng, H. Zhang, Y.-X. Zheng, W. Zhu and P.-T. Chou, *Adv. Mater.*, 2022, **34**, 2105080.

145 W. Yang, N. Li, J. Miao, L. Zhan, S. Gong, Z. Huang and C. Yang, *CCS Chem.*, 2022, **4**, 3463–3471.

146 Y.-C. Cheng, X.-C. Fan, F. Huang, X. Xiong, J. Yu, K. Wang, C.-S. Lee and X.-H. Zhang, *Angew. Chem., Int. Ed.*, 2022, **61**, e202212575.

147 W. Yang, J. Miao, F. Hu, Y. Zou, C. Zhong, S. Gong and C. Yang, *Adv. Funct. Mater.*, 2023, **33**, 2213056.

148 H. Mubarok, A. Amin, T. Lee, J. Jung, J.-H. Lee and M. H. Lee, *Angew. Chem., Int. Ed.*, 2023, **62**, e202306879.

149 J.-J. Hu, X.-F. Luo, Y.-P. Zhang, M.-X. Mao, H.-X. Ni, X. Liang and Y.-X. Zheng, *J. Mater. Chem. C*, 2022, **10**, 768–773.

150 G. Liu, H. Sasabe, K. Kumada, A. Matsunaga, H. Katagiri and J. Kido, *J. Mater. Chem. C*, 2021, **9**, 8308–8313.

151 J. Park, K. J. Kim, J. Lim, T. Kim and J. Y. Lee, *Adv. Mater.*, 2022, **34**, 2108581.

152 B. Lei, Z. Huang, S. Li, J. Liu, Z. Bin and J. You, *Angew. Chem., Int. Ed.*, 2023, **62**, e202218405.

153 X. Liang, Z.-P. Yan, H.-B. Han, Z.-G. Wu, Y.-X. Zheng, H. Meng, J.-L. Zuo and W. Huang, *Angew. Chem., Int. Ed.*, 2018, **57**, 11316–11320.

154 Y. Xu, Z. Cheng, Z. Li, B. Liang, J. Wang, J. Wei, Z. Zhang and Y. Wang, *Adv. Opt. Mater.*, 2020, **8**, 1902142.

155 M. Yang, I. S. Park and T. Yasuda, *J. Am. Chem. Soc.*, 2020, **142**, 19468–19472.

156 S. Xu, Q. Yang, Y. Zhang, H. Li, Q. Xue, G. Xie, M. Gu, J. Jin, L. Huang and R. Chen, *Chin. Chem. Lett.*, 2021, **32**, 1372–1376.

157 Y.-T. Lee, C.-Y. Chan, M. Tanaka, M. Mamada, U. Balijapalli, Y. Tsuchiya, H. Nakanotani, T. Hatakeyama and C. Adachi, *Adv. Electron. Mater.*, 2021, **7**, 2001090.

158 M. Yang, S. Shikita, H. Min, I. S. Park, H. Shibata, N. Amanokura and T. Yasuda, *Angew. Chem., Int. Ed.*, 2021, **60**, 23142–23147.

159 X. Yan, Z. Li, Q. Wang, Y. Qu, Y. Xu and Y. Wang, *J. Mater. Chem. C*, 2022, **10**, 15408–15415.

160 Y. Qi, W. Ning, Y. Zou, X. Cao, S. Gong and C. Yang, *Adv. Funct. Mater.*, 2021, **31**, 2102017.

161 Y. Zhang, G. Li, L. Wang, T. Huang, J. Wei, G. Meng, X. Wang, X. Zeng, D. Zhang and L. Duan, *Angew. Chem., Int. Ed.*, 2022, **61**, e202202380.

162 X. Cai, Y. Xu, Y. Pan, L. Li, Y. Pu, X. Zhuang, C. Li and Y. Wang, *Angew. Chem., Int. Ed.*, 2023, **62**, e202216473.

163 Y. Zhang, J. Wei, L. Wang, T. Huang, G. Meng, X. Wang, X. Zeng, M. Du, T. Fan, C. Yin, D. Zhang and L. Duan, *Adv. Mater.*, 2023, **35**, 2209396.

1688 | *Chem. Soc. Rev.*, 2024, **53**, 1624–1692

This journal is © The Royal Society of Chemistry 2024

164 F. Zhang, F. Rauch, A. Swain, T. B. Marder and P. Ravat, *Angew. Chem., Int. Ed.*, 2023, **62**, e202218965.

165 B. Du, K. Zhang, P. Wang, X. Wang, S. Wang, S. Shao and L. Wang, *J. Mater. Chem. C*, 2023, **11**, 9578–9585.

166 J. Liu, L. Chen, X. Wang, Q. Yang, L. Zhao, C. Tong, S. Wang, S. Shao and L. Wang, *Macromol. Rapid Commun.*, 2022, **43**, e2200079.

167 G. Liu, H. Sasabe, K. Kumada, H. Arai and J. Kido, *Chem. – Eur. J.*, 2022, **28**, e202201605.

168 Q. Li, Y. Wu, X. Wang, Q. Yang, J. Hu, R. Zhong, S. Shao and L. Wang, *Chem. – Eur. J.*, 2022, **28**, e202104214.

169 Q. Li, Y. Wu, Q. Yang, S. Wang, S. Shao and L. Wang, *ACS Appl. Mater. Interfaces*, 2022, **14**, 49995–50003.

170 J. Han, Z. Huang, X. Lv, J. Miao, Y. Qiu, X. Cao and C. Yang, *Adv. Opt. Mater.*, 2022, **10**, 2102092.

171 Z.-P. Yan, L. Yuan, Y. Zhang, M.-X. Mao, X.-J. Liao, H.-X. Ni, Z.-H. Wang, Z. An, Y.-X. Zheng and J.-L. Zuo, *Adv. Mater.*, 2022, **34**, 2204253.

172 Y. Zhang, D. Zhang, J. Wei, Z. Liu, Y. Lu and L. Duan, *Angew. Chem., Int. Ed.*, 2019, **58**, 16912–16917.

173 F. Liu, Z. Cheng, L. Wan, Z. Feng, H. Liu, H. Jin, L. Gao, P. Lu and W. Yang, *Small*, 2022, **18**, e2106462.

174 F. Huang, X.-C. Fan, Y.-C. Cheng, H. Wu, Y.-Z. Shi, J. Yu, K. Wang, C.-S. Lee and X.-H. Zhang, *Mater. Horiz.*, 2022, **9**, 2226–2232.

175 W. Xue, H. Yan, Y. He, L. Wu, X. Zhang, Y. Wu, J. Xu, J. He, C. Yan and H. Meng, *Chem. – Eur. J.*, 2022, **28**, e202201006.

176 Y.-H. He, F.-M. Xie, H.-Z. Li, K. Zhang, Y. Shen, F. Ding, C.-Y. Wang, Y.-Q. Li and J.-X. Tang, *Mater. Chem. Front.*, 2023, **7**, 2454–2463.

177 X.-F. Luo, H.-X. Ni, X. Liang, D. Yang, D. Ma, Y.-X. Zheng and J.-L. Zuo, *Adv. Opt. Mater.*, 2023, **11**, 2203002.

178 Y. Li, W. Li, J. Hu, X. Yao, L. Hua, W. Cai, S. Shi, C. Zhang, Z. Liu, S. Li, X. Chen, Z. Sun, Z. Ren, M.-C. Tang, G. Wei and Z. Fei, *Adv. Opt. Mater.*, 2023, **11**, 2300298.

179 Y. Xu, C. Li, Z. Li, Q. Wang, X. Cai, J. Wei and Y. Wang, *Angew. Chem., Int. Ed.*, 2020, **59**, 17442–17446.

180 Y.-T. Lee, C.-Y. Chan, M. Tanaka, M. Mamada, K. Goushi, X. Tang, Y. Tsuchiya, H. Nakanotani and C. Adachi, *Adv. Opt. Mater.*, 2022, **10**, 2200682.

181 X. Cai, Y. Pu, C. Li, Z. Wang and Y. Wang, *Angew. Chem., Int. Ed.*, 2023, **62**, e202304104.

182 Y. Zou, M. Yu, J. Miao, T. Huang, S. Liao, X. Cao and C. Yang, *Chem. Sci.*, 2023, **14**, 3326–3331.

183 J.-P. Liu, L. Chen, L. Zhao, C.-Y. Tong, S.-M. Wang, S.-Y. Shao and L.-X. Wang, *Chin. J. Polym. Sci.*, 2023, **41**, 802–810.

184 Y. Liu, X. Xiao, Y. Ran, Z. Bin and J. You, *Chem. Sci.*, 2021, **12**, 9408–9412.

185 M. Yang, R. K. Konidena, S. Shikita and T. Yasuda, *J. Mater. Chem. C*, 2023, **11**, 917–922.

186 X. Xiao, B. Lei, D. Wu and Z. Bin, *Chem. Commun.*, 2023, **59**, 6556–6559.

187 Q. Wu, J. Li, D. Liu, Y. Mei, B. Liu, J. Wang, M. Xu and Y. Li, *Dyes Pigm.*, 2023, **217**, 111421.

188 C.-Z. Du, Y. Lv, H. Dai, X. Hong, J. Zhou, J.-K. Li, R.-R. Gao, D. Zhang, L. Duan and X.-Y. Wang, *J. Mater. Chem. C*, 2023, **11**, 2469–2474.

189 Y. Zhang, D. Zhang, J. Wei, X. Hong, Y. Lu, D. Hu, G. Li, Z. Liu, Y. Chen and L. Duan, *Angew. Chem., Int. Ed.*, 2020, **59**, 17499–17503.

190 Y. Wei, K. Pan, X. Cao, Y. Li, X. Zhou and C. Yang, *CCS Chem.*, 2022, **4**, 3852–3863.

191 X.-F. Luo, H.-X. Ni, H.-L. Ma, Z.-Z. Qu, J. Wang, Y.-X. Zheng and J.-L. Zuo, *Adv. Opt. Mater.*, 2022, **10**, 2102513.

192 Y. Liu, X. Xiao, Z. Huang, D. Yang, D. Ma, J. Liu, B. Lei, Z. Bin and J. You, *Angew. Chem., Int. Ed.*, 2022, **61**, e202210210.

193 X.-F. Luo, S.-Q. Song, H.-X. Ni, H. Ma, D. Yang, D. Ma, Y.-X. Zheng and J.-L. Zuo, *Angew. Chem., Int. Ed.*, 2022, **61**, e202209984.

194 H. Chen, T. Fan, G. Zhao, D. Zhang, G. Li, W. Jiang, L. Duan and Y. Zhang, *Angew. Chem., Int. Ed.*, 2023, **62**, e202300934.

195 Y. Qiu, H. Xia, J. Miao, Z. Huang, N. Li, X. Cao, J. Han, C. Zhou, C. Zhong and C. Yang, *ACS Appl. Mater. Interfaces*, 2021, **13**, 59035–59042.

196 T. Hua, J. Miao, H. Xia, Z. Huang, X. Cao, N. Li and C. Yang, *Adv. Funct. Mater.*, 2022, **32**, 2201032.

197 F. Liu, Z. Cheng, Y. Jiang, L. Gao, H. Liu, H. Liu, Z. Feng, P. Lu and W. Yang, *Angew. Chem., Int. Ed.*, 2022, **61**, e202116927.

198 X. Xiong, Y.-C. Cheng, K. Wang, J. Yu and X.-H. Zhang, *Mater. Chem. Front.*, 2023, **7**, 929–936.

199 Y. Yang, N. Li, J. Miao, X. Cao, A. Ying, K. Pan, X. Lv, F. Ni, Z. Huang, S. Gong and C. Yang, *Angew. Chem., Int. Ed.*, 2022, **61**, e202202227.

200 J. Liu, Y. Zhu, T. Tsuboi, C. Deng, W. Lou, D. Wang, T. Liu and Q. Zhang, *Nat. Commun.*, 2022, **13**, 4876.

201 X.-F. Luo, H.-X. Ni, L. Shen, L. Wang, X. Xiao and Y.-X. Zheng, *Chem. Commun.*, 2023, **59**, 2489–2492.

202 D. H. Ahn, J. H. Maeng, H. Lee, H. Yoo, R. Lampande, J. Y. Lee and J. H. Kwon, *Adv. Opt. Mater.*, 2020, **8**, 2000102.

203 J. Park, J. Lim, J. H. Lee, B. Jang, J. H. Han, S. S. Yoon and J. Y. Lee, *ACS Appl. Mater. Interfaces*, 2021, **13**, 45798–45805.

204 J. Park, J. Moon, J. Lim, J. Woo, S. S. Yoon and J. Y. Lee, *J. Mater. Chem. C*, 2022, **10**, 12300–12306.

205 S. Oda, B. Kawakami, R. Kawasumi, R. Okita and T. Hatakeyama, *Org. Lett.*, 2019, **21**, 9311–9314.

206 J. A. Knöller, G. Meng, X. Wang, D. Hall, A. Pershin, D. Beljonne, Y. Olivier, S. Laschat, E. Zysman-Colman and S. Wang, *Angew. Chem., Int. Ed.*, 2020, **59**, 3156–3160.

207 X.-F. Luo, H.-X. Ni, A.-Q. Lv, X.-K. Yao, H.-L. Ma and Y.-X. Zheng, *Adv. Opt. Mater.*, 2022, **10**, 2200504.

208 X. Cai, J. Xue, C. Li, B. Liang, A. Ying, Y. Tan, S. Gong and Y. Wang, *Angew. Chem., Int. Ed.*, 2022, **61**, e202200337.

209 Y. Zhang, D. Zhang, T. Huang, A. J. Gillett, Y. Liu, D. Hu, L. Cui, Z. Bin, G. Li, J. Wei and L. Duan, *Angew. Chem., Int. Ed.*, 2021, **60**, 20498–20503.

210 J.-K. Li, X.-Y. Chen, Y.-L. Guo, X.-C. Wang, A. C.-H. Sue, X.-Y. Cao and X.-Y. Wang, *J. Am. Chem. Soc.*, 2021, **143**, 17958–17963.

211 Y. Zou, J. Hu, M. Yu, J. Miao, Z. Xie, Y. Qiu, X. Cao and C. Yang, *Adv. Mater.*, 2022, **34**, 2201442.

This journal is © The Royal Society of Chemistry 2024

Chem. Soc. Rev., 2024, **53**, 1624–1692 | **1689**

212 Y. Wang, K. Zhang, F. Chen, X. Wang, Q. Yang, S. Wang, S. Shao and L. Wang, *Chin. J. Chem.*, 2022, **40**, 2671–2677.

213 J.-K. Li, M.-Y. Zhang, L. Zeng, L. Huang and X.-Y. Wang, *Angew. Chem., Int. Ed.*, 2023, **62**, e202303093.

214 T. Fan, M. Du, X. Jia, L. Wang, Z. Yin, Y. Shu, Y. Zhang, J. Wei, D. Zhang and L. Duan, *Adv. Mater.*, 2023, **35**, 2301018.

215 I. S. Park, M. Yang, H. Shibata, N. Amanokura and T. Yasuda, *Adv. Mater.*, 2022, **34**, 2107951.

216 X.-C. Fan, K. Wang, Y.-Z. Shi, Y.-C. Cheng, Y.-T. Lee, J. Yu, X.-K. Chen, C. Adachi and X.-H. Zhang, *Nat. Photonics*, 2023, **17**, 280–285.

217 K. Matsui, S. Oda, K. Yoshiura, K. Nakajima, N. Yasuda and T. Hatakeyama, *J. Am. Chem. Soc.*, 2018, **140**, 1195–1198.

218 X. Lv, J. Miao, M. Liu, Q. Peng, C. Zhong, X. Hu, X. Cao, H. Wu, Y. Yang, C. Zhou, J. Ma, Y. Zou and C. Yang, *Angew. Chem., Int. Ed.*, 2022, **61**, e202201588.

219 J. Jin, C. Duan, H. Jiang, P. Tao, H. Xu and W.-Y. Wong, *Angew. Chem., Int. Ed.*, 2023, **62**, e202218947.

220 J. H. Kim, W. J. Chung, J. Kim and J. Y. Lee, *Mater. Today Energy*, 2021, **21**, 100792.

221 Y. Wang, Y. Duan, R. Guo, S. Ye, K. Di, W. Zhang, S. Zhuang and L. Wang, *Org. Electron.*, 2021, **97**, 106275.

222 H. J. Cheon, Y.-S. Shin, N.-H. Park, J.-H. Lee and Y.-H. Kim, *Small*, 2022, **18**, e2107574.

223 H.-J. Cheon, S.-J. Woo, S.-H. Baek, J.-H. Lee and Y.-H. Kim, *Adv. Mater.*, 2022, **34**, 2207416.

224 K. R. Naveen, S. J. Hwang, H. Lee and J. H. Kwon, *Adv. Electron. Mater.*, 2022, **8**, 2101114.

225 J. Bian, S. Chen, L. Qiu, N. Zhang, J. Zhang, C. Duan, C. Han and H. Xu, *Research*, 2022, **2022**, 9838120.

226 H. Lee, R. Braveenth, J. D. Park, C. Y. Jeon, H. S. Lee and J. H. Kwon, *ACS Appl. Mater. Interfaces*, 2022, **14**, 36927–36935.

227 Y.-N. Hu, X.-C. Fan, F. Huang, Y.-Z. Shi, H. Wang, Y.-C. Cheng, M.-Y. Chen, K. Wang, J. Yu and X.-H. Zhang, *Adv. Opt. Mater.*, 2023, **11**, 2202267.

228 E. Ravindran, H. E. Baek, H. W. Son, J. H. Park, Y.-H. Kim and M. C. Suh, *Adv. Funct. Mater.*, 2023, **33**, 2213461.

229 K. Di, R. Guo, Y. Wang, Y. Lv, H. Su, Q. Zhang, B. Yang and L. Wang, *J. Mater. Chem. C*, 2023, **11**, 6429–6437.

230 Y. Wang, K. Di, Y. Duan, R. Guo, L. Lian, W. Zhang and W. L. Wang, *Chem. Eng. J.*, 2022, **431**, 133221.

231 Y. Wang, R. Guo, A. Ying, K. Di, L. Chen, H. Gu, S. Liu, Y. Duan, H. Su, S. Gong and L. Wang, *Adv. Opt. Mater.*, 2023, **11**, 2202034.

232 C.-Y. Chan, S. Madayanad Suresh, Y.-T. Lee, Y. Tsuchiya, T. Matulaitis, D. Hall, A. M. Z. Slawin, S. Warriner, D. Beljonne, Y. Olivier, C. Adachi and E. Zysman-Colman, *Chem. Commun.*, 2022, **58**, 9377–9380.

233 Y. Lee and J.-I. Hong, *J. Mater. Chem. C*, 2022, **10**, 11855–11861.

234 M. Wang, Z. Fu, R. Cheng, J. Du, T. Wu, Z. Bin, D. Wu, Y. Yang and J. Lan, *Chem. Commun.*, 2023, **59**, 5126–5129.

235 N. Ikeda, S. Oda, R. Matsumoto, M. Yoshioka, D. Fukushima, K. Yoshiura, N. Yasuda and T. Hatakeyama, *Adv. Mater.*, 2020, **32**, 2004072.

236 T. Fan, Y. Zhang, L. Wang, Q. Wang, C. Yin, M. Du, X. Jia, G. Li and L. Duan, *Angew. Chem., Int. Ed.*, 2022, **61**, e202213585.

237 K. R. Naveen, H. Lee, L. H. Seung, Y. H. Jung, C. P. Keshavananda Prabhu, S. Muruganantham and J. H. Kwon, *Chem. Eng. J.*, 2023, **451**, 138498.

238 H. Tanaka, S. Oda, G. Ricci, H. Gotoh, K. Tabata, R. Kawasumi, D. Beljonne, Y. Olivier and T. Hatakeyama, *Angew. Chem., Int. Ed.*, 2021, **60**, 17910–17914.

239 K. R. Naveen, J. H. Oh, H. Lee and J. H. Kwon, *Angew. Chem., Int. Ed.*, 2023, **62**, e202306768.

240 K. Rayappa Naveen, H. Lee, R. Braveenth, K. Joon Yang, S. Jae Hwang and J. Hyuk Kwon, *Chem. Eng. J.*, 2022, **432**, 134381.

241 H. S. Kim, H. J. Cheon, D. Lee, W. Lee, J. Kim, Y.-H. Kim and S. Yoo, *Sci. Adv.*, 2023, **9**, eadf1388.

242 F. Huang, X.-C. Fan, Y.-C. Cheng, H. Wu, X. Xiong, J. Yu, K. Wang and X.-H. Zhang, *Angew. Chem., Int. Ed.*, 2023, **62**, e202306413.

243 S. Oda, B. Kawakami, Y. Yamasaki, R. Matsumoto, M. Yoshioka, D. Fukushima, S. Nakatsuka and T. Hatakeyama, *J. Am. Chem. Soc.*, 2022, **144**, 106–112.

244 S. Oda, B. Kawakami, M. Horiuchi, Y. Yamasaki, R. Kawasumi and T. Hatakeyama, *Adv. Sci.*, 2023, **10**, 2205070.

245 Y. Sano, T. Shintani, M. Hayakawa, S. Oda, M. Kondo, T. Matsushita and T. Hatakeyama, *J. Am. Chem. Soc.*, 2023, **145**, 11504–11511.

246 S. Nakatsuka, N. Yasuda and T. Hatakeyama, *J. Am. Chem. Soc.*, 2018, **140**, 13562–13565.

247 D. T. Yang, T. Nakamura, Z. He, X. Wang, A. Wakamiya, T. Peng and S. Wang, *Org. Lett.*, 2018, **20**, 6741–6745.

248 G. Meng, H. Dai, T. Huang, J. Wei, J. Zhou, X. Li, X. Wang, X. Hong, C. Yin, X. Zeng, Y. Zhang, D. Yang, D. Ma, G. Li, D. Zhang and L. Duan, *Angew. Chem., Int. Ed.*, 2022, **61**, e202207293.

249 G. Meng, H. Dai, J. Zhou, T. Huang, X. Zeng, Q. Wang, X. Wang, Y. Zhang, T. Fan, D. Yang, D. Ma, D. Zhang and L. Duan, *Chem. Sci.*, 2023, **14**, 979–986.

250 G. Meng, L. Liu, Z. He, D. Hall, X. Wang, T. Peng, X. Yin, P. Chen, D. Beljonne, Y. Olivier, E. Zysman-Colman, N. Wang and S. Wang, *Chem. Sci.*, 2022, **13**, 1665–1674.

251 S. Oda, K. Ueura, B. Kawakami and T. Hatakeyama, *Org. Lett.*, 2020, **22**, 700–704.

252 S. Uemura, S. Oda, M. Hayakawa, R. Kawasumi, N. Ikeda, Y.-T. Lee, C.-Y. Chan, Y. Tsuchiya, C. Adachi and T. Hatakeyama, *J. Am. Chem. Soc.*, 2023, **145**, 1505–1511.

253 S. Madayanad Suresh, L. Zhang, T. Matulaitis, D. Hall, C. Si, G. Ricci, A. M. Z. Slawin, S. Warriner, D. Beljonne, Y. Olivier, I. D. W. Samuel and E. Zysman-Colman, *Adv. Mater.*, 2023, **35**, 2300997.

254 S. Madayanad Suresh, L. Zhang, D. Hall, C. Si, G. Ricci, T. Matulaitis, A. M. Z. Slawin, S. Warriner, Y. Olivier, I. D. W. Samuel and E. Zysman-Colman, *Angew. Chem., Int. Ed.*, 2023, **62**, e202215522.

255 D. Karthik, D. H. Ahn, J. H. Ryu, H. Lee, J. H. Maeng, J. Y. Lee and J. H. Kwon, *J. Mater. Chem. C*, 2020, **8**, 2272–2279.

1690 | *Chem. Soc. Rev.*, 2024, **53**, 1624–1692

This journal is © The Royal Society of Chemistry 2024

256 D. Song, Y. Yu, L. Yue, D. Zhong, Y. Zhang, X. Yang, Y. Sun, G. Zhou and Z. Wu, *J. Mater. Chem. C*, 2019, **7**, 11953–11963.

257 Z. Huang, H. Xie, J. Miao, Y. Wei, Y. Zou, T. Hua, X. Cao and C. Yang, *J. Am. Chem. Soc.*, 2023, **145**, 12550–12560.

258 Q. Wang, Y. Xu, T. Yang, J. Xue and Y. Wang, *Adv. Mater.*, 2023, **35**, 2205166.

259 J. Hwang, H. Kang, J.-E. Jeong, H. Y. Woo, M. J. Cho, S. Park and D. H. Choi, *Chem. Eng. J.*, 2021, **416**, 129185.

260 Y. Xu, Q. Wang, X. Cai, C. Li and Y. Wang, *Adv. Mater.*, 2021, **33**, 2100652.

261 Y. Xu, C. Li, Z. Li, J. Wang, J, Xue, Q. Wang, X. Cai and Y. Wang, *CCS Chem.*, 2022, **4**, 2065–2079. (Previous citation CCS Chem., 2021, 3, 2077).

262 D. W. Lee, J. Hwang, H. J. Kim, H. Lee, J. M. Ha, H. Y. Woo, S. Park, M. J. Cho and D. H. Choi, *ACS Appl. Mater. Interfaces*, 2021, **13**, 49076–49084.

263 Z. Zhao, C. Zeng, X. Peng, Y. Liu, H. Zhao, L. Hua, S.-J. Su, S. Yan and Z. Ren, *Angew. Chem., Int. Ed.*, 2022, **61**, e202210864.

264 R. Braveenth, H. Lee, J. D. Park, K. J. Yang, S. J. Hwang, K. R. Naveen, R. Lampande and J. H. Kwon, *Adv. Funct. Mater.*, 2021, **31**, 2105805.

265 J. Hwang, C. W. Koh, J. M. Ha, H. Y. Woo, S. Park, M. J. Cho and D. H. Choi, *ACS Appl. Mater. Interfaces*, 2021, **13**, 61454–61462.

266 J. H. Maeng, D. H. Ahn, H. Lee, Y. H. Jung, D. Karthik, J. Y. Lee and J. H. Kwon, *Dyes Pigm.*, 2020, **180**, 108485.

267 J. Wang, J. Miao, C. Jiang, S. Luo, C. Yang and K. Li, *Adv. Opt. Mater.*, 2022, **10**, 2201071.

268 Y. Lee and J.-I. Hong, *Adv. Opt. Mater.*, 2021, **9**, 2100406.

269 T. Hua, Y.-C. Liu, C.-W. Huang, N. Li, C. Zhou, Z. Huang, X. Cao, C.-C. Wu and C. Yang, *Chem. Eng. J.*, 2022, **433**, 133598.

270 H. Xie, Z. Huang, N. Li, T. Hua, J. Miao and C. Yang, *J. Mater. Chem. C*, 2022, **10**, 11239–11245.

271 D. Karthik, Y. H. Jung, H. Lee, S. Hwang, B.-M. Seo, J.-Y. Kim, C. W. Han and J. H. Kwon, *Adv. Mater.*, 2021, **33**, 2007724.

272 Y. Watanabe, H. Sasabe and J. Kido, *Bull. Chem. Soc. Jpn.*, 2019, **92**, 716–728.

273 X.-Q. Gan, Z.-M. Ding, D.-H. Liu, W.-Q. Zheng, B. Ma, H. Zhang, X. Chang, L. Wang, Y. Liu, X. Wu, S.-J. Su and W. Zhu, *Adv. Opt. Mater.*, 2023, **11**, 2300195.

274 Y.-J. Yu, S.-N. Zou, C.-C. Peng, Z.-Q. Feng, Y.-K. Qu, S.-Y. Yang, Z.-Q. Jiang and L.-S. Liao, *J. Mater. Chem. C*, 2022, **10**, 4941–4946.

275 M. Godumala, J. Hwang, H. Kang, J.-E. Jeong, A. K. Harit, M. J. Cho, H. Y. Woo, S. Park and D. H. Choi, *ACS Appl. Mater. Interfaces*, 2020, **12**, 35300–35310.

276 E. Y. Park, J. H. Park, Y.-H. Kim and M. C. Suh, *J. Mater. Chem. C*, 2022, **10**, 4705–4716.

277 S. Wu, L. Zhang, J. Wang, A. Kumar Gupta, I. D. W. Samuel and E. Zysman-Colman, *Angew. Chem., Int. Ed.*, 2023, **62**, e202305182.

278 Y. Zhang, J. Wei, D. Zhang, C. Yin, G. Li, Z. Liu, X. Jia, J. Qiao and L. Duan, *Angew. Chem., Int. Ed.*, 2022, **61**, e202113206.

279 X. Song, S. Shen, S. Zou, F. Guo, Y. Wang, S. Gao and Y. Zhang, *Chem. Eng. J.*, 2023, **467**, 143557.

280 G. Chen, J. Wang, W.-C. Chen, Y. Gong, N. Zhuang, H. Liang, L. Xing, Y. Liu, S. Ji, H.-L. Zhang, Z. Zhao, Y. Huo and B. Z. Tang, *Adv. Funct. Mater.*, 2023, 2211893.

281 P. Jiang, J. Miao, X. Cao, H. Xia, K. Pan, T. Hua, X. Lv, Z. Huang, Y. Zou and C. Yang, *Adv. Mater.*, 2022, **34**, 2106954.

282 Y.-K. Qu, D.-Y. Zhou, F.-C. Kong, Q. Zheng, X. Tang, Y.-H. Zhu, C.-C. Huang, Z.-Q. Feng, J. Fan, C. Adachi, L.-S. Liao and Z.-Q. Jiang, *Angew. Chem., Int. Ed.*, 2022, **61**, e202201886.

283 T. Wang, X. Yin, X. Cao and C. Yang, *Angew. Chem., Int. Ed.*, 2023, **62**, e202301988.

284 T. Wang, Y. Zou, Z. Huang, N. Li, J. Miao and C. Yang, *Angew. Chem., Int. Ed.*, 2022, **61**, e202211172.

285 L. Yang, P. Wang, K. Zhang, S. Wang, S. Shao and L. Wang, *Dyes Pigm.*, 2023, **216**, 111371.

286 J. Z. Deng, D. V. Paone, A. T. Ginnetti, H. Kurihara, S. D. Dreher, S. A. Weissman, S. R. Stauffer and C. S. Burgey, *Org. Lett.*, 2009, **11**, 345–347.

287 F. Huang, X.-C. Fan, Y.-C. Cheng, Y. Xie, S. Luo, T. Zhang, H. Wu, X. Xiong, J. Yu, D.-D. Zhang, X.-K. Chen, K. Wang and X.-H. Zhang, *Adv. Opt. Mater.*, 2023, **11**, 2202950.

288 Y. Hu, J. Miao, C. Zhong, Y. Zeng, S. Gong, X. Cao, X. Zhou, Y. Gu and C. Yang, *Angew. Chem., Int. Ed.*, 2023, **62**, e202302478.

289 Y. Xu, Q. Wang, J. Wei, X. Peng, J. Xue, Z. Wang, S.-J. Su and Y. Wang, *Angew. Chem., Int. Ed.*, 2022, **61**, e202204652.

290 Q. Wang, Y. Xu, T. Huang, Y. Qu, J. Xue, B. Liang and Y. Wang, *Angew. Chem., Int. Ed.*, 2023, **62**, e202301930.

291 J. T. Reeves, C. A. Malapit, F. G. Buono, K. P. Sidhu, M. A. Marsini, C. A. Sader, K. R. Fandrick, C. A. Busacca and C. H. Senanayake, *J. Am. Chem. Soc.*, 2015, **137**, 9481–9488.

292 F. Huang, Y.-C. Cheng, H. Wu, X. Xiong, J. Yu, X.-C. Fan, K. Wang and X.-H. Zhang, *Chem. Eng. J.*, 2023, **465**, 142900.

293 J. Bian, S. Chen, L. Qiu, R. Tian, Y. Man, Y. Wang, S. Chen, J. Zhang, C. Duan, C. Han and H. Xu, *Adv. Mater.*, 2022, **34**, 2110547.

294 X.-J. Liao, D. Pu, L. Yuan, J. Tong, S. Xing, Z.-L. Tu, J.-L. Zuo, W.-H. Zheng and Y.-X. Zheng, *Angew. Chem., Int. Ed.*, 2023, **62**, e202217045.

295 N. Sharma, E. Spuling, C. Mattern, W. Li, O. Fuhr, Y. Tsuchiya, C. Adachi, S. Brase, I. Samuel and E. Zysman-Colman, *Chem. Sci.*, 2019, **10**, 6689–6696.

296 Z.-G. Wu, H.-B. Han, Z.-P. Yan, X.-F. Luo, Y. Wang, Y.-X. Zheng, J.-L. Zuo and Y. Pan, *Adv. Mater.*, 2019, **31**, 1900524.

297 M. Wu, N. Li, C. Shi, J. Song, R. Zeng, F. Li, Q. Li, A. Yuan and C. Yang, *Inorg. Chem. Front.*, 2023, **10**, 1262–1269.

298 C. Shi, F. Li, Q. Li, W. Zhao, Y. Cao, Q. Zhao and A. Yuan, *Inorg. Chem.*, 2021, **60**, 525–534.

This journal is © The Royal Society of Chemistry 2024

Chem. Soc. Rev., 2024, **53**, 1624–1692 | 1691

299 J. Wang, N. Li, C. Zhong, J. Miao, Z. Huang, M. Yu, Y. X. Hu, S. Luo, Y. Zou, K. Li and C. Yang, *Adv. Mater.*, 2023, **35**, 2208378.

300 J. Guo, Z. Li, X. Tian, T. Zhang, Y. Wang and C. Dou, *Angew. Chem., Int. Ed.*, 2023, **62**, e202217470.

301 G. Li, X. Liu, M. Wu, R. Zeng, Q. Li, A. Yuan and C. Shi, *Dyes Pigm.*, 2022, **208**, 110805.

302 K. Matsuo, S. Saito and S. Yamaguchi, *J. Am. Chem. Soc.*, 2014, **136**, 12580–12583.

303 Y. Qi, X. Cao, Y. Zou and C. Yang, *J. Mater. Chem. C*, 2021, **9**, 1567–1571.

304 T. Agou, J. Kobayashi and T. Kawashima, *Org. Lett.*, 2006, **8**, 2241–2244.

305 S. M. Suresh, E. Duda, D. Hall, Z. Yao, S. Bagnich, A. M. Z. Slawin, H. Bässler, D. Beljonne, M. Buck, Y. Olivier, A. Köhler and E. Zysman-Colman, *J. Am. Chem. Soc.*, 2020, **142**, 6588–6599.

306 K. Stavrou, S. Madayanad Suresh, D. Hall, A. Danos, N. A. Kukhta, A. M. Z. Slawin, S. Warriner, D. Beljonne, Y. Olivier, A. Monkman and E. Zysman-Colman, *Adv. Opt. Mater.*, 2022, **10**, 2200688.

307 X. Wang, Y. Zhang, H. Dai, G. Li, M. Liu, G. Meng, X. Zeng, T. Huang, L. Wang, Q. Peng, D. Yang, D. Ma, D. Zhang and L. Duan, *Angew. Chem., Int. Ed.*, 2022, **61**, e202206916.

1692 | *Chem. Soc. Rev.*, 2024, **53**, 1624–1692

This journal is © The Royal Society of Chemistry 2024